

Mechanistic Studies of π -Activation Catalysis by Cationic Gold(I) and Brønsted-acid

by

Rachel Elizabeth McKinney Brooner

Department of Chemistry
Duke University

Date: _____

Approved:

Ross A. Widenhoefer, Supervisor

Steven W. Baldwin

Katherine J. Franz

Qiu Wang

Dissertation submitted in partial fulfillment of
the requirements for the degree of Doctor
of Philosophy in the Department of
Chemistry in the Graduate School
of Duke University

2013

ABSTRACT

Mechanistic Studies of π -Activation Catalysis by Cationic Gold(I) and Brønsted-acid

by

Rachel Elizabeth McKinney Brooner

Department of Chemistry
Duke University

Date: _____

Approved:

Ross A. Widenhoefer, Supervisor

Steven W. Baldwin

Katherine J. Franz

Qiu Wang

An abstract of a dissertation submitted in partial
fulfillment of the requirements for the degree
of Doctor of Philosophy in the Department of
Chemistry in the Graduate School of
Duke University

2013

Copyright by
Rachel Brooner
2013

Abstract

Soluble gold(I) complexes are highly efficient catalysts for the functionalization of C–C multiple bonds through the addition of carbon- or heteroatom-nucleophiles across π -bonds or cycloisomerizations of enynes and related π -systems. Mechanisms involving outer-sphere attack of a nucleophile on the electrophilic π -ligand of a cationic gold π -complex are typically invoked for gold(I)-catalyzed hydrofunctionalization and cycloisomerization processes, but direct experimental evidence for this mechanism is limited.

As an extension of the pioneering research in the Widenhoefer lab on the synthesis and characterization of gold(I) π -complexes, a diverse family of 15 gold(I) π -complexes in three distinct series are reported herein. First, the synthesis, characterization, and solution behavior of a series of seven gold(I) π -diene complexes is reported. In each case, gold binds preferentially to the less substituted C=C bond of the diene, but intermolecular exchange of the complexed and uncomplexed C=C is facile. The gold–alkene interaction is stabilized via substitution-dependant donation of electron density from the uncomplexed C=C bond to the complexed C=C bond of the diene.

In addition, a pair of axially chiral dicationic, bis(gold) π -alkene complexes that contain a 2,2'-bis(phosphino)biphenyl ligand are reported. The complexes show no intramolecular Au–Au interactions or facial selectivity for complexation, but solution

analyses suggest that the environment about one gold center affects the behavior of the proximal gold center through a yet unknown mechanism. Gold(I) π -alkene, alkyne, diene, and allene complexes that bear a triphenylphosphine supporting ligand have also been synthesized and characterized *in situ*. The π -ligands in the triphenylphosphine gold complexes were considerably more labile than those bearing bulky, electron rich phosphine or *N*-heterocyclic carbene ligands, and the complexes decomposed in solution above -20 °C.

Mechanistic investigation of the gold-catalyzed cycloisomerization of a 7-aryl-1,6-enyne led to characterization of the first organometallic complex directly observed in the course of an enyne cycloisomerization. The complex is best described as a gold π -(bicyclo[3.2.0]heptane) complex with a domination metallacyclopropane binding interaction and undergoes an acid-catalyzed rearrangement to yield a stable bicyclo[3.2.0]heptane product which can further isomerize in the presence of Ag⁺. In a further effort to understand the reactive species in catalytic cycloisomerizations, the first example of a gold cyclopropyl carbene was synthesized and fully characterized.

Finally, in an effort understand the mechanistic distinctions between electrophilic metal-catalyzed hydrofunctionalization and similar Brønsted acid-catalyzed additions, the kinetics and stereochemistry of intramolecular acid-catalyzed hydrofunctionalization were studied. In all cases, the transformations were > 95 % selective for *anti*-addition and displayed rate-laws similar to those expected for metal-

catalyzed variants. A concerted C-H, C-X bond forming mechanism for addition is proposed.

Contents

Abstract	iv
List of Tables	xvii
List of Figures	xix
List of Schemes	xxvii
Acknowledgements	xxxii
1. Computational and Experimental Studies of the Structure and Binding of Cationic Gold(I) π -Complexes of Alkenes and Alkynes	1
1.1 Introduction: gold(I) π -activation catalysis	1
1.2 Binding models for cationic gold(I) π -complexes	3
1.2.1 The Dewar-Chatt-Duncanson model for binding in transition metal π -complexes	3
1.2.2 Relativistic effects on the chemistry of gold	4
1.2.3 Theoretical studies of bonding in Au ⁺ -ethylene and Au ⁺ -acetylene complexes	5
1.2.4 Theoretical studies of bonding in LAu ⁺ -alkene and LAu ⁺ -alkyne complexes	8
1.3 Experimental determination of structure and solution behavior in gold(I) π -complexes of alkenes and alkynes	10
1.3.1 Introduction	10
1.3.2 Synthesis, structural characterizations, and solution behavior of cationic gold(I) π -alkene complexes	12
1.3.2.1 Complexes bearing NHC supporting ligands	12
1.3.2.2 Complexes bearing bulky phosphine supporting ligands	17

1.3.3 Synthesis, structural characterizations, and solution behavior of cationic gold(I) π -alkyne complexes.....	21
1.3.3.1 Internal alkyne complexes bearing NHC supporting ligands.....	21
1.3.3.2. Complexes bearing a hindered alkyl phosphine ligand.....	24
1.4 Summary and discussion	27
2. Syntheses, X-ray Crystal Structures, and Solution Behavior of Cationic, Two-Coordinate Gold(I) η^2 -Diene Complexes.....	30
2.1 Introduction.....	30
2.1.1 Gold(I) catalyzed hydrofunctionalization of dienes.....	30
2.1.2 Coordination behavior in gold(I) π -alkene complexes.....	31
2.1.3 Transition metal η^2 - and η^4 -(1,3-diene) complexes	34
2.1.4 Project goals and scope.....	34
2.2 Results and discussion.....	35
2.2.1 Synthesis and characterization of the gold(I) η^2 -(<i>trans</i> -1,3-pentadiene) complex 2.6.....	35
2.2.1.1 Synthesis of [(P1)Au(η^2 -(<i>E</i>)-H ₂ C=C(H)C(H)=C(H)Me)] ⁺ SbF ₆ ⁻ (2.6).....	35
2.2.1.2 X-Ray crystal structure of 2.6	36
2.2.1.3 Solution characterization and fluxional behavior of 2.6.....	38
2.2.2 Synthesis and characterization of gold(I) η^2 -(diene) complexes 2.7 – 2.12.....	41
2.2.2.1 Synthesis of gold(I) η^2 -(diene) complexes 2.7 – 2.12	41
2.2.2.2 X-ray crystal structures of 2.7, 2.9, and 2.12	42
2.2.2.3 Solution characterization of 2.7 - 2.12.....	47
2.2.3 Fluxional behavior of gold(I) diene complexes.....	50

2.2.3.1 Fluxional behavior of complexes 2.6 and 2.8	50
2.2.3.2 Fluxional behavior of complexes 2.9-2.12.....	54
2.2.4 Intermolecular exchange behavior of gold(I) η^2 -diene complexes.....	63
2.2.4.1 Kinetics of intermolecular exchange of 2,4-dimethyl-1,3-pentadiene with 2.8	63
2.2.4.2 Relative binding affinities of dienes to gold(I).....	65
2.3 Conclusions and contemporary work	67
2.3.1 Experimental conclusions from this work	67
2.3.2 Contemporary work on the characterization of gold π -diene complexes.....	68
2.4 Experimental	71
2.4.1 General methods.....	71
2.4.2 Synthesis of Gold(I) η^2 -Diene Complexes.....	72
2.4.3 X-ray Crystal Structure Determinations.....	85
2.4.4 Kinetics of Intramolecular C=C Bond Exchange	87
2.4.5 Kinetics of Intermolecular Diene Exchange with 2.8.....	89
2.4.6 Determination of Diene Binding Constants.....	90
3. Synthesis and Structure of Dicationic, Bis(gold) π -Alkene Complexes Containing a 2,2'-Bis(phosphino)biphenyl Ligand	92
3.1 Introduction.....	92
3.1.1 Enantioselective gold(I) catalysis	92
3.1.2 Examples of structurally characterized chiral, neutral bis(gold) complexes	94
3.1.3 Project goals and scope.....	98
3.2 Results and discussion.....	98

3.2.1 Synthesis, characterization, and solution behavior of PP-isobutylene and 1-pentene.....	98
3.2.2 X-ray crystal structures of 3.6 and 3.7.....	101
3.2.3 Ligand exchange behavior in 3.6.....	105
3.2.3.1 Kinetics of intermolecular ligand exchange of 3.6 with isobutylene	105
3.2.3.2 Equilibrium binding affinity of isobutylene in 3.6	106
3.3 Summary of conclusions	108
3.4 Experimental	109
3.4.1 General Methods	109
3.4.2 Synthesis and characterization of bis(gold) complexes	109
3.4.3 Ligand exchange studies	112
3.4.3.1 Kinetics of isobutylene exchange with 3.6.....	112
3.4.3.2 Equilibrium Binding Studies	113
3.4.4 X-Ray crystal structures.....	114
3.4.4.1 X-ray crystal structure data for 3.6·CH ₂ Cl ₂	114
3.4.4.2 X-Ray Crystal Structure of 3.7·CH ₂ Cl ₂	116
4. Synthesis and Solution Behavior of Cationic, Two-Coordinate Gold(I) π -Complexes Bearing a Triphenylphosphine Ligand	118
4.1 Introduction.....	118
4.1.1 The use of triarylphosphines in gold(I) catalysis	118
4.1.2 Background on triarylphosphine gold(I) π -complexes	119
4.1.2.1 Examples of triarylphosphine gold(I) π -complexes.....	119
4.1.2.2 Reported <i>in situ</i> generation of [(PPh ₃)Au] ⁺ π -complexes	121

4.1.3 Project goals and scope.....	123
4.2 Results and discussion.....	124
4.2.1 Triphenylphosphine gold π -alkene complexes.....	124
4.2.1.1 Synthesis and characterization of [(PPh ₃)Au(η^2 -Me(H)C=CMe ₂)] ⁺ SbF ₆ ⁻ (4.8·SbF ₆).....	124
4.2.1.2 Effect of stoichiometry on the synthesis of 4.8·SbF ₆	126
4.2.1.3 Effect of counterion on the synthesis of 4.8·SbF ₆	130
4.2.2 Triphenylphosphine gold π -(vinyl arene) complex 4.7.....	131
4.2.3 Triphenylphosphine gold π -(3-hexyne) complex 4.9.....	134
4.2.4 Triphenylphosphine gold π -(1,3-cyclohexadiene) complex 4.10.....	137
4.2.5 Triphenylphosphine gold π -allene complexes.....	140
4.2.5.1 Synthesis, characterization, and fluxional behavior of 1,1-dimethylallene complex 4.11.....	140
4.2.5.2 Synthesis, characterization, and fluxional behavior of 1,3-disubstituted allene complex 4.13.....	142
4.2.5.3 Effect of counterion and solvent on the synthesis and reactivity of 4.13.....	147
4.2.5.4 The role of 4.13 in the hydroamination of 1,7-diphenyl-3,4-heptadiene with methyl carbazate.....	148
4.3 Summary of conclusions.....	151
4.4 Experimental.....	152
4.4.1 General methods.....	152
4.4.2 Complex synthesis and characterization.....	153
4.4.3 Kinetics of intermolecular 3-alkyne exchange with 4.9.....	157

4.4.4 Kinetics of π -face exchange in complexes 4.10, 4.11, and 4.13	158
5. Mechanistic studies of the gold-catalyzed intramolecular cycloisomerizations of 1,6-enynes	161
5.1 Introduction.....	161
5.1.1 Gold(I) catalyzed cycloisomerization of 1,6-enynes.....	161
5.1.2 Proposed mechanism(s) of gold(I) catalyzed enyne cycloisomerization.....	162
5.1.3 Project goals and scope.....	164
5.2 Results and discussion.....	166
5.2.1 Generation and characterization of gold π -(bicyclo[3.2.0]hept-1(7)-ene) complex 5.9.....	166
5.2.1.1 Stoichiometric generation of gold π -enyne complexes 5.7 and 5.8 and their conversion to π -(Bicyclo[3.2.0]hept-1(7)-ene) complex 5.9.....	166
5.2.1.2 Characterization of 5.9 and isotopomers	170
5.2.2 Reactivity of gold π -(bicyclo[3.2.0]hept-1(7)-ene) complex 5.9	173
5.2.2.1 Generation of free bicyclo[3.2.0]hept-1(7)-ene 5.10	173
5.2.2.2 Hydroarylation of 5.9 with 1,3-dimethoxybenzene	175
5.2.3 Conversion of 5.9 to 5.11.....	177
5.2.3.1 Characterization of gold 6-phenylbicyclo-[3.2.0]-hept-6-ene complex 5.11	177
5.2.3.2 Kinetics of the conversion of 5.9 to 5.11	179
5.2.3.3 Skeletal rearrangement of 5.11- ¹³ C ₃	185
5.2.4 Catalytic enyne cycloisomerizations.....	189
5.2.4.1 Mechanistic studies of the catalytic conversion of 5.5 to 5.6.....	189

5.2.4.2 Catalytic tandem cyclization/hydroarylation of 5.5 and 1,3-dimethoxybenzene	191
5.3 Summary and conclusions	192
5.4 Experimental	194
5.4.1 General methods.....	194
5.4.2 Syntheses and characterization of complexes	195
5.4.2.1 Syntheses and characterization of enyne 5.5 and isotopomers	195
5.4.2.2 Syntheses and characterization of gold π -enyne complexes 5.7 and 5.8 and isotopomers.....	201
5.4.2.3 Syntheses and characterization of gold η^2 -bicyclo-[3.2.0]-hept-1(7)ene 5.9 and isotopomers.....	201
5.4.2.4 Syntheses and characterization of free bicyclo-[3.2.0]-hept-1(7)ene 5.10 and isotopomers.....	208
5.4.2.5 Syntheses and characterization of gold bicyclo-[3.2.0]-hept-6-ene 5.11 and isotopomers.....	210
5.4.2.6 Syntheses and characterization of free bicyclo-[3.2.0]-hept-6-ene isotopomers 5.6- $^{13}\text{C}_1$ and 5.6- d_x	212
5.4.3 Determination of equilibrium binding affinities of 5.10 and 5.6 for [(P1)Au] $^+$	213
5.4.4 Kinetics of the conversion of 5.9 and isotopomers to 5.11 and isotopomers ..	214
5.4.4.1 Kinetic analyses of the conversions of 5.9 and isotopomers to 5.11 without added acid.....	214
5.4.4.2 Kinetic analyses of the conversions of 5.9 and isotopomers to 5.11 with added acid.....	218
5.4.5 "Gold-free" and silver-free stoichiometric transformations	222
5.4.5.1 Reaction of 5.10 with HOTf	222

5.4.5.2	Generation and isomerization of 5.2-4,5,6- ¹³ C ₃	223
5.4.6	Catalytic Reactions	224
5.4.6.1	Gold-catalyzed enyne cycloisomerization.....	224
5.4.6.2	Gold catalyzed tandem cyclization/hydroarylation of 5.5 and 1,3-dimerthoxybenzene.....	226
6.	Synthesis and Characterization of a Gold Cyclopropyl Carbene Compound	227
6.1	Introduction.....	227
6.1.1	Questions on the electronic structure of gold carbenes	227
6.1.2	Synthesis and structure of stabilized gold carbenes.....	228
6.1.3	Project goals and scope.....	233
6.2	Results and discussion.....	233
6.2.1	Synthesis of gold cyclopropyl Fischer-carbene 6.11	233
6.2.2	Solution characterization of 6.11	235
6.2.3	X-ray crystal structure of 6.11	237
6.3	Summary and conclusions	239
6.4	Experimental	239
6.4.1	General methods.....	239
6.4.2	Synthesis and characterization of carbene complexes	240
6.4.3	X-ray crystal structure determination	241
7.	Stereochemistry and Mechanism of the Brønsted Acid Catalyzed Intramolecular Hydrofunctionalization of an Unactivated Cyclic Alkene	244
7.1	Introduction.....	244
7.1.1	Transition metal- and acid-catalyzed hydrofunctionalizations.....	244

7.1.2 Mechanism of the intermolecular acid-catalyzed alkene hydrofunctionalization	246
7.1.2.1 Alkene hydration	246
7.1.2.2 Addition of hydrogen halides to alkenes	247
7.1.3 Mechanism of the intramolecular acid-catalyzed alkene hydrofunctionalizations	250
7.1.4 Project goals and scope.....	250
7.2 Results and discussion.....	252
7.2.1 Stereochemistry of intramolecular hydrofunctionalization	252
7.2.1.1 Intramolecular hydroamination.....	252
7.2.1.2 Intramolecular hydroalkoxylation and hydroacyloxylation:	258
7.2.1.3 Effect of solvent and acid on hydrofunctionalization.....	261
7.2.2 Kinetics of the hydroamination.....	263
7.2.2.1 Conversion of 7.1 to 7.2.....	263
7.2.2.2 α -Secondary kinetic isotope effect.....	267
7.2.3 Mechanism of the acid-catalyzed conversion of 7.1 to 7.2.....	270
7.3 Summary and conclusions	274
7.4 Experimental	276
7.4.1 General methods.....	276
7.4.2 Syntheses of substrates 7.1, 7.3, and 7.5 and isotopomers.....	277
7.4.2.1 Syntheses and characterization of isotopomers of 7.1	277
7.4.2.2 Syntheses and characterization of isotopomers of 7.3 and 7.5	282

7.4.3 Acid-catalyzed hydrofunctionalizations and characterizations of bicyclic products.....	285
7.4.3.1 Synthesis and characterization of 7.2 and isotopomers.....	285
7.4.3.2 Synthesis and characterization of 7.4 and isotopomers.....	292
7.4.3.3 Synthesis and characterization of 7.6 and isotopomers.....	296
7.4.3 Kinetic experiments.....	299
7.4.3.1 Kinetics of the HOTf catalyzed conversion of 7.1 to 7.2.....	299
7.4.3.2 α -Secondary KIE for the conversion of 7.1 to 7.2.....	301
References	304
Biography	329

List of Tables

Table 1: Calculated bond distances (Å) and interaction energies (kcal mol ⁻¹) for Au ⁺ -ethylene and Au ⁺ -acetylene complexes.....	7
Table 2: Calculated bond lengths (Å) and energies (kcal mol ⁻¹) for [(L)Au(alkyne)] ⁺ and [(L)Au(alkene)] ⁺ complexes.	10
Table 3: Relevant ¹³ C and ¹ H NMR data for [(IPr)Au(π-alkene)] ⁺ complexes in CDCl ₃ . Displacement from free alkene (Δδ) is shown parenthetically (ppm). ^a	14
Table 4: Relevant ¹³ C, ¹ H, and ³¹ P NMR data for [(phosphine)Au(π-alkene)] ⁺ complexes in CDCl ₃ . Displacement from free alkene is shown parenthetically (ppm). ^a	19
Table 5: ¹³ C chemical shifts (ppm) and C-P coupling constants (Hz) of the sp ² carbon atoms of the complexes 2.6 – 2.12 in CD ₂ Cl ₂ and chemical shift difference (Δδ, ppm) relative to free diene.	48
Table 6: Line-broadening data and observed rate constants (<i>k</i> _{obs}) for the exchange of the 2,4-dimethyl-1,3-pentadiene ligand of 2.8 ([2.8] = 161 mM) with free 2,4-Dimethyl-1,3-pentadiene in CD ₂ Cl ₂ at 25 °C.	64
Table 7: Equilibrium constants for displacement of isobutylene from [(P1)Au(η ² -H ₂ C=CMe ₂)] ⁺ SbF ₆ ⁻ (2.1) with dienes in CD ₂ Cl ₂ at -70 °C.....	66
Table 8: Crystal and structure refinement data for complexes 2.6, 2.7, 2.9, and 2.12.	86
Table 9: Observed rate constants for the intermolecular exchange of bound and free isobutylene with complex 3.6.....	105
Table 10: Crystal and structure refinement data for complexes 3.6-CD ₂ Cl ₂ and 3.7-CD ₂ Cl ₂	117
Table 11: ³¹ P NMR Chemical shifts of relevant triphenylphosphine gold σ-complexes in CD ₂ Cl ₂	122
Table 12: ³¹ P NMR chemical shifts of the synthesized triphenylphosphine gold π-complexes in CD ₂ Cl ₂	124
Table 13: Observed rate constants for the intermolecular exchange of 3-hexyne with complex 4.9.	135

Table 14: Observed rate constants and selectivities for the conversions of 5.9 ([5.9] ₀ = 0.76 M) and isotopomers to 5.11 or 5.11- <i>d_x</i> in CD ₂ Cl ₂ without added acid and with [HOTf] = 0.019 M.....	184
Table 15: Crystal and structure refinement data for complex 6.11	243
Table 16: Brønsted acid-catalyzed intramolecular hydrofunctionalization of substrates 7.1-1',3'- <i>d</i> ₂ , 7.3-1',3'- <i>d</i> ₂ , and 7.5-1',3'- <i>d</i> ₂ at 85 °C for 48 h as a function of the solvent and the acid (5 mol %).....	263
Table 17: Observed rate constants for the conversion of 7.1 ([7.1] ₀ = 0.5 M) to 7.2 catalyzed by HOTf in toluene as a function of temperature and [HOTf].....	266
Table 18: Total conversion and isotope ratios as a function of time for the reaction of a 47.6:52.4 mixture of 7.1 and 7.1-2'- <i>d</i> ₁ catalyzed by HOTf (5 mol %) in toluene at 59.5 °C as determined from LC/MS analysis.....	302

List of Figures

- Figure 1: Orbital diagrams (left) and skeletal structures (right) depicting the two predominant binding modes described by the Dewar-Chatt-Duncanson model. 3
- Figure 2: ORTEP diagrams and skeletal structures of phosphine gold(I) η^1 - and η^2 -arene π -complexes 1.9 and 1.10. Hydrogen atoms and counterions have been removed for clarity. 11
- Figure 3: ORTEP diagrams of [(IPr)Au(η^2 -alkene)]⁺ complexes 1.15 (top left), 1.16 (right), and 1.18 (bottom left). Hydrogen atoms and counterions have been removed for clarity. 16
- Figure 4: ORTEP diagrams of [(phosphine)Au(η^2 -alkene)]⁺ complexes 1.19 (top left), 1.20 (bottom left), 1.22 (top right) and 1.24 (bottom right). Hydrogen atoms and counterions have been removed for clarity..... 20
- Figure 5: ORTEP diagrams of [(NHC)Au(η^2 -alkyne)]⁺ complexes 1.4 (top left), 1.5 (bottom left), and 1.29 (right). Hydrogen atoms and counterions have been removed for clarity. 24
- Figure 6: ORTEP diagram of [(^tBu₃P)Au(η^2 -alkyne)]⁺ (1.30). Hydrogen atoms and counterion have been removed for clarity. 26
- Figure 7: Cationic, three-coordinate gold(I) π -alkene complexes 2.4 and 2.5..... 33
- Figure 8: ORTEP diagram of 2.6 showing partial atom numbering scheme. Ellipsoids are shown at the 50% probability level. Hydrogen atoms and counterion have been removed for clarity. 38
- Figure 9: ORTEP diagram of 2.7 showing partial atom numbering scheme. The major conformer of the diene ligand (2.7a) is shown in dark gray ellipsoids, and the minor conformer (2.7b) is shown in white ellipsoids. Ellipsoids are shown at the 50% probability level. Hydrogen atoms and counterion have been removed for clarity. 43
- Figure 10: ORTEP diagram of 2.9 showing partial atom numbering scheme. The major conformer of the diene ligand (2.9a) is shown in dark gray ellipsoids, and the minor conformer (2.9b) is shown in white ellipsoids. Ellipsoids are shown at the 50% probability level. Hydrogen atoms and counterion have been removed for clarity. 45

Figure 11: ORTEP diagram of 2.12 showing partial atom numbering scheme. Ellipsoids are shown at the 50% probability level. Hydrogen atoms and counterion have been removed for clarity.	47
Figure 12: Temperature dependence of the quaternary <i>tert</i> -butyl ¹³ C NMR resonance of 2.6 from -50 to -80 °C in CD ₂ Cl ₂	52
Figure 13: Temperature dependence of the quaternary <i>tert</i> -butyl ¹³ C NMR resonances of 2.8 from -90 °C to -60 °C in CD ₂ Cl ₂	53
Figure 14: Temperature dependence of the vinylic ¹ H NMR resonances of 2.9 from -90 °C to 15 °C in CD ₂ Cl ₂ . The small multiplets at δ 6.3, 5.2, and 5.1 correspond to free 1,3-butadiene.....	56
Figure 15: Temperature dependence of the vinylic (left column) and diene methyl (right column) ¹ H NMR resonances of 2.10 in CD ₂ Cl ₂ from -60 °C to 20 °C. Resonances at δ 5.0 and 1.88 correspond to free diene and the resonance at δ ~1.65 corresponds to water. Vertical and horizontal scale is not consistent between the two sets of spectra.	58
Figure 16: Temperature dependence of the vinylic (left column) and allylic (right column) ¹ H NMR resonances of 2.11 from -85 °C to 0 °C in CD ₂ Cl ₂ . The resonance indicated with an “x” corresponds to an unknown impurity. Vertical and horizontal scale is not consistent between the two sets of spectra.....	60
Figure 17: Temperature dependence of the vinylic ¹ H NMR resonances of 2.12 from -70 °C to -20 °C in CD ₂ Cl ₂	61
Figure 18: Plot of <i>k</i> _{obs} versus [2,4-dimethyl-1,3-pentadiene] for the intermolecular exchange of the 2,4-dimethyl-1,3-pentadiene ligand of 2.8 ([2.8] = 161 mM) with free 2,4-dimethyl-1,3-pentadiene from 93 to 245 mM at 25 °C in CD ₂ Cl ₂	64
Figure 19: Potential η ² -coordination modes of the 2,5-dimethyl-2,4-hexadiene ligand in complex 2.13	70
Figure 20: Partial HMQC spectrum of 2.6 at 25 °C.....	73
Figure 21: Partial HMBC of 2.8 in CD ₂ Cl ₂ at 25 °C.	77
Figure 22: Partial ¹ H- ¹ H COSY spectrum of 2.9 in CD ₂ Cl ₂ at -90 °C. The cross-peak at δ 4.4 × δ 6.3 (indicated with boxes) corresponds to a pair of strongly coupled protons in an impurity that is undetected in the 1-D NMR spectra. Repeated concentration/dissolution	

of pure samples of 2.9 leads to the appearance of resonances in the ^1H NMR spectrum at δ 6.3, 4.45, 3.2. A wider expansion of the COSY spectrum of 2.9 also shows a crosspeak between the δ 6.3 and 3.2 resonances.	79
Figure 23: Partial HMQC of 2.9 in CD_2Cl_2 at -90°C	80
Figure 24: Partial COSY of 2.11 in CD_2Cl_2 at -85°C	83
Figure 25: Temperature dependence of the vinylic ^{13}C NMR resonances of 2.11 in CD_2Cl_2 from -85°C to 27°C in CD_2Cl_2	84
Figure 26: Experimental (left) and simulated (right) ^1H NMR spectra of internal vinyl protons H2 and H3 of complex 2.9.	88
Figure 27: Experimental (left) and simulated (right) ^1H NMR spectra of vinyl methyl protons of complex 2.10.	88
Figure 28: Experimental (left) and simulated (right) ^1H NMR spectra of internal vinyl protons H3 (δ 6.0 ppm) and H2 (δ 5.38 ppm) of complex 2.11.	89
Figure 29: Experimental (left) and simulated (right) ^1H NMR spectra of vinyl protons H1/H2 and H4/H5 of complex 2.12.	89
Figure 30: ORTEP and skeletal diagrams of bis(gold chloride) complexes 3.2 (upper structure) and 3.3 (lower structure). ¹⁰⁹ Ellipsoids are shown at the 50% probability level. Hydrogen atoms and counterion have been removed for clarity.	95
Figure 31: ORTEP and skeletal diagrams of [(biphep)(AuX) ₂] complexes 3.4 (upper structure) ¹¹⁴ and 3.5 (lower structure) ¹⁰⁸ . π - π stacking is indicated by the dashed line. Ellipsoids are shown at the 50% probability level. Hydrogen atoms and counterion have been removed for clarity.	97
Figure 32: Two ORTEP diagrams of 3.6 showing partial atom numbering scheme. Ellipsoids are shown at the 50% probability level. Hydrogen atoms and counterion have been removed for clarity.	103
Figure 33: ORTEP diagram of 3.7. Ellipsoids are shown at the 50% probability level. Hydrogen atoms and counterion have been removed for clarity.	104
Figure 34: Plot of k_{obs} versus [isobutylene] for the intermolecular exchange of the isobutylene ligands of 3.6 with free isobutylene from 14 to 61 mM at 25°C in CD_2Cl_2	106

Figure 35: Cationic, multimeric gold(I) π -complexes containing triarylphopshine supporting ligands.....	120
Figure 36: Thermally unstable cationic, monomeric gold(I) π -complexes containing triarylphopshine supporting ligands.	121
Figure 37: Variable-temperature ^{31}P NMR spectra of the solutions generated from reaction of (a) a 2:2:1 mixture of $[(\text{PPh}_3)\text{AuCl}]$, AgSbF_6 , and 2-methyl-2-butene in CD_2Cl_2 at $-78\text{ }^\circ\text{C}$ (left); and (b) a 2:1:2 mixture of $[(\text{PPh}_3)\text{AuCl}]$, AgSbF_6 , and 2-methyl-2-butene in CD_2Cl_2 at $-78\text{ }^\circ\text{C}$ (right). Vertical amplitude is not consistent between spectra.	128
Figure 38: Variable-temperature ^{31}P NMR spectra of the solutions generated from reaction of (a) a 1:1:1.15 mixture of $[(\text{PPh}_3)\text{AuCl}]$, AgBF_4 , and 4-methylstyrene in CD_2Cl_2 at $-78\text{ }^\circ\text{C}$ (left); and (b) a 1:1:1 mixture of $[(\text{PPh}_3)\text{AuCl}]$, AgSbF_6 , and 4-methylstyrene in CD_2Cl_2 at $-78\text{ }^\circ\text{C}$ (right). Vertical amplitude is not consistent among the spectra.	133
Figure 39: Plot of k_{obs} versus [3-hexyne] for the intermolecular exchange of the 3-hexyne ligand of 4.9-SbF_6 ($[4.9\text{-SbF}_6] = 80\text{ mM}$) from 18 to 60 mM at $-85\text{ }^\circ\text{C}$ in CD_2Cl_2	136
Figure 40: Temperature dependence of the alkenyl (left) and aliphatic (right) ^1H NMR resonances of 4.10-SbF_6 from -94 to $-25\text{ }^\circ\text{C}$ in CD_2Cl_2	139
Figure 41: Temperature dependence of the allenyl methyl ^1H (left) and ^{13}C (right) NMR resonances of 4.11-SbF_6 in CD_2Cl_2 . Amplitude is not consistent between spectra.	142
Figure 42: Temperature dependence of the ^{31}P resonances (left) and allenyl ^1H resonances (right) of 4.13-SbF_6 in CD_2Cl_2 . Amplitude is not consistent between spectra.....	145
Figure 43: Partial ^1H - ^{13}C HMQC spectrum of 4.13-SbF_6 in CD_2Cl_2 at $-90\text{ }^\circ\text{C}$. The cross-peak at $\delta 5.2 \times \delta 90.6$ (indicated with a box) corresponds to equivalent sp^2 allenyl protons/carbons of free 1,7-diphenyl-3,4-heptadiene.	146
Figure 44: ^{31}P NMR resonances of: (a) a 1:1 mixture of $\text{Ph}_3\text{PAuNTf}_2$ and methyl carbazate in CD_3NO_2 at $25\text{ }^\circ\text{C}$; (b) sample from (a) plus 1 equiv. 1,7-diphenyl-3,4-heptadiene after 10 minutes at $25\text{ }^\circ\text{C}$; (c) sample from (b) after 1 h at $25\text{ }^\circ\text{C}$; (d) sample from (b) after 12 h at $25\text{ }^\circ\text{C}$; (e) a 1:1 mixture of $\text{Ph}_3\text{PAuNTf}_2$ and carbazate 4.14 in CD_3NO_2 at $-20\text{ }^\circ\text{C}$	151
Figure 45: Partial ^1H - ^1H COSY spectrum of 4.13-SbF_6 in CD_2Cl_2 at $-90\text{ }^\circ\text{C}$. The cross-peaks at $\delta = 5.2 \times \delta = 2.1$ (indicated with boxes) corresponds to protons of free 1,7-diphenyl-3,4-heptadiene.....	156

Figure 46: Experimental (left) and simulated (right) ^1H NMR spectra of the vinyl protons used to approximate the rate constant and free energy of activation for the intramolecular alkene exchange in 4.10·SbF ₆	159
Figure 47: Experimental (left) and simulated (right) ^1H NMR spectra of the diastereotopic methyl groups used to approximate the rate constant and free energy of activation for the intramolecular alkene exchange in 4.11·SbF ₆	160
Figure 48: Experimental (left) and simulated (right) ^{31}P NMR spectra of the phosphorus resonances used to approximate the rate constant and free energy of activation for the intramolecular alkene exchange in 4.13·SbF ₆	160
Figure 49: Skeletal rearrangements in the gold-catalyzed cycloisomerizations of 1,6-enynes.....	162
Figure 50: Possible cationic intermediates in the ligand- and substrate-dependent pathways for enyne cycloaddition catalyzed by electrophilic noble metal complexes. .	163
Figure 51: Partial atom numbering scheme of 5.9 and complexes which aided in the characterization of 5.9.....	171
Figure 52: Partial atom numbering scheme for 5.11.....	178
Figure 53: First order plot of the conversion of 5.9 to 5.11 ($[\text{5.9}]_0 = 0.076 \text{ M}$) in CD ₂ Cl ₂ at 25 °C.....	180
Figure 54: Analysis of the cycloisomerization of 5.5 ($[\text{5.5}]_0 = 0.10 \text{ M}$) to 5.6 via 5.10 catalyzed by a mixture of [(P1)AuCl] (5 mol %) and AgSbF ₆ (5 mol %) in CD ₂ Cl ₂ at 25 °C.	190
Figure 55: The overall conversion of 5.5- $^{13}\text{C}_3$ to 5.11-4,5,6- $^{13}\text{C}_3$ and 5.11-1,2,6- $^{13}\text{C}_3$ in the presence of [(P1)Au] ⁺ , Ag ⁺ , and H ⁺	193
Figure 56: Partial $^{13}\text{C}\{^1\text{H}\}$ NMR spectrum of 5.5- $^{13}\text{C}_3$ showing resonances corresponding to the labeled carbon atoms (CDCl ₃ , 25 °C).....	198
Figure 57: Partial atom numbering scheme for 5.9.....	201
Figure 58: Selected coupling constants (left) and NOE enhancements observed in NMR spectra of 5.9.	203

Figure 59: Partial ^1H - ^1H COSY spectrum of 5.9 in CD_2Cl_2 at $-20\text{ }^\circ\text{C}$. Resonances are labeled in accord with the numbering scheme depicted in Figure 57.....	204
Figure 60: Partial ^1H - ^1H NOESY spectrum of 5.9 in CD_2Cl_2 at $-20\text{ }^\circ\text{C}$. Resonances are labeled in accord with the numbering scheme depicted in Figure 57.....	205
Figure 61: Partial atom numbering scheme for 5.6.....	208
Figure 62: First order plot of the conversion of 5.9- d_2 to 5.11- d_x ($[\text{5.9-}d_2]_0 = 0.076\text{ M}$) in CD_2Cl_2 at $25\text{ }^\circ\text{C}$	216
Figure 63: First order plot of the conversion of <i>trans</i> -5.9- d_1 to 5.11- d_x ($[\textit{trans}\text{-5.9-}d_1]_0 = 0.073\text{ M}$) in CD_2Cl_2 at $25\text{ }^\circ\text{C}$	217
Figure 64: First order plot of the conversion of <i>cis</i> -5.9- d_1 to 5.11- d_x ($[\textit{cis}\text{-5.9-}d_1]_0 = 0.076\text{ M}$) in CD_2Cl_2 at $25\text{ }^\circ\text{C}$	218
Figure 65: First order plot of the conversion of 5.9 to 5.11 ($[\text{5.9}]_0 = 0.076\text{ M}$) with HOTf ($[\text{HOTf}] = 0.019\text{ M}$) in CD_2Cl_2 at $-21\text{ }^\circ\text{C}$	219
Figure 66: First order plot of the conversion of 5.9- d_2 to 5.11- d_x ($[\text{5.9-}d_2]_0 = 0.076\text{ M}$) with HOTf ($[\text{HOTf}] = 0.019\text{ M}$) in CD_2Cl_2 at $-21\text{ }^\circ\text{C}$	220
Figure 67: First order plot of the conversion of <i>trans</i> -5.9- d_1 to 5.11- d_x ($[\textit{trans}\text{-5.9-}d_1]_0 = 0.070\text{ M}$) with HOTf ($[\text{HOTf}] = 0.019\text{ M}$) in CD_2Cl_2 at $-21\text{ }^\circ\text{C}$	221
Figure 68: First order plot of the conversion of <i>cis</i> -5.9- d_1 to 5.11- d_x ($[\textit{cis}\text{-5.9-}d_1]_0 = 0.076\text{ M}$) with HOTf ($[\text{HOTf}] = 0.019\text{ M}$) in CD_2Cl_2 at $25\text{ }^\circ\text{C}$	222
Figure 69: Possible canonical forms for the structure of $[(\text{L})\text{Au-C}(\text{H})\text{R}]^+$, including the carbene form (6.I) and the stabilized carbocation form (6.II).....	228
Figure 70: Structurally characterized neutral Fischer-type gold carbene. ²⁰¹	229
Figure 71: ^{13}C chemical shifts of cyclopropyl carbons of cationic metal carbenes and neutral organic cyclopropanes.	237
Figure 72: ORTEP diagram of 6.11 showing partial atom numbering scheme. Ellipsoids are shown at the 50% probability level. Hydrogen atoms and counterion have been removed for clarity.	238

Figure 73: ORTEP diagram of 7.2 showing partial atom numbering scheme. Ellipsoids are shown at the 50% probability level. Hydrogen atoms and aromatic portion of tosyl group removed for clarity.....	254
Figure 74: (a) Partial ^1H NMR spectrum of 7.2; (b),(c) Partial ^1H and ^2H NMR spectra of 7.2-3a,7 _{eq-d2} ; (d),(e) Partial ^1H and ^2H NMR spectra of 7.2-7 _{ax-d1} ; (f) Partial ^2H NMR spectrum of 7.2-7a-d ₁	256
Figure 75: ^1H (a) and ^2H NMR analysis of the DOTf-catalyzed conversion of 7.1-N-d ₁ to 7.2-7 _{ax-d1} quenched at ~50% conversion with NEt ₃	258
Figure 76: (a) Partial ^1H NMR spectrum of 7.4; (b),(c) Partial ^1H and ^2H NMR spectra of 7.4-3a,7 _{eq-d2}	260
Figure 77: (a) Partial ^1H NMR spectrum of 7.6; (b),(c) Partial ^1H and ^2H NMR spectra of 7.6-3a,7 _{eq-d2}	261
Figure 78: First-order plots for the conversion of 7.1 ($[\text{7.1}]_0 = 0.50 \text{ M}$) to 7.2 catalyzed by triflic acid ($[\text{HOTf}] = 5.0 (\diamond), 12.6 (\square), \text{ and } 25.2 (\triangle) \text{ mM}$) in toluene at 62 °C.	264
Figure 79: Plot of k_{obs} versus the concentration of triflic acid for the conversion of 7.1 ($[\text{7.1}]_0 = 0.50 \text{ M}$) to 7.2 in toluene at 62 °C.	265
Figure 80: Eyring plot for the conversion of 7.1 ($[\text{7.1}]_0 = 0.50 \text{ M}$) to 7.2, catalyzed by HOTf (25 mM) in toluene over the temperature range 39 °C – 72 °C.....	266
Figure 81: First order plot for the conversion of 7.1 to 7.2 (O) and 7.1-2'-d ₁ to 7.2-7a-d ₁ (◇) catalyzed by triflic acid (5 mol %) in toluene at 60 °C.....	270
Figure 82: Numbering scheme (left structure), relevant ^1H - ^1H coupling constants (center structure), and key NOESY interactions (right structure) for compound 7.1.	287
Figure 83: ^1H - ^1H COSY (800 MHz) NMR spectrum of 7.2 at 45 °C in CDCl ₃	288
Figure 84: ^1H - ^1H NOESY (800 MHz) NMR spectrum of 7.2 at 25 °C in CDCl ₃	289
Figure 85: Numbering scheme and key NOESY interactions for compounds 7.4.	293
Figure 86: ^1H - ^1H COSY (500 MHz) NMR spectrum of 7.4 at 25 °C in CDCl ₃	294
Figure 87: ^1H - ^1H NOESY (500 MHz) NMR spectrum of 7.4 at 25 °C in CDCl ₃	295

Figure 88: ^1H - ^1H COSY (800 MHz) NMR spectrum of 7.6 at 25 °C in CDCl_3	297
Figure 89: ^1H - ^1H NOESY (800 MHz) NMR spectrum of 7.6 at 25 °C in CDCl_3	298
Figure 90: First-order plots for the conversion of 7.1 ($[\text{7.1}]_0 = 0.50 \text{ M}$) to 7.2 catalyzed by triflic acid in toluene: $[\text{HOTf}] = 12.6 \text{ mM}$ at 72 °C (\circ); $[\text{HOTf}] = 25.2 \text{ mM}$ at 62.5 °C (\diamond); $[\text{HOTf}] = 25.2 \text{ mM}$ at 53.0 °C (\square); $[\text{HOTf}] = 25.2 \text{ mM}$ at 39 °C (\triangle); and $[\text{HOTf}] = 25.1 \text{ mM}$ at 45.5 °C (\times).....	301

List of Schemes

Scheme 1: Proposed mechanism π -activation by cationic gold(I).....	2
Scheme 2: Synthesis of select [(IPr)Au(η^2 -alkene)] ⁺ complexes. Ar = 2,6-diisopropylphenyl.....	13
Scheme 3: Synthesis of select [(IPr)Au(η^2 -alkyne)] ⁺ complexes. Ar = 2,6-diisopropylphenyl.....	22
Scheme 4: Proposed mechanism for degenerate alkene exchange in gold(I) π -alkene complexes.....	32
Scheme 5: Synthesis of [(P1)Au(η^2 -(E)-H ₂ C=C(H)C(H)=C(H)Me)] ⁺ SbF ₆ ⁻ (2.6)	36
Scheme 6: Resonance structures depicting depletion of electron density at the C4 position of the 1,3-pentadiene ligand in 2.6.	40
Scheme 7: Synthesis of cationic, monomeric gold(I) η^2 -diene complexes 2.6 - 2.12	42
Scheme 8: Proposed mechanism for racemization of complex 2.6 via intramolecular, associative exchange of prochiral alkene π -faces	54
Scheme 9: Proposed mechanism for intramolecular π -face exchange in complex 2.13	71
Scheme 10: Enantioselective enyne alkocycloisomerization catalyzed by the chiral bis(gold) BINAP complex 3.1. ¹⁰⁶	93
Scheme 11: Synthesis of chiral, dicationic bis(gold) complexes 3.6 and 3.7.....	99
Scheme 12: Successive equilibrium displacement of 4-trifluoromethylbenzotrile (NCArF') from 3.8 to give 3.9 and from 3.9 to give 3.6 by isobutylene.....	107
Scheme 13: Low temperature generation of triphenylphosphine gold π -alkene complex 4.8·SbF ₆ and its decomposition to 4.6·SbF ₆	125
Scheme 14: Reaction of an equimolar mixture of [(PPh ₃)AuCl] and 2-methyl-2-butene with a deficiency of AgSbF ₆ to form an equilibrating mixture of 4.8·SbF ₆ and 4.5·SbF ₆ ..	130
Scheme 15: Competitive binding of 2-methyl-2-butene and the NTf ₂ ⁻ (eq. 1) and OTf (eq. 2) counterions for [(PPh ₃)Au] ⁺	131

Scheme 16: Hydroamination of 1,7-diphenyl-3,4-heptadiene with methyl carbazate catalyzed by [(PPh ₃)AuNTf ₂] in CH ₃ NO ₂ in the absence (eq. 1) and the presence (eq. 2) of PPh ₃	149
Scheme 17: Hydroamination of 1,7-diphenyl-3,4-heptadiene by stoichiometric gold carbazate complex 4.15 (1 equiv.) to give gold bound product 4.16 with concomitant generation of decomposition product 4.6.....	150
Scheme 18: Trapping of a gold cyclopropyl carbene complex by oxidation with Ph ₂ SO. ¹⁶⁰	164
Scheme 19: Trapping of a gold cyclopropyl carbene complex with methanol. ¹⁵⁴	164
Scheme 20: Cycloisomerization of 7-phenyl-1,6-enyne 5.1 to the 6-phenylbicyclo[3.2.0]hept-6-ene 5.2 catalyzed by [(P1)Au(NCMe)] ⁺ SbF ₆ ⁻	165
Scheme 21: Formation of gold π-alkyne complex 5.7 and gold π-alkene complex 5.8....	166
Scheme 22: Formation of isotopically labeled gold π-alkyne complex 5.7- ¹³ C ₃ and gold π-alkene complex 5.8- ¹³ C ₃	167
Scheme 23: Conversion of 5.7 and 5.8 to 5.9 at -20 °C in CD ₂ Cl ₂ . Three canonical structures of 5.9 are shown.	169
Scheme 24: Conversion of enyne isotopomers 5.5- ¹³ C ₁ , 5.5- ¹³ C ₃ , 5.5- <i>d</i> ₅ , 5.5- <i>d</i> ₂ , <i>cis</i> -5.5- <i>d</i> ₁ , and <i>trans</i> -5.5- <i>d</i> ₁ to gold bicyclo[3.2.0]heptene isotopomers 5.9- ¹³ C ₁ , 5.9- ¹³ C ₃ , 5.9- <i>d</i> ₅ , 5.9- <i>d</i> ₂ , <i>cis</i> -5.9- <i>d</i> ₁ , and <i>trans</i> -5.9- <i>d</i> ₁	170
Scheme 25: Generation of the thermally sensitive bicyclo[3.2.0]hept-1(7)-ene 5.10 from 5.9 and regeneration of 5.9 from 5.10.	173
Scheme 26: Equilibrium binding affinities of 5.9 (eq. 1) and 5.6 (eq. 2) to [(P1)Au] ⁺ relative to NCA _{RF} [NCA _{RF} = 3,5-bis(trifluoromethyl)benzotrile]......	174
Scheme 27: Hydroarylation of 5.9 with 1,3-dimethoxybenzene to give 5.13.....	176
Scheme 28: Control reactions showing that 5.10 (eq. 1), 5.11 (eq. 2), and 5.6 (eq. 3) do not undergo hydroarylation with 1,3-dimethoxybenzene.....	177
Scheme 29: The conversion of 5.9 to 5.11, and independent synthesis of 5.11 from 5.6.	178

Scheme 30: Thermal rearrangement of 5.9- ¹³ C ₁ to 5.11- ¹³ C ₁ and displacement of gold to form 5.6- ¹³ C ₁	179
Scheme 31: Conversion of 5.9- <i>d</i> ₂ to 5.11- <i>d</i> _x	180
Scheme 32: E ₂ -like mechanism for conversion of 5.9 to 5.11 through gold σ-alkyl species 5.V.....	181
Scheme 33: Conversion of <i>trans</i> -5.9- <i>d</i> ₁ (eq. 1) and <i>cis</i> -5.9- <i>d</i> ₁ (eq. 2) to 5.11- <i>d</i> _x	182
Scheme 34: Conversion of 5.10 to 5.6 with HOTf (25 mol %).	185
Scheme 35: Mechanism of the conversion of 5.9 to 5.11 by the acid-catalyzed isomerization of 5.10 to 5.6 through intermediate 5.VI.	185
Scheme 36: Conversion of 5.9- ¹³ C ₃ to 5.11-4,5,6- ¹³ C ₃ and 5.11-1,2,6- ¹³ C ₃	186
Scheme 37: Synthesis of 5.6-4,5,6- ¹³ C ₃ from the [(P1)Au(NCArF)] (5.12) catalyzed cyclization of 5.5- ¹³ C ₃ to 5.9- ¹³ C ₃ and 5.10- ¹³ C ₃ followed by H ⁺ catalyzed isomerization.	187
Scheme 38: Silver catalyzed isomerization of 5.6-4,5,6- ¹³ C ₃ to 5.6-1,2,6- ¹³ C ₃	188
Scheme 39: The Ag ⁺ catalyzed isomerization of tricyclo[4.1.0.0]heptanes to bicyclo[3.2.0]hept-6-enes (eq. 1) ¹⁸⁶⁻¹⁸⁸ , and the proposed mechanism for the Ag ⁺ catalyzed isomerization of 5.6-4,5,6- ¹³ C ₃ to 5.6-1,2,6- ¹³ C ₃ (eq. 2).....	189
Scheme 40: The cycloisomerization of 5.5 to 5.6 catalyzed by [(P1)Au] ⁺ without (eq. 1) and with (eq. 2) added HOTf.	191
Scheme 41: Gold-catalyzed tandem cyclization/hydroarylation protocol for the conversion of 5.5 and 1,3-dimethoxybenzene to 5.13.	192
Scheme 42: Gas phase synthesis of gold carbene complex 6.1 employing collision-induced dissociation (CID). Mes = 2,4,6-trimethylphenyl.....	228
Scheme 43: Gold-mediated rearrangement of dioxaspiro[2.5]oct-1-ene to form stabilized gold carbenoids 6.3.	230
Scheme 44: Observation of a cationic intermediate in the course of the gold catalyzed cyclization of 2-methyl-5-phenyl-2,3-pentadienoate.	231

Scheme 45: Generation of gold allenylidene 6.6 from gold acetylide 6.5, and four possible canonical forms of 6.6.....	232
Scheme 46: Synthesis of gold Fischer-carbene complexes 6.7. ¹⁹⁹	233
Scheme 47: Synthesis of gold cyclopropyl carbene complexes 6.10 and 6.11.....	234
Scheme 48: Gold(I)- and HOTf-catalyzed hydroalkoxylation of cyclohexene with phenols. ^{181, 243}	245
Scheme 49: General mechanism for the acid-catalyzed hydration of alkenes.....	246
Scheme 50: Proposed preassociation mechanism for the acid-catalyzed hydration of alkenes.	247
Scheme 51: The HCl-catalyzed addition of HCl to 1,3,3-trideuteriocyclohexene via an Ad _E 3 mechanism (eq. 1), and the HCl-catalyzed addition of HOAc to 1,3,3-trideuteriocyclohexene via an Ad _E 2 mechanism (eq.2). ²⁸⁰	248
Scheme 52: The <i>syn</i> selective addition of DBr to <i>trans</i> -1-phenylpropene in dichloromethane via an Ad _E 2 mechanism. ²⁹²	249
Scheme 53: Proposed mechanism for the acid-catalyzed intramolecular addition of sulfonamides across vinyl arenes. ¹⁸⁰	250
Scheme 54: Gold-catalyzed intramolecular <i>syn</i> -hydroamination of doubly deuterated γ -cyclohexenyl sulfonamide 7.1-1',3'-d ₂ . ¹⁴⁰	251
Scheme 55: HOTf-catalyzed intramolecular <i>syn</i> -hydroamination of doubly deuterated γ -cyclohexenyl sulfonamide 7.1-1',3'-d ₂	252
Scheme 56: HOTf-catalyzed intramolecular hydroamination of γ -cyclohexenyl sulfonamide 7.1.	253
Scheme 57: Generation and DOTf-catalyzed cyclization of 7.1- <i>N</i> -d ₁ to 7.2-7 _{ax} -d ₁	257
Scheme 58: HOTf-catalyzed intramolecular <i>syn</i> -hydroalkoxylation of doubly deuterated γ -cyclohexenyl alcohol 7.3-1',3'-d ₂	259
Scheme 59: HOTf-catalyzed intramolecular <i>syn</i> -hydroacyloxylation of doubly deuterated γ -cyclohexenyl carboxylic acid 7.5-1',3'-d ₂	261

Scheme 60: The HOTf-catalyzed hydroamination of a ~1:1 mixture of 7.1 and 7.1-2'- <i>d</i> ₁ to 7.2 and 7.2-7a- <i>d</i> ₁ (eq. 1) and the HOTf catalyzed isomerization of 7.1-2'- <i>d</i> ₁ to 7.2-7a- <i>d</i> ₁ (eq. 2).....	269
Scheme 61: Proposed mechanism for the DOTf-catalyzed intramolecular <i>syn</i> -hydroamination of 7.1- <i>N</i> - <i>d</i> ₁	274

Acknowledgements

Rachel would first like to thank Ross Widenhoefer and the Duke Chemistry Department faculty and staff for their guidance throughout her time as a research and teaching assistant. Rachel would also like to recognize her parents, Alice and Stan, easily the best parents she ever had. To the Widenhoefer lab members, past and present, who offered Rachel advice and counsel throughout her years, she extends many thanks. During the dissertation writing process, Rachel conned many editors into proofreading, among them Marina Leed, Kristina Butler, Jason King and Robert Harris. Lastly, Rachel would like to show appreciation for her husband Matt. His patience, companionship, and ability to keep her computer alive were the base without which she may have never finished graduate school.

1. Computational and Experimental Studies of the Structure and Binding of Cationic Gold(I) π -Complexes of Alkenes and Alkynes

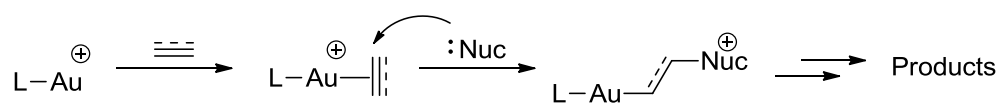
Portions of this chapter are in press in *Angewandte Chemie* and *Angewandte Chemie, International Edition*.

1.1 Introduction: gold(I) π -activation catalysis

It has been said recently that transition metals have magical powers.¹ Homogeneous transition metal catalysis has been widely adopted by the pharmaceuticals and fine chemicals communities because of the variety of selective, efficient, atom-economical methodologies the field provides for the functionalization of complex molecules.² Since the 1998 report by Teles, et al that soluble, cationic gold(I) complexes catalyze the addition of alcohols to alkynes,³ the development of homogeneous gold catalysts for organic transformations has been a broad and important area of research. Gold(I) complexes are especially efficient in effecting the addition of carbon and heteroatom nucleophiles across C-C multiple bonds (hydrofunctionalization)⁴⁻⁸ and the cycloisomerization of 1,*n*-enynes.⁹⁻¹¹ More recently, a number of enantioselective variants of these transformations have been reported that employ dinuclear gold catalysts supported by axially chiral bis(phosphine) ligands.¹²⁻¹⁴

Mechanisms involving outer-sphere attack of a nucleophile on the electrophilic π -ligand of a cationic gold(I) π -complex are typically invoked for gold(I)-catalyzed hydrofunctionalization processes (Scheme 1), but direct experimental evidence for this

mechanism is limited.^{6, 9-10, 15-17} Notably, the direct observation of the addition of a nucleophile to a gold π -complex has not been reported. Because of the similarities in the electronic properties and reactivity of gold(I), platinum(II) and mercury (II), it is not surprising that the proposed mechanisms for π -activation by these three metals closely parallel one another.^{9, 15, 18-19}



Scheme 1: Proposed mechanism π -activation by cationic gold(I).

Despite the surge in methodology development centered on π -activation by gold(I), prior to 2006 no examples of cationic gold(I) π -complexes existed in the literature. Information about the structure of these important complexes was inferred from the observed catalytic activity, computational studies of simple model systems, and structural analyses of neutral gold π -complexes.¹⁵ It was not until 2009 that a diverse collection of well characterized examples of cationic gold(I) π -complexes of alkenes and alkynes has become available. Summarized below are the computational models used to explain the nature of binding in gold(I) π -complexes as well as examples of well-characterized complexes of the form $[(\text{L})\text{Au}(\pi\text{-ligand})]^+$ [L = carbene or phosphine supporting ligand, π -ligand = alkene or alkyne].

1.2 Binding models for cationic gold(I) π -complexes

1.2.1 The Dewar-Chatt-Duncanson model for binding in transition metal π -complexes

The nature of the bond(s) formed to transition metals by π -ligands, including alkenes, alkynes, and allenes, is generally described by the Dewar-Chatt-Duncanson (DCD) model.²⁰⁻²¹ Essentially, the DCD partitions the metal- π -interaction into a σ -donation component, in which electron density is donated from the filled π -orbital on the ligand into an empty metal hybrid orbital of appropriate symmetry, and a π -backbonding component, in which electron density is donated from a filled metal d-orbital into the π^* -orbital of the ligand (Figure 1).

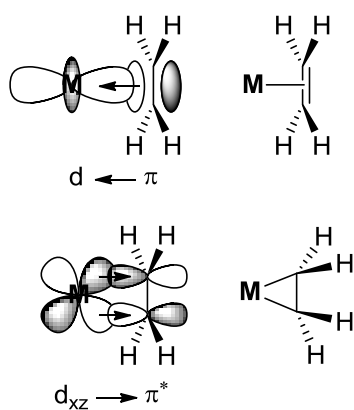


Figure 1: Orbital diagrams (left) and skeletal structures (right) depicting the two predominant binding modes described by the Dewar-Chatt-Duncanson model.

The balance between ligand to metal σ -donation (abbreviated herein as $L \rightarrow M$) and metal to ligand π -backbonding ($M \rightarrow L$) has important implications on the structure and reactivity of transition metal π -complexes. Complexes with relatively strong $L \rightarrow M$ interactions generally have low energy barriers for the rotation of the π -ligand about the

M-L bond axis, while complexes with significant contributions from $M \rightarrow L$ backbonding adopt a more metallacyclopropane-like structure and are more conformationally rigid. Both components can cause structural changes in the π -ligand, including lengthening of the C-C bond and distortion of the bound atoms from their typical geometries. Strong predomination of one component over the other also affects reactivity; net depletion of the electron density from the π -ligand through strong $L \rightarrow M$ interaction renders it electrophilic.

1.2.2 Relativistic effects on the chemistry of gold

The chemistry of gold is thought to be dominated by large relativistic effects, which are attributed to the significantly high velocity of electrons moving near a heavy nucleus with respect to the speed of light.²²⁻²⁵ For gold, these effects result in a contraction of the s- and p-orbitals to an extent unmatched in elements in which $Z < 100$.²⁶ Contracted s- and p-orbitals result in shielding of the d- and f-electrons from attractive nuclear forces and cause expansion and diffusion of the d- and f-orbitals. Consequently, gold complexes exhibit short, unusually strong bonds to soft Lewis bases such as phosphines and alkenes. Relativistic effects are also invoked to explain the stabilization of the Au-Au interaction, which is on the order of a hydrogen bond, and the strong tendency of gold to adopt linear, two-coordinate geometry.²⁷⁻²⁸

1.2.3 Theoretical studies of bonding in Au⁺-ethylene and Au⁺-acetylene complexes.

Before 2006, most of the information available regarding the structure of gold π -complexes came from computational studies on simplified systems; the most studied of these systems is the cationic gold(I)-ethylene complex Au⁺-(C₂H₄) (**1.1**). A number of computational methods have been used to determine the optimal geometry of **1.1** and the relative contributions of electrostatic (ΔE_{elstat}) and orbital (ΔE_{orb}) interactions to the binding energy (ΔE_{int}) of the complex (Table 1).²⁹⁻³³ Further, relative contributions of the L \rightarrow M and M \rightarrow L type interactions to the orbital interaction energy are computed. The first of these studies was reported in 1979 by Ziegler and Rauk and utilized the semi-empirical Hartree-Fock-Slater (HFS) transition state method.²⁹ The study concluded that electrostatic interactions contributed 65% of the 50 kcal mol⁻¹ attractive bonding energy. Of the 35% remaining that was attributed to orbital interactions, 74% of this was predicted to be from L \rightarrow M σ -donation and 20% from M \rightarrow L π -backbonding. The remaining 6% of the orbital interaction component is attributed to minimal contributions from interactions of the orbitals perpendicular to the Au-C-C plane. However, these early computations did not account for relativistic effects, resulting in a rather long computed M-C distance ($d_{\text{M-C}}$) of 2.47 Å.

In 1996, a similar study was published using hybrid density functional theory/Hartree-flock (DFT/HF) methods employing an augmented local density approximation (LDA/BP) to account for relativistic effects.³⁰ As expected, this study

predicts a shorter (2.18 Å), stronger (69.0 kcal mol⁻¹) metal alkene bond. Furthermore, the quasi-relativistic Morokuma bond decomposition analysis attributes only ~50% of the attractive bonding energy to electrostatic interactions. The remaining orbital interaction is partitioned into a ~5:1 ratio of L → M donation to M → L backbonding and is expected to result in the elongation of the C-C ethylene bond by 0.032 Å (2.4 %).

A more recent 2004 study using DFT at the BP86/TZP theory level and energy partitioning analysis (EPA) predicts an even stronger, shorter Au-olefin interaction but with about the same relative contribution of L → M and M → L donation.³¹ Although this study found the orbital interaction to contribute only 43% to the overall attractive bonding energy, the large absolute magnitude of these interactions (101.6 kcal mol⁻¹) results in lengthening of the C-C bond of ethylene by 0.081 Å (6.1%). More importantly, this study compares the calculated bond energies of **1.1** with the analogous gold acetylene complex Au⁺-(C₂H₂) (**1.2**). They found that the gold-acetylene bond is shorter but less stable by almost 10 kcal mol⁻¹. Energy decomposition analysis (EDA) shows that the relative contributions of the different interactions are about the same in **1.1** and **1.2**, but M → L backbonding is slightly more important in the alkyne complex.

Table 1: Calculated bond distances (Å) and interaction energies (kcal mol⁻¹) for Au⁺-ethylene and Au⁺-acetylene complexes.

Theory (Year)	Au ⁺ (C ₂ H ₄)			Au ⁺ (C ₂ H ₂)
	HFS (1979) ²⁹	DFT/HF (1996) ³⁰	DFT (2004) ³¹	DFT (2004) ³¹
<i>d</i> M-C	2.47	2.18	2.165	2.135
<i>d</i> C-C	---	1.371 ^a	1.414 ^b	1.250 ^c
ΔE_{int}^d	-50	-69.0	-79.1	-70.8
$\Delta E_{\text{elstat}}^e$	-57 (65%)	-73.62 (50.8%)	-134.7 (57.0%)	-134.1 (57.8%)
ΔE_{orb}^e	-31 (35%)	-71.25 (49.2%)	-101.6 (43.0%)	-97.8 (42.2%)
L→M σ -donation ^f	-23 (74%)	-54.81 (76.9%)	-68.0 (67.0%)	-63.1 (64.6%)
M→L π -backbonding ^f	-6.3 (20%)	-11.22 (15.7%)	-25.5 (25.0%)	-26.5 (27.1%)

^aCalculated *d*_{CC} for free ethylene = 1.339 Å.³⁰ ^bCalculated *d*_{CC} for free ethylene = 1.333 Å.³¹ ^cCalculated *d*_{CC} for free acetylene = 1.206 Å.³¹ ^dThe balance of the interaction energy is attributed to Pauli repulsion forces.

^ePercentages are of total attractive binding energies ($\Delta E_{\text{elstat}} + \Delta E_{\text{orb}}$). ^fPercentages are of ΔE_{orb} .

A pair of publications using natural bond orbital (NBO)³² and multiconfigurational self-consistent field (MCSCF)³³ calculations attempt to assess the importance of metal to ligand π -back bonding in **1.1** based on electron density in the olefin π^* -orbital relative to free ethylene. However, the reports are inconsistent, with the former claiming a large electron population in the π^* orbital due to strong donation from the metal cation and the later reporting a decrease in electron density in the ethylene π^* orbital relative to free ethylene. Furthermore, neither report compares the relative

magnitude of π -backbonding to σ -donation or total orbital interaction energy, so the significance of the data is difficult to assess.

1.2.4 Theoretical studies of bonding in LAu^+ -alkene and LAu^+ -alkyne complexes.

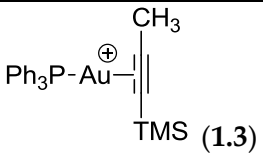
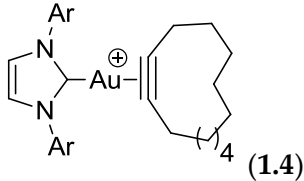
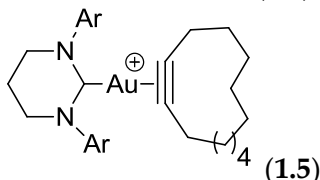
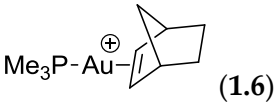
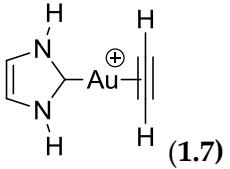
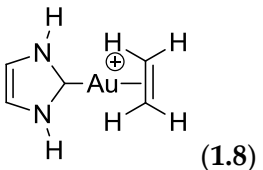
While the studies outlined above are informative to the global understanding of gold π -ligand binding, gold(I) catalysis typically employs cationic gold catalyst bearing a phosphine or carbene supporting ligand. More recently, computational studies have been carried out on more catalytically relevant model cationic gold π -complexes of the form $[\text{LAu}-(\pi\text{-ligand})]^+$ [L = phosphine or NHC supporting ligand; π -ligand = alkene or alkyne], often in conjunction with experimental characterization of similar complexes (see below). In 2008, Toste reported a DFT/NBO analysis of phosphine gold-alkyne complex **1.3** (Table 2).³⁴ Geometry optimization of **1.3** gave results described as consistent with a similar isolated dimeric complex, but commentary on the geometrical changes of the alkyne ligand upon complexation to gold were not included. NBO analysis of **1.3** revealed a L \rightarrow M interaction of 56.6 kcal mol⁻¹ and M \rightarrow L interaction of 13.3 kcal mol⁻¹, consistent in magnitude and ratio with the orbital interaction energies computed for **1.1**.³⁰

A similar study on cationic NHC-gold-cyclododecyne complexes **1.4** and **1.5** (Table 2) revealed the same ~4:1 ratio of L \rightarrow M donation and M \rightarrow L π -backbonding as was predicted for **1.3**, but the magnitudes of the total orbital interactions for the complexes were larger.³⁵ While the Au-alkyne bond in **1.4** is computed to be ~6.5 kcal

mol⁻¹ stronger than the Au-alkyne bond in **1.5**, the C≡C bond of the cyclododecyne ligand is expected to lengthen by ~0.03 Å upon complexation to either [(NHC)Au]⁺ fragment. Subsequently, Russell et al published the EPA analysis of [(Me₃P)Au(norbornene)]⁺ (**1.6**). Overall orbital interaction is predicted to be weaker in this complex than in any of the others studied, and M → L backbonding was calculated to contribute a full 25% to this bond.³⁶

In a slightly different approach, Tarantelli et al used DFT and the charge-displacement (CD) function to analyze the shift in electron density upon complexation of acetylene (**1.7**) or ethylene (**1.8**) to a simplified NHC-Au⁺ fragment.³⁷ The BDE for the gold-(π-ligand) bond was found to be 36.9 kcal mol⁻¹ in **1.7** and 38.8 kcal mol⁻¹ in **1.8**. For **1.7**, metal to ligand π-backbonding contributed ~34% to the overall orbital interactions with the remaining 66% from ligand to metal σ-donation, causing a 12° bend in the C–C–H bond-angle of the acetylene ligand. For **1.8**, π back-donation was calculated to contribute 45% to the total orbital interaction energy.

Table 2: Calculated bond lengths (Å) and energies (kcal mol⁻¹) for [(L)Au(alkyne)]⁺ and [(L)Au(alkene)]⁺ complexes.

	<i>d</i> C-C	<i>d</i> M-C	BDE	L → M	M → L
 (1.3)	1.258	2.249, 2.386	--	56.6 (81.0%)	13.3 (19.0%)
 (1.4)	1.246 ^a	--	39.60	77.4 (79.6%)	19.8 (20.4%)
 (1.5)	1.247 ^a	--	33.08	69.7 (77.4%)	20.3 (22.6%)
 (1.6)	--	--	--	45.2 (75%)	15 (25%)
 (1.7)	1.23 ^b	2.17	36.9	(66%)	(34%)
 (1.8)	1.37 ^c	2.20	38.8	(55%)	(45%)

^aCalculated *d*_{C-C} for free cyclododecyne = 1.216 Å. ^bCalculated *d*_{C-C} for free acetylene = 1.21. ^cCalculated *d*_{C-C} for free ethylene = 1.33 Å.

1.3 Experimental determination of structure and solution behavior in gold(I) π-complexes of alkenes and alkynes

1.3.1 Introduction

The first examples of isolated cationic, monomeric gold π-complexes of the form [(L)Au(π-ligand)] were reported in 2006 by Echavarren and coworkers. Four gold(I) π-

arene complexes bearing bulky phosphine ligands of the form $[(PR_{2o}\text{-biphenyl})Au(\text{arene})]^+$ [$R = t\text{-Bu}$, arene = *p*-xylene (**1.9**), toluene; $R = \text{cyclohexyl}$, arene = *p*-xylene, toluene (**1.10**)] were synthesized by ligand exchange in and crystallization from the corresponding aromatic solvent for characterization in the solid state (Figure 2).³⁸ Xylene complexes exhibited η^2 -arene interactions, while toluene complexes exhibited an Au- η^1 -C3 bond. Fluxionality of the weakly bound π -arene ligands precluded meaningful spectroscopic analysis of the complexes in solution.

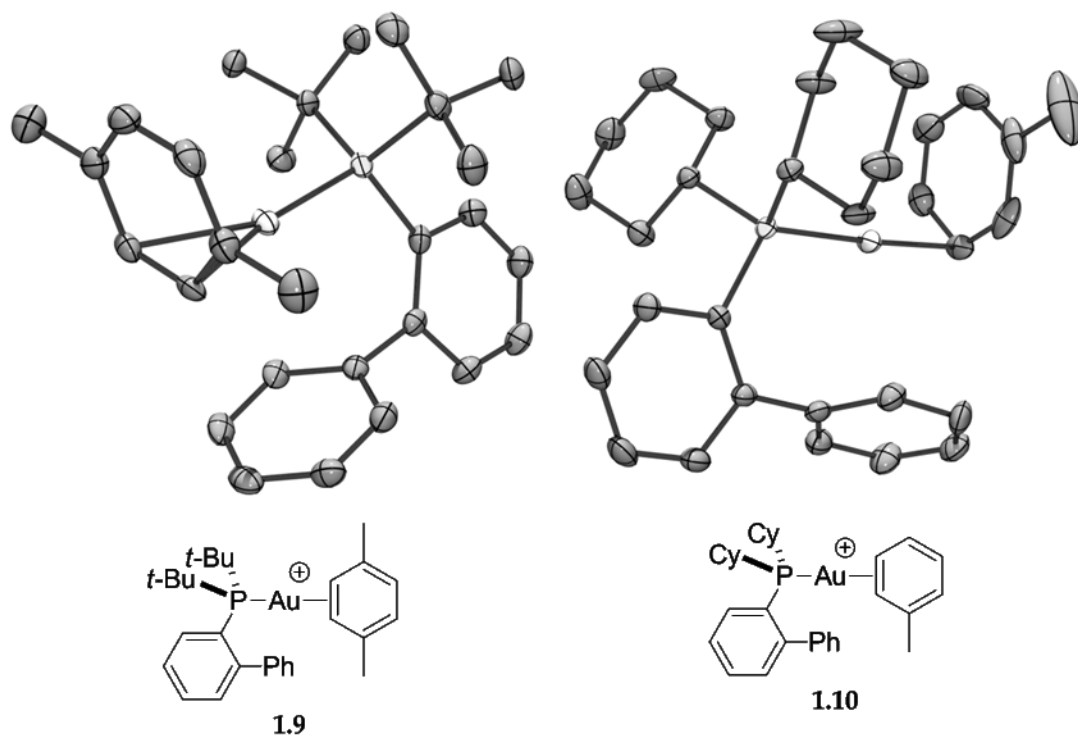


Figure 2: ORTEP diagrams and skeletal structures of phosphine gold(I) η^1 - and η^2 -arene π -complexes **1.9** and **1.10**. Hydrogen atoms and counterions have been removed for clarity.

Shortly thereafter, Sadighi reported isolation and solution characterization of the stable gold(I) π -alkyne complex $[(\text{SIPr})Au(\eta^2\text{-EtC}\equiv\text{CEt})]^+ \text{BF}_4^-$ [$\text{SIPr} = 1,3\text{-bis}(2,6\text{-}$

diisopropylphenyl)imidazolin-2-ylidene] (**1.11**).³⁹ Since then, a diverse collection of gold(I) π -complexes has been reported, including complexes of alkenes, alkynes, arenes, allenes, dienes, enol ethers, and enamines with a number of different supporting ligands. Highlighted below are examples of monomeric, cationic, two-coordinate gold(I) π -complexes of alkenes and alkynes of the form $[(L)Au(\pi\text{-ligand})]^+$ with either an N-heterocyclic carbene (NHC) or a bulky phosphine supporting ligand. Examples of gold(I) π -diene complexes and gold(I) π -complexes bearing either a chiral (bis)phosphine or triarylphosphine supporting ligand are considered in detail in chapters 2, 3, and 4, respectively.

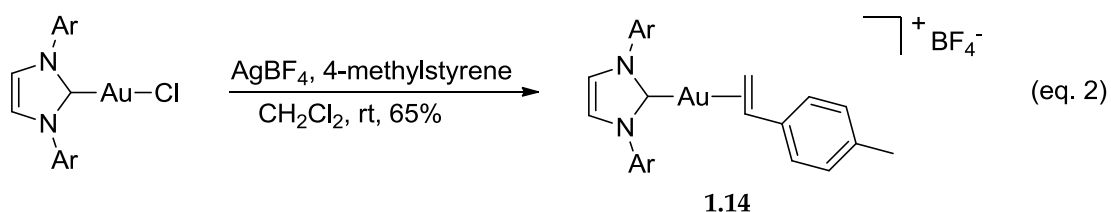
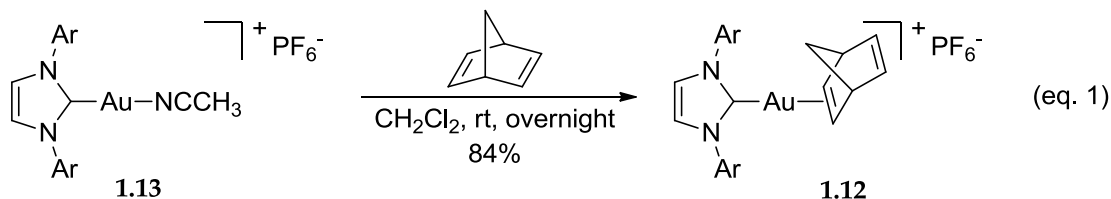
1.3.2 Synthesis, structural characterizations, and solution behavior of cationic gold(I) π -alkene complexes

1.3.2.1 Complexes bearing NHC supporting ligands

In 2009, Nolan reported the synthesis of the complex $[(IPr)Au(\eta^2\text{-norbornadiene})]^+ PF_6^-$ [$IPr = 1,3\text{-bis}(\text{diisopropylphenyl})\text{imidazol-2-ylidene}$] (**1.12**) by displacement of acetonitrile from the common gold precatalyst $[(IPr)AuNCCH_3]^+ PF_6^-$ (**1.13**) (Scheme 2, eq. 1).⁴⁰ In the same year, Macchioni reported the synthesis and isolation of $[(IPr)Au(\eta^2\text{-4-methylstyrene})]^+ BF_4^-$ (**1.14**) through halide abstraction from $(IPr)AuCl$ with $AgBF_4$ in the presence of 4-methylstyrene.⁴¹ Subsequently, Widenhoefer and co-workers reported use of a similar procedure to synthesize a diverse family of NHC-gold-alkene complexes of the form $[(IPr)Au(\eta^2\text{-alkene})]^+ SbF_6^-$ [alkene =

isobutylene (**1.15**), norbornene (**1.16**), 2-methyl-2-butene (**1.17**), 2,3-dimethyl-2-butene (**1.18**), methylene cyclohexane, *cis*-2-butene, 1-hexene, and 4-methylstyrene] (Table 3).⁴²

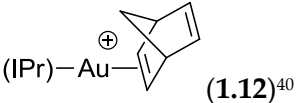
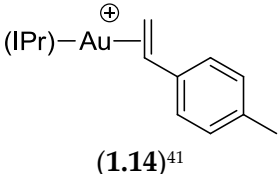
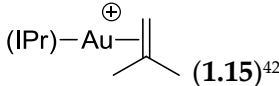
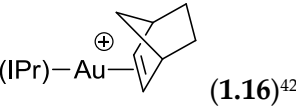
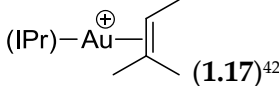
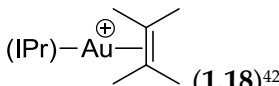
Scheme 2: Synthesis of select [(IPr)Au(η^2 -alkene)]⁺ complexes. Ar = 2,6-diisopropylphenyl



Because of its sensitivity to the electronic environment of atoms, ¹³C NMR spectroscopy was used to confirm binding of the cationic [(IPr)Au]⁺ fragment to alkenes in solution (Table 3). For complexes **1.12**, **1.16** and **1.18** with symmetrically-substituted alkenes, the alkenyl ¹³C resonances were shifted upfield relative to the free alkene. Complexes of an aliphatic terminal olefin (**1.15**) or unsymmetrically substituted internal olefin (**1.17**) displayed the same upfield shift of the resonance corresponding to the less-substituted alkene terminus and a downfield shift of the resonance corresponding to the more-substituted alkene terminus. This pattern points to slippage of gold toward the less-substituted terminus of the alkene with depletion of electron density from the more substituted terminus; the magnitude of this slippage increases with increased differentiation of the two alkene termini. Interestingly, 4-methylstyrene complex **1.14**

displays a very large upfield shift of the terminal carbon resonance ($\Delta\delta = 28.4$ ppm) and a smaller upfield shift of the internal alkene resonance relative to free alkene, indicating either less slippage of gold toward the unsubstituted alkene carbon or reduced donation of electron density from the more substituted terminus. ^1H NMR resonances corresponding to the vinyl protons of bound alkenes were all shifted upfield regardless of substitution patterns, albeit to different degrees ($\Delta\delta = -0.05 - -0.77$ ppm).

Table 3: Relevant ^{13}C and ^1H NMR data for $[(\text{IPr})\text{Au}(\pi\text{-alkene})]^+$ complexes in CDCl_3 . Displacement from free alkene ($\Delta\delta$) is shown parenthetically (ppm).^a

Alkene Complex	$\text{H}_2\text{C}=\text{C}$	$\text{R}_2\text{C}=\text{C}$	$\text{R}(\text{H})\text{C}=\text{C}$	$\text{H}_2\text{C}=\text{C}$	$\text{R}(\text{H})\text{C}=\text{C}$
 (1.12) ⁴⁰			δ 134.4 ^b (-8.8)		δ 6.52 ^b (-0.33)
 (1.14) ⁴¹	δ 84.7 ^c (-28.4)		δ 129.4 ^c (-9.0)	δ 5.01, 4.90 ^c (-0.77, -0.52)	δ 6.56 ^c (-0.18)
 (1.15) ⁴²	δ 88.2 (-22.3)	δ 155.2 (13.0)		δ 4.38 (-0.22)	
 (1.16) ⁴²			123.5 (-11.7)		5.71 (-0.24)
 (1.17) ⁴²		δ 137.2 (5.2)	δ 105.3 (-12.7)		δ 5.07 (-0.05)
 (1.18) ⁴²		δ 122.1 (-1.6)			

^aNegative values indicate upfield shifts, positive values indicate downfield shifts. ^bResonances broad.

^cSpectra recorded in CD_2Cl_2 .

Analysis of the isotopomer **1.15**- $^{13}\text{C}_1$ showed only a minor diminution of the $^1J_{\text{C}=\text{C}}$ coupling constant of the isobutylene ligand relative to free isobutylene. This points to minimal deviation of the bound isobutylene from sp^2 hybridization and, hence, nominal contribution of π -backbonding to the gold–alkene bond. Multinuclear, two-dimensional NMR studies into the interionic structure of **1.14** reveal that the tetrafluoroborate counterion is positioned predominantly (65-83% occupancy) near the IPr imidazole ring, suggesting minimal charge transfer from the π -ligand to the cationic gold moiety.⁴¹

Complexes **1.15**, **1.16** and **1.18** were also analyzed in the solid state (Figure 3).⁴² All complexes display η^2 -coordination and adopt distorted linear, two-coordinate geometries about the central gold atom [$\text{C}(\text{carbene})\text{--Au--C}=\text{C}(\text{centroid}) = 172\text{--}177^\circ$] with no significant elongation of the coordinated $\text{C}=\text{C}$ bond relative to free alkene. The $\text{Au--C}=\text{C}(\text{centroid})$ distances ranged from 2.128 Å in **1.16** to 2.141 Å in **1.15**. Consistent with the ^{13}C NMR spectroscopy, the gold π -isobutylene complex **1.15** displayed significant slippage of gold toward the less substituted alkene terminus, binding through a shorter Au--CH_2 and a longer Au--CMe_2 bond ($\Delta d = 0.086$ Å). In comparison, the Au--C bonds of complex **1.16** differed by only 0.024 Å, and those of complex **1.18** differed by less than 0.01 Å. Complex **1.12** was not characterized in the solid-state as it decomposed via P–F bond cleavage to form $[(\text{IPrAu})_2(\mu\text{-PF}_4)]^+ \text{PF}_4^-$ upon attempted crystallization.⁴⁰

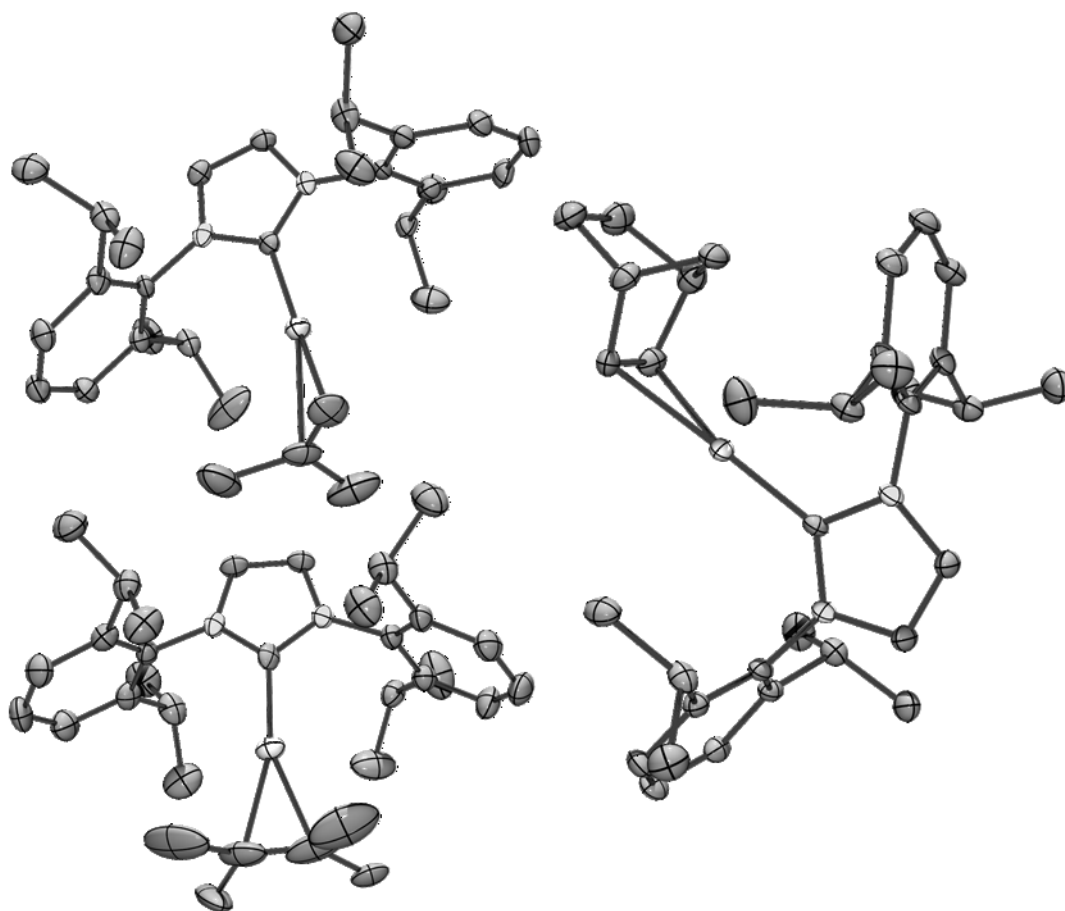


Figure 3: ORTEP diagrams of [(IPr)Au(η²-alkene)]⁺ complexes **1.15 (top left), **1.16** (right), and **1.18** (bottom left). Hydrogen atoms and counterions have been removed for clarity.**

To better understand the structure and reactivity of the gold π -alkene complexes, a number of studies on the solution behavior of the complexes were performed. Kinetic analysis of intermolecular isobutylene exchange with **1.15** established an [isobutylene] dependent pathway for exchange with an energy barrier of $\Delta G^{\ddagger}_{318\text{K}} = 16 \text{ kcal mol}^{-1}$ arising from a modest enthalpy of activation ($\Delta H^{\ddagger} = 8 \text{ kcal mol}^{-1}$) and large negative entropy of activation ($\Delta S^{\ddagger} = -27 \text{ eu}$). These data are consistent with an associative pathway for

isobutylene exchange involving the unobserved, 16-electron, bis(alkene) intermediate $[(\text{IPr})\text{Au}(\eta^2\text{-H}_2\text{C}=\text{CMe}_2)_2]^+ \text{SbF}_6^-$.

Toward further evaluating the σ -donation/ π -backbonding nature of the gold-alkene bond,⁴³⁻⁴⁵ Widenhoefer and Brown determined the relative binding affinities of *p*-substituted vinyl arenes to the 12 electron gold fragment $[(\text{IPr})\text{Au}]^+$ by measuring the equilibrium displacement of 3,5-bis(trifluoromethyl)benzotrile (NC_{ArF}) from $[(\text{IPr})\text{Au}(\text{NC}_{\text{ArF}})]^+ \text{SbF}_6^-$.⁴² A plot of $\log K_{\text{eq}}$ versus the Hammett σ -parameter produced a reaction constant of $\rho = -2.4 \pm 0.2$, which is significantly more negative than those obtained for related late transition metal complexes (Ag⁺: $\rho = -0.77$,⁴³ Pt(II): $\rho = -1.32$,⁴⁴ Pd(II): $\rho \approx -1.39$ ⁴⁵). These observations indicate that the bonding interaction for cationic gold alkene complexes is biased toward σ -donation and away from π -backbonding to an extent unprecedented for late transition metal π -alkene complexes.

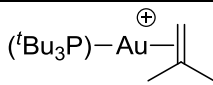
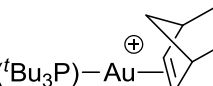
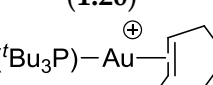
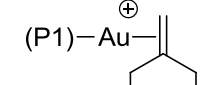
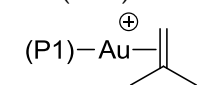
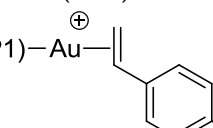
1.3.2.2 Complexes bearing bulky phosphine supporting ligands

Concurrent with Widenhoefer's report of IPr gold π -alkene complexes, and in conjunction with the DFT study of complex **1.6** (section 1.2.4), Green and Russell reported the synthesis of gold complexes of the form $[(\text{P}^t\text{Bu}_3)\text{Au}(\pi\text{-alkene})]^+ \text{SbF}_6^-$ [alkene = isobutylene (**1.19**), norbornene (**1.20**), *trans*-cyclooctene (**1.21**), and norbornadiene] (Table 4).³⁶ Subsequently, Widenhoefer and Brown reported the isolation of eleven compounds of the form $[(\text{P}1)\text{Au}(\pi\text{-alkene})]^+ \text{SbF}_6^-$ [alkene = methylenecyclohexane (**1.22**), isobutylene (**1.23**), 4-methylstyrene (**1.24**),

cis-2-butene, 1-hexene, 2,3-dimethyl-2-butene, *trans*-2-butene, 2-methyl-2-butene, styrene, 4-bromostyrene, and 4-trifluoromethylstyrene; P1 = P(*t*-Bu)₂o-biphenyl].⁴⁶

Complexes **1.19** - **1.24** displayed similar patterns and magnitudes of chemical shifts as were observed for the corresponding alkene complexes bearing the NHC ligands (Table 4). Unlike the NHC complexes, vinyl proton resonances corresponding to alkenes complexed to [(*t*Bu₃P)Au]⁺ (**1.19** – **1.21**) were universally shifted downfield relative to free alkene ($\Delta\delta = 0.54 - 0.65$), while [(P1)Au(π -alkene)]⁺ complexes (**1.22** – **1.24**) displayed an upfield shift of the vinyl protons corresponding to the less substituted alkene terminus and a downfield shift of those corresponding to the more-substituted terminus.

Table 4: Relevant ^{13}C , ^1H , and ^{31}P NMR data for [(phosphine)Au(π -alkene)]⁺ complexes in CDCl_3 . Displacement from free alkene is shown parenthetically (ppm).^a

Complex	$\text{H}_2\text{C}=\text{C}$	$\text{R}_2\text{C}=\text{C}$	$\text{R}(\text{H})\text{C}=\text{C}$	$\text{H}_2\text{C}=\text{C}$	$\text{R}(\text{H})\text{C}=\text{C}$	^{31}P
 (1.19) ³⁶	δ 96.2 (-14.3)	δ 162.1 (19.7)		δ 5.19 (0.59)		δ 100.4
 (1.20) ³⁶			δ 132.3 (-2.9)		δ 6.60 (0.65)	δ 98.1
 (1.21) ³⁶			δ 130.6 (-3.3)		δ 6.04 (0.54)	δ 99.1
 (1.22) ^{b,42}	δ 91.8 (-14.6)	δ 169.4 (19.4)		δ 3.93 (-0.62)		δ 64.7
 (1.23) ^{b,42}	δ 95.1 (-15.4)	δ 163.3 (20.9)		δ 3.92 (-0.68)		δ 64.9
 (1.24) ⁴²	δ 89.5 (-23.2)		δ 135.5 (-1.2)	δ 4.75, 4.32 (-0.41, -0.38)	δ 6.82 (0.17)	δ 67.0

^aNegative values reflect upfield shifts, positive values reflect downfield shifts. ^bSpectra recorded in CD_2Cl_2 .

Complexes **1.19**, **1.20**, **1.22** and **1.24** were further characterized by X-ray crystallography (Figure 4). Like their NHC analogues, these complexes adopted distorted linear, two-coordinate geometries with minimal elongation of the η^2 -bound alkene. The phosphine complexes displayed slightly longer Au-C=C(centroid) distances ranging from 2.155 Å (**1.24**) to 2.186 Å (**1.19** and **1.20**). As compared to IPr gold complex **1.15**, solid-state analysis of the 1,1-disubstituted alkene complexes **1.19** and **1.22** revealed

more pronounced slippage of the alkene ligand toward the unsubstituted terminus [Δd Au–C1/Au–C2 = 0.126 (**1.19**) and 0.155 Å (**1.22**)]. Also evident from X-ray structural analysis was the pronounced steric influence of the protruding phenyl ring of the P1 ligand, which was manifested in the more significant deviation from linearity [P–Au–C=C(centroid) = 161–165 °] relative to both the P^tBu₃ and IPr complexes.

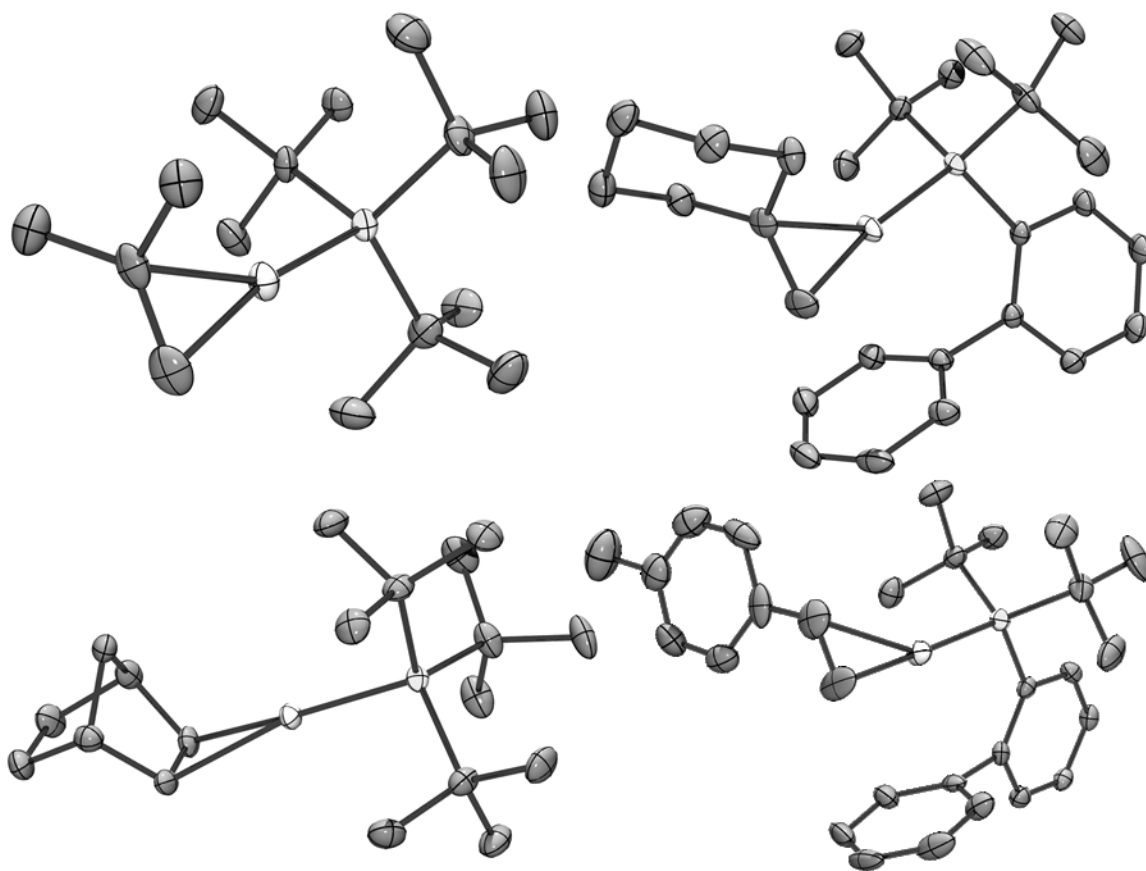


Figure 4: ORTEP diagrams of [(phosphine)Au(η^2 -alkene)]⁺ complexes **1.19 (top left), **1.20** (bottom left), **1.22** (top right) and **1.24** (bottom right). Hydrogen atoms and counterions have been removed for clarity.**

Kinetic analysis of intermolecular isobutylene exchange with **1.23** established the presence of an [isobutylene] dependent pathway with activation parameters ($\Delta H^\ddagger = 5$

kcal/mol, $\Delta S^\ddagger = -33$ eu) similar to those of IPr complex **1.15**. Hammett analysis of the binding affinities of substituted vinyl arenes to the 12 electron gold fragment (P1)Au⁺ produced a reaction constant of $\rho = -3.4$, which significantly exceeded that determined for the binding of vinyl arenes to (IPr)Au⁺. This observation points to the greater electrophilicity of a gold fragment bearing an alkyl phosphine ligand relative to the corresponding gold fragments bearing and NHC ligand.

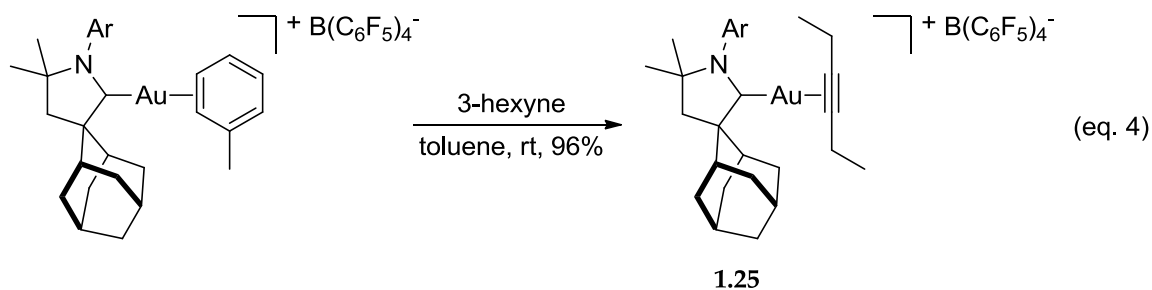
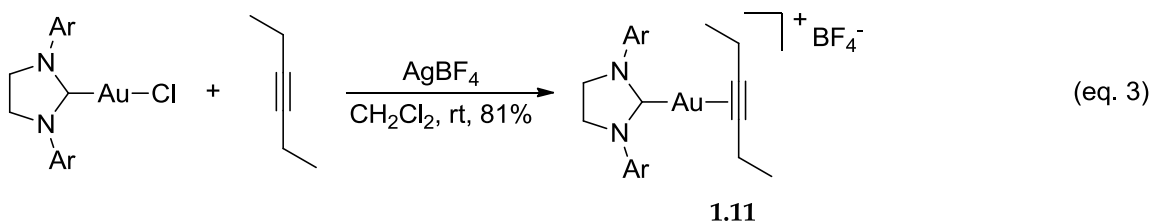
1.3.3 Synthesis, structural characterizations, and solution behavior of cationic gold(I) π -alkyne complexes

1.3.3.1 Internal alkyne complexes bearing NHC supporting ligands

In 2007, Sadighi reported the isolation of the cationic gold alkyne complex [(SIPr)Au(η^2 -EtC \equiv CEt)]⁺ BF₄⁻ (**1.11**) via chloride abstraction from (SIPr)AuCl with AgBF₄ in the presence of 3-hexyne (Scheme 3, eq. 3).³⁹ The following year, Bertrand reported the synthesis of the analogous cyclic alkyl amino carbene complex (CAAC)Au(η^2 -EtC \equiv CEt)]⁺ B(C₆F₅)₄⁻ (**1.25**) via ligand displacement from the corresponding π -toluene complex with 3-hexyne (Scheme 3, eq. 4).⁴⁷ These early successes sparked a number of studies of internal alkyne complexes of the form [(L)Au(π -alkyne)]⁺ in the following years. Along with an aforementioned DFT study, Furstner et. al. reported the generation and *in situ* and solid-state characterization of [(NHC)Au(η^2 -cyclododecyne)]⁺ SbF₆⁻ [NHC = IPr (**1.4**), 1,3-Bis(2,6-diisopropylphenyl)hexahydropyrimidin-2-ylidene (**1.5**)].³⁵ Subsequently, the syntheses and study of stable complexes [(IPr)Au(η^2 -MeC \equiv CPr)]⁺ BF₄⁻ (**1.26**)⁴⁸ and [(IPr)Au(π -alkyne)]⁺ SbF₆⁻ [alkyne = 3-hexyne (**1.27**), 1-phenylpropyne (**1.28**)] were

reported.⁴⁹ Dias has recently reported the synthesis and solid-state structure of the cyclooctyne complex $[(\text{SIPr})\text{Au}(\eta^2\text{-cyclooctyne})]^+ \text{SbF}_6^-$ (**1.29**), which, in contrast to **1.4** and **1.5**, was thermally stable in solution.⁵⁰

Scheme 3: Synthesis of select $[(\text{IPr})\text{Au}(\eta^2\text{-alkyne})]^+$ complexes. Ar = 2,6-diisopropylphenyl



Unlike the complexes of symmetrically substituted alkenes, for 3-hexyne complexes **1.11**, **1.25**, and **1.27**, the alkyne carbon resonances were shifted downfield by ~ 6.5 ppm relative to free alkyne in the ^{13}C NMR spectra. Similarly, the C2 and C3 alkyne carbons in 2-hexyne **1.26** were shifted downfield by 6.8 and 6.6 ppm, respectively, suggesting that the methyl and propyl substituents are not sterically or electronically different enough to cause slippage of gold toward one alkyne terminus. For the cycloalkyne complexes, the greater donicity of the IPr ligand of **1.4** relative to the NHC ligands of **1.5** and **1.29** was reflected in the greater shielding of the alkyne carbon

resonances of **1.4** ($\Delta\delta = 6.3$ ppm) as compared to those of **1.5** ($\Delta\delta = 4.9$ ppm) and **1.29** ($\Delta\delta = 2.5$ ppm) in the ^{13}C NMR spectra.

Studies by Macchioni et al on 2-hexyne complex **1.26** suggest that the solution structure and behavior of gold(I) π -alkyne complexes are similar to analogous alkene complexes. Kinetic analysis of the intermolecular exchange of 2-hexyne with **1.26** established the presence of a [2-hexyne] dependent pathway with an energy barrier of $\Delta G^{\ddagger}_{298\text{K}} = 15.5$ kcal/mol, and interionic analysis suggests that the BF_4^- counterion locates proximal to the NHC ligand.⁵¹

Of the complexes discussed herein, only the cycloalkyne complexes **1.4**, **1.5** and **1.29** have been characterized in the solid state (Figure 5). The Au-C \equiv C(centroid) distances of 2.115 Å (**1.29**) and 2.14 Å (**1.4** and **1.5**) are in the same range as [(NHC)Au(π -alkene)]⁺ complexes. The C \equiv C bond of IPr complex **1.4** is lengthened slightly ($\Delta d = 0.01$ Å) and the C \equiv C-C angle (168 °) is diminished slightly relative to free cyclododecyne (176 °). Despite the significant differences in the NMR spectra of **1.4** and **1.5**, the C-C bond length of **5** was not significantly different from that of **4** and the compressed C \equiv C-C of **5** (160 °) was attributed to steric rather than electronic effects.

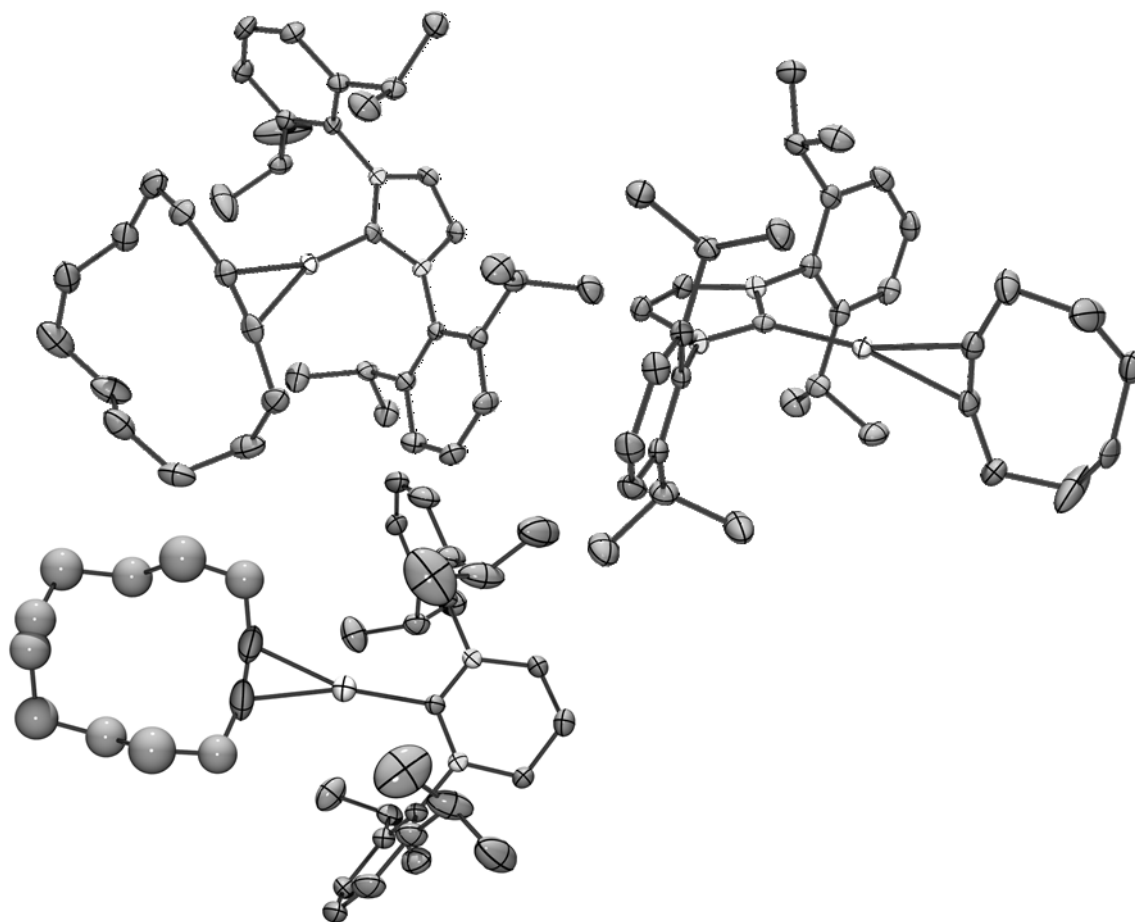


Figure 5: ORTEP diagrams of [(NHC)Au(η^2 -alkyne)]⁺ complexes 1.4 (top left), 1.5 (bottom left), and 1.29 (right). Hydrogen atoms and counterions have been removed for clarity.

1.3.3.2. Complexes bearing a hindered alkyl phosphine ligand

As compared to the NHC complexes discussed above, fewer examples of alkyne complexes bearing hindered alkyl phosphine ligands have been reported. In 2010, Green and Russell reported the synthesis and solid state characterization of the gold π -alkyne complexes [(P^tBu₃)Au(RC≡CCMe₃)]⁺ SbF₆⁻ [R = Me (**1.30**), SiMe₃ (**1.31**)].⁵² Widenhoefer and Brown subsequently reported the synthesis and solution behavior of a family of

gold π -alkyne complexes of the form $[(P1)Au(R^1C\equiv CR^2)]^+ SbF_6^-$ [$R^1 = R^2 = Et$ (**1.32**); $R^1 = Me, R^2 = tBu$ (**1.33**), Ph, Me, nPr].⁴⁹ Recently, Macchioni reported the synthesis of the 3-hexyne complexes $[(L)Au(EtC\equiv CEt)]^+ BF_4^-$ [$L = P1$ (**1.34**), P^tBu_3 (**1.35**)] in conjunction with a combined NMR/DFT study of this and previously known gold(I) π -alkyne complexes.⁵³

Complex **1.32** and related linear alkynes displayed downfield shifts of the bound alkyne ~ 4 ppm greater than the corresponding IPr complexes ($\Delta\delta$ 10-11 ppm) in the ^{13}C NMR spectrum, suggesting more charge transfer from the alkyne ligand to the $[(P1)Au]^+$ fragment relative to the less electron deficient $[(NHC)Au]^+$ fragment. Complexes **1.30**, and **1.33**, bearing the bulky tBu substituted alkyne, displayed larger downfield shifts of both sp carbons of the bound alkyne relative to free alkyne ($\Delta\delta$ 12-15 ppm), despite the significant steric and electronic differences between the two alkyne termini and the enhanced donicity of the trialkylphosphine supporting ligand relative to P1. Unlike complexes of the alkyl-substituted alkynes, the ^{13}C spectrum of complex **1.31** did suggest asymmetric binding of gold to the trimethylsilyl substituted ligand with significant slippage of gold toward the $CSiMe_3$ terminus ($\Delta\delta = 8$ ppm) and away from the $CCMe_3$ terminus ($\Delta\delta = 17$ ppm).

While no formal Hammett analysis of binding in gold(I) π -internal-alkyne complexes has been reported, Widenhoefer et al. did measure the equilibrium binding affinity of several alkynes to $[(L)Au]^+$ ($L = IPr, P1$) relative to $NCAr_F$.⁴⁹ In general, the more electron rich aliphatic alkynes bound more strongly to gold than those bearing

aromatic substituents. Equilibrium displacement of NCAR_F from both the NHC complex and the phosphine complex by butyne was essentially equivalent, but 1-phenyl-1-propyne displayed significantly lower affinity for $[(\text{P1})\text{Au}]^+$ relative to $[(\text{IPr})\text{Au}]^+$. Macchioni analysed the anion/cation structure of the 3-hexyne complexes **1.34** and **1.35** by $^{19}\text{F},^1\text{H}$ HOESY NMR and found the counterion positioned primarily near the alkyne ligand.⁵³

X-ray crystal structures are reported for complexes **1.30** and **1.31**, but orientational disorder in **1.31** precluded meaningful structural analysis (Figure 6). The X-ray structure of **1.30** revealed symmetrical, η^2 -coordination of the 4,4-dimethylpent-2-yne ligand to gold with an $\text{Au}-\text{C}\equiv\text{C}(\text{centroid})$ distance of 2.153 Å and a $\text{P}-\text{Au}-\text{C}\equiv\text{C}(\text{centroid})$ angle of 175.73°. No significant lengthening of the $\text{C}\equiv\text{C}$ bond relative to free 4,4-dimethylpent-2-yne was observed, although the alkyne substituents were bent away from the $(\text{P}^t\text{Bu}_3)\text{Au}$ moiety ($\text{C}\equiv\text{C}-\text{C} = 165\text{-}168^\circ$).

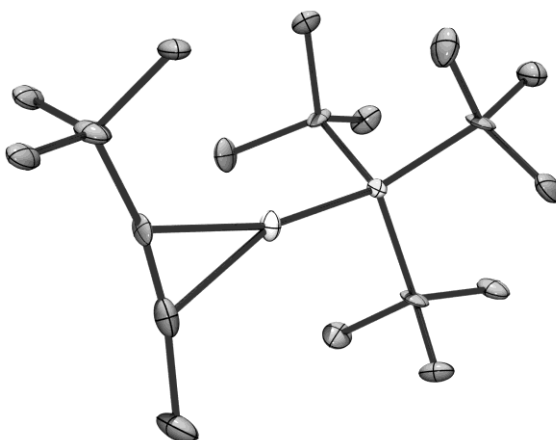


Figure 6: ORTEP diagram of $[(^t\text{Bu}_3\text{P})\text{Au}(\eta^2\text{-alkyne})]^+$ (**1.30**). Hydrogen atoms and counterion have been removed for clarity.

1.4 Summary and discussion

Computational and experimental studies conclude that cationic gold(I) favorably forms π -complexes with alkenes and alkynes and that attractive orbital interactions are dominated by $L \rightarrow M$ σ -donation. Beyond these conclusions, ambiguity remains regarding the nature of binding in gold(I) π -complexes.

Computational studies of **1.1** and **1.2** predict that 35-50% of the attractive forces in the metal-(π -ligand) bond come from favorable orbital overlap between the two components as described by the DCD-model. The magnitude of this stabilization differs by study, as does the relative contribution of $M \rightarrow L$ π -backbonding, which is predicted to account for 15-27% of stabilization gained by orbital interactions. A direct comparison of ethylene and acetylene binding show the alkene complex **1.1** to be ~ 10 kcal mol⁻¹ more stable than alkyne complex **1.2**. Because of the variety of complexes studied, general trends are more difficult to reduce from computational studies of [(L)Au(π -ligand)]⁺ complexes **1.3** – **1.8**. The electrostatic component of the gold- π -ligand interaction is largely ignored in these studies, and the predicted relative contribution of $M \rightarrow L$ π -backbonding ranges from $\sim 20\%$ in NBO/EDA experiments to 45% in CD studies.

While very little comparable experimental data exists regarding the energetics of binding in gold(I) π -complexes, computational and experimental results can easily be compared on the basis of geometry. All but the earliest theoretical works predict an Au-(π -ligand) bond length of 2.1 – 2.2 Å. Isolated π -complexes exhibit Au-alkene and Au-

alkyne distances within this computationally predicted range, with the [(NHC)Au]⁺ complexes generally exhibiting closer Au-(π -ligand) interactions than the corresponding bulky phosphine ligands. However, DFT calculations also predict a 0.02 – 0.08 Å elongation of a C–C π -bond upon complexation to gold, and this effect is almost completely absent in the structurally characterized complexes. The lack of elongation and distortion of alkenes and alkynes in π -complexes has been used to partially support claims that M \rightarrow L backbonding contributes minimally to binding in gold(I) π -complexes, but the implications of these observations on the importance of L \rightarrow M σ -donation remains unexplained.

Perhaps the most important conclusion that can be drawn from the experimental data regarding cationic gold(I) π -complexes is the sensitivity of this interaction to changes in substitution on the π -ligand. The strength of the bond between [(L)Au]⁺ and a π -system depends more on the steric and electronic effects of substitution on the π -system than the identity of the π -system itself (alkene vs. alkyne, etc.). Furthermore, the degree of $\eta^2 \rightarrow \eta^1$ slippage in these complexes is highly sensitive to steric and electronic differentiation between the two carbon termini of the π -ligand, especially in [(L)Au(alkene)]⁺ complexes.

Together, the computational and experimental data described above have been used to explain the high efficiency with which cationic gold(I) catalyzes hydrofunctionalization of C–C π -bonds. However, with the exception of the

intermolecular ligand exchange discussed herein and the corresponding intramolecular process in complexes of allenes and dienes, little is known about the reactivity of these complexes. Addition of a nucleophile to a gold(I) π -complex has not been directly observed, although this mechanism is almost universally proposed. Despite the great advances in only the last few years, much remains to be learned about the structure and reactivity of gold(I) π -complexes and their role in π -activation catalysis.

2. Syntheses, X-ray Crystal Structures, and Solution Behavior of Cationic, Two-Coordinate Gold(I) η^2 -Diene Complexes

Portions of this chapter have been published: Brooner, R. E. M.; Widenhoefer, R. A. *Organometallics*, **2011**, *30*, 3182. X-ray crystal structures were solved and refined by Dr. Paul D. Boyle at North Carolina State University.

2.1 Introduction

2.1.1 Gold(I) catalyzed hydrofunctionalization of dienes

Included in the body of gold(I)-catalyzed hydrofunctionalizations developed in recent years are a number of methods for the addition of a weakly basic, neutral nucleophile across a conjugated diene. Specifically, cationic gold(I) complexes catalyze the intermolecular 1,2-addition of the X–H bond of sulfonamides,⁵⁴⁻⁵⁵ carbamates,⁵⁴ thiols,⁵⁶ or indoles⁵⁷ to the less substituted C=C bond of a conjugated diene and the intramolecular 1,4-addition of the N–H bond of a sulfonamide across a tethered 1,3-cyclohexadiene moiety.⁵⁸ The selective 1,2-addition of the nucleophile across the less substituted C=C bond in the gold(I)-catalyzed intermolecular hydrofunctionalization of conjugated dienes distinguishes these transformations from other transition metal-catalyzed diene hydrofunctionalization processes, which typically occur with net 1,4-addition⁵⁹⁻⁶⁰ and/or telomerization.⁶⁰⁻⁶¹

Gold(I)-catalyzed diene hydrofunctionalization has been proposed to occur via initial π -coordination of the diene to gold, either through the less substituted C=C bond

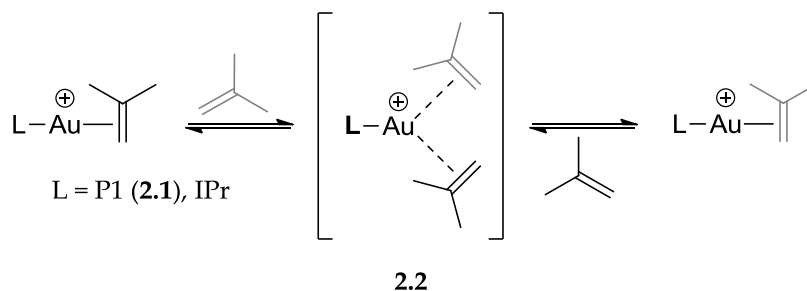
(η^2 -complexation)⁵⁵⁻⁵⁸ or to both C=C bonds (η^4 -complexation),⁵⁴ followed by outer-sphere addition of the nucleophile and subsequent protodeauration. An outer-sphere pathway involving attack of the nucleophile on a gold η^2 -diene intermediate was further supported by computational analysis of the gold(I)-catalyzed intramolecular hydroamination of 3-methyl-1,3-pentadiene with benzyl carbamate.⁶² Despite the potential role of cationic gold(I) π -diene complexes in the gold(I)-catalyzed hydrofunctionalization of conjugated dienes, prior to 2011, no well-characterized gold π -diene complexes had been documented. Formation of a gold(I) π -diene complex from a mixture of (PPh₃)AuCl, AgOTf, 3-methyl-1,3-pentadiene, and benzyl carbamate was proposed on the basis of *in situ* ³¹P and ¹³C NMR analysis; however, neither isolation nor full characterization of the purported gold(I) π -diene complex was reported.⁵⁴ As such, information regarding the structure, bonding, and fluxional behavior of cationic gold(I) π -diene complexes was limited to that provided by computational analysis⁵⁹ or that gleaned from related gold π -alkene or allene complexes or transition metal 1,3-diene complexes.

2.1.2 Coordination behavior in gold(I) π -alkene complexes

It is well documented that gold(I) forms stable, two-coordinate, monomeric, cationic π -complexes with mono-olefins of the form [(L)Au(η^2 -alkene)]⁺ X⁻ [L = NHC or hindered alkyl phosphine, X⁻ = weakly coordinating counterion such as SbF₆⁻ or BF₄⁻].^{36, 40-42, 46, 51, 63} While no 1,3-diene complexes were included in these pioneering experiments,

several interesting questions about the nature of gold(I) π -diene complexes arise from the observations therein. For example, kinetic analysis of intermolecular ligand exchange of isobutylene with $[(L)Au(\eta^2\text{-isobutylene})]^+ SbF_6^-$ [$L = P1$ (**2.1**), IPr] suggests that exchange occurs via an associative pathway through unobserved 16-electron, three-coordinate bis-alkene intermediates or transition states such as **2.2**. Furthermore, this exchange is facile ($\Delta G^\ddagger = 15.0 \text{ kcal mol}^{-1}$ for **2.1**) and occurs with a low entropy of activation ($\Delta H^\ddagger = 5.0 \text{ kcal mol}^{-1}$) (Scheme 4).^{42, 46} Presumably, linking the two alkene ligands (as in a 1,3-diene) would decrease the entropy of activation for formation of the three-coordinate bis-alkene species, making this process less unfavorable provided that tethering the ligands does not result in increased strain in the complexes.

Scheme 4: Proposed mechanism for degenerate alkene exchange in gold(I) π -alkene complexes.



Another question about the structure of gold(I) π -diene complexes arises from the observed preference of $[(L)Au]^+$ for complexation of highly-substituted alkenes. For the series of complexes $[(P1)Au(\eta^2\text{-alkene})]^+ SbF_6^-$ [alkene = isobutylene (**2.1**), 1-hexene (**2.3**), 2-methyl-2-butene), equilibrium binding affinity increased in the order 1-hexene < isobutylene < 2-methyl-2-butene.⁴⁶ However, gold(I) catalysts specifically add

nucleophiles across the less-substituted bond of a differentially-substituted 1,3-diene, suggesting activation of this less-substituted bond, presumably through coordination to gold. While preferential formation of an η^2 -complex at the more-substituted alkene of the diene would not preclude addition across the less-substituted alkene, additional study would be necessary to explain the observed regioselectivity.

In addition to the isolated complexes described above, limited examples of cationic, three-coordinate gold(I) π -alkene complexes are known. Most of these complexes are formed with a strong bidentate ligand and take the form $[(\kappa^2\text{-L})\text{Au}(\eta^2\text{-alkene})]^+ \text{X}^-$; for example, the three-coordinate complex $[(\kappa^2\text{-bipy}^{\text{ip}})\text{Au}(\text{styrene})]^+ \text{SbF}_6^-$ [bipy^{ip} = 6-isopropyl-2,2'-bipyridine] (**2.4**, Figure 7) was generated from the reaction of a cationic gold(III) oxo complex with styrene.⁶⁴ Recently, Dias and coworkers reported that the reaction of AuCl with AgSbF₆ in CH₂Cl₂ in the presence of ethylene formed the air-sensitive tris-ethylene complex $[\text{Au}(\text{C}_2\text{H}_4)_3]^+ \text{SbF}_6^-$ (**2.5**, Figure 7).⁶⁵

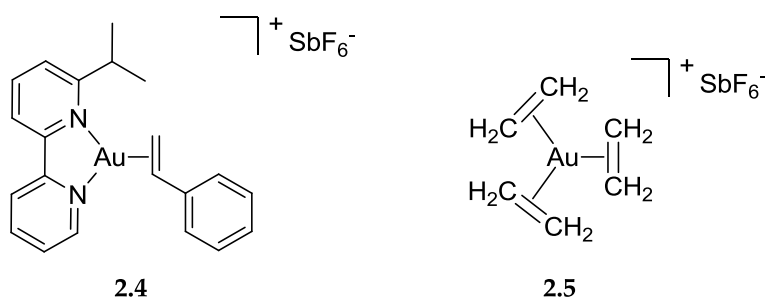


Figure 7: Cationic, three-coordinate gold(I) π -alkene complexes 2.4 and 2.5.

2.1.3 Transition metal η^2 - and η^4 -(1,3-diene) complexes

Complexes of 1,3-dienes are well known for transition metals through group 9. These complexes display a strong preference toward η^4 -coordination of the diene,⁶⁶⁻⁷⁰ but η^2 -coordination is not unknown. Thermolysis of $(\eta^5\text{-C}_5\text{Me}_5)\text{W}(\sigma\text{-alkyl})(\pi\text{-allyl})$ complexes generates 16-electron η^2 -diene intermediates that can be trapped as their 18-electron PMe_3 adducts.⁷¹⁻⁷³ Photolysis of tungsten,⁷⁴⁻⁷⁵ molybdenum,⁷⁵⁻⁷⁶ rhenium,⁷⁷ and cobalt⁷⁸ carbonyl compounds in the presence of diene also forms η^2 -diene compounds. Similarly, treatment of molybdenum η^4 -diene compounds with a tertiary phosphine or CO forms the corresponding molybdenum η^2 -diene compound.⁷⁹ Iron η^2 -diene complexes have been isolated from rearrangements of iron-allylidene compounds⁸⁰ and from the reaction of iron σ -alkenyl compounds with triphenylcarbenium-hexafluorophosphate.⁸¹

Examples of group 10 transition metal η^2 -diene complexes include three-coordinate palladium, platinum, and nickel complexes that contain both an η^2 -1,3-butadiene ligand and a chelating bis(phosphine) ligand.⁸² Of the group 11 metals, both copper and silver salts are known to form dimeric or polymeric η^2 -diene complexes through bridging 1,3-diene ligands.⁸³⁻⁸⁶

2.1.4 Project goals and scope

Computational studies have predicted both η^2 - and η^4 -complexation of 1,3-dienes by gold(I), either of which could be supported by experimental studies of cationic

gold(I) π -alkene complexes. Furthermore, analogy to known 1,3-diene complexes of late transition metals suggest that gold(I) may form either monomeric η^2 - or η^4 -complexes or polymeric η^2 -diene-bridged structures. As gold(I) π -diene complexes are often cited as key intermediates in the catalytic hydrofunctionalization of dienes, a general understanding of their structure and solution behavior is critical to the understanding of the mechanism of these reactions. To this end, we sought to synthesize and study gold(I) π -diene complexes using techniques previously developed in the lab to generate and characterize monomeric, cationic gold(I) π -alkene complexes. We sought to determine the preferential binding mode(s) in the synthesized diene complexes, as well as study their intra- and intermolecular exchange behavior. Concurrent with publication of this work, Russell et al reported a combined experimental/DFT study of a similar family of gold(I) η^2 -diene complexes.⁸⁷⁻⁸⁸ The results of this and subsequent studies are discussed in the context of the present work in section 2.3.2.⁸⁹

2.2 Results and discussion

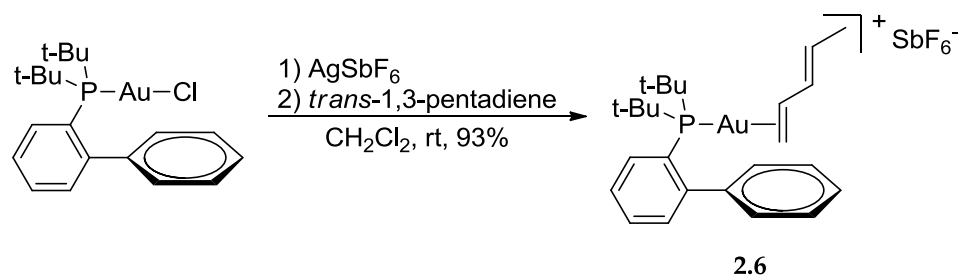
2.2.1 Synthesis and characterization of the gold(I) η^2 -(*trans*-1,3-pentadiene) complex 2.6

2.2.1.1 Synthesis of [(P1)Au(η^2 -(*E*)-H₂C=C(H)C(H)=C(H)Me)]⁺ SbF₆⁻ (2.6)

The synthesis of the cationic gold(I) complex of *trans*-1,3-pentadiene was completed employing a procedure similar to that used to prepare cationic gold(I) η^2 -alkene complexes.^{42, 46} A 1:1 mixture of (P1)AuCl [P1 = P(*t*-Bu)₂₀-biphenyl] and AgSbF₆ suspended in methylene chloride was treated with *trans*-1,3-pentadiene (10 equiv) under

an atmosphere of N₂, resulting in formation of a new white precipitate which settles out of solution. The mixture was stirred for 6 h at room temperature, filtered through Celite, and concentrated and dried to yield [(P1)Au(η²-(E)-H₂C=C(H)C(H)=C(H)Me)]⁺SbF₆⁻ (**2.6**) in 93% yield (Scheme 5). Solid-state and solution characterization confirmed the isolation of a two-coordinate, η²-diene complex (see below). As was the case with analogous complexes of simple alkenes, **2.6** was an air- and thermally-stable white solid.

Scheme 5: Synthesis of [(P1)Au(η²-(E)-H₂C=C(H)C(H)=C(H)Me)]⁺SbF₆⁻ (2.6**)**



2.2.1.2 X-Ray crystal structure of 2.6

Slow diffusion of hexanes into a CH₂Cl₂ solution of **2.6** at 4 °C gave colorless crystals of **2.6** suitable for single-crystal X-ray analysis (Figure 8). The crystal structure of **2.6** established it as a monomeric complex with η²-complexation of the *trans*-1,3-pentadiene ligand by gold through the less-substituted C1=C2 bond. Complex **2.6** adopts a distorted linear conformation in the solid state, with a P–Au–C1=C2_(centroid) angle of 169.3° and with the diene ligand unsymmetrically bonded to gold with a shorter Au–C1 and longer Au–C2 interaction (Δ*d* = 0.113 Å). The coordinated C1=C2 bond of the diene is elongated relative to the uncomplexed C3=C4 bond (Δ*d* = 0.049 Å), and the

diene moiety adopts a near planar *s-trans* configuration with a C1–C2–C3–C4 dihedral angle of 169.9°. The diene ligand is positioned such that the plane defined by Au–C1–C2 is rotated by ~12° relative to the plane defined by Au–P–C14 with the C=C(H)Me group directed away from the protruding phenyl ring and along the Au–P–C14 plane.

The protruding phenyl group of the *o*-biphenyl phosphine moiety is not perpendicular to the P-bound aryl ring, but instead is rotated toward the C6 quaternary carbon atom with a C14–C19–C20–C21 dihedral angle of 70.6°. The distance between the gold atom and the plane of the protruding phenyl group is 2.88 Å with a distance of Au–C20 = 3.018 Å, suggesting the presence of a weak Au–arene interaction. Similar Au–arene interactions have been observed for gold dialkyl(*o*-biphenyl)phosphine^{38, 90-92} and related gold complexes,⁹³⁻⁹⁴ although the Au–arene distance of **2.6** is shorter than is typically observed (Au–arene_(plane) = 3.0–3.2 Å,^{38, 90} Au–C_{ipso} = 3.16–3.36 Å⁹¹⁻⁹²).

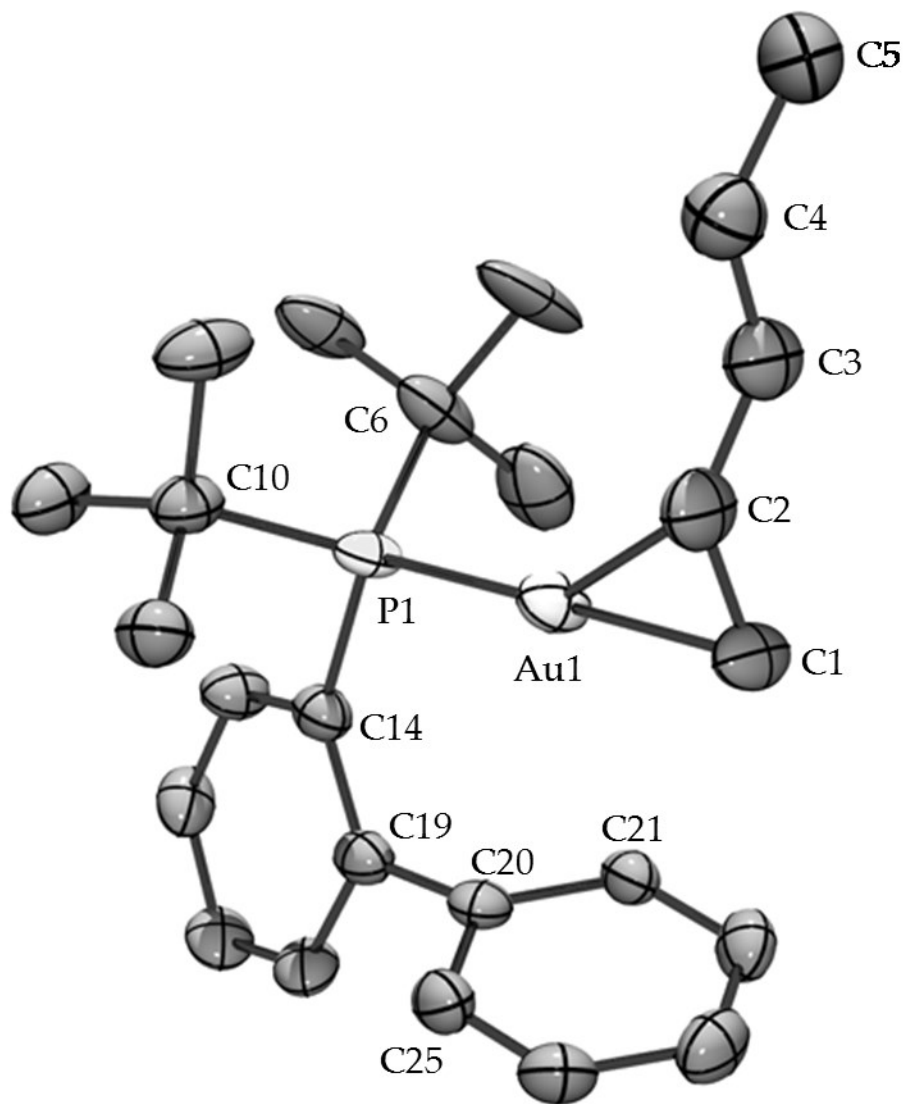


Figure 8: ORTEP diagram of 2.6 showing partial atom numbering scheme. Ellipsoids are shown at the 50% probability level. Hydrogen atoms and counterion have been removed for clarity.

2.2.1.3 Solution characterization and fluxional behavior of 2.6

As with the gold(I) π -alkene and alkyne complexes, the solution-state structure of *trans*-1,3-pentadiene complex 2.6 was probed spectroscopically. The ^1H and ^{13}C NMR

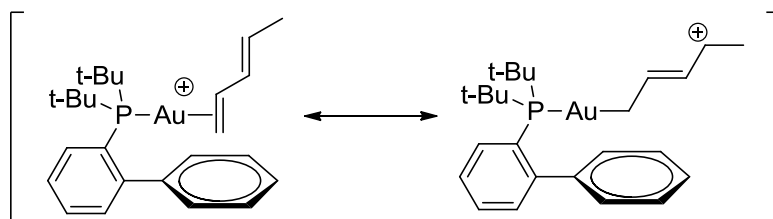
resonances corresponding to the diene ligand of complex **2.6** were unambiguously assigned through one- and two-dimensional analyses (see section 2.4.2). In the ^{13}C NMR spectrum of **2.6** at $-80\text{ }^\circ\text{C}$, the resonance corresponding to the C1 carbon atom of bound *trans*-1,3-pentadiene (δ 90.6, d, $J_{\text{CP}} = 10.1$ Hz) was shifted ~ 24 ppm to lower frequency relative to that of the free diene (δ 114.4), while the C2 (δ 137.1) and C3 (δ 129) diene resonances of **2.6** were only slightly perturbed ($\Delta\delta < 4$ ppm) relative to the resonances of free *trans*-1,3-pentadiene (Table 5, section 2.2.2.3). In comparison, the C4 diene resonance of **2.6** (δ 144.3) was shifted to higher frequency by ~ 14 ppm relative to that of free diene (δ 129.8).

The shift patterns were similar in the ^1H NMR spectrum of **2.6**. The C1 diene protons of **2.6** [δ 4.17, 4.11] were shifted ~ 0.8 ppm to lower frequency relative to those of free *trans*-1,3-pentadiene (δ 5.06, 4.93), while the C2 (δ 6.51) and C3 (δ 5.99) diene resonances of **2.6** differed by ≤ 0.2 ppm relative to those of free *trans*-1,3-pentadiene. In comparison, the C4 proton of **2.6** (δ 6.26) was shifted to higher frequency by ~ 0.5 ppm relative to that of free diene.

To better understand the bonding information in the spectra of **2.6**, comparisons can be made to the cationic gold 1-hexene complex $[(\text{P1})\text{Au}(\eta^2\text{-H}_2\text{C}=\text{C}(\text{H})(\text{CH}_2)_3\text{CH}_3)]^+ \text{SbF}_6^-$ (**2.3**).⁴⁶ The ^{13}C NMR spectrum of **2.3** displays a large shift ($\Delta\delta \approx -16$) of the C1 alkene carbon atom to lower frequency and small shift of the C2 carbon atom to higher frequency ($\Delta\delta \approx 2$) relative to the corresponding resonances of free 1-hexene. Likewise,

the terminal alkene protons of **2.3** are shifted ~ 0.5 ppm to lower frequency, while the internal alkenes protons are shifted ~ 0.3 ppm to higher frequency. These patterns have been attributed to slippage of gold toward the unsubstituted alkene terminus with a stronger Au–C1 interaction relative to the Au–C2 interaction, a contention that was supported by X-ray crystallographic studies.⁴⁶ Therefore, the significant shifts of the C1 diene carbon atom and C1 diene protons of **2.6** to higher frequency, as well as the splitting of the C1 carbon resonance due to carbon-phosphorus coupling, indicate that the diene binds to gold through the C1=C2 bond, as was observed in the solid state. Unlike the 1-hexene complex **2.3**, the resonances corresponding to the C4 carbon and C4 vinyl protons of **2.6** were shifted to higher frequency relative to free diene. These observations point to stabilization of the gold- π interaction of **2.6** through donation of electron density from the uncomplexed C3=C4 bond to the complexed C1=C2 bond, leading to depletion of electron density at the C4 diene carbon atom of **2.6** (Scheme 6).

Scheme 6: Resonance structures depicting depletion of electron density at the C4 position of the 1,3-pentadiene ligand in 2.6.

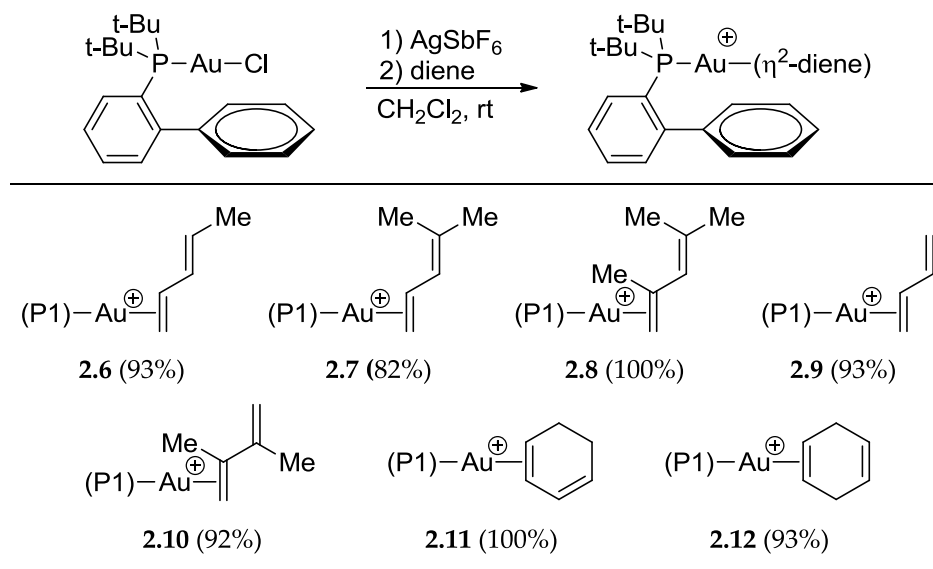


2.2.2 Synthesis and characterization of gold(I) η^2 -(diene) complexes 2.7 – 2.12

2.2.2.1 Synthesis of gold(I) η^2 -(diene) complexes 2.7 – 2.12

Employing a procedure similar to that employed to synthesize and isolate **2.6**, the cationic gold(I) η^2 -diene complexes [(P1)Au(η^2 -diene)]⁺SbF₆⁻ [diene = 4-methyl-1,3-pentadiene (**2.7**), 2,4-dimethyl-1,3-pentadiene (**2.8**), 1,3-butadiene (**2.9**), 2,3-dimethyl-2-butene (**2.10**), 1,3-cyclohexadiene (**2.11**), and 1,4-cyclohexadiene (**2.12**) were isolated in >80% yield as air- and thermally-stable white solids (Scheme 7). Although stable indefinitely in the solid state, the gold π -diene complexes **2.6** – **2.12** were only modestly stable in solution and tended to decompose when concentrated. This behavior complicated purification, and solutions of these complexes typically contained traces (~5%) of the free diene. More specifically, complexes **2.7** and **2.8** were effectively crystallized from concentrated CH₂Cl₂ solutions, which, in the case of **2.7**, also produced X-ray quality crystals. Conversely, crystallization of **2.6**, **2.9**, and **2.12** from concentrated CH₂Cl₂ solutions produced X-ray quality crystals but also formed amorphous material that degraded the bulk purity of the sample. Attempted crystallization of **2.10** and **2.11** led to degradation of the sample without crystal formation. Nevertheless, all complexes displayed satisfactory combustion analysis and were unambiguously characterized in solution by ¹H, ¹³C, and ³¹P NMR spectroscopy; complexes **2.7**, **2.9**, and **2.12** were also characterized in the solid state by X-ray crystallography.

Scheme 7: Synthesis of cationic, monomeric gold(I) η^2 -diene complexes 2.6 - 2.12



2.2.2.2 X-ray crystal structures of 2.7, 2.9, and 2.12

In addition to *trans*-1,3-pentadiene complex **2.6**, 4-methyl-1,3-butadiene complex **2.7**, 1,3-butadiene complex **2.9**, and 1,4-cyclohexadiene complex **2.12** were analyzed by X-ray crystallography (Figures 9-11). Refinement of the structure of **2.7** was complicated by an orientational disorder of the 4-methyl-1,3-pentadiene ligand, which precluded meaningful analysis of the bond distances and angles within the 4-methyl-1,3-pentadiene ligand. Nevertheless, the crystal structure of **2.7** revealed a distorted linear η^2 -diene complex with the gold atom bound unsymmetrically to the less-substituted $\text{C1}=\text{C2}$ bond of the diene with a shorter $\text{Au}-\text{C1}$ and longer $\text{Au}-\text{C2}$ interaction, as was observed for complex **2.6** (Figure 9). In the major conformer of **2.7** (**2.7a**, 57% occupancy), the diene ligand is positioned so that the $\text{Au}-\text{C1}-\text{C2}$ plane is rotated by 77.4° relative to the $\text{Au}-\text{P}-\text{C15}$ plane with the C3 carbon atom directed away from the protruding phenyl

ring of the *o*-biphenylphosphine ligand. In the minor conformer (**2.7b**, 43% occupancy), the coordinated C1=C2' bond is bound through the opposite π -face relative to **2.7a** and is positioned such that the Au–C1–C2' plane is rotated by 66.8° relative to the Au–P–C15 plane with the C3' carbon atom directed toward the protruding phenyl group. In both **2.7a** and **2.7b**, the protruding phenyl group of the *o*-biphenyl phosphine moiety is rotated toward the C7 quaternary carbon atom with C15–C20–C21–C22 = 80.2° and with an Au–arene(plane) distance of 3.02 Å.

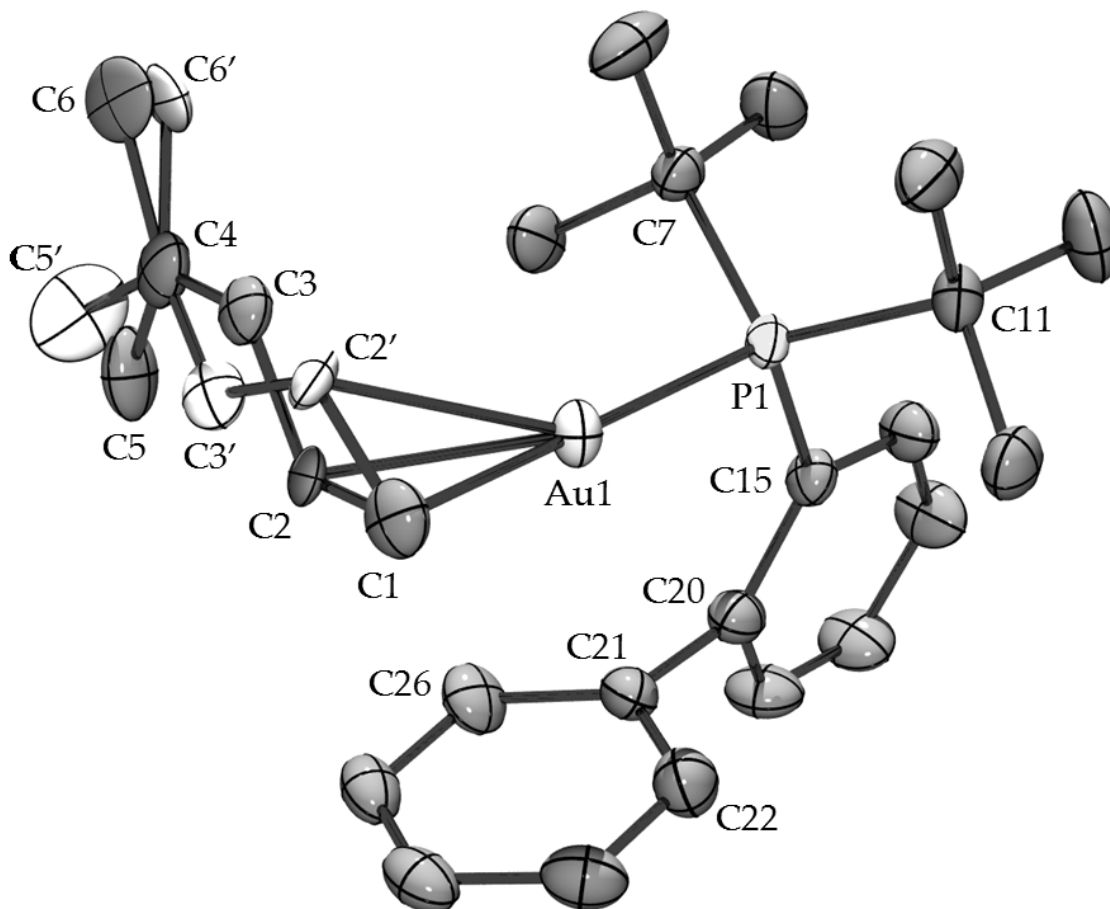


Figure 9: ORTEP diagram of **2.7** showing partial atom numbering scheme. The major conformer of the diene ligand (**2.7a**) is shown in dark gray ellipsoids, and the minor

conformer (2.7b) is shown in white ellipsoids. Ellipsoids are shown at the 50% probability level. Hydrogen atoms and counterion have been removed for clarity.

Similar to **2.7**, complex **2.9** suffered from an orientational disorder of the 1,3-butadiene ligand. In both conformers of **2.9**, gold adopts a distorted linear conformation [P–Au–alkene_(cent) = 166–168 °] with the η²-butadiene ligand bound unsymmetrically to gold through a shorter Au–C1 and longer Au–C2 interaction ($\Delta d = 0.09\text{--}0.10$ Å; Figure 10). In the major conformer of **2.9** (**2.9a**, 64% occupancy), the coordinated C1=C2 bond of the diene (as defined by the Au–C1–C2 plane) is rotated ~38° relative to the Au–P–C14 plane with the unbound C3=C4 group directed away from the *o*-phenyl ring and along the Au–P–C14 plane. In the minor conformer of **2.9** (**2.9b**, 36% occupancy), the diene ligand is bound through the opposite π-face relative to **2.9a** and is positioned such that the Au–C1'–C2' plane is rotated ~20 ° relative to the Au–P–C13 plane with the unbound C3'=C4' moiety directed away from the proximal phenyl group. In both conformers, the protruding phenyl group of the *o*-biphenylphosphine moiety is rotated toward the C9 quaternary carbon atom with a C13–C14–C19–C24 dihedral angle of 63.5 ° and with an Au–arene_(plane) distance of 2.96 Å.

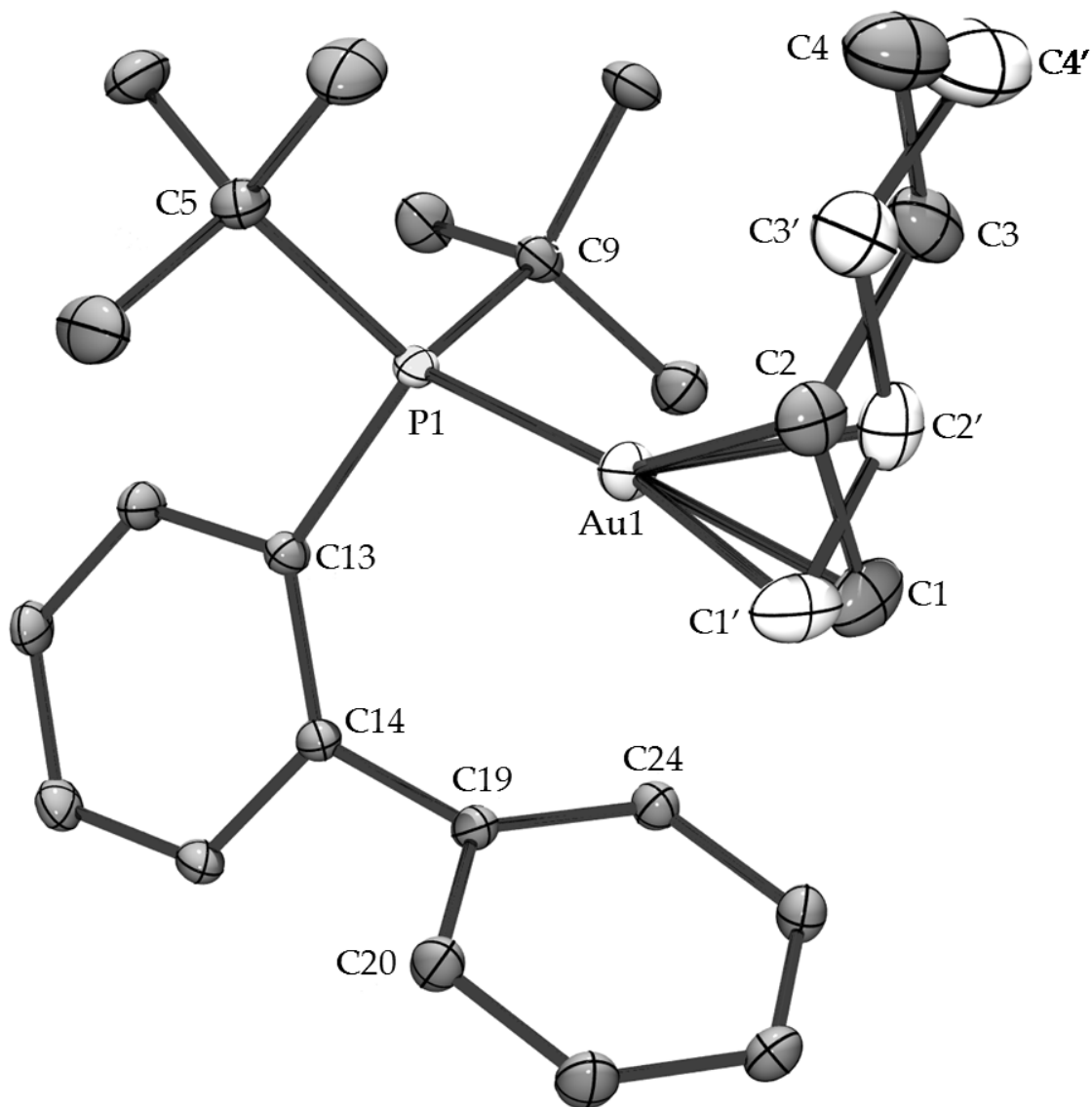


Figure 10: ORTEP diagram of 2.9 showing partial atom numbering scheme. The major conformer of the diene ligand (2.9a) is shown in dark gray ellipsoids, and the minor conformer (2.9b) is shown in white ellipsoids. Ellipsoids are shown at the 50% probability level. Hydrogen atoms and counterion have been removed for clarity.

Complex **2.12**, which contains a nonconjugated 1,4-cyclohexadiene ligand, adopts a slightly distorted linear conformation ($P-Au-alkene_{(cent)}$ angle of 171.3°) with the diene ligand bound more symmetrically to gold ($\Delta d Au-C1/Au-C2 = 0.031 \text{ \AA}$;

Figure 11) than was observed for acyclic 1,3-diene complexes **2.6**, **2.7**, and **2.9**. The coordinated C1=C2 bond of the cyclohexadiene ligand is positioned roughly parallel to the protruding phenyl ring of the *o*-biphenyl moiety with the remainder of the cyclohexadiene ligand directed away from the proximal phenyl group. The two aryl rings of the *o*-biphenylphosphine ligand are perpendicular to one another with a C15–C20–C21–C22 dihedral angle of 91.0°. Within the 1,4-cyclohexadiene moiety, the coordinated C1=C2 bond is elongated by 0.038 Å relative to the uncomplexed C3=C4 bond, and the C–C=C–C groupings associated with both the complexed and uncomplexed C=C bonds are planar, with C6–C1–C2–C3 and C3–C4–C5–C6 dihedral angles of < 2°. Interestingly, the 1,4-cyclohexadiene ligand adopts a boat-like conformation with an angle of ~18° between the C6–C1–C2–C3 and C3–C4–C5–C6 planes with the concave face directed toward the *tert*-butyl groups.

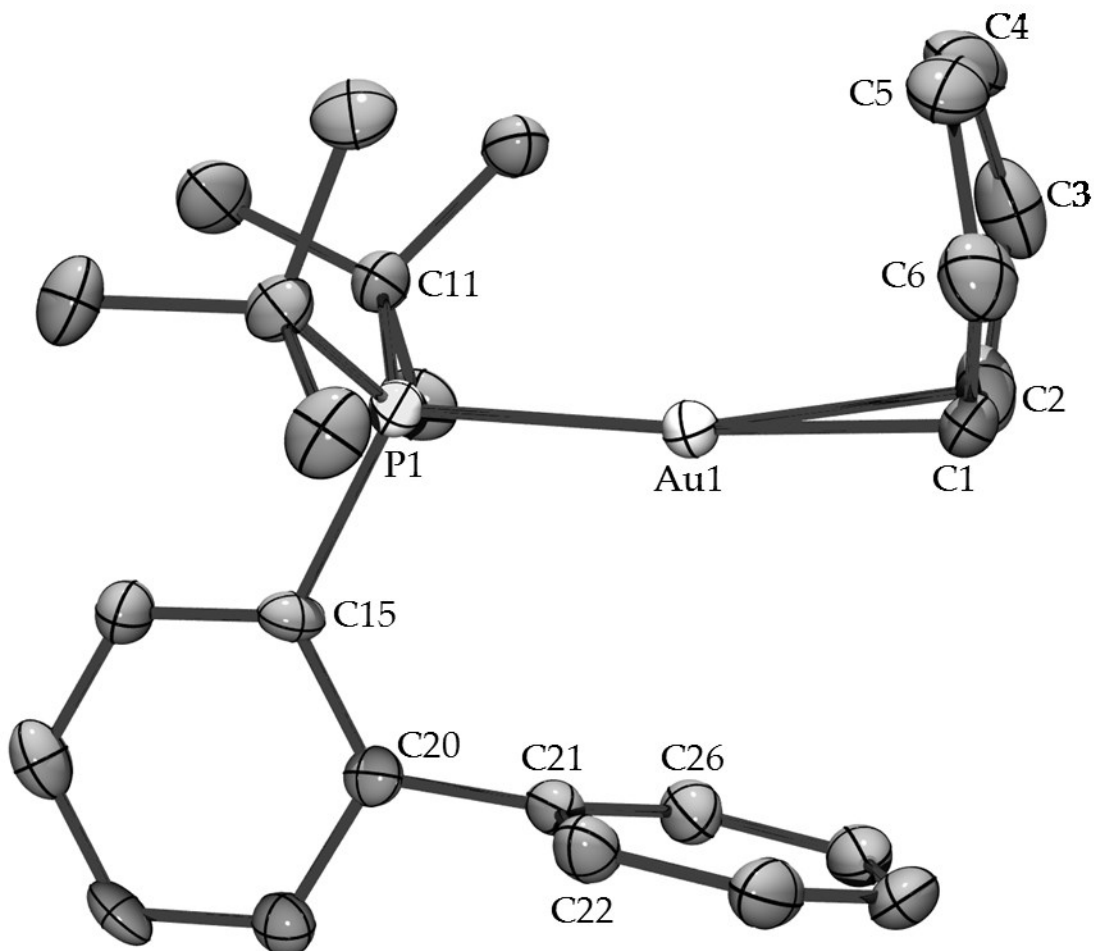


Figure 11: ORTEP diagram of 2.12 showing partial atom numbering scheme. Ellipsoids are shown at the 50% probability level. Hydrogen atoms and counterion have been removed for clarity.

2.2.2.3 Solution characterization of 2.7 - 2.12

As with **2.6**, NMR spectroscopy was used to elucidate the solution structure of complexes **2.7 – 2.12**. Often, low temperature analysis was employed due to fluxional behavior of the diene ligand at room temperature (see section 2.2.3). The vinylic protons and sp^2 diene carbon atoms of complexes **2.8**, **2.9**, and **2.11** were unambiguously

assigned from the ^1H and ^{13}C NMR spectra supported by various combinations of ^1H - ^1H COSY, HMQC, HMBC, and variable-temperature ^{13}C NMR spectroscopy; the vinylic protons and sp^2 diene carbon atoms of complexes **2.7**, **2.10**, and **2.12** were confidently assigned from the ^1H and ^{13}C NMR spectra and by analogy to the spectroscopy of complexes **2.6**, **2.8**, **2.9**, and **2.11**. As was the case with **2.6**, assignment of ^{13}C resonances was aided by the presence of phosphorus coupling to the C1 diene carbon atom with J_{CP} ranging from 12.6 to 16.3 Hz for acyclic diene complexes **2.7**–**2.10** and 8.3 Hz for cyclohexadiene complex **2.11** (Table 5). Details regarding these ^1H and ^{13}C assignments are provided in section 2.4.2.

Table 5: ^{13}C chemical shifts (ppm) and C-P coupling constants (Hz) of the sp^2 carbon atoms of the complexes **2.6 – **2.12** in CD_2Cl_2 and chemical shift difference ($\Delta\delta$, ppm) relative to free diene.**

complex	temp ($^{\circ}\text{C}$)	C1		C2		C3	C4
		δ ($\Delta\delta^a$)	J_{PC} (Hz)	δ ($\Delta\delta^a$)	J_{PC} (Hz)	δ ($\Delta\delta^a$)	δ ($\Delta\delta^a$)
2.6	-80	90.6 (-23.8)	10.1	137.1 (-0.1)		129 ^b (-3.6)	144.3 (14.5)
2.7	25	90.6 (-23.8)	15.0	134.3 (0.8)		123.5 (-2.6)	153.1 (17.5)
2.8	25	91.7 (-21.9)	16.3	158.7 (16.3)		125.1 ^c (-2.3)	149.4 (15.5)
2.9^d	-90	94.9 (-22.6)	12.6	133.5 (-4.6)	2.5	133.3 (-4.8)	128.6 (11.1)
2.10^d	-60	91.9 (-21.2)	15.0	154.7 (10.9)		140.2 (-3.4)	124.2 (11.1)
2.11^d	-70	114.7 (-11.6)	8.3	117.4 (-7.0)	6.2	121.1 (-3.3)	136.4 (10.1)
2.12		120.7 (-3.4) ^e	6.9				123.4 (-0.7) ^f

^aNegative $\Delta\delta$ corresponds to a shift of the complex to lower frequency relative to free diene; positive $\Delta\delta$ corresponds to a shift of the complex to higher frequency relative to free diene. ^bC3 diene resonance overlaps with an aromatic resonance of P1. ^c $J_{\text{PC}} = 5.2$ Hz. ^dC1 and C2 are defined as the termini of the gold-bound alkene. ^eChemical shift of equivalent C1 and C2 atoms. ^fChemical shift of equivalent C4 and C5 atoms.

The trends in the ^{13}C NMR spectroscopy of complexes **2.6- 2.11** are descriptive of an η^2 -bond between the less-substituted alkene of diene ligand and gold that is sensitive to the substitution of the conjugated π -system (Table 5). Each of the complexes **2.6-2.11** displayed a shift of the C1 diene carbon resonance to lower frequency and a shift of the uncomplexed C4 diene carbon to higher frequency relative to the corresponding resonances of free diene, as was observed for **2.6**. In the cases of complexes **2.7** and **2.8**, which possess dissimilarly substituted C=C double bonds, these features established binding of the diene to gold in solution through the less substituted C1=C2 bond, as was observed for **2.6**. Further comparison of the ^{13}C spectra of complexes **2.6**, **2.7**, and **2.9**, which differ in the degree of methyl substitution at the C4 carbon atom, reveals that the shift of the C4 carbon atom to higher frequency relative to free diene increases with increasing substitution at the C4 carbon atom in the order **2.9** ($\Delta\delta = 11.1$) < **2.6** ($\Delta\delta = 14.5$) < **2.7** ($\Delta\delta = 17.5$). This behavior may be indicative of increased donation from the uncomplexed to complexed C=C bond with increasing methyl substitution of the C4 carbon atom. Conversely, complexes **2.8** and **2.10**, which possess a C2 methyl group, displayed a more pronounced shift of the C2 diene carbon atom to higher frequency ($\Delta\delta = -16.3$ for **2.8** and $\Delta\delta = -11.1$ for **2.10**) than did the complexes lacking substitution at the C2 carbon atom. This behavior may suggest a more even distribution of partial positive charge between the C2 and C4 carbon atoms of complexes **2.8** and **2.10** relative to complexes lacking substitution at the diene C2 position.

As compared to the acyclic, C1-unsubstituted complexes, the C1 carbon resonance of complex **2.11** exhibited a smaller shift to lower frequency, and both the C2 and C3 carbon resonances were also shifted slightly to lower frequency. This suggests that slippage of gold toward C1 and away from C2 in the bound alkene of 1,3-cyclohexadiene ligand occurs to a lesser degree in **2.11** than in complexes **2.6 – 2.10**. Likewise, the magnitude of the higher-frequency shift of the C4 carbon resonance in **2.11** was similar to that of complexes **2.9** and **2.10** with C4-unsubstituted diene ligands. In contrast, the non-conjugated 1,4-cyclohexadiene ligand of complex **2.12** binds to gold symmetrically in solution, as in the solid-state. The C1 and C2 carbons of **2.12** are equivalent, producing a single resonance which is shifted only slightly to lower frequency ($\Delta\delta = -3.4$ ppm) in the ^{13}C NMR spectrum, as are the C4 and C5 carbons, whose resonance is relatively unperturbed compared to free diene ($\Delta\delta = -0.7$ ppm). Close similarity of the steric environment of the two cyclohexadiene ligands suggests that the slippage observed in complex **2.11** is induced by the electronic differentiation of the C1 and C2 alkene termini of 1,3-cyclohexadiene.

2.2.3 Fluxional behavior of gold(I) diene complexes

2.2.3.1 Fluxional behavior of complexes 2.6 and 2.8

Because the C1=C2 bonds of the 1,3-diene ligands are prochiral, static solution structures of the gold(I) η^2 -(1,3-diene) complexes bearing the P1 ligand described herein are expected to possess diastereotopic *tert*-butyl groups. For example, ^{13}C NMR

spectroscopy of a static structure of **2.6** should indicate two pairs of resonances corresponding to the diastereotopic C6 and C10 atoms, as they are depicted in the solid state structure (Figure 8). Indeed, at -80 °C the ^{13}C NMR spectrum of **2.6** displayed a pair of phosphorus-coupled doublets at δ 37.1 and 36.9 ($J_{\text{CP}} = 24$ Hz), corresponding to the quaternary *tert*-butyl carbon atoms (Figure 12). As the temperature was raised, these doublets both shifted to higher frequency and broadened, forming a single phosphorus-coupled doublet at δ 37.5 ($J_{\text{CP}} = 24$ Hz) at -50 °C that sharpened further upon warming to room temperature. Simulation of the temperature-dependence of the ^{13}C NMR spectra of **2.6** to obtain a rate constant for the exchange was unsatisfactory, due in part to the significant change in chemical shifts of the C6 and C10 resonances over the relevant temperature range. However, the temperature-dependent behavior of the quaternary *tert*-butyl ^{13}C resonances of **2.6** was independent of the presence of free *trans*-1,3-pentadiene (0 - 150 mM), which argues against an intermolecular pathway for interconversion of the phosphorus-bound *tert*-butyl groups.

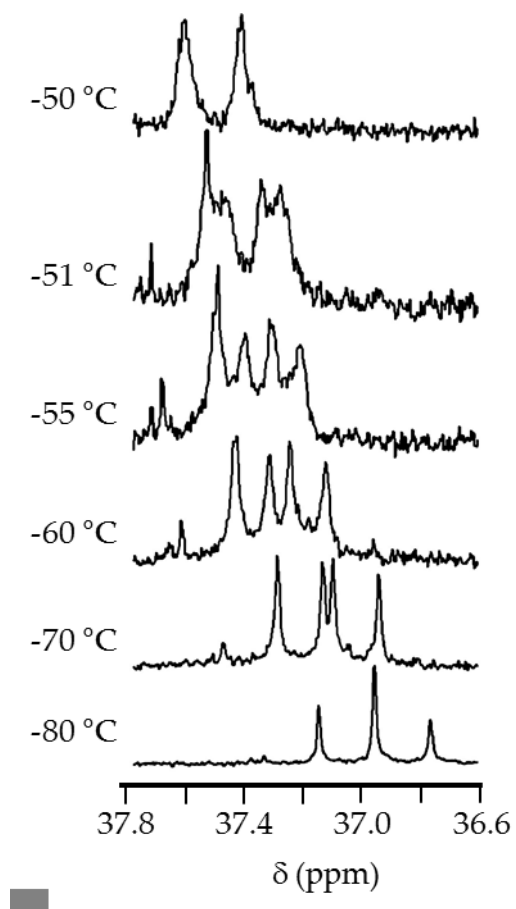


Figure 12: Temperature dependence of the quaternary *tert*-butyl ^{13}C NMR resonance of **2.6 from -50 to -80 °C in CD_2Cl_2**

As was observed for 1,3-pentadiene complex **2.6**, 2,4-dimethyl-1,3-pentadiene complex **2.8** displayed fluxional behavior which equilibrated the quaternary carbons of the diastereotopic *tert*-butyl groups of a static structure of **2.8**. The ^{13}C NMR spectrum of **2.8** at -90 °C displayed a pair of phosphorus-coupled doublets at δ 36.3 and 36.2 ($J_{\text{CP}} = 24$ Hz) corresponding to these inequivalent quaternary carbon atoms (Figure 13). As the temperature was raised, the resonances broadened and coalesced, forming a single phosphorus-coupled doublet at δ 36.8 ($J_{\text{CP}} = 24$ Hz) at -60 °C. As was the case for **2.6**, the

coalescence behavior was unaffected by the presence of free 2,4-dimethyl-1,3-pentadiene up to 150 mM.

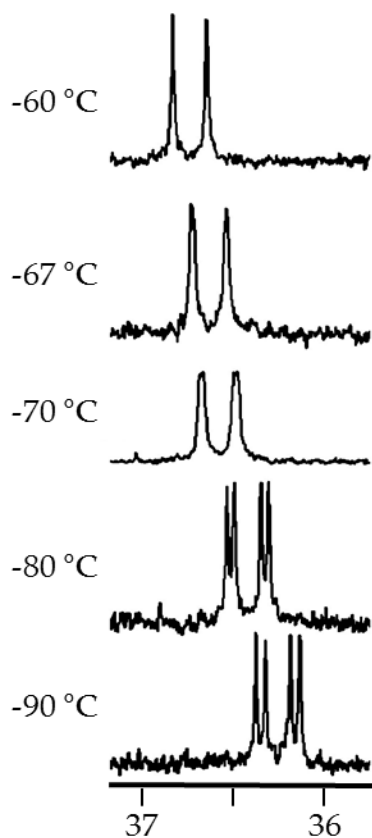
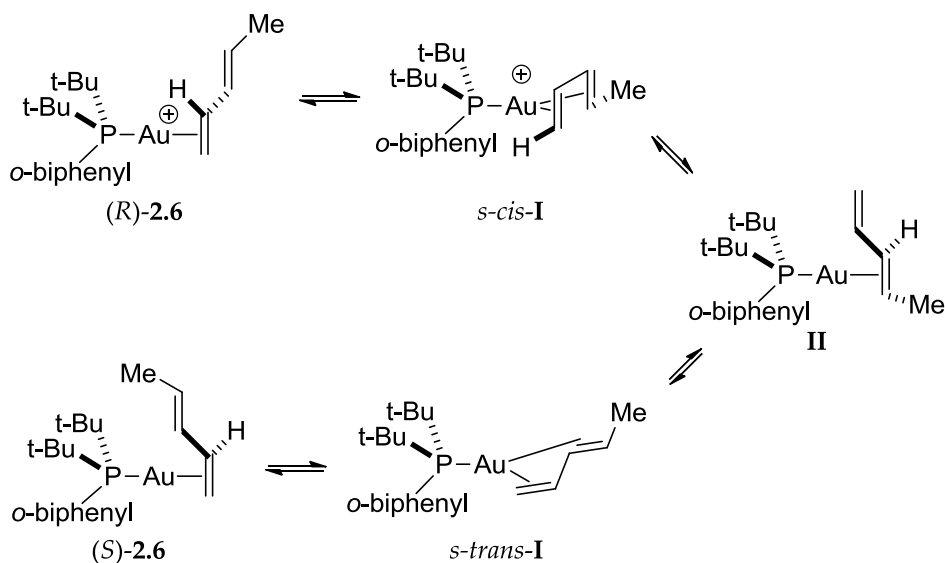


Figure 13: Temperature dependence of the quaternary *tert*-butyl ^{13}C NMR resonances of 2.8 from -90 °C to -60 °C in CD_2Cl_2 .

The presence of inequivalent *tert*-butyl groups in the low temperature ^{13}C NMR spectra of **2.6** and **2.8** which equilibrate at temperatures > -50 °C points to a facile fluxional process that exchanges the prochiral faces of the 1,3-diene ligands in these complexes. Although exchange of alkene π -faces without displacement has been documented in the case of a cationic rhenium complex,⁹⁵ a more likely mechanism for racemization of **2.6** and **2.8** involves intramolecular exchange of the complexed and

uncomplexed C=C bonds of the ligands through *s-cis* and *s-trans* η^4 -diene transition states and/or intermediates. For example, intramolecular ligand exchange of (*R*)-**2.6** via the *s-cis* η^4 -diene intermediate *s-cis*-I would form the undetected C3=C4-bound isomer **II** (Scheme 8). A second intramolecular ligand exchange via the *s-trans* η^4 -diene intermediate *s-trans*-I would form (*S*)-**2.6**. Note that both *s-cis* and *s-trans* η^4 -diene intermediates are required for racemization of **2.6** and **2.8**; a mechanism involving either *s-cis* or *s-trans* η^4 -diene intermediates would lead to exchange of the complexed and uncomplexed diene C=C bonds without racemization of the complexes.

Scheme 8: Proposed mechanism for racemization of complex **2.6 via intramolecular, associative exchange of prochiral alkene π -faces**



2.2.3.2 Fluxional behavior of complexes **2.9-2.12**

Complexes **2.9-2.12**, which contain diene ligands composed of identically substituted C=C groups, displayed variable-temperature NMR behavior consistent with

facile intramolecular exchange of the complexed and uncomplexed C=C bonds of the diene ligand. For example, the ^1H NMR spectrum of 1,3-butadiene complex **2.9** at $-90\text{ }^\circ\text{C}$ displayed two one-proton multiplets at δ 6.48 and 6.18, corresponding to the C2 and C3 vinylic protons, and four one-proton multiplets at δ 5.66, 5.56, 4.11, and 3.93 corresponding to the C4 (higher frequency) and C1 (lower frequency) vinylic resonances (Figure 14). As the temperature was raised, the resonances corresponding to C2 and C3 protons broadened and coalesced at $-60\text{ }^\circ\text{C}$ to form a multiplet at δ 6.40 at $15\text{ }^\circ\text{C}$. Over the same temperature range, the resonances corresponding to the C1 and C4 protons broadened and coalesced at $-45\text{ }^\circ\text{C}$ to form a two-proton multiplet at $\delta \sim 5.0$ at $15\text{ }^\circ\text{C}$.

The presence of distinct resonances corresponding to the bound and unbound alkenes within the 1,3-butadiene ligand of **2.9** in the ^1H NMR of the complex at $-90\text{ }^\circ\text{C}$ indicates that alkene exchange is slow relative to the NMR timescale at this temperature. The temperature-dependent broadening and coalescence indicates significant exchange on the NMR timescale, eventually resulting in a time-average spectrum of the resonances of the bound and unbound alkene which are equilibrated through exchange. Significantly, broadening of the vinylic resonances of **2.9** occurred prior to detectable broadening of the vinylic resonances of residual 1,3-butadiene, arguing against an intermolecular pathway for the exchange. Line shape simulation of the C2/C3 diene resonances near the coalescence temperature ($\tau_c = -59\text{ }^\circ\text{C}$) was used to calculate an

energy barrier of $\Delta G^{\ddagger}_{214} = 9.6 \text{ kcal mol}^{-1}$ for interconversion of the diene C=C bonds of **2.9**. Details of this analysis are included in section 2.4.4.

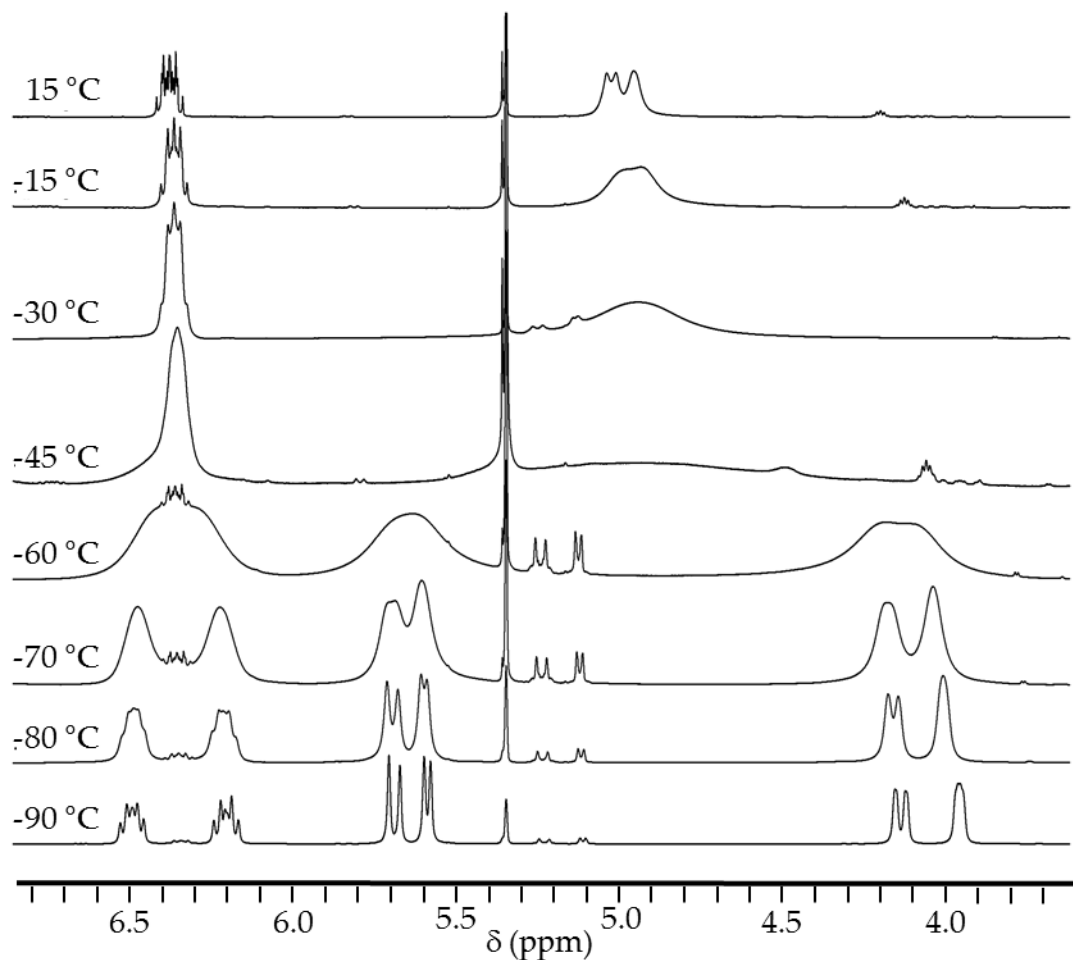


Figure 14: Temperature dependence of the vinylic ¹H NMR resonances of **2.9 from -90 °C to 15 °C in CD₂Cl₂. The small multiplets at δ 6.3, 5.2, and 5.1 correspond to free 1,3-butadiene.**

The ¹H NMR spectrum of 2,3-dimethyl-1,3-butadiene complex **2.10** at -60 °C displayed a 1:1 ratio of three-proton singlets at δ 2.25 and 1.73 corresponding to the diene methyl protons and a 1:1:1:1 ratio of one-proton resonances at δ 5.65, 5.48, 3.99,

and 3.64 corresponding to the C4 (higher frequency) and C1 (lower frequency) vinylic protons (Figure 15). As the temperature was raised, the diene methyl resonances broadened and coalesced at -12 °C, forming a broad singlet ($\nu_{1/2} = 19$ Hz) at 2.04 at 20 °C. Over the same temperature range, the vinylic resonances broadened and coalesced, forming a broad four-proton multiplet at $\delta \sim 4.8$ at 20 °C. As was the case with **2.9**, significant broadening of the vinylic and diene methyl resonances of **2.10** occurred prior to detectable broadening of the resonances of residual 2,3-dimethyl-1,3-butadiene, arguing against an intermolecular pathway for the exchange. An energy barrier of $\Delta G^{\ddagger}_{261K} = 11.9$ kcal mol⁻¹ for the diene C=C bonds of **2.10** was determined from line shape analysis of the diene methyl resonances at the coalescence temperature ($\tau_c = -12$ °C).

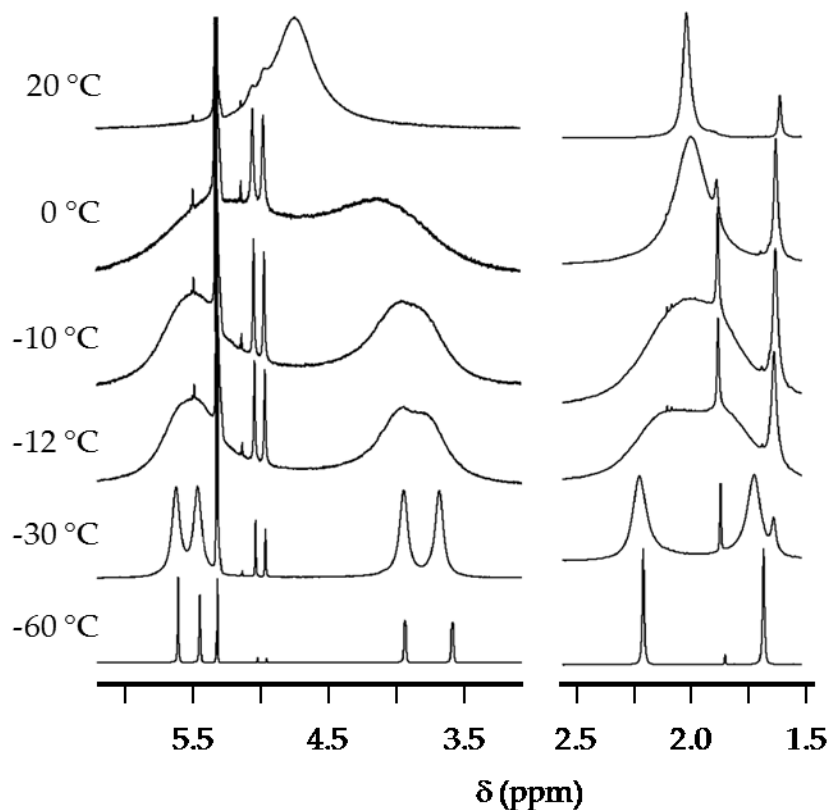


Figure 15: Temperature dependence of the vinylic (left column) and diene methyl (right column) ^1H NMR resonances of 2.10 in CD_2Cl_2 from $-60\text{ }^\circ\text{C}$ to $20\text{ }^\circ\text{C}$. Resonances at δ 5.0 and 1.88 correspond to free diene and the resonance at δ \sim 1.65 corresponds to water. Vertical and horizontal scale is not consistent between the two sets of spectra.

The ^1H NMR spectrum of 1,3-cyclohexadiene complex 2.11 at $-85\text{ }^\circ\text{C}$ displayed a 1:1:1:1 ratio of broad one-proton singlets at δ 6.18, 6.01, 5.59, and 5.13, corresponding to the H4, H3, H2, and H1 vinyl protons, respectively. As the temperature was raised, the H2/H3 pair of vinylic resonances at δ 6.01 and 5.59 broadened and coalesced at $\sim -40\text{ }^\circ\text{C}$, forming a broad singlet at δ 5.89 at $0\text{ }^\circ\text{C}$. Over the same temperature range, the H1/H4 pair of vinylic resonances at δ 6.18 and 5.13 broadened and coalesced at $\sim -30\text{ }^\circ\text{C}$, forming a broad singlet at \sim 5.7 at $0\text{ }^\circ\text{C}$ (Figure 16). An energy barrier of $\Delta G^\ddagger_{233\text{K}} = 10.4\text{ kcal}$

mol⁻¹ for exchange of the complexed and uncomplexed C=C bonds of **2.11** was determined from line shape analysis of the H2/H3 vinylic resonances near the coalescence point ($\tau_c = -40$ °C).

Significantly, the fast exchange spectrum (0 °C) of **2.11** contains a 1:1 pair of multiplets at δ 2.46 and 2.32 ($\Delta\nu = 71$ Hz), which correspond to the time-averaged C5/C6 protons positioned either *cis* or *trans* to the gold phosphine group (Figure 16). The presence of chemically inequivalent *cis* and *trans* C5/C6 protons establishes that the interconversion of complexed and uncomplexed C=C bonds of the 1,3-cyclohexadiene ligand of **2.11** occurs without concomitant exchange of the two faces of the 1,3-cyclohexadiene ligand. Because an intermolecular pathway for exchange of the complexed and uncomplexed C=C bonds of the 1,3-cyclohexadiene ligand of **2.11** would also interconvert the *cis*-C5/C6 and *trans*-C5/C6 protons, we can safely rule out an intermolecular pathway for exchange of the complexed and uncomplexed C=C bonds of the 1,3-cyclohexadiene ligand of **2.11**.

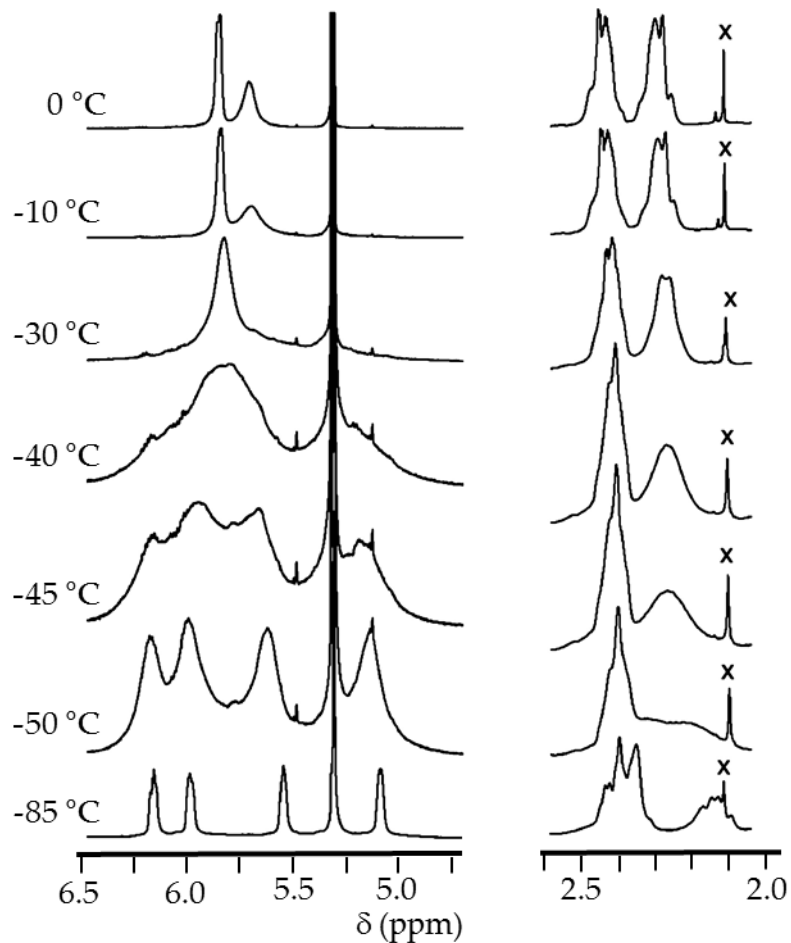


Figure 16: Temperature dependence of the vinylic (left column) and allylic (right column) ^1H NMR resonances of 2.11 from $-85\text{ }^\circ\text{C}$ to $0\text{ }^\circ\text{C}$ in CD_2Cl_2 . The resonance indicated with an “x” corresponds to an unknown impurity. Vertical and horizontal scale is not consistent between the two sets of spectra.

The ^1H NMR spectrum of 1,4-cyclohexadiene compound **2.12** at $-70\text{ }^\circ\text{C}$ displayed a 1:1 ratio of resonances at δ 5.57 and 5.71 corresponding to the vinylic protons of the complexed and uncomplexed $\text{C}=\text{C}$ bond of the diene, respectively (Figure 17). As the temperature was raised, the vinylic resonances broadened and coalesced at $-45\text{ }^\circ\text{C}$, forming a single resonance at δ 5.7 at $-10\text{ }^\circ\text{C}$. An energy barrier of $\Delta G^\ddagger_{233} = 10.9\text{ kcal}$

mol⁻¹ for exchange of the complexed and uncomplexed C=C bonds of **2.12** was determined from line shape analysis of the -45 °C spectrum. The ¹H NMR spectrum of **2.12** at -70 °C also displayed a four-proton multiplet at δ 2.85 corresponding to the allylic protons, which shifted slightly to higher frequency with increasing temperature, but remained otherwise unchanged over the temperature range -70 to -20 °C. As was the case with 1,3-cyclohexadiene complex **2.11**, this observation argues against an intermolecular process for C=C bond exchange in **2.12** that would equilibrate the *cis* and *trans* allylic protons, leading to collapse of the allylic multiplet.

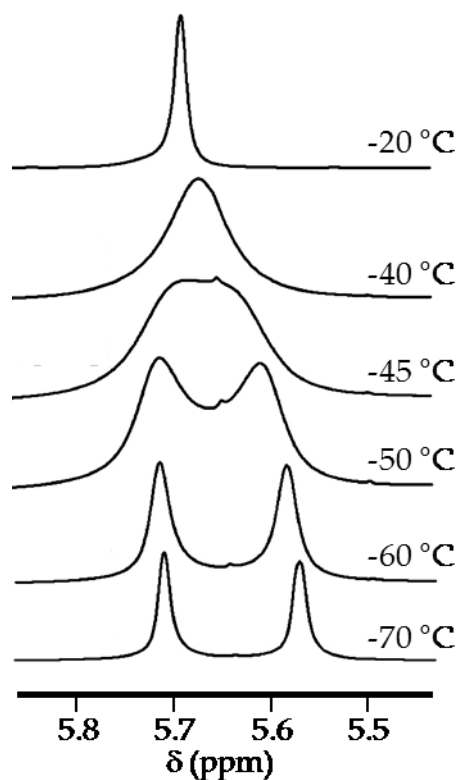


Figure 17: Temperature dependence of the vinylic ¹H NMR resonances of **2.12** from -70 °C to -20 °C in CD₂Cl₂.

Observations regarding the intramolecular exchange of the complexed and uncomplexed C=C bonds of the diene ligands of complexes **2.9–2.12** provide insight into the general solution behavior of gold(I) π -(1,3diene) complexes. The energy barriers for exchange of complexed and uncomplexed C=C bonds for complexes **2.9–2.12** fall in the range $\Delta G^\ddagger = 9.6\text{--}11.9$ kcal mol⁻¹, with butadiene complex **2.9** displaying the lowest barrier for exchange ($\Delta G_{233}^\ddagger = 9.6$ kcal mol⁻¹) and 2,3-dimethyl-1,3-butadiene complex **2.10** displayed the highest barrier for exchange ($\Delta G_{261}^\ddagger = 11.9$ kcal mol⁻¹). Although we cannot rule out ground-state destabilization of **2.9** relative to **2.10** as the origin of these differences, the higher energy barrier for exchange in the case of **2.10** presumably reflects increased steric destabilization of the transition state for formation of the three-coordinate, η^4 -diene intermediate.

In the case of complexes **2.9** and **2.10**, exchange of the complexed and uncomplexed C=C bonds of the diene ligand through either *s-cis* or *s-trans* η^4 -diene intermediates and/or transition states fully accounts for the observed fluxional behavior. In the case of 1,3-cyclohexadiene complex **2.10**, exchange must occur solely through *s-cis* η^4 -diene intermediates and/or transition states. Although we were unable to obtain satisfactory simulations of the temperature-dependent ¹³C NMR spectra of complexes **2.6** and **2.8**, the facile racemization of **2.6** and **2.8** suggests that both the *s-cis* and *s-trans* η^4 -diene intermediates and/or transition states are easily accessible. Furthermore, the similar energy barriers observed for C=C bond exchange of 1,3-

cyclohexadiene complex **2.11** and 1,4-cyclohexadiene complex **2.12** further suggest that the stability of the three-coordinate intermediates is only modestly sensitive to the geometry of the two alkene ligands and also that conjugation plays no significant role in the energetics of C=C bond exchange.

2.2.4 Intermolecular exchange behavior of gold(I) η^2 -diene complexes

2.2.4.1 Kinetics of intermolecular exchange of 2,4-dimethyl-1,3-pentadiene with **2.8**

In addition to the observations regarding the exchange of complexed and uncomplexed C=C bonds of diene complexes **2.6** and **2.8** – **2.12** which argue against intermolecular pathways for C=C bond exchange, we sought to differentiate the two processes by independently determining the rate of an intermolecular exchange pathway. To this end, we measured the rate of 2,4-dimethyl-1,3-pentadiene exchange with **2.8** as a function of [2,4-dimethyl-1,3-pentadiene] in CD₂Cl₂ at 25 °C employing ¹H NMR line-broadening techniques.⁹⁶ Addition of 2,4-dimethyl-1,3-pentadiene (93 mM) to a solution of **2.8** (160 mM) in CD₂Cl₂ at 25 °C led to excess line broadening of the C3 vinylic proton resonance at δ 5.74 of $\Delta\nu_{1/2}(\text{excess}) = 4.0$ Hz, which corresponds to a first-order rate constant for exchange of $k_{\text{obs}} = \pi[\Delta\nu_{1/2}(\text{excess})] = 12.7$ s⁻¹ (Table 6). The linear relationship between k_{obs} and [2,4-dimethyl-1,3-pentadiene] over the concentration range 0.093–0.25 M indicated a second order process with a rate constant for intermolecular exchange of 2,4-dimethyl-1,3-pentadiene with **2.8** of $k_{\text{ex}} = 169 \pm 1$ M⁻¹s⁻¹ ($\Delta G_{298}^\ddagger = 14.40 \pm 0.01$ kcal mol⁻¹; Figure 18).

Table 6: Line-broadening data and observed rate constants (k_{obs}) for the exchange of the 2,4-dimethyl-1,3-pentadiene ligand of 2.8 ([2.8] = 161 mM) with free 2,4-Dimethyl-1,3-pentadiene in CD_2Cl_2 at 25 °C.

[2,4-dimethyl-1,3-pentadiene] (M)	$\Delta\nu_{1/2}$ (Hz)	$\Delta\nu_{1/2(\text{excess})}$ (Hz)	k_{obs} (s^{-1})
0.09	11.0	4.0	12.7
0.14	13.7	6.8	21.3
0.18	15.8	8.9	27.9
0.22	17.9	10.9	34.3
0.25	19.2	12.3	38.5

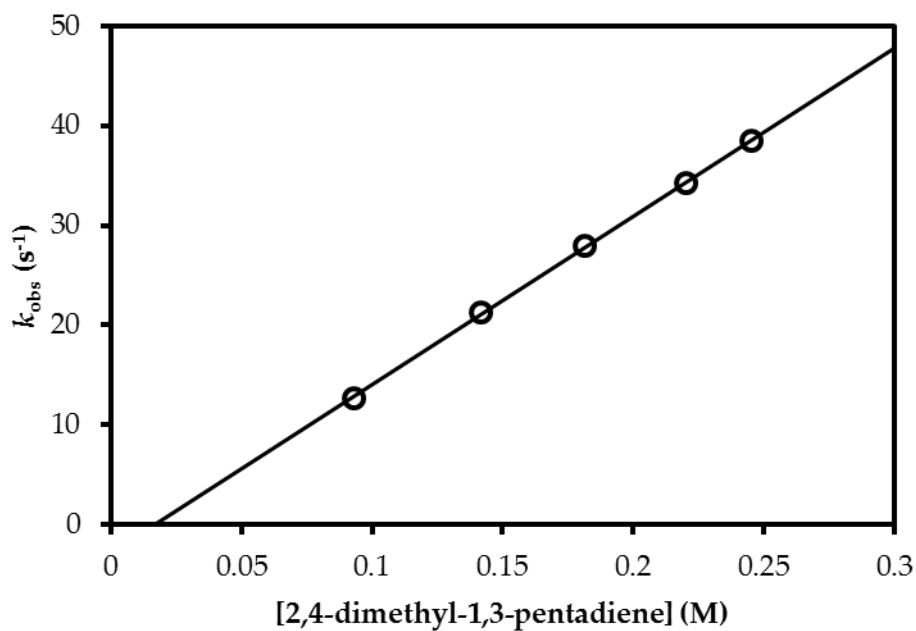


Figure 18: Plot of k_{obs} versus [2,4-dimethyl-1,3-pentadiene] for the intermolecular exchange of the 2,4-dimethyl-1,3-pentadiene ligand of 2.8 ([2.8] = 161 mM) with free 2,4-dimethyl-1,3-pentadiene from 93 to 245 mM at 25 °C in CD_2Cl_2 .

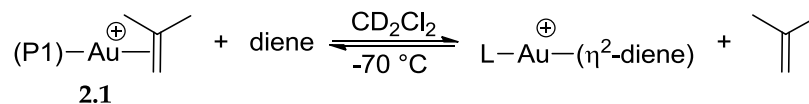
These data support an associative pathway for intermolecular diene exchange through the cationic, three-coordinate bis(η^2 -diene) intermediate $[(\text{P}1)\text{Au}(\eta^2\text{-H}_2\text{C}=\text{C}(\text{Me})\text{C}(\text{H})=\text{CMe}_2)_2]^+ \text{SbF}_6^-$. As expected, the energy barrier for intermolecular

diene exchange of 14.4 kcal mol⁻¹ is considerably higher than was observed for the intramolecular exchange of complexed and uncomplexed C=C bonds in complexes **2.9** – **2.12** ($\Delta G^\ddagger = 9.6$ – 11.9 kcal mol⁻¹). Additionally, the rate of intermolecular exchange of 2,4-dimethyl-1,3-pentadiene with **2.8** is only slightly lower than the rate of isobutylene exchange with [(P1)Au(η^2 -H₂C=CMe₂)]⁺SbF₆⁻ (**2.1**; $\Delta G^\ddagger_{298} = 15.0 \pm 0.01$ kcal mol⁻¹).⁴⁶

2.2.4.2 Relative binding affinities of dienes to gold(I)

In order to draw direct comparisons among the binding of conjugated dienes, aliphatic monoenes, and vinyl arenes, and also to determine the effect of diene substitution on the binding affinity of the dienes to gold(I), we sought to determine the relative binding affinities of conjugated dienes to the cationic 12-electron gold fragment [(P1)Au]⁺. To this end, equilibrium constants for the displacement of isobutylene from **2.1** with several diene ligands were measured in CD₂Cl₂ at -70 °C employing ¹H NMR analysis (Table 7). Of the diene ligands studied, only 1,3-cyclohexadiene displayed a higher binding affinity for gold than did isobutylene. The relative binding affinities of the dienes were only modestly sensitive to substitution and/or conjugation and decreased by a factor of ~13 in the order 1,3-cyclohexadiene > 2,4-dimethyl-1,3-pentadiene > 1,4-cyclohexadiene > 2,3-dimethyl-1,3-butadiene > *trans*-1,3-pentadiene (Table 7). Furthermore, addition of butadiene to a solution of **2.1** in CD₂Cl₂ at -70 °C led to no detectable formation of butadiene complex **2.9**, suggesting that 1,3-butadiene binds less tightly to gold than does *trans*-1,3-pentadiene.

Table 7: Equilibrium constants for displacement of isobutylene from [(P1)Au(η^2 -H₂C=CMe₂)]⁺ SbF₆⁻ (2.1) with dienes in CD₂Cl₂ at -70 °C.



diene	K_{eq}
1,3-cyclohexadiene	1.21 ± 0.05
2,4-dimethyl-1,3-pentadiene	0.93 ± 0.06
1,4-cyclohexadiene	0.6 ± 0.2
2,3-dimethyl-1,3-butadiene	0.14 ± 0.02
<i>trans</i> -1,3-pentadiene	0.09 ± 0.01
1,4-butadiene ^a	< 0.09

^aNo bound diene was observed under experimental conditions.

We have previously shown that aliphatic monoenes displayed significantly higher binding affinities to gold(I) than did vinyl arenes, presumably due to the electron-withdrawing nature of the sp² substituent of the vinyl arenes.⁴⁶ For example, the relative binding affinity of isobutylene exceeded that of styrene by a factor of ~60 at -60 °C ($\Delta G = 1.73 \text{ kcal mol}^{-1}$). In contrast, comparison of the relative binding affinities of 1,3-cyclohexadiene ($K_{\text{eq}} = 1.21 \pm 0.05$) and 1,4-cyclohexadiene ($K_{\text{eq}} = 0.60 \pm 0.2$) points to conjugation as a nominally stabilizing feature of gold π -diene complexes. Just as the binding affinities of *p*-substituted vinyl arenes to the cationic gold fragment [(P1)Au]⁺ increased significantly with the increasing electron density of the aryl group, the relative binding affinity of acyclic, C1-unsubstituted diene ligands increased with increasing substitution at the uncomplexed C4 carbon atom in the order 1,3-butadiene < *trans*-1,3-

pentadiene < 2,4-dimethyl-1,3-pentadiene. This observation further supports the bonding model of conjugated dienes to cationic gold(I) involving stabilization of the gold π -interaction through donation of electron density from the uncomplexed C=C bond to the complexed C=C bond of the diene ligand, as was also suggested by ^{13}C NMR analysis of cationic gold η^2 -diene complexes.

2.3 Conclusions and contemporary work

2.3.1 Experimental conclusions from this work

A number of binding modes have been proposed for cationic gold(I) π -(1,3-diene) complexes. While other transition metals predominantly form η^4 -diene complexes, monomeric and polymeric η^2 -complexes of 1,3-dienes are known. To better understand the binding of gold(I) to 1,3-dienes, we have synthesized seven cationic gold π -diene complexes that contain the sterically hindered $\text{P}(t\text{-Bu})_2\text{O}$ -biphenyl ligand. These complexes have been characterized by variable-temperature NMR spectroscopy and, in four cases, by X-ray crystallography. All evidence points to formation of gold(I) η^2 -diene complexes both in solution and in the solid state. The η^2 -coordination of the diene ligands, as opposed to η^4 -coordination, is not surprising owing to the pronounced tendency of gold(I) to form two-coordinate 14-electron complexes, rather than three-coordinate, 16-electron complexes.^{27-28, 97}

Both in solution and in the solid state, dienes that contain dissimilarly substituted C=C bonds bind to gold(I) selectively through the less substituted C=C

bond. This observation is seemingly contradictory to previous studies of gold π -alkene complexes, which reported that the binding affinity of an alkene ligand for $[(L)Au]^+$ increases with increasing alkyl substitution at gold.^{42, 46} However, analysis of the ^{13}C NMR chemical shifts of the bound diene ligands and of diene binding affinities for the complexes reported herein points to stabilization of the gold π -diene interaction through donation of electron density from the uncomplexed C=C bond to the complexed C=C bond of the gold(I) π -diene complex. Thus, electronic difference between the two alkenes of the 1,3-diene ligand is minimized, and complexes of the less substituted alkene are favored, possibly due to sterics.

Variable-temperature NMR analysis established the fluxional behavior of cationic gold(I) π -diene complexes involving the facile ($\Delta G^\ddagger = 9.6\text{--}11.9$ kcal mol⁻¹) intramolecular exchange of the complexed and uncomplexed C=C bonds of the diene ligand, presumably involving 16-electron gold η^4 -diene intermediates and transition states. The energy barrier for this process is significantly lower than that measured for the intermolecular, associative exchange of 2,4-dimethyl-1,3-pentadiene with complex **2.8** ($\Delta G_{298}^\ddagger = 14.40 \pm 0.01$ kcal mol⁻¹) and that reported for isobutylene exchange with **2.1** ($\Delta G_{298}^\ddagger = 15.0 \pm 0.01$ kcal mol⁻¹).⁴⁶

2.3.2 Contemporary work on the characterization of gold π -diene complexes

Concurrent with the publication of the results included in this chapter, Russell *et al* reported the synthesis and characterization of a similar family of cationic gold(I)

π -diene complexes of the form $[(L)Au(\eta^2\text{-diene})]^+ SbF_6^-$ [$L = P1$, diene = 2,5-dimethyl-2,4-hexadiene (**2.13**), 2,3-dimethoxy-1,3-butadiene; $L = tBu_3P$, diene = 2,3-dimethyl-1,3-butadiene].⁸⁷⁻⁸⁸ The following year, corresponding complexes of 1,3-cyclopentadiene and 1,3-cyclohexadiene were reported from the same group.⁸⁹

While an in-depth summary of the structural features reported for these complexes would be redundant, several of the reported observations add to our general understanding of binding in gold(I) π -diene complexes. For example, **2.13** has three possible η^2 -coordination modes: one in which the $[(L)Au]^+$ fragment is bound symmetrically to one of the two equivalent alkenes of the 2,5-dimethyl-2,4-hexadiene ligand (**2.13a**), one in which gold is slipped toward the more substituted C2 alkene terminus and electron density is donated from the uncomplexed C4=C5 to the complexed C2=C3 (**2.13b**), and one in which gold is slipped toward the less substituted C3 terminus of the complexed C2=C3 and no donation from the uncomplexed alkene occurs (**2.13c**) (Figure 19). X-ray crystallographic analysis of **2.13** suggests that the complex in the solid state adopts a structure in which gold is slipped toward the less substituted C3 alkene terminus ($Au-C2 = 2.335(3) \text{ \AA}$, $Au-C3 = 2.270(3) \text{ \AA}$) as in **2.13c**. Unfortunately, equilibration of the complexed and uncomplexed alkene units of the 2,5-dimethyl-2,4-hexadiene ligand of **2.13**, presumably due to facile intramolecular π -face exchange, precluded spectroscopic solution characterization, even at $-90 \text{ }^\circ\text{C}$.

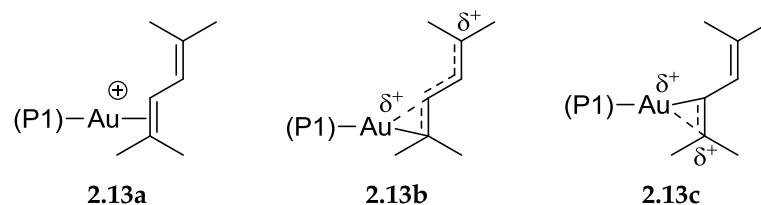
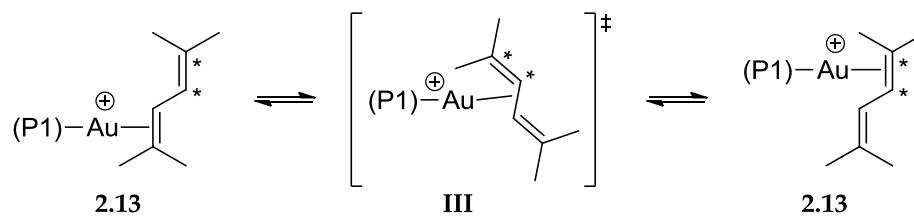


Figure 19: Potential η^2 -coordination modes of the 2,5-dimethyl-2,4-hexadiene ligand in complex 2.13

On the basis of their experimental observations and DFT computation, Russell and coworkers proposed a pathway for intramolecular π -face exchange in **2.13** that involves gold “gliding” between the two alkene units through the transition state **III** in which gold is η^2 -bound to the central C3–C4 bond (Scheme 9). This proposal is an alternative to the associative pathway described above which proceeds through a gold η^4 -diene intermediate or transition state (Scheme 8). While neither pathway is supported directly by experimental evidence, circumstantial support of either can be provided. For example, the “gliding” pathway requires conjugation of the exchanging alkenes, while the associative mechanism does not. We have shown that the rate of intramolecular π -face exchange in the conjugated 1,3-cyclohexadiene ligand of **2.11** and in the non-conjugated 1,4-cyclohexadiene ligand of **2.12** proceed with approximately the same energy barrier, suggesting that the exchange process is very similar between these two complexes. On the other hand, the presence of time-averaged resonances corresponding to rapidly equilibrating alkenes in the ^{13}C NMR spectrum 2,5-dimethyl-2,4-hexadiene ligand of **2.13** at $-90\text{ }^\circ\text{C}$ suggests that intramolecular π -face exchange is faster in this complex than in complexes **2.9** – **2.11**. This rate can be explained by the gliding pathway,

as the [(P1)Au]⁺ unit is already slipped significantly towards an η¹-bond with the C3 alkene terminus in **2.13**, while in **2.9 – 2.11**, [(P1)Au]⁺ is slipped toward C1 and away from the central C2–C3 bond.

Scheme 9: Proposed mechanism for intramolecular π-face exchange in complex 2.13



2.4 Experimental

2.4.1 General methods

Reactions were performed under a nitrogen atmosphere employing standard Schlenk and glovebox techniques unless specified otherwise. Elemental analysis was performed by Complete Analysis Laboratories (Parsippany, NJ). NMR spectra were obtained on a Varian spectrometer operating at 500 MHz for ¹H NMR, 125 MHz for ¹³C NMR, 470 MHz for ¹⁹F NMR, and 202 MHz for ³¹P NMR in CD₂Cl₂ at room temperature with noted exceptions. Methylene chloride was purified by passage through columns of activated alumina under nitrogen. CDCl₃ and CD₂Cl₂ were dried over CaH₂ prior to use. [(P1)Au(η²-H₂C=CMe₂)]⁺SbF₆⁻ (**2.1**) was synthesized using a published procedure.⁴⁶ (P1)AuCl, AgSbF₆, hexanes, 4-methylpentadiene, *trans*-1,3-pentadiene, 2,4-dimethyl-1,3-pentadiene, 1,3-butadiene, 2,3-dimethyl-1,3-butadiene, 1,3-cyclohexadiene, 1,4-cyclohexadiene, and isobutylene were purchased from major chemical suppliers and

used as received. Line shape analysis was performed using WINDNMR-Pro.⁹⁸ NMR probe temperatures were calibrated using a neat methanol thermometer.

2.4.2 Synthesis of Gold(I) η^2 -Diene Complexes

[(P1)Au(η^2 -(*E*)-H₂C=C(H)C(H)=C(H)Me)]⁺ SbF₆⁻ (2.6) A mixture of (P1)AuCl (40 mg, 7.5×10^{-2} mmol), AgSbF₆ (26 mg, 7.5×10^{-2} mmol), and *trans*-1,3-pentadiene (51 mg, 0.75 mmol) was dissolved in CH₂Cl₂ (2 mL), forming a white suspension. The suspension was stirred in a sealed flask in the dark at room temperature for 6 h, then filtered through Celite. Volatile material was evaporated under vacuum to give **2.6** as a white solid (56 mg, 93%). ¹H NMR (30 °C): δ 7.92–7.86 (m, 1 H), 7.67–7.54 (m, 5 H), 7.32–7.18 (m, 3 H), 6.51 (ddd, $J = 9.0, 10.5, 16.0$ Hz, 1 H), 6.26 (qd, $J = 7.0, 13.5$ Hz, 1 H), 5.99 (ddd, $J = 1.0, 10.5, 14.5$ Hz, 1 H), 4.17 (d, $J = 16.5$ Hz, 1 H), 4.11 (d, $J = 8.5$ Hz, 1 H), 1.91 (dd, $J = 1.0, 7.0$ Hz, 3 H), 1.38 (d, $J = 16.0$ Hz, 18 H). ¹³C NMR (-80 °C): δ 147.4 (d, $J = 13.9$ Hz), 144.3, 142.6 (d, $J = 7.4$ Hz), 137.3, 133.5, 132.6 (d, $J = 7.4$ Hz), 131.0, 129.0, 129.0, 128.8, 128.3, 127.6 (d, $J = 7.4$ Hz), 127.3, 123.7 (d, $J = 47.3$ Hz), 90.6, 37.0 (d, $J = 23.5$ Hz), 36.9 (d, $J = 23.6$ Hz), 29.6 (br s), 18.4. ³¹P{¹H} NMR: δ 65.9 Anal. Calcd (found) for C₂₅H₃₅AuF₆PSb: H, 4.32 (4.41); C, 37.46 (37.57).

The ¹H NMR resonances corresponding to the vinylic protons of the *trans*-1,3-pentadiene ligand of **2.6** were unambiguously assigned as follows from analysis of the ³J_{HH} coupling constants in the 1-D ¹H NMR spectrum: δ 6.51 (ddd, $J = 9.0, 10.5, 16.0$ Hz, H2), 6.26 (qd, $J = 7.0, 13.5$ Hz, H4), 5.99 (ddd, $J = 1.0, 10.5, 14.5$ Hz, H3), 4.17

(d, $J = 16.5$ Hz, H1_{cis}), 4.11 (d, $J = 8.5$ Hz, H1_{trans}), 1.91 (dd, $J = 1.0, 7.0$ Hz, H5). The ^{13}C NMR resonances corresponding to the carbon atoms of the *trans*-1,3-pentadiene ligand of **2.6** were unambiguously assigned as follows from the 2-D HMQC spectrum (Figure 20): δ 144.5 (C4), 138.1 (C2), 128.2 (C3), 92.1 (C1), 18.2 (C5).

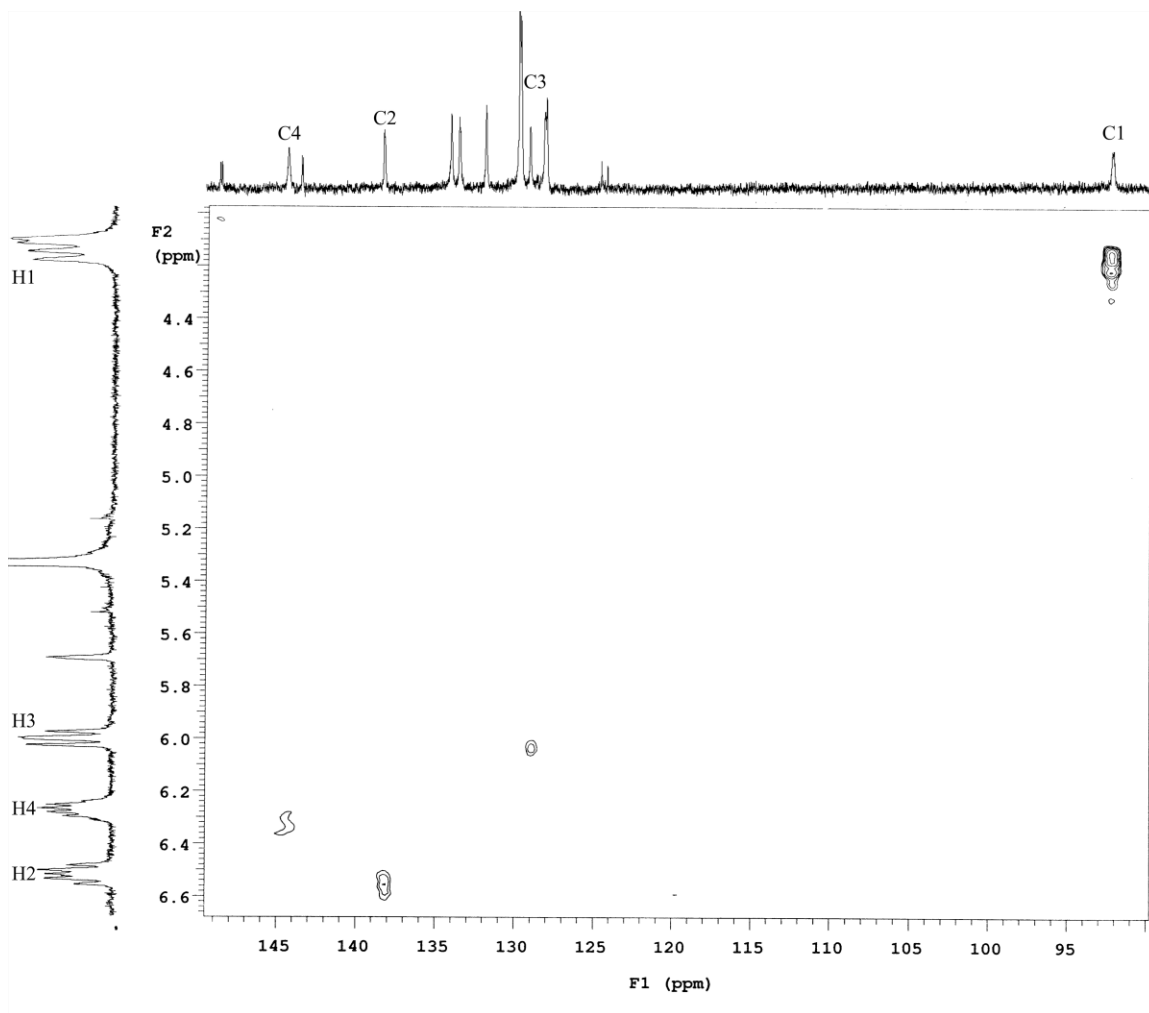


Figure 20: Partial HMQC spectrum of **2.6** at 25 °C.

$[(\text{P1})\text{Au}(\eta^2\text{-H}_2\text{C}=\text{C}(\text{H})\text{C}(\text{H})=\text{CMe}_2)]^+\text{SbF}_6^-$ (**2.7**) A mixture of (P1)AuCl (40 mg, 7.5×10^{-2} mmol), AgSbF₆ (26 mg, 7.5×10^{-2} mmol), and 4-methyl-1,3-pentadiene (12 mg,

0.15 mmol) was dissolved in CH₂Cl₂ (2 mL), forming a white suspension. The suspension was stirred in a sealed flask in the dark at room temperature for 6 h, then filtered through a plug of Celite, eluting with CH₂Cl₂. The filtrate was concentrated to ~2 mL, diluted with hexanes (2 mL), and cooled at 4 °C overnight to form **2.7** (50 mg, 82%) as a white solid. ¹H NMR (25 °C): δ 7.95–7.91 (m, 1 H), 7.70–7.60 (m, 5 H), 7.35–7.22 (m, 3 H), 6.81 (ddd, *J* = 8.5, 11.5, 16.0 Hz, 1 H), 5.85 (d, *J* = 11.5 Hz, 1 H), 4.13 (d, *J* = 16.0 Hz, 1 H), 4.08 (d, *J* = 8.0 Hz, 1 H), 1.97 (s, 3 H), 1.95 (s, 3 H), 1.40 (d, *J* = 16.5 Hz, 18 H). ¹³C{¹H} NMR (25 °C): δ 153.1, 148.8 (d, *J* = 13.7 Hz), 143.7 (d, *J* = 6.3 Hz), 134.9, 134.3, 133.7 (d, *J* = 7.5 Hz), 132.1, 130.0, 129.8, 128.4 (d, *J* = 6.2 Hz), 128.3, 124.7 (d, *J* = 46.3 Hz), 123.5, 90.6 (d, *J* = 15.0 Hz), 38.6 (d, *J* = 23.7 Hz), 30.8 (d, *J* = 7.5 Hz), 26.4, 19.5. ³¹P{¹H} NMR: δ 67.3. Anal. Calcd (found) for C₂₆H₃₇AuF₆PSb: H, 4.59 (4.70); C, 38.40 (38.42).

The diene ¹H NMR resonances of complex **2.7** were assigned as follows from analysis of the ³*J*_{HH} coupling constants in the ¹H NMR spectrum and from the diagnostic upfield shift of the H1 protons: δ 6.81 (ddd, *J* = 8.5, 11.5, 16.0 Hz, 1 H, *H*₂), 5.85 (d, *J* = 11.5 Hz, 1 H, *H*₃), 4.13 (d, *J* = 16.0 Hz, 1 H, *H*_{1_{cis}}), 4.08 (d, *J* = 8.0 Hz, 1 H, *H*_{1_{trans}}). The diene ¹³C NMR resonances of complex **2.7** were assigned by analogy to the chemical shift behavior displayed by complexes **2.6**, **2.8**, **2.9**, and **2.11**. In addition, the C1 diene carbon resonance of **2.7** was assigned on the basis of the diagnostic phosphorous–carbon coupling observed for this resonance.

[(P1)Au(η^2 -H₂C=C(Me)C(H)=CMe₂)]⁺SbF₆⁻ (2.8**)** Complex **2.8** was isolated as a white solid (62 mg, 100%) from the reaction of 2,4-dimethyl-1,3-pentadiene, (P1)AuCl, and AgSbF₆ employing a procedure similar to that used to synthesize **2.7**. ¹H NMR (25 °C): δ 7.93–7.88 (m, 1 H), 7.65–7.55 (m, 5 H), 7.28–7.20 (m, 3 H), 5.04 (s, 1 H), 3.89 (d, J = 3.5 Hz, 1 H), 3.81 (d, J = 4.0 Hz, 1 H), 2.27 (s, 3 H), 1.96 (s, 3 H), 1.92 (s, 3 H), 1.37 (d, J = 16.5 Hz, 18 H). ¹³C{¹H} NMR (25 °C): δ 158.7, 149.4, 148.8 (d, J = 13.8 Hz), 143.7 (d, J = 7.5 Hz), 134.3 (d, J = 2.5 Hz), 133.8 (d, J = 7.5 Hz), 132.0 (d, J = 2.5 Hz), 130.0, 129.8, 128.3 (d, J = 7.5 Hz), 128.3, 125.1 (d, J = 5.0 Hz), 124.8 (d, J = 47.5 Hz), 91.7 (d, J = 16.3 Hz), 37.8 (d, J = 22.5 Hz), 30.7 (d, J = 6.2 Hz), 28.8, 28.0, 21.3. ³¹P{¹H} NMR: δ 67.5. Anal. Calcd (found) for C₂₇H₃₉AuF₆PSb: H, 4.68 (4.75); C, 39.09 (39.20).

The ¹H NMR resonances corresponding to the vinylic protons of the 2,4-dimethyl-1,3-pentadiene ligand of **2.8** were assigned as follows from the diagnostic upfield shifts of the H1 protons in the 1-D ¹H NMR spectrum: δ 5.04 (s, H3), δ 3.89 (d, J = 3.5 Hz, H1) and 3.81 (d, J = 4.0 Hz, H1); the three methyl resonances at δ 2.27, 1.96, and 1.92 were not distinguished. Assignment of the ¹³C NMR resonances corresponding to the 2,4-dimethyl-1,3-pentadiene ligand of **2.8** was determined through 2-D HMBC analysis (Figure 21). The resonances at δ 91.5 and 158.1 showed cross peaks to H3 and one methyl group at δ 2.27, confirming their assignments as C1 and C2, respectively; this also confirmed the δ 2.27 resonance as the C2 methyl group and the δ 1.96, and 1.92 resonances as the C4 methyl groups. The absence of the anticipated C2–H1 correlation

precluded distinction between C1 and C2 by HMBC analysis. However, the resonance at δ 91.5 was identified as C1 owing to the diagnostic phosphorous–carbon coupling constant of $J_{CP} = 16.3$ Hz. The ^{13}C resonance at δ 122.6 displayed correlation with the H1 vinyl protons and all three methyl groups, establishing this resonance as C3. The ^{13}C resonance at δ 149 showed a weak correlation to H3 and strong correlations to the protons of both C4 methyl groups, establishing this resonance as C4.

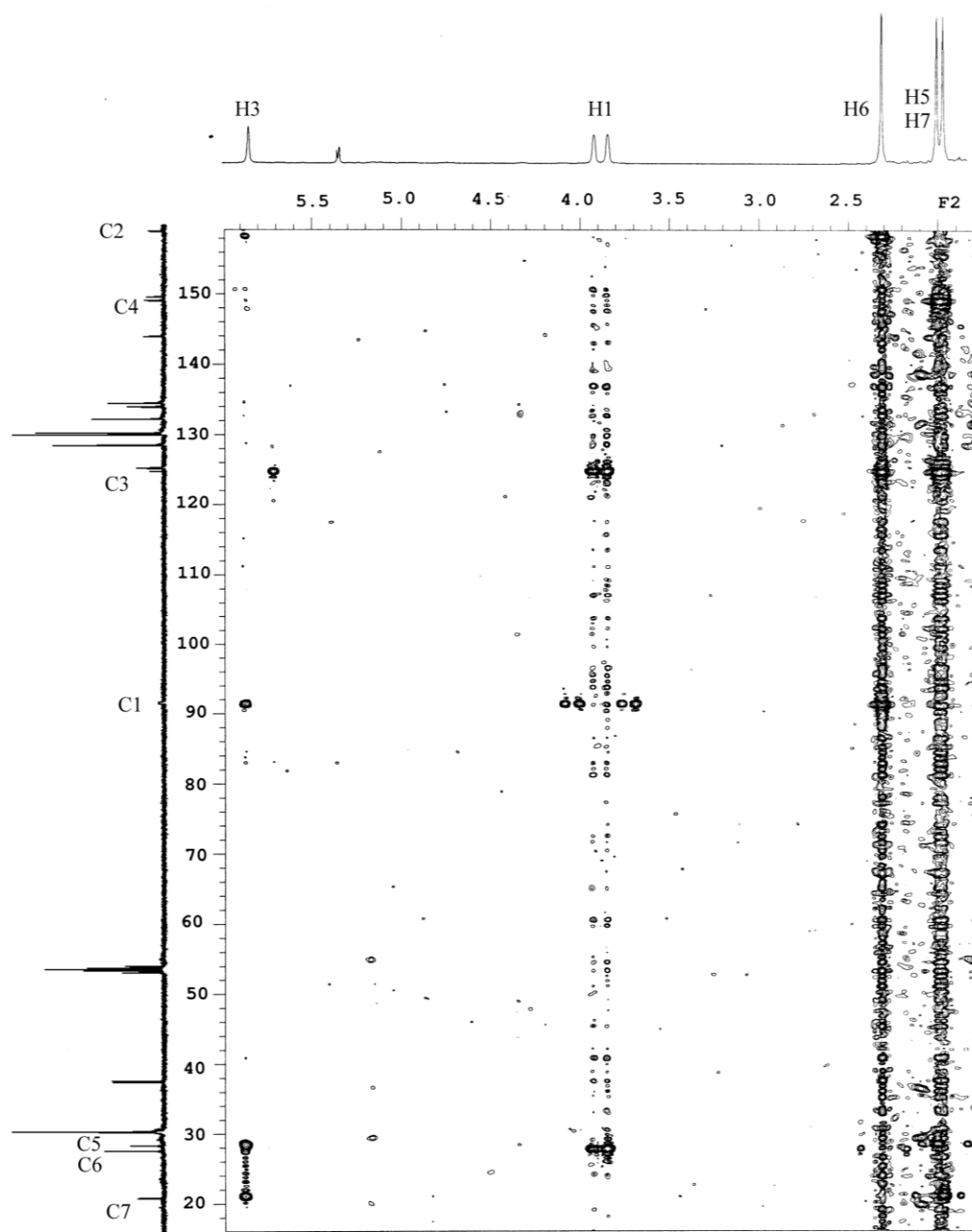


Figure 21: Partial HMBC of 2.8 in CD_2Cl_2 at 25 °C.

$[(\text{P1})\text{Au}(\eta^2\text{-H}_2\text{C}=\text{C}(\text{H})\text{C}(\text{H})=\text{CH}_2)]^+\text{SbF}_6^-$ (2.9) Methylene chloride (2 mL) was added to a mixture of $(\text{P1})\text{AuCl}$ (40 mg, 7.5×10^{-2} mmol) and AgSbF_6 (26 mg, 7.5×10^{-2} mmol).

² mmol) under 1,3-butadiene atmosphere. 1,3-Butadiene was bubbled through the resulting suspension with stirring for 6 h at room temperature in the dark. The resulting suspension was filtered through Celite, and volatile material was evaporated under vacuum to give **2.9** (55 mg, 93%) as a white solid. ¹H NMR (-90 °C): δ 7.84–7.78 (m, 1 H), 7.59–7.52 (m, 5 H), 7.21–7.13 (m, 3 H), 6.48 (td, *J* = 10, 17.8 Hz, 1 H), 6.18 (td, *J* = 10, 17.0 Hz, 1 H), 5.66 (d, *J* = 16.8 Hz, 1 H), 5.56 (d, *J* = 9.8 Hz, 1 H), 4.11 (d, *J* = 16.0 Hz, 1 H), 3.93 (br dd, *J* = 4.1, 7.2 Hz, 1 H), 1.26 (d, *J* = 16.7 Hz, 18 H). ¹³C{¹H} NMR (-90 °C): δ 147.2 (d, *J* = 12.5 Hz), 142.5 (d, *J* = 7.5 Hz), 134.7 (d, *J* = 2.5 Hz), 133.5 (d, *J* = 2.5 Hz), 133.3, 132.4 (d, *J* = 7.5 Hz), 130.9 (d, *J* = 1.2 Hz), 129.1, 129.1, 128.9, 128.6, 128.5, 127.6 (d, *J* = 6.9 Hz), 127.3, 123.5 (d, *J* = 47.2 Hz), 94.9 (d, *J* = 12.6 Hz), 36.8 (d, *J* = 23.4 Hz), 36.5 (d, *J* = 23.6 Hz), 29.5. ³¹P{¹H} NMR: δ 63.3. Anal. Calcd (found) for C₂₄H₃₃AuF₆PSb: H, 4.24 (4.33); C, 36.71 (36.67).

The pairs of protons, H₂/H₃, H₁_{trans}/H₄_{trans}, and H₁_{cis}/H₄_{cis} were unambiguously assigned based on analysis of splitting patterns in the slow-exchange 1-D ¹H NMR spectrum (-90 °C) and from the coalescence of each of these pairs of protons in the variable temperature NMR spectra (Figure 14). The protons of **2.9** were further grouped as either H₁_{cis}/H₁_{trans}/H₂ or H₄_{cis}/H₄_{trans}/H₃ from low temperature (-90 °C) ¹H–¹H COSY analysis (Figure 22). The two sets of protons are distinguished by the strong upfield shifts of the H₁ protons (δ 4.11 and 3.93) and through HMQC correlation to the C₁ carbon atom (see below). The ¹³C resonance at δ 94.9 was assigned as C₁ from the large

phosphorous-carbon coupling constant of $J_{CP} = 12.6$ Hz. From this assignment and the low temperature (-90 °C) HMQC spectrum (Figure 23), all of the diene carbon and proton resonances were assigned as follows from. ^1H : δ 6.48 (td, $J = 10, 17.8$ Hz, 1 H, H_2), 6.18 (td, $J = 10, 17.0$ Hz, 1 H, H_3), 5.66 (d, $J = 16.8$ Hz, 1 H_{4cis}), 5.56 (d, $J = 9.8$ Hz, 1 H, H_{4trans}), 4.11 (d, $J = 16.0$ Hz, 1 H, H_{1cis}), 3.93 (br dd, $J = 4.1, 7.2$ Hz, 1 H, H_{1trans}); ^{13}C : δ 133.5 (d, $J = 2.5$ Hz, C2), 133.3 (C3), 128.6 (C4), 94.9 (d, $J = 12.6$ Hz, C1).

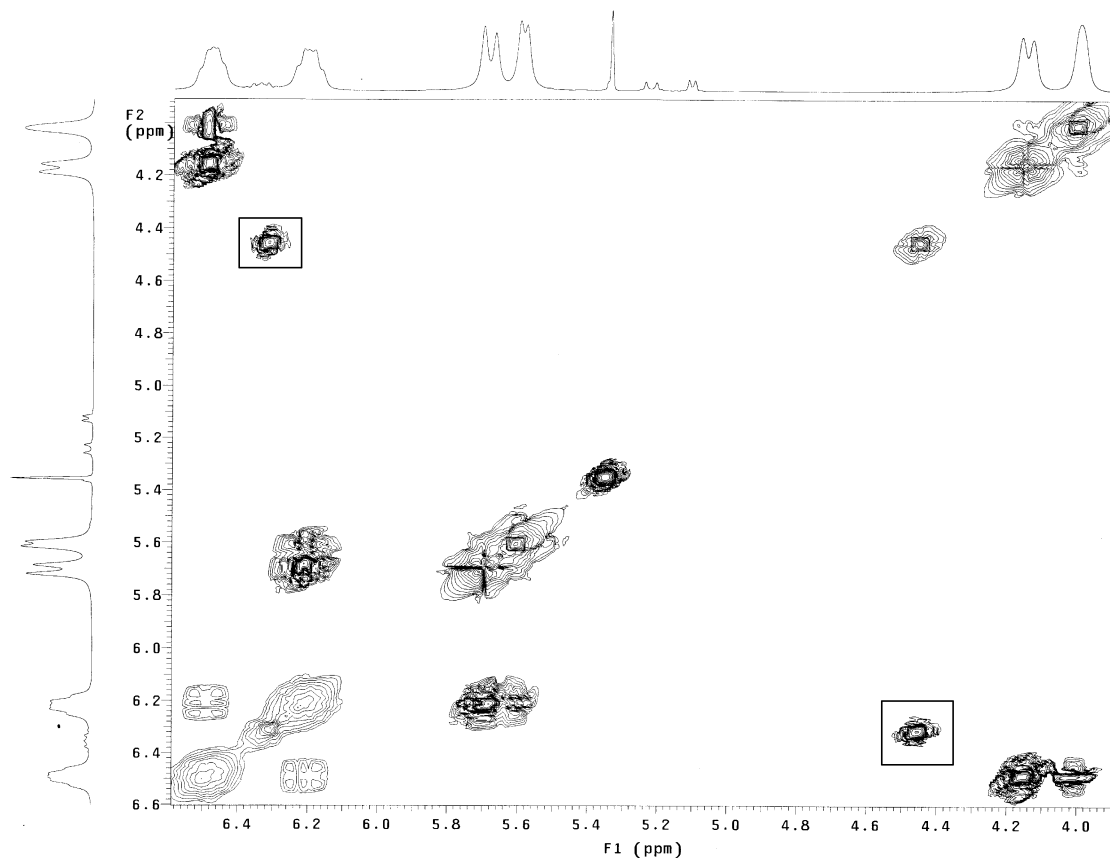


Figure 22: Partial ^1H - ^1H COSY spectrum of 2.9 in CD_2Cl_2 at -90 °C. The cross-peak at δ $4.4 \times \delta$ 6.3 (indicated with boxes) corresponds to a pair of strongly coupled protons in an impurity that is undetected in the 1-D NMR spectra. Repeated concentration/dissolution of pure samples of 2.9 leads to the appearance of resonances

in the ^1H NMR spectrum at δ 6.3, 4.45, 3.2. A wider expansion of the COSY spectrum of 2.9 also shows a crosspeak between the δ 6.3 and 3.2 resonances.

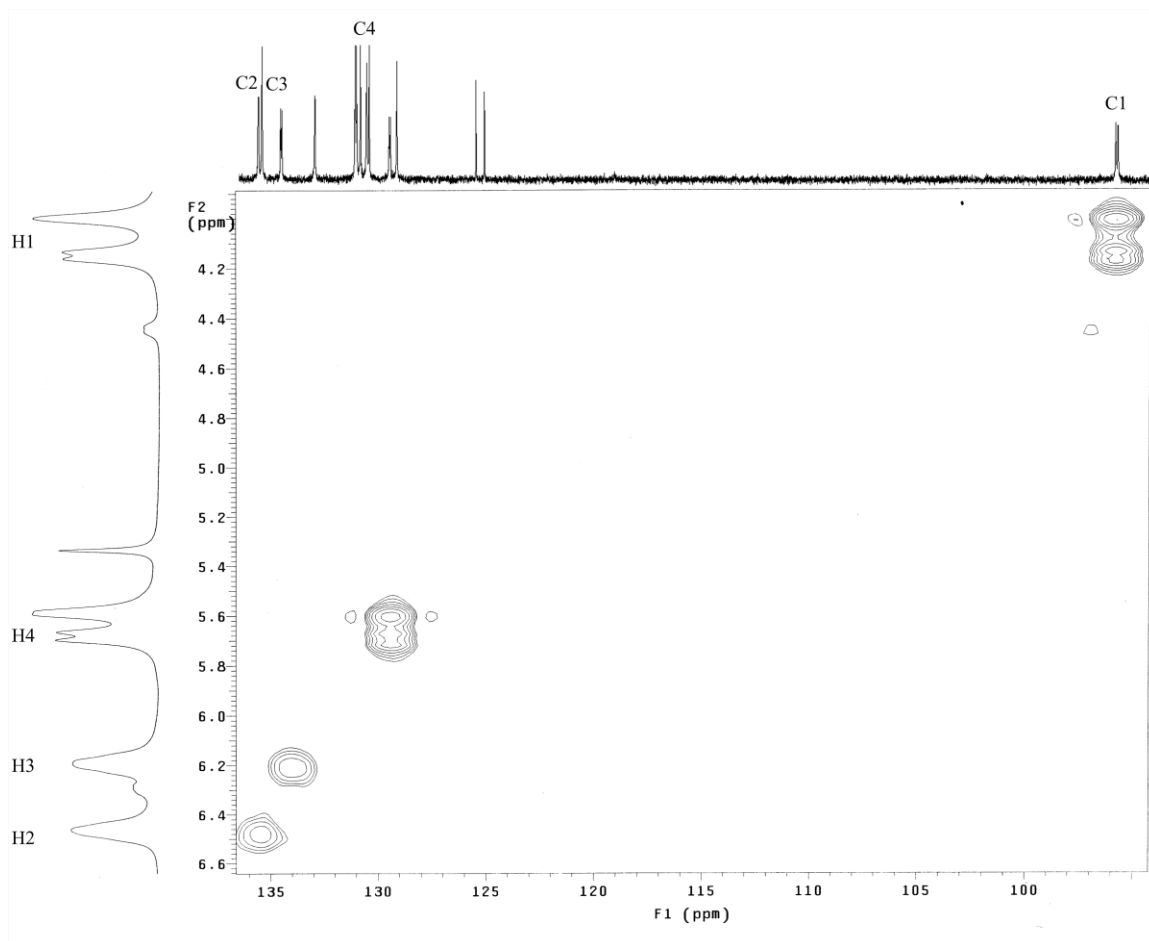


Figure 23: Partial HMQC of 2.9 in CD_2Cl_2 at -90 °C.

$[(\text{P}1)\text{Au}(\eta^2\text{-H}_2\text{C}=\text{C}(\text{Me})\text{C}(\text{Me})=\text{CH}_2)]^+\text{SbF}_6^-$ (**2.10**) Complex **2.10** was isolated as a white solid (56 mg, 92%) from the reaction of 2,3-dimethyl-1,3-butadiene with $(\text{P}1)\text{AuCl}$ and AgSbF_6 employing a procedure similar to that used to synthesize **2.6**. ^1H NMR (-50 °C): δ 7.90–7.85 (m, 1 H), 7.67–7.58 (m, 5 H), 7.26–7.20 (m, 3 H), 5.65 (s, 1 H), 5.48 (s, 1 H), 3.99 (br d, $J = 3.5$ Hz, 1 H), 3.64 (br d, $J = 4.0$ Hz, 1 H), 2.25 (s, 3 H), 1.74 (s, 3 H), 1.36 (d, $J = 16.5$ Hz, 9 H), 1.25 (d, $J = 17.0$ Hz, 9 H). $^{13}\text{C}\{^1\text{H}\}$ NMR (-60 °C): δ 154.7,

147.6 (d, $J = 15.0$ Hz), 143.1 (d, $J = 7.5$ Hz), 140.2, 133.7, 132.9 (d, $J = 6.3$ Hz), 131.3, 129.5, 129.4, 129.3, 128.9, 127.8 (d, $J = 7.5$ Hz), 127.7, 124.2, 123.9 (d, $J = 47.5$ Hz), 91.9 (d, $J = 15.0$ Hz), 36.4 (d, $J = 23.7$ Hz), 36.2 (d, $J = 23.7$ Hz), 30.2 (d, $J = 5.0$ Hz), 29.5 (d, $J = 6.2$ Hz), 24.0, 20.1. $^{31}\text{P}\{^1\text{H}\}$ NMR (-60 °C): δ 63.5. Anal. Calcd (found) for $\text{C}_{26}\text{H}_{37}\text{AuF}_6\text{PSb}$: H, 4.59 (4.52); C, 38.40 (38.46).

The diene ^1H NMR resonances of complex **2.10** were assigned as follows from the diagnostic upfield shift of the H1 protons: δ 5.65 (s, 1 H, *H4*), 5.48 (s, 1 H, *H4*), 3.99 (br d, $J = 3.5$ Hz, 1 H, *H1*), 3.64 (br d, $J = 4.0$ Hz, 1 H, *H1*). The diene ^{13}C NMR resonances of complex **2.10** were assigned by analogy to the chemical shift behavior displayed by complexes **2.6**, **2.8**, **2.9**, and **2.11**. In addition, the C1 diene carbon resonance of **2.10** was assigned on the basis of the diagnostic phosphorous–carbon coupling observed for this resonance.

$[(\text{P1})\text{Au}(\eta^2\text{-}\overline{\text{C}(\text{H})=\text{C}(\text{H})\text{C}(\text{H})=\text{C}(\text{H})\text{CH}_2\text{CH}_2})]^+ \text{SbF}_6^-$ (**2.11**) Complex **2.11** was isolated as a white solid (61 mg, 100%) from the reaction of 1,3-cyclohexadiene with $(\text{P1})\text{AuCl}$ and AgSbF_6 following the procedure used to synthesize **2.6**. ^1H NMR (-70 °C): δ 7.86–7.79 (m, 1 H), 7.61–7.52 (m, 5 H), 7.26–7.18 (m, 3 H), 6.18 (br s, 1 H), 6.01 (br s, 1 H), 5.59 (br s, 1 H), 5.13 (br s, 1 H), 2.46–2.31 (m, 3 H), 2.21–2.08 (m, 1 H), 1.32 (d, $J = 16.5$ Hz, 9 H), 1.28 (d, $J = 16.5$ Hz, 9 H). $^{13}\text{C}\{^1\text{H}\}$ NMR (-70 °C): δ 147.4 (d, $J = 13.2$ Hz), 142.6 (d, $J = 6.5$ Hz), 136.4, 133.5, 132.5 (d, $J = 7.2$ Hz), 131.0, 129.3, 129.1, 128.7, 128.5, 127.5 (d, $J = 6.6$ Hz), 127.2, 123.4, 123.0 (d, $J = 5.0$ Hz), 121.1, 117.4 (d, $J = 6.2$ Hz), 114.6 (d, $J = 8.3$ Hz),

37.4 (d, $J = 24.0$ Hz), 37.2 (d, $J = 23.8$ Hz), 29.8 (d, $J = 15.2$ Hz), 24.4, 21.7. $^{31}\text{P}\{^1\text{H}\}$ NMR (-70 °C): δ 61.9. Anal. Calcd (found) for $\text{C}_{26}\text{H}_{35}\text{AuF}_6\text{PSb}$: H, 4.35 (4.43); C, 38.49 (38.44).

The vinyl proton resonances in the slow exchange ^1H NMR spectrum of **2.11** were assigned based on COSY analysis at -85 °C (Figure 24). Cross peaks between proton resonances at δ 6.18 and 5.13 and between each of these resonances and the allylic proton multiplets at δ 2.5 and 2.1 established the δ 6.18 and 5.13 resonances as the H1/H4 pair, with the upfield resonance at δ 5.13 assigned to H1 and the downfield resonance at δ 6.18 assigned to H4, based on analogy to complexes **2.6**, **2.7** and **2.8**. Cross peaks between the resonances at δ 6.01 and 5.59 and the absence of cross peaks between these resonances and the allylic protons established the δ 6.0 and 5.59 resonances as the H2/H3 pair. A cross peak between the δ 5.59 and δ 5.13 resonances therefore established δ 5.59 as H2 while a cross peak between the δ 6.18 and δ 6.01 resonances established δ 6.01 as H3. In the ^{13}C NMR spectrum of **2.11** at -85 °C, resonances at δ 114.7 (δ , $J = 8.2$ Hz) and δ 117.4 (d, $J = 6.0$ Hz) were assigned as the C1/C2 pair based on their ^{13}C - ^{31}P coupling with the δ 114.7 assigned to C1 on the basis of the larger J_{PC} . As the solution was warmed, the C1 resonance at δ 114.7 coalesced with the resonance at δ 136.4, forming a broad singlet at $\delta \sim 126$ at 27 °C (Figure 25). Likewise, the C2 resonance at δ 117.4 coalesced with the resonance at δ 121.3, forming a singlet at δ 120 at 27 °C. From this temperature-dependent behavior, we assign the resonance at δ 136.4 as C4 and the resonance at δ 121.3 as C3.

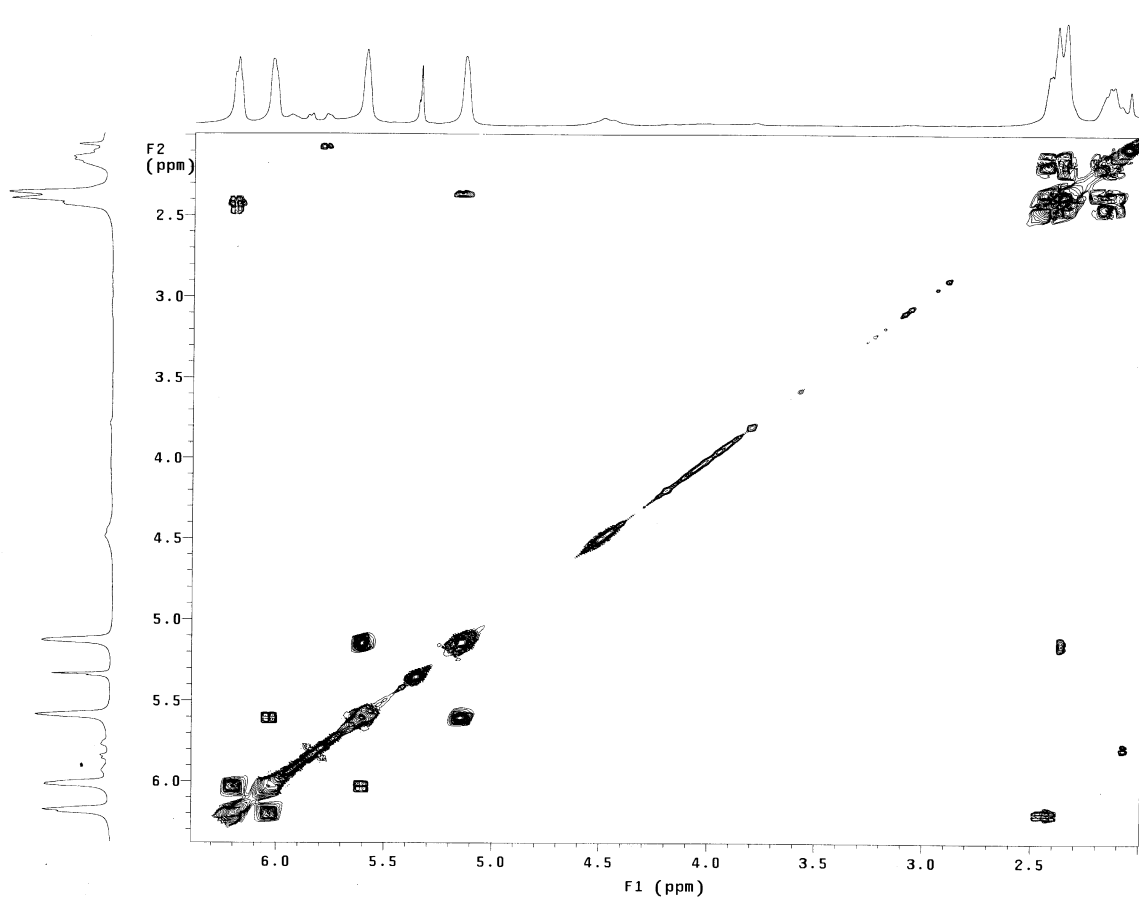


Figure 24: Partial COSY of 2.11 in CD₂Cl₂ at -85 °C.

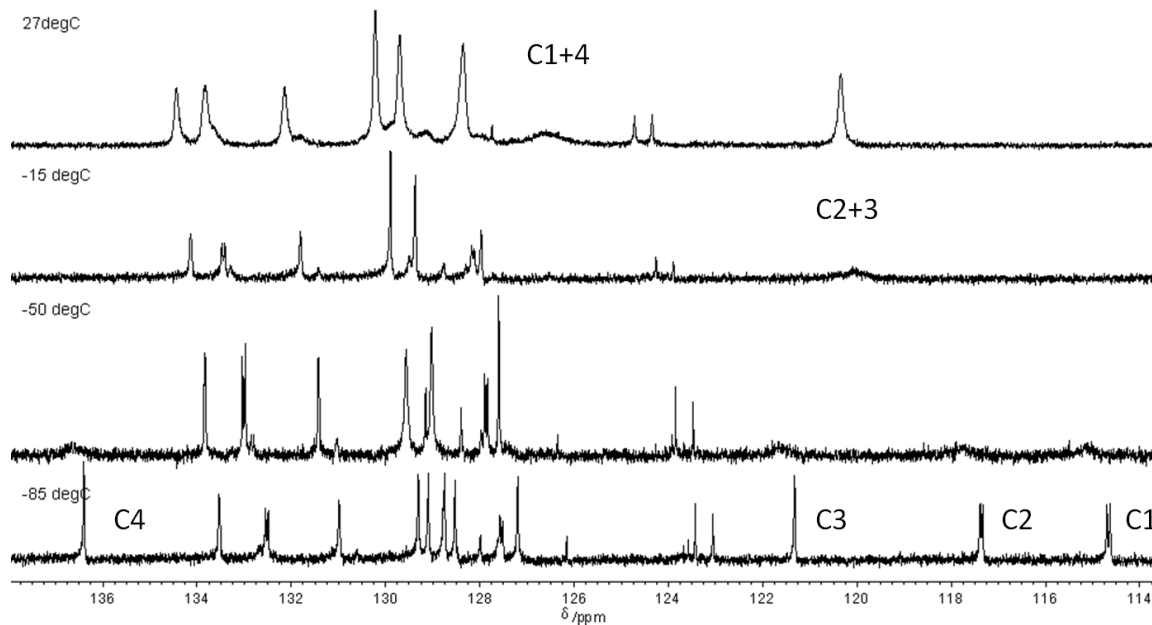


Figure 25: Temperature dependence of the vinylic ^{13}C NMR resonances of 2.11 in CD_2Cl_2 from $-85\text{ }^\circ\text{C}$ to $27\text{ }^\circ\text{C}$ in CD_2Cl_2 .

$[(\text{P1})\text{Au}(\eta^2\text{-}\overline{\text{C}(\text{H})=\text{C}(\text{H})\text{CH}_2\text{C}(\text{H})=\text{C}(\text{H})\text{CH}_2})]^+ \text{SbF}_6^-$ (**2.12**) Complex **2.12** was

isolated as a white solid (61 mg, 93%) from the reaction of 1,4-cyclohexadiene with $(\text{P1})\text{AuCl}$ and AgSbF_6 employing a procedure similar to that used to synthesize **2.6**. ^1H NMR ($-60\text{ }^\circ\text{C}$): δ 7.86–7.79 (m, 1 H), 7.62–7.52 (m, 5 H), 7.25–7.22 (m, 1 H), 7.21–7.14 (m, 2 H), 5.71 (s, 2 H), 5.58 (s, 2 H), 2.95–2.76 (m, 1 H), 1.31 (d, $J = 17.0$ Hz, 18 H). $^{13}\text{C}\{^1\text{H}\}$ NMR ($-85\text{ }^\circ\text{C}$): δ 147.4 (d, $J = 13.0$ Hz), 142.5 (d, $J = 7.0$ Hz), 133.4 (d, $J = 3.0$ Hz), 132.5 (d, $J = 7.5$ Hz), 131.0, 129.2, 128.5, 127.5 (d, $J = 6.4$ Hz), 127.2, 123.4, 122.9 (d, $J = 47.3$ Hz), 120.7 (d, $J = 6.9$ Hz), 36.9 (d, $J = 24.1$ Hz), 29.8, 27.0. $^{31}\text{P}\{^1\text{H}\}$ NMR ($-60\text{ }^\circ\text{C}$): δ 62.2. Anal. Calcd (found) for $\text{C}_{26}\text{H}_{35}\text{AuF}_6\text{PSb}$: H, 4.32 (4.35); C, 38.40 (38.49).

2.4.3 X-ray Crystal Structure Determinations

Crystals of **2.6**, **2.7**, **2.9**, and **2.12** were obtained from slow diffusion of hexanes into CH₂Cl₂ solutions of the respective complexes at 4 °C. The crystals were mounted on a Mitegen polyimide micromount with a small amount of Paratone N oil. Diffraction data were obtained with graphite-monochromated Mo K α radiation ($\lambda = 0.71073$ Å) on a Bruker-Nonius Kappa Axis X8 Apex2 diffractometer at 110 K. Crystallographic data for complexes of **2.6**, **2.7**, **2.9**, and **2.12** are collected in Table 8. The data collection strategy employed ω and ϕ scans that collected data up to 2θ . The frame integration was performed using SAINT.⁹⁹ The resulting raw data were scaled and absorption corrected using a multiscan averaging of symmetry equivalent data using SADABS.¹⁰⁰ The structures of **2.6**, **2.9**, and **2.12** were solved by direct methods using the XS program;¹⁰¹ the structure of complex **2.7** was solved by direct methods using the SIR92 program.¹⁰² All non-hydrogen atoms were obtained from the initial solution. The hydrogen atoms were introduced at idealized positions and were allowed to ride on the parent atom. The structural models were fit to the data using full matrix least-squares based on F^2 . The calculated structure factors included corrections for anomalous dispersion from the usual tabulation. The structures were refined using the XL program from SHELXTL;¹⁰³ graphic plots were produced using the NRCVAX crystallographic program suite.

Table 8: Crystal and structure refinement data for complexes 2.6, 2.7, 2.9, and 2.12.

	2.6	2.7	2.9	2.12
Empirical formula	C _{25.50} H ₃₅ AuClF ₆ PSb	C ₂₆ H ₃₇ AuF ₆ PSb	C ₂₄ H ₃₃ AuF ₆ PSb	C ₂₆ H ₃₅ AuF ₆ PSb
fw	840.67	813.24	785.19	811.23
cryst size (mm ³)	0.31 × 0.20 × 0.07	0.32 × 0.18 × 0.06	0.37 × 0.29 × 0.28	0.16 × 0.14 × 0.11
color and habit	colorless prism	colorless prism	colorless prism	colorless plate
<i>T</i> (K)	110(2)	110(2)	110(2)	110(2)
λ (Å)	0.71073	0.71073	0.71073	0.71073
cryst syst	monoclinic	orthorhombic	triclinic	monoclinic
space group	<i>P</i> 2(1)/ <i>n</i>	<i>Pca</i> 2 ₁	<i>P</i> $\bar{1}$	<i>P</i> 2 ₁ / <i>n</i>
unit cell dimens	<i>a</i> = 10.488(2) Å <i>b</i> = 17.861(4) Å <i>c</i> = 15.443(3) Å β = 93.948(10)°	<i>a</i> = 12.7007(4) Å <i>b</i> = 11.9861(4) Å <i>c</i> = 18.9847(6) Å	<i>a</i> = 9.4763(8) Å <i>b</i> = 9.8824(8) Å <i>c</i> = 14.0672(11) Å α = 83.970(3)° β = 87.373(4)° γ = 81.222(4)°	<i>a</i> = 9.9305(6) Å <i>b</i> = 24.7210(15) Å <i>c</i> = 11.5076(7) Å β = 94.593(3)°
<i>V</i> (Å ³)	2886.0(10)	2890.08(16)	1294.14(18)	2815.9(3)
<i>Z</i>	4	4	2	4
<i>D</i> _{calc} (g/cm ³)	1.935	1.869	2.015	1.913
2 θ _{max} (deg)	56.66	72.58	86.78	68.88
abs coeff (mm ⁻¹)	6.214	6.112	6.821	6.273
total no. of reflns	91 845	98 369	73 102	67 039
no. of unique reflns	6 678	12 497	15 686	11 764
no. params refined/restraints	6 678/311	12 497/360	15 686/341	11 764/322
<i>F</i> (000)	1616	1568	752	1560
goodness-of-fit on <i>F</i> ²	1.188	1.033	1.002	1.029
final <i>R</i> indices [<i>I</i> > 2 σ (<i>I</i>)]	<i>R</i> ₁ = 0.0265, <i>wR</i> ₂ = 0.0595	<i>R</i> ₁ = 0.0364, <i>wR</i> ₂ = 0.0722	<i>R</i> ₁ = 0.0260, <i>wR</i> ₂ = 0.0604	<i>R</i> ₁ = 0.0463, <i>wR</i> ₂ = 0.1033
<i>R</i> indices (all data)	<i>R</i> ₁ = 0.0346, <i>wR</i> ₂ = 0.0619	<i>R</i> ₁ = 0.0624, <i>wR</i> ₂ = 0.0848	<i>R</i> ₁ = 0.0312, <i>wR</i> ₂ = 0.0619	<i>R</i> ₁ = 0.0942, <i>wR</i> ₂ = 0.1172
max., min. $\Delta\rho$ (e/Å ³)	-2.044, 1.907	-0.710, 1.857	-2.359, 4.902	-1.264, 2.295

The 4-methyl-1,3-pentadiene ligand of complex **2.7** exhibited an orientational disorder. Atoms C2 and C5 occupied single positions, while atoms C1, C3, C4, and C6 occupied a second set of sites denoted as C1', C3', C4', and C6', respectively. The occupancies for the orientations were refined and normalized to 0.574(11) and 0.426(11) for the unprimed and primed sites respectively. The 1,3-butadiene ligand of **2.9** was

likewise disordered over two orientations. The refined occupancy for the major component was 0.643(8).

2.4.4 Kinetics of Intramolecular C=C Bond Exchange

An NMR tube containing a solution of **2.9** (0.55 mg, 0.070 mmol) in CD₂Cl₂ (0.5 mL) was placed in the probe of an NMR spectrometer precooled to -90 °C, allowed to equilibrate for 10 min, and analyzed by ¹H NMR spectroscopy. The solution was warmed incrementally, equilibrated at -80, -70, -60, -59, -45, -30, -15, and 15 °C, and analyzed at each temperature by ¹H NMR spectroscopy. Simulation of the portion of the ¹H NMR spectrum containing the C2/C3 vinylic resonances (δ 6.1–6.6) at -59 °C employing the parameters $\Delta\omega = 144.9$ Hz, $\omega_a = 5$ Hz, $\omega_b = 4$ Hz, $J_{AB} = 10.0$ Hz, $J_{Atrans} = 17.8$, $J_{Acis} = 8.8$ Hz, $J_{Bcis} = 10.2$ Hz, $J_{Btrans} = 17.0$ Hz gave a best fit with an exchange rate of $k_{ex} = 701$ s⁻¹ ($\Delta G_{214}^\ddagger = 9.6$ kcal mol⁻¹, Figure 26). Peak separations ($\Delta\omega$) were obtained directly from the -90 °C ¹H NMR spectrum of **2.9**; coupling constants (J) were obtained from the -90 °C ¹H NMR spectrum of **2.9** and then varied within ± 0.2 Hz to best reproduce the slow-exchange spectrum. Natural peak widths (ω) were estimated by averaging the peak width at half-height of the outer lines of the respective multiplets.

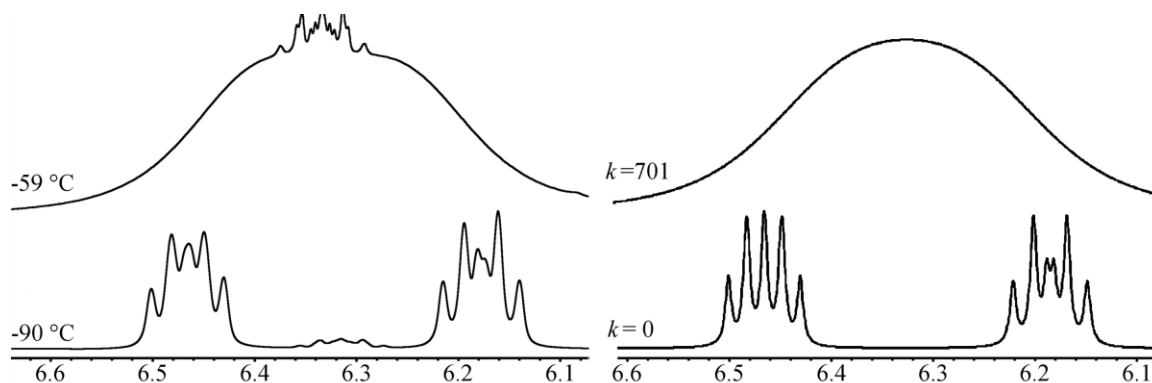


Figure 26: Experimental (left) and simulated (right) ^1H NMR spectra of internal vinyl protons H2 and H3 of complex 2.9.

The energy barriers for interconversion of the diene $\text{C}=\text{C}$ bonds of complexes **2.10** – **2.12** were determined through similar analyses. Comparisons of experimental and simulated ^1H NMR spectra are included as Figures 27–29.

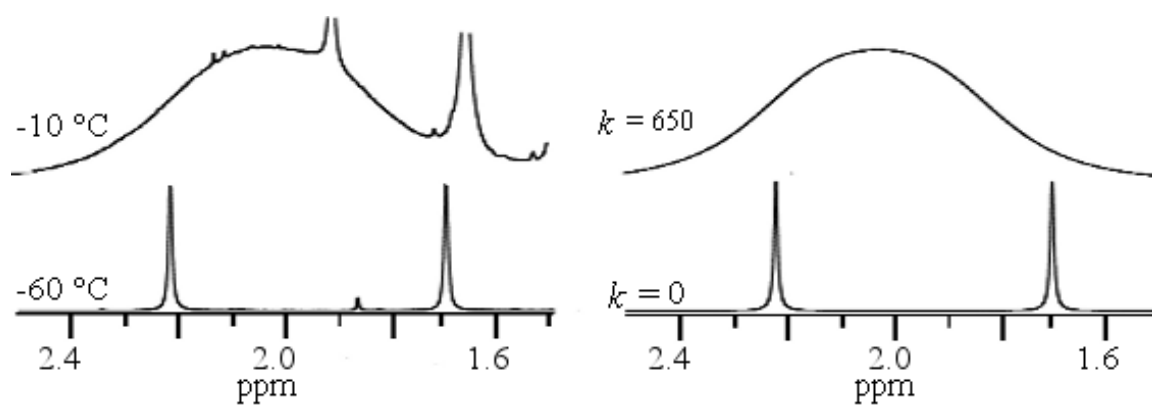


Figure 27: Experimental (left) and simulated (right) ^1H NMR spectra of vinyl methyl protons of complex 2.10.

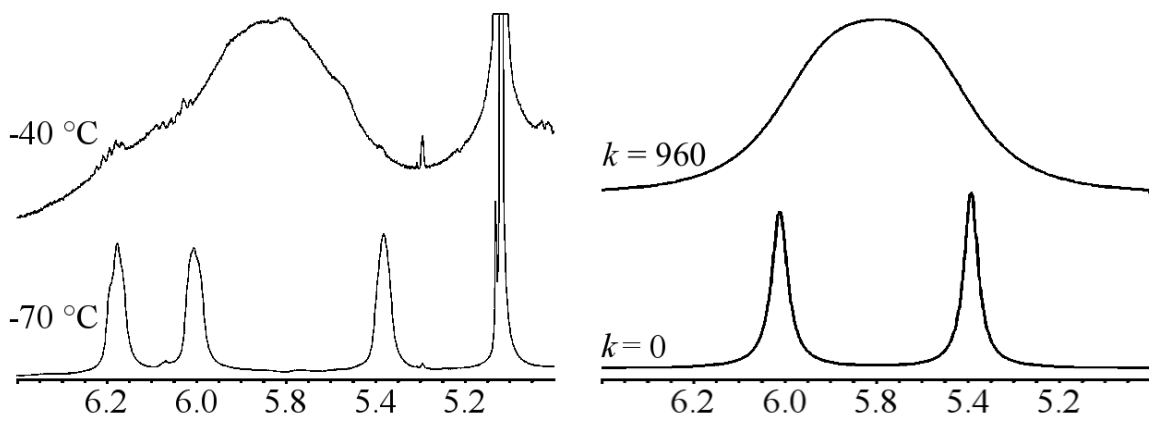


Figure 28: Experimental (left) and simulated (right) ^1H NMR spectra of internal vinyl protons H3 (δ 6.0 ppm) and H2 (δ 5.38 ppm) of complex 2.11.

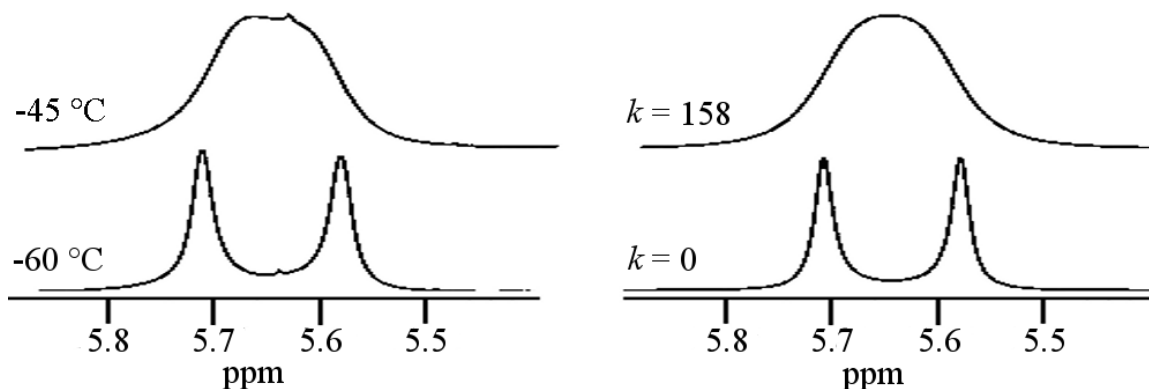


Figure 29: Experimental (left) and simulated (right) ^1H NMR spectra of vinyl protons H1/H2 and H4/H5 of complex 2.12.

2.4.5 Kinetics of Intermolecular Diene Exchange with 2.8

An NMR tube capped with a rubber septum that contained a solution of **2.8** (59 mg, 0.072 mmol) and 1,3-dimethoxybenzene (0.018 mmol, 2.4 μL , internal standard) in CD_2Cl_2 (0.445 mL) was placed in the probe of an NMR spectrometer maintained at 298 K. Analysis of the singlet at δ 5.74 corresponding to the C3 proton of the 2,4-dimethyl-1,3-pentadiene ligand of **2.8** in the ^1H NMR spectrum gave a peak width at half-height of

$\Delta v_{1/2} = 6.9$ Hz (Table 6). The tube was removed from the probe, and 2,4-dimethyl-1,3-pentadiene was added via syringe. The tube was inverted several times, returned to the probe, and allowed to equilibrate for 10 min. The concentration of free 2,4-dimethyl-1,3-pentadiene was determined as 0.09 M by integration of the C3 proton resonance of free 2,4-dimethyl-1,3-pentadiene at δ 5.65 relative to the multiplet at δ 6.48 corresponding to the C4, C5, and C6 aryl protons of 1,3-dimethoxybenzene. The peak width at half-height for the singlet at δ 5.74 was $\Delta v_{1/2} = 11.0$ Hz, corresponding to an excess broadening of $\Delta v_{1/2(\text{excess})} = 4.0$ Hz (Table 7). Using this value, the rate of exchange of the diene ligand with **2.8** was determined through application of the slow exchange approximation to be $k_{\text{obs}} = \pi(\Delta v_{1/2(\text{excess})}) = 12.7$ s⁻¹. The first-order rate constant for diene exchange with **2.8** was determined in a similar manner at [2,4-dimethyl-1,3-pentadiene] = 0.14, 0.18, 0.22, and 0.25 M (Table 6). The second-order rate constant for the rate of exchange of the diene ligand of **2.8** was determined from the slope of a plot of k_{obs} versus [2,4-dimethyl-1,3-pentadiene] where $k_{\text{ex}} = 169 \pm 1$ M⁻¹ s⁻¹ ($\Delta G^\ddagger = 14.40 \pm 0.01$ kcal mol⁻¹) (Table 6, Figure 18).

2.4.6 Determination of Diene Binding Constants

2,3-Dimethyl-1,3-butadiene (2.4 mg, 0.029 mmol) was added via syringe to a CD₂Cl₂ solution of [(P1)Au(η^2 -H₂C=CMe₂)]⁺SbF₆⁻ (**2.1**; 20 mg, 0.029 mmol) in an NMR tube sealed with a rubber septum. The contents of the tube were thoroughly mixed, placed in the probe of an NMR spectrometer precooled to -70 °C, and maintained at this

temperature for 10 min. The relative concentrations of **2.1**, free isobutylene, **2.10**, and free 2,3-dimethyl-1,3-butadiene were measured by integrating the resonances corresponding to the vinyl protons of bound (δ 3.73) and free (δ 4.59) isobutylene and the vinyl protons of bound (δ 5.60, 5.44, 3.95, 3.52) and free (δ 5.01, 4.95) 2,3-dimethyl-1,3-butadiene. An equilibrium constant of $K_{eq} = ([\mathbf{2.10}][\text{isobutylene}])/([\mathbf{2.1}][\text{2,3-dimethyl-1,3-butadiene}]) = 0.13 \pm 0.02$ was determined as the average of two separate experiments (Table 7). To ensure that equilibrium was achieved under these conditions, a similar experiment was performed through addition of isobutylene (0.017 mmol) to a CD_2Cl_2 solution of **2.10** (0.025 mmol). An equilibrium constant of $K_{eq} = ([\mathbf{2.10}][\text{isobutylene}])/([\mathbf{2.1}][\text{2,3-dimethyl-1,3-butadiene}]) = 0.12 \pm 0.01$ was determined, which is not significantly different from that obtained by treatment of **2.1** with 2,3-dimethyl-1,3-butadiene. The relative binding affinities of 1,3-cyclohexadiene, 2,4-dimethyl-1,3-pentadiene, 1,4-cyclohexadiene, and *trans*-1,3-pentadiene relative to isobutylene at -70 °C were determined employing procedures analogous to that used to determine the binding affinity of 2,3-dimethyl-1,3-butadiene (Table 7).

3. Synthesis and Structure of Dicationic, Bis(gold) π -Alkene Complexes Containing a 2,2'-Bis(phosphino)biphenyl Ligand

Portions of this chapter have been published: Brooner, R. E. M.; Widenhoefer, R.

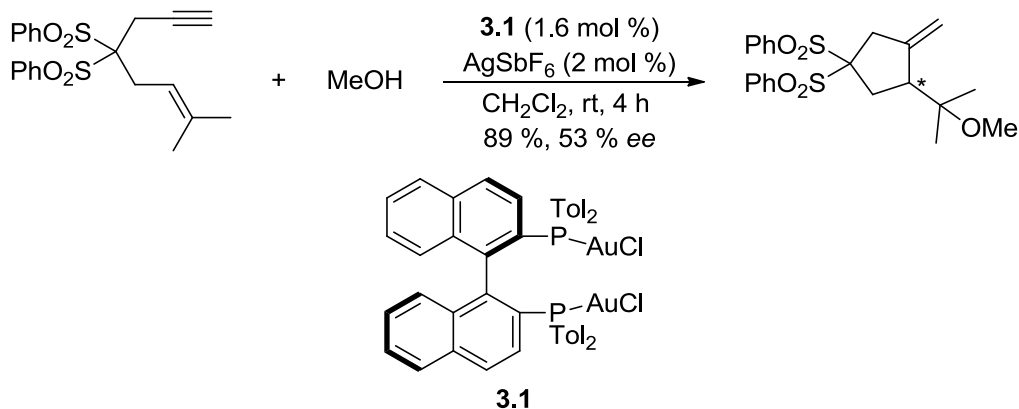
A. *Organometallics*, **2012**, *31*, 768. X-ray crystal structures were solved and refined by Dr. Paul D. Boyle at North Carolina State University.

3.1 Introduction

3.1.1 Enantioselective gold(I) catalysis

Development of new methods for achieving enantioselective transformations using gold(I) has been a major area of research since the early days of the field.^{12-14, 104} In fact, the first report of enantioselective gold(I) catalysis, Hayashi's 1986 disclosure of the addition of isocyanoacetate to aldehydes catalyzed by a chiral ferrocenylphosphine-gold(I) complex,¹⁰⁵ predates Teles's pioneering report of gold(I) catalyzed alkyne hydration by a full decade.³ However, only in the last eight years have further examples of enantioselective gold(I) catalysis emerged. Pivotal to this renewed activity in enantioselective gold(I) catalysis was Echavarren's demonstration of enantioselective enyne cyclization catalyzed by cationic, bis(gold) BINAP complexes such as **3.1** (Scheme 10).¹⁰⁶ Since then, enantioselective gold(I) π -activation catalysis has relied heavily on bis(gold) phosphine complexes that contain an axially chiral 2,2'-bis(phosphino)biaryl ligand as catalysts.^{12-14, 104}

Scheme 10: Enantioselective enyne alkokycloisomerization catalyzed by the chiral bis(gold) BINAP complex 3.1.¹⁰⁶



Unlike other late transition metals such as platinum and palladium, which form chelated mononuclear complexes with bidentate bis(phosphine) ligands, chiral bis(phosphine) gold complexes are formed as dinuclear species in which each phosphorus is bound to a two-coordinate gold(I) atom. With the exception of a recently reported example of an axially-chiral bis(gold) phosphine complex acting as a chiral proton source,¹⁰⁷ involvement of one of the gold centers of a bis(gold) phosphine complex appears obligatory in effecting a given enantioselective transformation. However, the role of the second gold phosphine moiety as a reactive or stereocontrolling element remains unclear. Although it is possible that the two gold centers do not operate as equivalent and independent catalytic sites, a large body of circumstantial evidence suggests otherwise, including the marked sensitivity of many enantioselective gold(I) transformations to the ratio of bis(gold chloride) precatalyst and chloride abstracting silver salt.^{106, 108-113}

3.1.2 Examples of structurally characterized chiral, neutral bis(gold) complexes

To address these issues, the structures of a number of neutral, axially chiral bis(gold) phosphine complexes bearing anionic ligands have been interrogated for potential geometry-controlling intramolecular interactions.^{108-109, 113-120} As expected, each gold center in these complexes adopts a nearly linear, two-coordinate geometry with one phosphine of the ligand and one anionic ligand; no indication of interaction with the second phosphine is observed. For example, Zhang and coworkers have reported the X-ray crystal structures of a pair of common bis(gold chloride) precatalysts [(L)(AuCl)₂] [L = (*R*)-C₁-tunephos (**3.2**), (*R*)-MeO-dtbn-biphep (**3.3**)] (Figure 30).¹⁰⁹ Complex **3.2** exhibits a C25-C30-C37-C36 dihedral angle of 68.08 ° and a close Au-Au distance of 2.994 Å, which is characteristic of an bond between the two atoms.²² On the other hand, complex **3.3** has a much larger dihedral C1-C6-C7-C8 dihedral angle (105.74 °) and a long Au-Au distance of 5.316 Å, precluding any aurophilic interaction. The authors postulate that the smaller “bite angle” and Au-Au bond in **3.2** makes this complex more rigid than **3.3**; further, they speculate that the enhanced rigidity explains the enhanced enantioselectivity shown by **3.2** relative to **3.3** for the tandem cycloization/[3+3] cycloaddition of 2-(1-alkynyl)-2-alken-1-ones with nitrones.

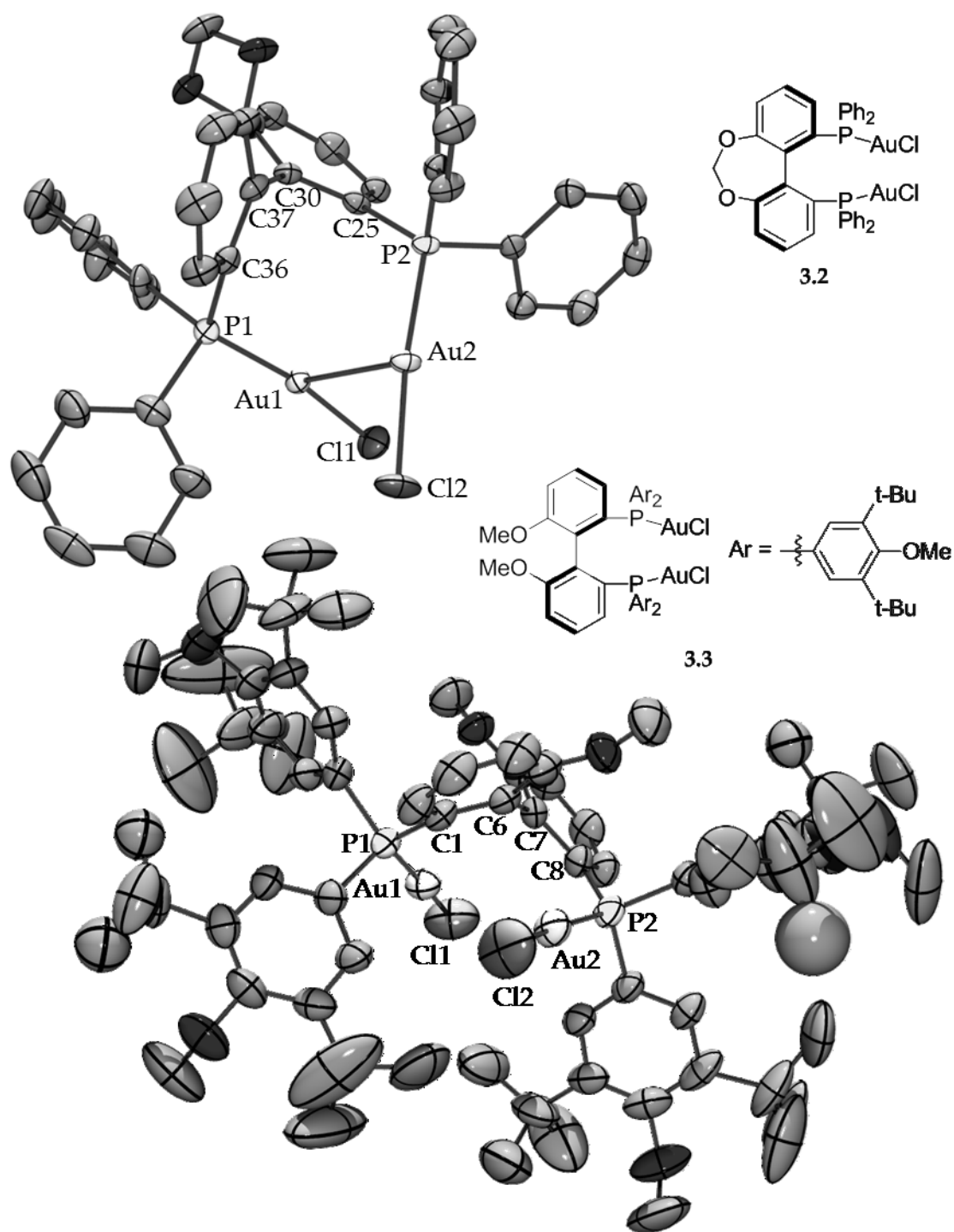


Figure 30: ORTEP and skeletal diagrams of bis(gold chloride) complexes 3.2 (upper structure) and 3.3 (lower structure).¹⁰⁹ Ellipsoids are shown at the 50% probability level. Hydrogen atoms and counterion have been removed for clarity.

However, information gleaned from these neutral complexes, especially the bis(gold chloride) precatalysts, is only tangentially relevant to catalysis as these complexes are not considered to be active in the catalytic cycle. Furthermore, while the examples above demonstrate that the chiral bis(phosphine) ligand greatly influences the structure of the bis(gold) precatalysts, the anionic ligand also affects the structure significantly. Comparison of the solid state structure of complex [(biphep)(AuCl)₂] (**3.4**)¹¹⁴ to that of [(biphep)(AuNTf₂)₂] (**3.5**)¹⁰⁸ with the same chiral supporting ligand but a bulky, weakly coordinating anionic ligand reveals a close Au-Au interaction (3.0992 Å) in the former that is absent in the later (Au-Au distance = 6.6818(6) Å) (Figure 31). The long Au-Au distance in **3.5** was attributed not to the steric influence of the NTf₂ ligand but rather to the presence of stabilizing, rigidifying π - π stacking interactions between phenyl substituents on the two phosphorus atoms of the biphep ligand.

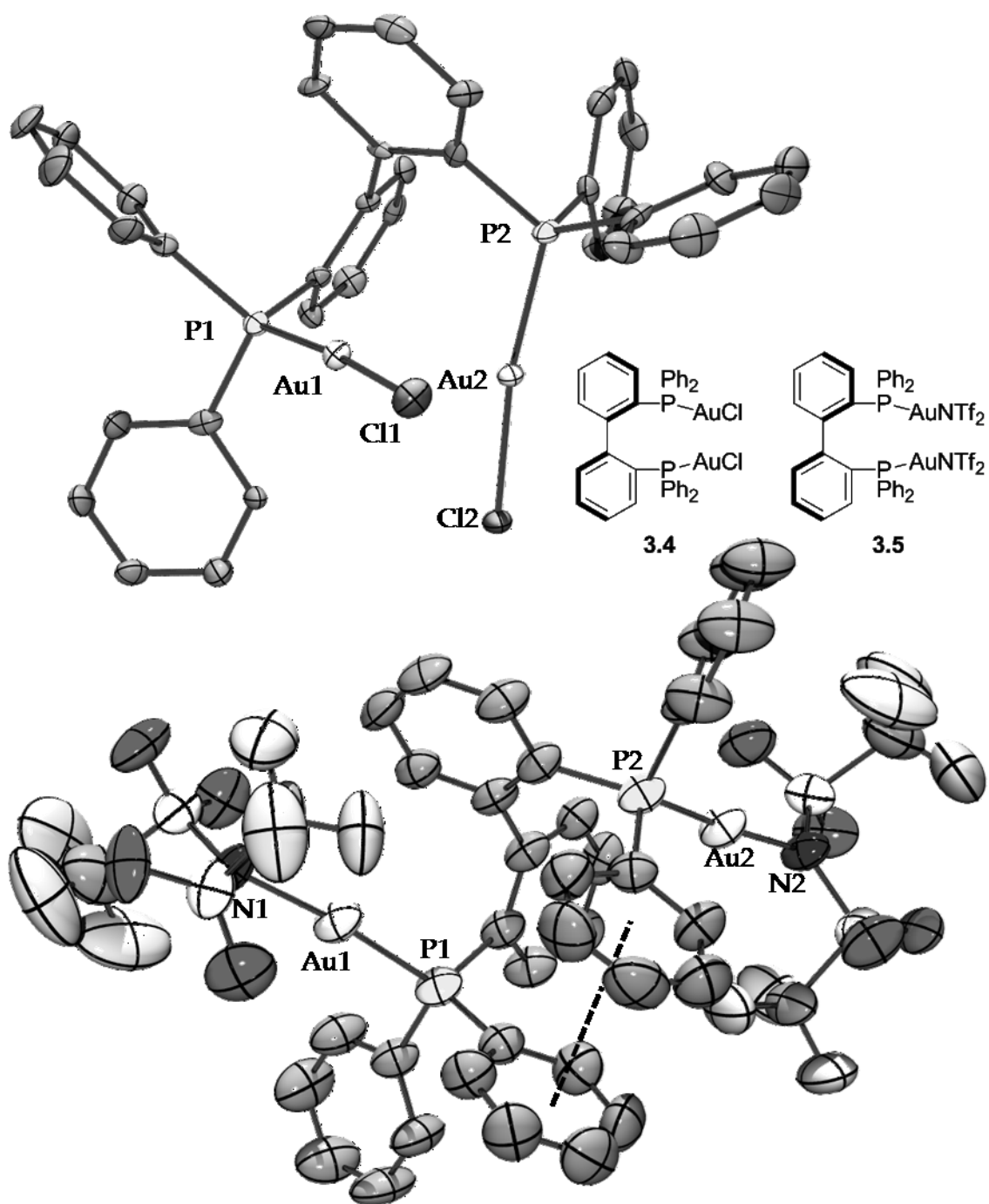


Figure 31: ORTEP and skeletal diagrams of [(biphep)(AuX)₂] complexes 3.4 (upper structure)¹¹⁴ and 3.5 (lower structure)¹⁰⁸. π - π stacking is indicated by the dashed line. Ellipsoids are shown at the 50% probability level. Hydrogen atoms and counterion have been removed for clarity.

3.1.3 Project goals and scope

Despite the growing body of structurally characterized neutral, chiral bis(gold) complexes bearing anionic ligands, before 2011 no information regarding the structure and behavior of more catalytically relevant cationic bis(gold) complexes bearing π -bound ligands was available. As both the structure of the chiral supporting ligand and the second ligand on each gold atom within these complexes has been shown to influence the structure of the complex, we sought to explore the structure of cationic bis(gold) π -alkene complexes. To that end, we have reported the syntheses, solid-state and solution structures, and ligand-binding behavior of a pair of dicationic, bis(gold) π -alkene complexes that contain a 2,2'-bis(phosphino)biphenyl ligand.

3.2 Results and discussion

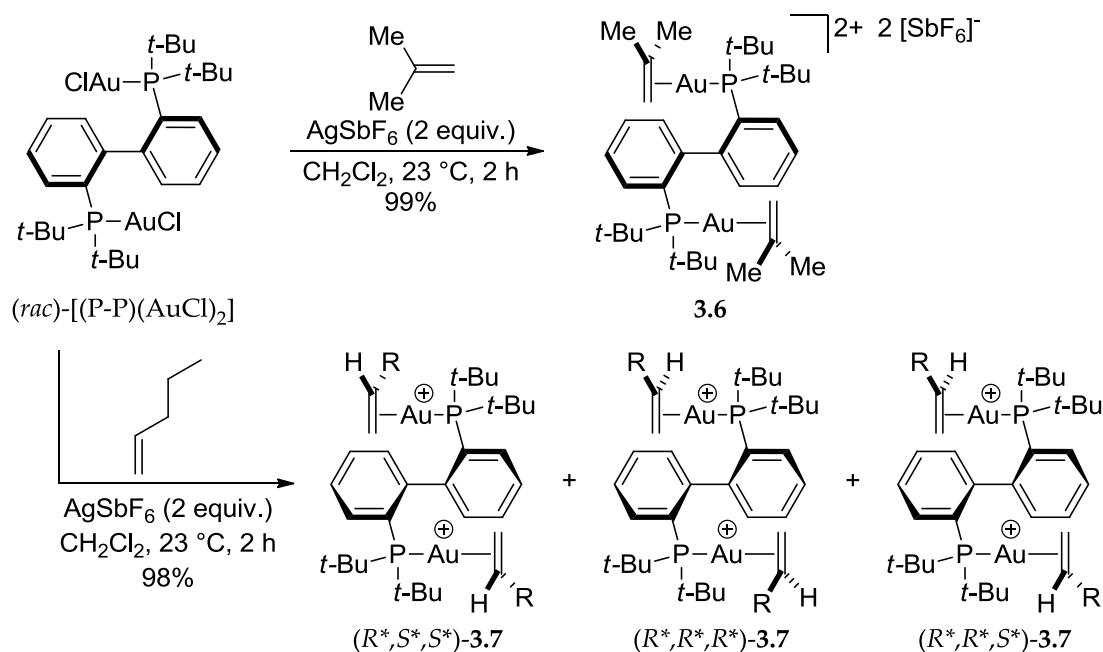
3.2.1 Synthesis, characterization, and solution behavior of PP-isobutylene and 1-pentene

Initial experiments were directed toward the synthesis of bis(gold) π -alkene complexes employing bis(diarylphosphino) ligands, such as binap or biphep derivatives, as these are the ligands commonly used in enantioselective gold(I) catalysis. However, all attempts at generation of these complexes, either for isolation or *in situ* characterization, were unsuccessful. Based on the extant body of work regarding cationic, two-coordinate gold π -complexes, which is dominated by complexes of di- and tri-alkylphosphine ligands, it was thought that a more electron-rich phosphine ligand

might facilitate π -complex formation. For this reason, we proceeded using the chiral, racemic 2,2'-bis(di-*t*-Bu-phosphino)biphenyl (P-P).

Treatment of a 1:2 suspension of (*rac*)-[(P-P)(AuCl)₂] and AgSbF₆ with isobutylene in CH₂Cl₂ at room temperature for 2 h led to isolation of (*rac*)-[(P-P)(Au(η^2 -H₂C=CMe₂))₂]²⁺ 2SbF₆⁻ (**3.6**) in 99% yield as an air- and thermally stable white solid (Scheme 11). Likewise, treatment of (*rac*)-[(P-P)(AuCl)₂] and AgSbF₆ with the prochiral alkene 1-pentene led to isolation of (*rac*)-[(P-P)(Au(η^2 -H₂C=C(H)CH₂CH₂CH₃))₂]²⁺ 2SbF₆⁻ (**3.7**) in 98% yield as a statistical ~1:1:2 mixture of the three possible chemically inequivalent stereoisomers (*R*^{*},*S*^{*},*S*^{*})-**3.7**, (*R*^{*},*R*^{*},*R*^{*})-**3.7**, and (*R*^{*},*R*^{*},*S*^{*})-**3.7** (Scheme 11; *R*-phosphine series depicted).

Scheme 11: Synthesis of chiral, dicationic bis(gold) complexes 3.6 and 3.7



Binding of isobutylene to gold in solution was established using ^{13}C NMR spectroscopy. The terminal olefinic C1 carbon resonance of bound isobutylene (δ 94.1) was shifted to lower frequency relative to free isobutylene ($\Delta\delta = -16.4$), and the ^{13}C resonance corresponding to methyl-substituted C2 alkene terminus of bound isobutylene (δ 167.2) was shifted to higher frequency relative to free isobutylene ($\Delta\delta = 24.8$). In comparison, the ^{13}C NMR spectrum of mono(gold) isobutylene complex $[(\text{P1})\text{Au}(\eta^2\text{-isobutylene})]^+ \text{SbF}_6^-$ displayed similar shifts of the resonances corresponding to the C1 and C2 of bound relative to free isobutylene ($\Delta\delta = -15.4, 20.9$, respectively).⁴⁶ A single, sharp resonance at δ 64.9 in the ^{31}P NMR spectrum of **3.6** over the temperature range of -50 to 25 °C established the chemical equivalence of the phosphorus atoms in **3.6**. On the other hand, the presence of resonances corresponding to diastereotopic isobutylene vinyl protons (δ 4.06 and 3.89), isobutylene methyl groups (δ 2.20 and 2.11), and phosphine methyl groups (δ 1.44, 1.40; $J_{\text{PH}} = 16.5$ Hz) in the ^1H NMR spectrum of **3.6** over the temperature range of 25 – 60 °C established that both aryl–aryl bond rotation and isobutylene exchange were slow on the NMR time scale over this temperature range.

Unambiguous assignment of the resonances corresponding to the 1-pentene ligand in the ^{13}C and ^1H NMR spectra of **3.7** was precluded by the presence of diastereomers; however, the presence of resonances in a 1:2 ratio of at δ 6.4 – 6.3 and δ 4.6 – 4.2 is indicative of a $[(\text{P1})\text{Au}(\eta^2\text{-(1-alkene)})]^+$ alkene complex.⁴⁶ Key to the characterization and determination of the isomeric composition of **3.7** was the presence

of a ~1:1:1:1 ratio of sharp resonances at δ 62.1, 62.0, 61.8, and 61.7 in the ^{31}P NMR spectrum of **3.7**. The two phosphorus atoms of both the (R^*,S^*,S^*) -**3.7** and the (R^*,R^*,R^*) -**3.7** isomers are chemically equivalent, giving rise to one ^{31}P resonance for each isomer, whereas the phosphorus atoms of the (R^*,R^*,S^*) -**3.7** isomer are chemically inequivalent, giving rise to two ^{31}P NMR resonances that are distinct from each other and those of the (R^*,S^*,S^*) -**3.7** and (R^*,R^*,R^*) -**3.7** isomers. The 1:1:1:1 ratio of the four resonances suggests that (R^*,S^*,S^*) -**3.7**, (R^*,R^*,R^*) -**3.7**, and (R^*,R^*,S^*) -**3.7** are formed in a statistic 1:1:2 ratio, thus the cationic gold centers complex 1-penene with a lack of π -face discrimination. On the other hand, the presence of four distinct resonances in the ^{31}P spectrum, despite the absence of alkene π -face discrimination, indicates that the chemical environment of one gold coordination site affects that of the second coordination site.

3.2.2 X-ray crystal structures of **3.6** and **3.7**

Slow diffusion of pentane into a CH_2Cl_2 solution of **3.6** at 4 °C formed colorless crystals of **3.6**· CH_2Cl_2 suitable for X-ray analysis (Figure 32). The solid-state structure of **3.6**· CH_2Cl_2 revealed two similar but crystallographically inequivalent $[\text{Au}(\eta^2\text{-isobutylene})]$ moieties related by a pseudo- C_2 symmetry axis that runs perpendicular to the C22–C23 bond vector. Both gold centers adopt a distorted linear geometry with P–Au–alkene_{centroid} angles of 162.54° and 163.05° for the Au1 and Au2 centers, respectively. Both isobutylene ligands bind unsymmetrically to gold with a shorter Au–CH₂ and longer Au–CMe₂ interaction ($\Delta d = 0.186$ Å for Au1, $\Delta d = 0.181$ Å for Au2), and both

isobutylene ligands are oriented such that the C=C bond vector is roughly parallel to the associated Au–P–C_{ipso} plane with the CMe₂ terminus directed away from the perpendicularly oriented arene ring. The solid-state structure **3.6** is comparable to that of the mono-gold complex [(P1)Au(η^2 -methylene cyclohexane)]⁺SbF₆⁻, although the latter demonstrated slightly less deviation from linearity about gold (P–Au–alkene_{centroid} angle = 165.1°) and marginally less asymmetry in the binding of the alkene to gold ($\Delta\delta$ Au–CH₂/Au–CR₂ = 0.155 Å) than in **3.6**.⁴⁶ Presumably, this increased deviation from optimal geometry observed for **3.6** reflects increases steric bulk of the bis(phosphine) ligand.

The biphenyl arene rings of **3.6** deviate significantly from a perpendicular arrangement, with a C17–C22–C23–C24 dihedral angle of 124.04°. As such, complex **3.6** exhibits a long Au1–Au2 distance of 5.4821 Å, much too far for any intramolecular Au–Au interaction.^{22, 121} Conversely, the proximity of each gold atom to the perpendicularly oriented arene ring [Au–arene_{plane} = 2.9–3.0 Å, Au–arene_{ipso} = 3.0–3.2 Å] suggests the presence of Au–arene interactions similar to those observed for some mono(gold) dialkyl(*o*-biphenyl)phosphine complexes.^{91, 122-124} These Au–arene interactions could explain the resistance of **3.6** to rotation about the C22–C23 bond, even in the absence of rigidifying Au–Au or π – π interactions.

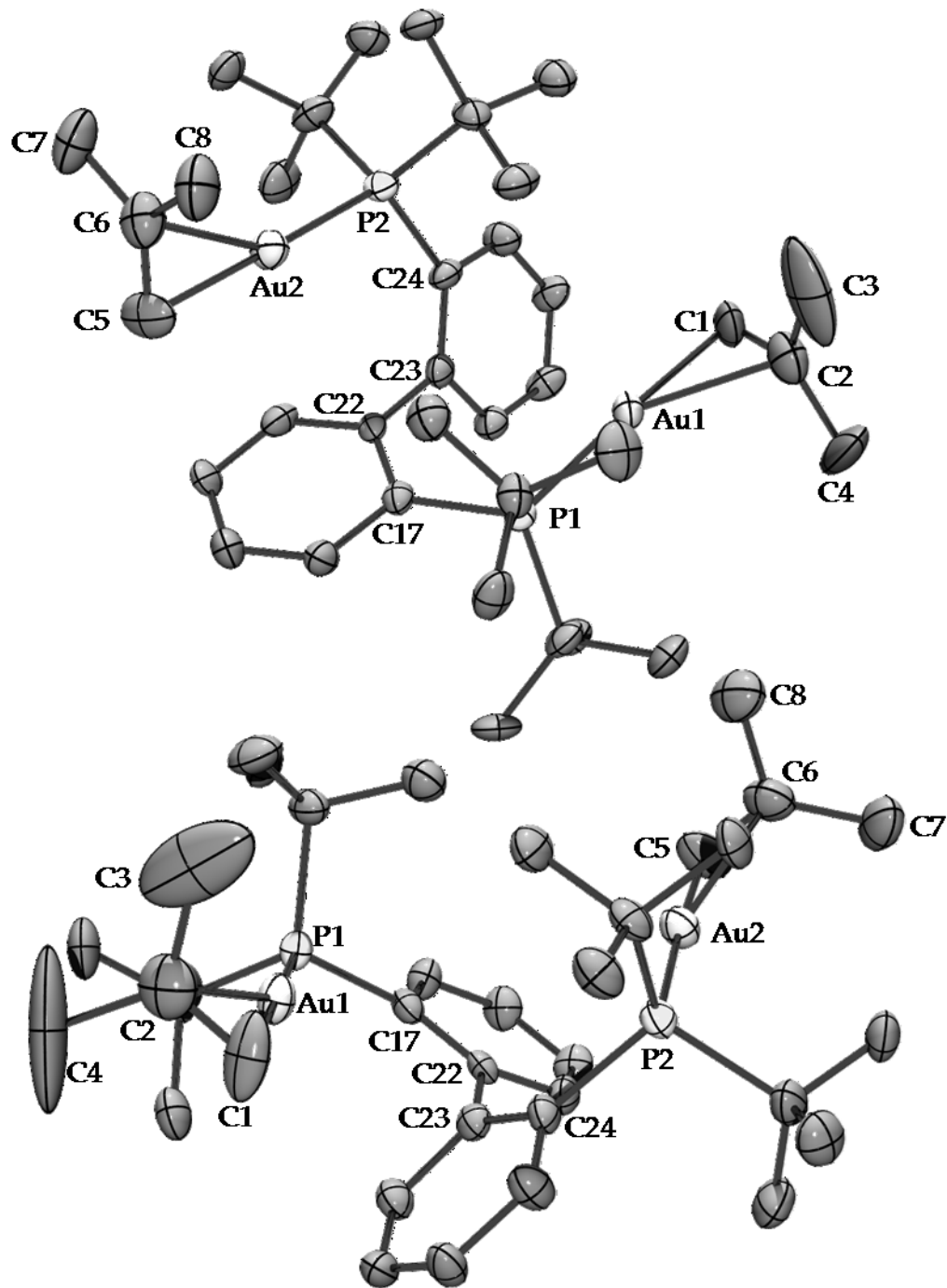


Figure 32: Two ORTEP diagrams of 3.6 showing partial atom numbering scheme. Ellipsoids are shown at the 50% probability level. Hydrogen atoms and counterion have been removed for clarity.

Slow diffusion of pentane into a C_2Cl_2 solution of **3.7** at 4 °C led to selective crystallization of the (R^*,R^*,S^*)-**3.7**· CH_2Cl_2 diastereomer, as determined by X-ray analysis (Figure 33). Unfortunately, the resulting structure was of low quality owing to twinning of the crystals, which precluded more detailed analysis of the molecular geometrical parameters.

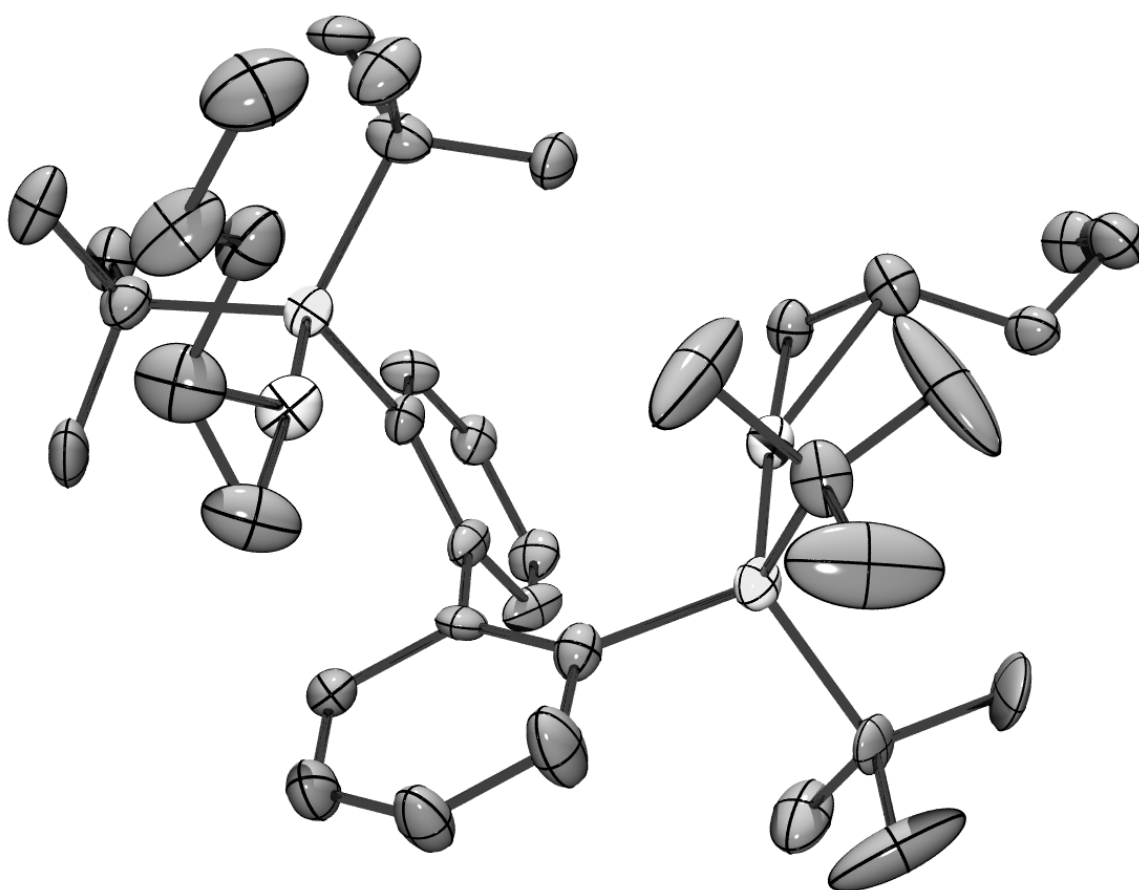


Figure 33: ORTEP diagram of **3.7. Ellipsoids are shown at the 50% probability level. Hydrogen atoms and counterion have been removed for clarity.**

3.2.3 Ligand exchange behavior in 3.6

3.2.3.1 Kinetics of intermolecular ligand exchange of 3.6 with isobutylene

Kinetic analyses of degenerate intermolecular ligand exchange in gold(I) π -complexes has led to valuable insight into the solution coordination behavior of these complexes. In order to gain learn more about the coordination behavior of a bis(gold) π -alkene complex, we sought to directly compare the ligand-exchange behavior of 3.6 to an analogous mono(gold) π complex. To this end, we studied the kinetics of isobutylene exchange with 3.6 (47 mM) as a function of [isobutylene] from 14 to 61 mM in CH_2Cl_2 at 25 °C employing ^1H NMR spin-saturation transfer techniques (Table 9).¹²⁵⁻¹²⁶

Experimental details are included in section 3.4.3.1.

Table 9: Observed rate constants for the intermolecular exchange of bound and free isobutylene with complex 3.6.

[Isobutylene] (mM)	k_{obs} (s^{-1}) (1 st trial)	k_{obs} (s^{-1}) (2 nd trial)
14	1.0	1.0
31	1.1	1.1
48	1.3	1.2
61	1.4	1.4

A benefit of analyzing ligand-exchange kinetics using spin-saturation transfer is the technique allows for discrimination of [ligand]-dependent, associative (k_2) and [ligand]-independent, solvent-assisted (k_1) pathways for exchange. In fact, a plot of k_{obs} versus [isobutylene] was linear with a nonzero y intercept (Figure 34), which established the two-term rate law for intermolecular isobutylene exchange with 3.6 of a rate = $k_1[3.6] + k_2[3.6][\text{isobutylene}]$, where $k_1 = 0.86 \pm 0.02 \text{ s}^{-1}$ ($\Delta G^\ddagger_{298\text{K}} = 17.52 \pm 0.01 \text{ kcal}$

mol⁻¹) and $k_2 = 8.3 \pm 0.5 \text{ M}^{-1} \text{ s}^{-1}$ ($\Delta G^\ddagger_{298\text{K}} = 16.18 \pm 0.03 \text{ kcal mol}^{-1}$). The energy barrier for the isobutylene-dependent exchange pathway of **3.6** is $\sim 1.2 \text{ kcal mol}^{-1}$ higher than that for the isobutylene-dependent exchange pathway for the analogous mono(gold) complex $[(\text{P1})\text{Au}(\eta^2\text{-H}_2\text{C}=\text{CMe}_2)]^+\text{SbF}_6^-$;⁴⁶ this rate decrease is indicative of the increased steric congestion about the gold centers in the bis(gold) complex relative to the mono(gold) complex.

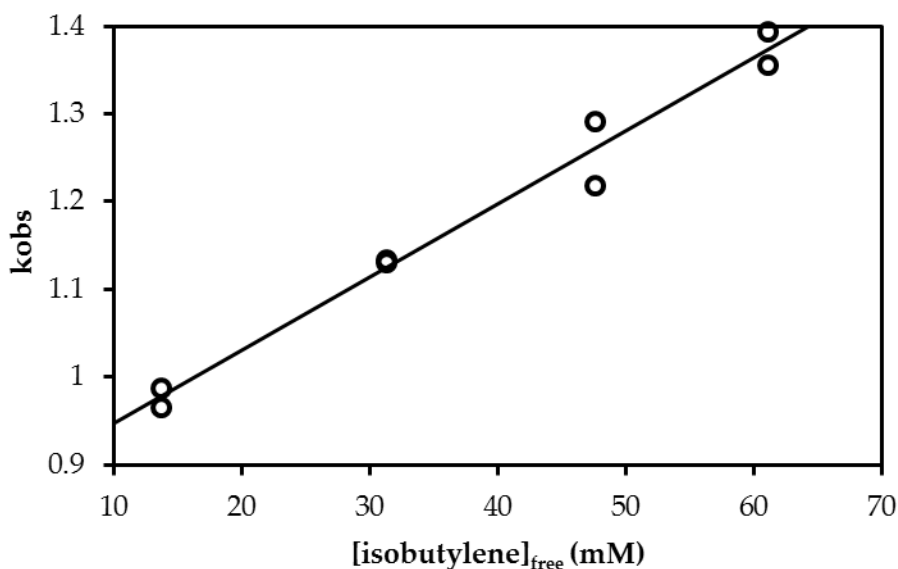


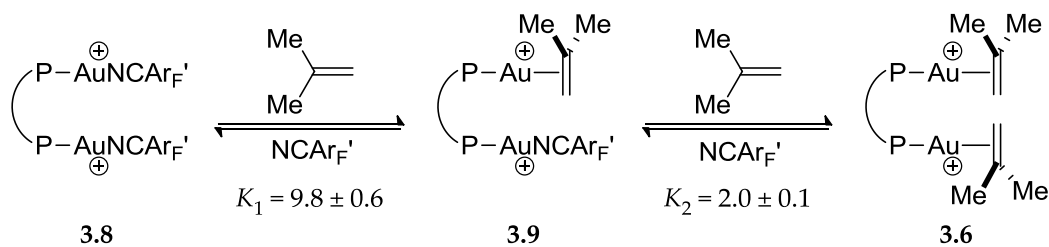
Figure 34: Plot of k_{obs} versus [isobutylene] for the intermolecular exchange of the isobutylene ligands of **3.6** with free isobutylene from 14 to 61 mM at 25 °C in CD_2Cl_2 .

3.2.3.2 Equilibrium binding affinity of isobutylene in **3.6**

As both another point of comparison to mono-gold alkene complexes and a method to evaluate the extent to which complexation of one π -alkene ligand affects complexation of the second alkene ligand in dicationic $[(\text{P-P})(\text{AuL})_2]^{2+}$ complexes, we determined equilibrium constants for the successive displacement of NCArF' [$\text{NCArF}' =$

4-trifluoromethylbenzotrile] from $[(P-P)Au(NCAr_F')_2]^{2+} 2SbF_6^-$ (**3.8**) with isobutylene in CD_2Cl_2 at $-50\text{ }^\circ C$ using a combination of 1H , ^{31}P , and ^{19}F NMR spectroscopies (Scheme 12). Experimental details are included in section 3.4.3.2. The equilibrium constant for displacement of one $NCAr_F'$ ligand from **3.8** with isobutylene to form $[(P-P)(Au(NCAr_F'))(Au(\eta^2-H_2C=CMe_2))]^{2+}$ (**3.9**) was $K_1 = 9.8 \pm 0.6$, and the equilibrium constant for displacement of the $NCAr_F'$ ligand from **3.9** to give **3.6** was $K_2 = 2.00 \pm 0.09$. The overall equilibrium constant for the conversion of **3.8** to **3.6** is $K_3 = ([3.1][NCAr_F']^2)/([3.3][isobutylene]^2) = 20 \pm 1$.

Scheme 12: Successive equilibrium displacement of 4-trifluoromethylbenzotrile ($NCAr_F'$) from **3.8 to give **3.9** and from **3.9** to give **3.6** by isobutylene.**



The observation of different equilibrium constants for the displacement of one $NCAr_F'$ from **3.8** and **3.9** by isobutylene reveals that binding of isobutylene to gold is affected by the environment of the proximal gold center, although the origin of this effect remains unclear. The long internuclear Au–Au separation in the solid-state structure of **3.6** appears to preclude steric interaction between the two isobutylene ligands. Likewise, it is difficult to envision that the minor electronic perturbation caused by exchange of $NCAr_F'$ with isobutylene would be transferred efficiently to the second

gold atom. However, the observation corroborated the preliminary conclusion that one gold center can influence the other drawn from the ^{31}P NMR of **3.7**.

3.3 Summary of conclusions

In summary, we have synthesized the dicationic bis(gold) π -alkene complexes **3.6** and **3.7**, which represent the first examples bis(gold) phosphine π - complexes that contain a 2,2'-bis(phosphino)biaryl ligand. Both in solution and in the solid state, complex **3.6** appears to be very similar to the mono-gold complex $[(\text{P}1)\text{Au}(\eta^2\text{-isobutylene})]^+$. Slight differences in structure and exchange behavior are attributed to the increased steric bulk of the bis(phosphine) ligand. The 1-pentene complex **3.7** is formed as a statistical mixture of the three possible chemically inequivalent stereoisomers, revealing the absence of facial selectivity for the coordination of the prochiral 1-pentene ligand to the chiral bis(gold) phosphine moiety. Neither complex displays rotation around the aryl-aryl bond of the ligand backbone in solution on the timescale; this rigidity is explained by the close Au-arene contacts observed in the solid-state structure of **3.6**.

Intermolecular isobutylene exchange with **3.6** occurs via competing isobutylene-independent ($\Delta G^\ddagger \approx 17.5 \text{ kcal mol}^{-1}$) and isobutylene-dependent ($\Delta G^\ddagger \approx 16 \text{ kcal mol}^{-1}$) pathways, which is expected based on the comparison described above. Surprisingly, equilibrium analysis of the displacement of 4-trifluoromethylbenzotrile from **3.8** with

isobutylene revealed that the binding affinity of isobutylene to gold is affected by the coordination environment of the proximal gold center.

3.4 Experimental

3.4.1 General Methods

Reactions were performed under a nitrogen atmosphere employing standard Schlenk and glovebox techniques unless specified otherwise. NMR spectra were obtained on a Varian spectrometer operating at 500 MHz for ^1H NMR, 125 MHz for ^{13}C NMR, 470 MHz for ^{19}F NMR, and 202 MHz for ^{31}P NMR in CD_2Cl_2 at room temperature with noted exceptions. Elemental analysis was performed by Complete Analysis Laboratories (Parsippany, NJ). Methylene chloride was purified by passage through columns of activated alumina under nitrogen. CDCl_3 and CD_2Cl_2 were dried over CaH_2 prior to use. 2,2'-Bis(di-*tert*-butylphosphino)biphenyl (P-P), AgSbF_6 , pentane, 4-trifluoromethylbenzonitrile (NCA_{TF}), and isobutylene were purchased from major chemical suppliers and used as received.

3.4.2 Synthesis and characterization of bis(gold) complexes

$[(\text{P-P})(\text{AuCl})_2]$ Thiodiethanol (370 mg, 3.0 mmol) was added dropwise over 45 min to a stirred solution of $\text{NaAuCl}_4 \cdot 2\text{H}_2\text{O}$ (400 mg, 1.0 mmol) in H_2O (4 mL) at 4 °C. To this colorless solution was added 2,2'-bis(di-*tert*-butylphosphino)biphenyl [P-P; 0.22 g, 0.50 mmol] in CHCl_3 dropwise at 4 °C, and the resultant biphasic mixture was stirred for 1 h at 4 °C. Chloroform was evaporated under vacuum, and the resultant white

precipitate was collected by vacuum filtration and washed with minimal cold methanol to give [(P-P)(AuCl)₂] (0.45 g, 99%) as a white solid. ¹H NMR: δ 7.92 (t, *J* = 8.2 Hz, 2H), 7.68 (t, *J* = 7.4 Hz, 2H), 7.48 (t, *J* = 7.6 Hz, 2H), 7.39–7.33 (m, 2H), 1.55 (d, *J* = 16.0 Hz, 18H), 1.43 (d, *J* = 15.3 Hz, 18H). ¹³C NMR: δ 148.0 (m), 135.7 (d, *J* = 3.2 Hz), 135.5 (d, *J* = 9.6 Hz), 130.2 (d, *J* = 2.1 Hz), 128.2 (d, *J* = 7.7 Hz), 127.2 (d, *J* = 43.3 Hz), 39.1 (d, *J* = 24.4 Hz), 38.9 (d, *J* = 24.5 Hz), 33.1 (d, *J* = 6.6 Hz), 31.2 (d, *J* = 5.8 Hz). ³¹P{¹H} NMR: δ 58.5. Anal. Calcd (found) for C₂₈H₄₄Au₂Cl₂P₂: H, 4.89 (4.79); C, 37.06 (36.94).

[(P-P)(Au(η²-H₂C=CMe₂))₂]²⁺ 2(SbF₆⁻) (3.6) Methylene chloride (2 mL) was added to a mixture of [(P-P)(AuCl)₂] (40 mg, 4.4 × 10⁻² mmol) and AgSbF₆ (30 mg, 8.8 × 10⁻² mmol) under an isobutylene atmosphere, and additional isobutylene was bubbled into the solution for ~10 s. The resulting suspension was stirred for 2 h at room temperature in the dark and filtered through Celite. The filtrate was concentrated under vacuum to give **3.6** (63 mg, 99%) as a white solid. ¹H NMR: δ 8.03 (t, *J* = 7.5 Hz, 2H), 7.84 (t, *J* = 7.5 Hz, 2H), 7.77 (t, *J* = 7.5 Hz, 2H), 7.42–7.38 (m, 2H), 4.06 (dd, *J* = 2.5, 4.5 Hz, 2H), 3.89 (dd, *J* = 2.5, 4.5 Hz, 2H), 2.20 (s, 6H), 2.11 (s, 6H), 1.44 (d, *J* = 16.5 Hz, 18H), 1.40 (d, *J* = 17 Hz, 18H). ¹³C{¹H} NMR: δ 167.2 (d, *J* = 2.9 Hz), 147.4–147.1 (m), 137.3 (d, *J* = 3 Hz), 135.8 (d, *J* = 7.0 Hz), 132.8 (d, *J* = 1.9 Hz), 129.5 (d, *J* = 7.3 Hz), 126.8 (d, *J* = 41 Hz), 94.1 (d, *J* = 13.7 Hz), 39.9 (d, *J* = 23 Hz), 38.2 (d, *J* = 23 Hz), 32.4 (d, *J* = 6.2 Hz), 31.5 (d, *J* = 5.7 Hz), 28.9 (s), 28.8 (s). ³¹P{¹H} NMR: δ 64.9. Anal. Calcd (found) for C₃₆H₆₀Au₂F₁₂P₂Sb₂: H, 4.26 (4.14); C, 30.44 (30.29).

[(P-P)(Au(η^2 -H₂C=CH(CH₂)₂CH₃))₂]²⁺ 2(SbF₆⁻) (3.7) Complex **3.7** was isolated as a white solid (62 mg, 98%) from the reaction of P-P(AuCl)₂, AgSbF₆, and 1-pentene employing a procedure similar to that used to synthesize **3.6**. ¹H NMR: δ 8.15–8.06 (m, 2H), 7.95–7.82 (m, 4H), 7.52–7.42 (m, 2H), 7.42–7.38 (m, 2H), 6.36 (br s, 2H), 4.60–4.42 (m, 3H), 4.24 (br s, 1H), 2.54–2.42 (m, 2H), 2.28–2.06 (m, 2H), 1.68–1.34 (m, 40H), 0.96 (q, J = 7.0 Hz, 6H). ¹³C{¹H} NMR: δ 147.3–147.0 (m), 144.6–144.2 (m), 137.3 (d, J = 3 Hz), 135.8 (d, J = 7 Hz), 135.3 (d, J = 7 Hz), 132.9 (br s), 132.8 (br s), 129.5 (br s), 127.0–126.6 (m), 100.8 (d, J = 10.5 Hz), 100.6 (d, J = 10.3 Hz), 41.0–40.5 (m), 39.4–38.7 (m), 38.2 (br), 32.3, 31.5, 22.4, 13.3. ³¹P{¹H} NMR: δ 62.1, 62.0, 61.8, 61.7. Anal. Calcd (found) for C₃₈H₆₄Au₂F₁₂P₂Sb₂: H, 4.45 (4.37); C, 31.51 (31.48).

[(P-P)(Au(NCAr^r'))₂]²⁺ 2(SbF₆⁻) (3.8) A solution of 4-trifluoromethylbenzonitrile (19 mg, 0.11 mmol) in CH₂Cl₂ (2 mL) was added to a mixture of (P-P)(AuCl)₂ (40 mg, 4.4 \times 10⁻² mmol) and AgSbF₆ (30 mg, 8.8 \times 10⁻² mmol), and the resultant suspension was stirred for 6 h at room temperature in the dark. The reaction mixture was filtered through Celite, and the filtrate was diluted with pentane (2 mL) and cooled at 4 °C overnight to form **3.8** (25 mg, 41%) as a white solid. ¹H NMR (CD₂Cl₂): δ 8.14–8.07 (m, 6H), 7.90 (d, J = 7.8 Hz, 4H), 7.88–7.79 (m, 4H), 7.57 (t, J = 5.5, 2H), 1.59 (d, J = 16.5 Hz, 18H), 1.53 (d, J = 16.5 Hz, 18H). ¹³C NMR: δ 147.4 (q, J = 5.4 Hz), 136.4 (d, J = 6.6 Hz), 136.3 (d, J = 2.0 Hz), 135.0, 132.3, 128.9 (d, J = 7.7 Hz), 127.5, 125.9 (d, J = 47 Hz), 123.2 (q, J = 273.5 Hz), 118.2, 40.4 (d, J = 26.9), 39.0 (d, J = 26.8 Hz). ³¹P{¹H} NMR: δ 57.6. ¹⁹F{¹H} NMR:

δ -64.2. Anal. Calcd (found) for $C_{44}H_{52}Au_2F_{12}N_2P_2Sb_2$: H, 3.18 (3.15); C, 32.02 (31.87); N, 1.70 (1.54).

3.4.3 Ligand exchange studies

3.4.3.1 Kinetics of isobutylene exchange with 3.6

Isobutylene (~300 μ L, 6.9×10^{-3} mmol; 14 mM) was added via gas-tight syringe to a solution of 3.6 (2.4×10^{-2} mmol; 47 mM) and 1,3- dimethoxybenzene (internal standard, 1.5×10^{-2} mmol) in CD_2Cl_2 (0.50 mL) in an NMR tube sealed with a rubber septum. The mixture was shaken vigorously and placed in an NMR probe maintained at 25 °C for ≥ 10 minutes prior to analysis. The resonance corresponding to the vinyl protons of free isobutylene (δ 4.65) was saturated by irradiating at -155.9 Hz at a power of -9dB for 10 seconds, resulting in a loss of intensity of the vinyl resonances of bound isobutylene at δ 4.15 and δ 3.96. Resonance intensities without (S_0) and with (S) saturation at δ 4.65 were measured by integrating the resonances at δ 4.15 and δ 3.96 relative to the resonance at δ 6.5 corresponding to H4, H5, and H6 of the 1,3-dimethoxybenzene internal standard.

From these values and from the independent determination of the spin-lattice relaxation times (T_1) of bound and free isobutylene, a first-order rate constant for intermolecular isobutylene exchange with 3.6 of $k = 2 \times (1/T_{1free})[(S_0/S)-1] = 1.0 \text{ s}^{-1}$ was determined; the standard equation for magnetization transfer must be multiplied by the stoichiometric factor of 2 owing the presence of two equivalent isobutylene ligands.¹²⁶ Analyses were performed in duplicate over a range of concentrations of free isobutylene

from 14 - 61 mM. A plot of k_{obs} versus [isobutylene] was linear with a non-zero intercept, which established the two-term rate law for intermolecular isobutylene exchange with **3.6** of rate = $k_1[\mathbf{3.6}] + k_2[\mathbf{3.6}][\text{isobutylene}]$ where $k_1 = 0.86 \pm 0.02 \text{ s}^{-1}$ ($\Delta G^\ddagger_{298K} = 17.52 \pm 0.01 \text{ kcal mol}^{-1}$) and $k_2 = 8.3 \pm 0.5 \text{ M}^{-1}$ ($\Delta G^\ddagger = 16.18 \pm 0.03 \text{ kcal mol}^{-1}$).¹²⁵ Error values correspond to the standard error of the intercept and slope, respectively, of this plot.

3.4.3.2 Equilibrium Binding Studies

Isobutylene (500 μL , 0.67 mg, 1.2×10^{-2} mmol) was added via gas-tight syringe to an NMR tube sealed with a rubber septum containing a solution of **3.8** (4.8 mg, 3.0×10^{-3} mmol) and NCArF' (0.33 mg, 1.9×10^{-3} mmol) in CD_2Cl_2 (0.50 mL) and a sealed capillary containing a solution of PPh_3 in CD_2Cl_2 (0.48 M, external standard). The tube was inverted several times, placed into the probe of an NMR spectrometer pre-cooled at -50°C , and maintained at this temperature for 10 minutes. The concentrations of **3.8**, **3.9**, and **3.6** were determined by integrating the ^{31}P resonances corresponding to **3.8** (δ 55.6), **3.9** [δ 55.7 and 65.1 (1:1)], and **3.6** (δ 65.2) relative to the resonance corresponding to PPh_3 (δ -6.0). The concentration of free isobutylene was calculated from the experimentally determined concentrations of **3.6** and **3.9** and from the ratio of free:bound isobutylene, determined by integrating the ^1H resonances corresponding to the vinylic protons of free isobutylene (δ 4.60), and bound isobutylene [δ 4.05 and δ 3.76 (1:1, **3.6** and **3.9**)], using the formula: $[\text{isobutylene}]_{\text{free}} = (\text{ratio free:bound isobutylene}) \times (2[\mathbf{3.6}] \times [\mathbf{3.9}])$. Similarly,

the ratio of free $\text{NCA}_{\text{rF}'}$ calculated from the experimentally determined concentrations of **3.8** and **3.9** and from the ratio of free:bound $\text{NCA}_{\text{rF}'}$, determined by integrating the ^{19}F resonance corresponding to free $\text{NCA}_{\text{rF}'}$ ($\delta -63.4$) and bound $\text{NCA}_{\text{rF}'}$ [$\delta -63.7$ (both **3.8** and **3.9**)], using the formula: $[\text{NCA}_{\text{rF}'}]_{\text{free}} = (\text{ratio free:bound } \text{NCA}_{\text{rF}'}) \times (2[\mathbf{3.8}] \times [\mathbf{3.9}])$.

Analogous experiments were performed as a function of $[\text{isobutylene}]_{\text{total}}$ from 27-85 mM. From these data, equilibrium constants were determined for the conversion of **3.8** to **3.9** (K_1), **3.9** to **3.6** (K_2) and **3.8** to **3.6** (K_3); the reported values refer to the averages determined from multiple experiments with $[\text{isobutylene}]_{\text{total}}$ ranging from 27-85 mM and the reported error values refer to the standard deviation among the respective sets of data.

To ensure that equilibrium was achieved under these conditions, a similar experiment was performed through addition of $\text{NCA}_{\text{rF}'}$ to a solution of **3.6** (15.7 mM) in CD_2Cl_2 at $-50\text{ }^\circ\text{C}$. Equilibrium constants were calculated as outlined above as a function of $[\text{NCA}_{\text{rF}'}]_{\text{total}}$ from 14-159 mM; equilibrium constants determined in this manner did not differ significantly from those obtained from reaction of **3.8** and isobutylene.

3.4.4 X-Ray crystal structures

3.4.4.1 X-ray crystal structure data for $\mathbf{3.6}\cdot\text{CH}_2\text{Cl}_2$

Slow diffusion of pentane into a CH_2Cl_2 solution of **3.6** at $4\text{ }^\circ\text{C}$ formed colorless crystals of $\mathbf{3.6}\cdot\text{CH}_2\text{Cl}_2$ suitable for X-ray analysis (Figure 32, Table 10). The sample was mounted on a Mitegen polyimide micromount with a small amount of Paratone N oil.

All X-ray measurements were made on a Bruker-Nonius Kappa Axis X8 Apex2 diffractometer at a temperature of 110 K. The unit cell dimensions were determined from a symmetry constrained fit of 9764 reflections with $4.72^\circ < 2\theta < 46.04^\circ$. The data collection strategy was a number of ω and φ scans which collected data up to $57.5^\circ (2\theta)$. The frame integration was performed using SAINT.⁹⁹ The resulting raw data was scaled and absorption corrected using a multi-scan averaging of symmetry equivalent data using SADABS.¹⁰⁰ The structure was solved by direct methods using the SIR92 program.¹⁰² Most non-hydrogen atoms were obtained from the initial solution. The remaining non-hydrogen atom positions were obtained from subsequent difference Fourier maps. The hydrogen atoms were introduced at idealized positions and were allowed to ride on the parent atom. The C2—C3 bond length was restrained to a target value of 1.54 Å and refined to a value of 1.579(9) Å. The model also showed high amplitude motion in the alkene bonded to Au1. The difference map was scrutinized for suggestions of an orientational disorder, but a set of peaks representing an alternative orientation could not be found. The structural model was fit to the data using full matrix least-squares based on F^2 . The calculated structure factors included corrections for anomalous dispersion from the usual tabulation. The structure was refined using the XL program from SHELXTL,¹⁰³ graphic plots were produced using the NRCVAX crystallographic program suite.

3.4.4.2 X-Ray Crystal Structure of 3.7·CH₂Cl₂

Slow diffusion of pentane into a CH₂Cl₂ solution of 3.7 at 4 °C formed colourless crystals of 3.7·CH₂Cl₂ suitable for X-ray analysis (Figure 33, Table 10). The sample was mounted on a Mitegen polyimide micromount with a small amount of Paratone N oil. All X-ray measurements were made on a Bruker-Nonius Kappa Axis X8 Apex2 diffractometer at a temperature of 110 K. The unit cell dimensions were determined from a symmetry constrained fit of 2769 reflections with $4.82^\circ < 2\theta < 55.96^\circ$. The data collection strategy was a number of ω and ϕ scans which collected data up to 61.22° (2θ). The frame integration was performed using SAINT.⁹⁹ The resulting raw data was scaled and absorption corrected using a multi-scan averaging of symmetry equivalent data using TWINABS.¹²⁷ The crystal was a multiple domained “twin”. Indexing was stopped at 5 domains. However, integration of more than 2 components led to unsatisfactory integrations. The data was fit to a two component twin. The structure was solved by direct methods using the XS program.¹⁰¹ All non-hydrogen atoms were obtained from the initial solution. The hydrogen atoms were introduced at idealized positions and were allowed to ride on the parent atom. The data was integrated as a two component twin. However, using this data gave worse results than using the data only from the primary domain (the “detwinned” data), but even this was not completely satisfactory. The final refinements were done using the detwinned data. The structural model was fit to the data using full matrix least-squares based on F^2 . The calculated structure factors

included corrections for anomalous dispersion from the usual tabulation. The structure was refined using the XL program from SHELXTL¹⁰³ and graphic plots were produced using the NRCVAX crystallographic program suite.

Table 10: Crystal and structure refinement data for complexes 3.6·CD₂Cl₂ and 3.7·CD₂Cl₂.

	3.6·CD ₂ Cl ₂	3.7·CD ₂ Cl ₂
empirical formula	C ₃₇ H ₆₂ Au ₂ Cl ₂ F ₁₂ P ₂ Sb ₂	C ₃₉ H ₆₅ Au ₂ Cl ₂ F ₁₂ P ₂ Sb ₂
fw	1505.14	1532.18
crystal size (mm ³)	0.18 x 0.08 x 0.04	0.24 x 0.12 x 0.07
Color and habit	colorless prism	colorless prism
T (K)	110(2)	110(2)
λ (Å)	0.71073	0.71073
crystal system	orthorhombic	monoclinic
space group	Pbca	P2 ₁ /c
unit cell dimensions	a = 13.7610(4) Å b = 17.2858(5) Å c = 39.9274(12) Å	a = 19.0763(6) Å b = 15.7558(5) Å β = 93.1807(18)° c = 16.9063(5) Å
V (Å ³)	9497.5(5)	5073.6(3)
Z	8	4
D _{calc} (g/cm ³)	2.105	2.006
2θ _{max} (deg)	57.5	61.22
abs coeff (cm ⁻¹)	7.539	7.058
total no. of reflns	154134	15425
no. of unique reflns	12303	15425
no. params. refined/restraints	12303/514	15425/532
F(000)	5728	2924
goodness-of-fit on F ²	1.085	1.075
final R indices [I>2σ(I)]	R1 = 0.0529, wR2 = 0.1268	R1 = 0.0716, wR2 = 0.1693
R indices (all data)	R1 = 0.0918, wR2 = 0.1453	R1 = 0.1178, wR2 = 0.1817
max,min Δρ, (e/Å ⁻³)	-3.174, 3.702	-3.819, 6.445

4. Synthesis and Solution Behavior of Cationic, Two-Coordinate Gold(I) π -Complexes Bearing a Triphenylphosphine Ligand

Portions of this chapter have been published: Brooner, R. E. M.; Brown, T. J.; Widenhoefer, R. A. *Chem.-Eur. J.* **2013**, *19*, 8276. Synthesis, characterization, and variable-temperature NMR studies of complex **4.11** were performed by Dr. T. J. Brown.

4.1 Introduction

4.1.1 The use of triarylphosphines in gold(I) catalysis

It is undeniable that the surge of information regarding the structure and solution behavior of gold(I) complexes in recent years has greatly increased general understanding of the mechanisms operative in gold(I) π -activation catalysis. However, despite boasting a wide variety of different π -ligands, isolated gold(I) π -complexes bear almost exclusively sterically hindered, electron-rich supporting ligands such as *N*-heterocyclic carbenes (NHC) or dialkyl *o*-biphenylphosphines. While these ligands have been employed to good effect in gold(I) π -catalysis, the simplest triarylphosphine, triphenylphosphine, remains the workhorse ligand in gold(I) catalysis. Similarly, axially chiral bis(triarylphosphines) remain the most common utilized in enantioselective gold π -activation catalysis.

As demonstrated previously, a great interest in the understanding of the nature of gold(I) π -complexes has arisen out of their purported role in catalysis. Unfortunately, no cationic, mononuclear gold(I) π -complex bearing a triphenylphosphine ligand has

been isolated. Rather, information regarding the structure, bonding, and reactivity of these complexes is gleaned either from characterization of mononuclear, cationic gold(I) complexes of π -alkene,^{36, 42, 46, 128} alkyne,^{49, 52, 129} allene,¹³⁰⁻¹³¹ conjugated diene,^{88-89, 122} or arene^{38, 90, 132} π -ligands that bear a sterically hindered, electron-rich supporting ligand or from reports of complexes generated and observed spectroscopically only *in situ* (see below).

4.1.2 Background on triarylphosphine gold(I) π -complexes

4.1.2.1 Examples of triarylphosphine gold(I) π -complexes

Although triphenylphosphine gold(I) π -complexes have escaped isolation, a limited number of examples of π -complexes bearing other triarylphosphine ligands have been reported. In 2008, Toste and coworkers reported the synthesis of the polymeric, cationic gold π -alkene complex **4.1** and dimeric gold π -alkyne complex **4.2**, which contained triarylphosphine supporting ligands tethered to π -ligands by an alkyl chain (Figure 35)¹³³ Single crystal X-ray analysis of **4.1** established the presence of a distorted gold η^2 -alkene π -bond with a shorter Au-CHR and a longer Au-CMe₂ interaction ($\Delta d = \sim 0.1$ Å). Likewise, for complex **4.2** in the solid state, gold is η^2 -bound to the silylalkyne moiety but is slipped toward the tri-*iso*-propylsilyl group through a shorter Au-C1 and longer Au-C2 bond ($\Delta d = 0.073$ Å); the alkyne substituent on **4.2** is bent away from gold [C \equiv C-C = 167.2°, C \equiv C-Si = 164.4°]. Detailed solution characterization of **4.1** and **4.2** was precluded by facile disproportionation of the complexes.

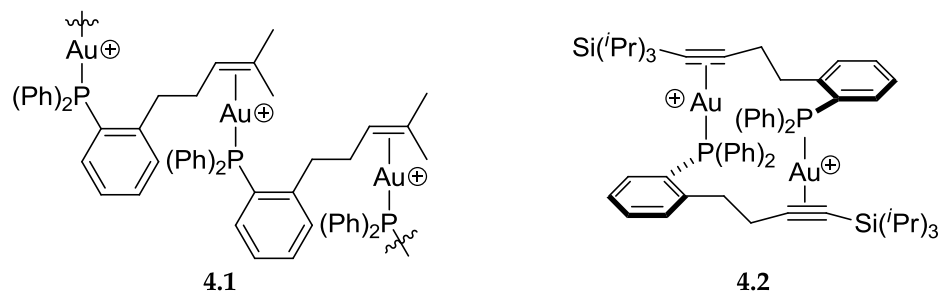


Figure 35: Cationic, multimeric gold(I) π -complexes containing triarylphosphine supporting ligands.

Later, Macchioni and coworkers reported *in situ* generation and characterization of the thermally sensitive triarylphosphine gold π -alkyne complex $[(\text{PAr}_3)\text{Au}(\eta^2\text{-MeC}\equiv\text{C}^n\text{Pr})]^+ \text{BF}_4^-$ [Ar = 3,5-bis(trifluoromethyl)phenyl (**4.3**)] (Figure 36), which was characterized without isolation at -69°C .⁴⁸ Spectroscopically, ^{19}F - ^1H HOESY analysis indicated that the BF_4^- counterion was located near the gold atom in an area between the phosphine and alkyne π -ligand, which the authors suggested is an indication that the positive charge locates mainly on the gold atom in these complexes. Recently, Dias has reported synthesis and structural characterization of the cyclooctyne complex $[(\text{Mes}_3\text{P})\text{Au}(\eta^2\text{-cyclooctyne})]^+ \text{SbF}_6^-$ (**4.4**; Figure 36).⁵⁰ Although **4.4** decomposed slowly in solution at room temperature, it is significantly more stable than complex **4.3**, which decomposes readily in solution near room temperature.

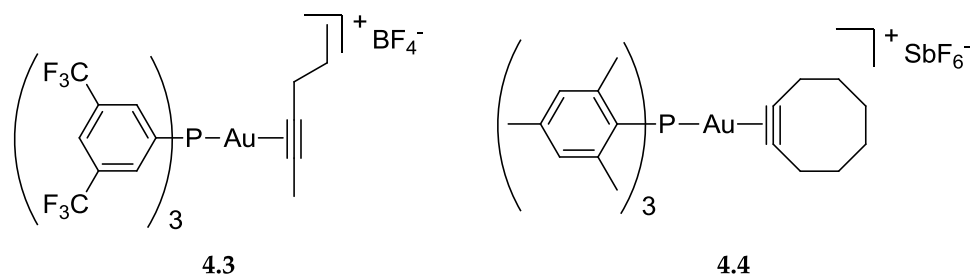


Figure 36: Thermally unstable cationic, monomeric gold(I) π -complexes containing triarylphosphine supporting ligands.

In addition to the complexes above, the synthesis and X-ray crystal structures of a pair of stable, cationic triphenylphosphine gold enamine complexes have been reported.¹³⁴ However, in contrast to gold complexes of alkyl and aliphatic alkenes, X-ray analysis of these complexes revealed η^1 -coordination of the nitrogen-substituted ligand with no significant contribution of the corresponding η^2 - canonical form. Furthermore, the stability and reactivity of these complexes is more similar to triphenylphosphine gold(I) σ -alkyl complexes, which are well known in the literature.¹³⁵⁻¹³⁶

4.1.2.2 Reported *in situ* generation of [(PPh₃)Au]⁺ π -complexes

As with some of the less-stable triarylphosphine gold(I) π -complexes, a number of triphenylphosphine gold(I) π -complexes have been purportedly generated *in situ* from reaction of a π -ligand with either a mixture of [(PPh₃)AuCl] and silver salt or a single-component gold complex, such as [(PPh₃)AuNTf₂].^{3, 41, 115, 137-141} However, there are a number of inconsistencies in the reported spectroscopy and solution behavior of these complexes that warrant further investigation. In most cases, characterization of the purported triphenylphosphine gold π -complex rests solely on ³¹P NMR analysis

recorded at or above room temperature, which often shows full conversion of [(PPh₃)AuX] to a new complex with reported chemical shifts ranging from $\delta = 28$ to 45 ppm. We found the broad range of chemical shifts disconcerting given the narrow range of phosphorous chemical shifts ($\delta = 65 \pm 3$ ppm) observed for a family of more than 30 complexes of the form [(P1)Au(π -ligand)]⁺ SbF₆⁻.^{38, 46, 49, 88-90, 122, 130-131} Furthermore, the lower frequency value of $\delta = 28$ ppm is similar to that of weak σ -complexes, such as [(PPh₃)AuOTf]¹⁴², [(PPh₃)AuNTf₂]¹⁴³ and [((PPh₃)Au)₂(μ -Cl)]⁺ SbF₆⁻ (**4.5**),¹⁴⁴ whereas the higher frequency value of $\delta = 45$ ppm is similar to the bis(phosphine) cation [(PPh₃)₂Au]⁺ (**4.6**) (Table 11).¹⁴⁵ Both of these complexes can be envisioned as byproducts or decomposition products formed in the generation of triphenylphosphine gold π -complexes.

Table 11: ³¹P NMR Chemical shifts of relevant triphenylphosphine gold σ -complexes in CD₂Cl₂.

σ -complex	δ at 25 °C	δ at -90 °C
Ph ₃ PAuCl	32.7	30.6
Ph ₃ PAuOTf	30.6	28.0
Ph ₃ PAuNTf ₂	29.9	27.8
(Ph ₃ P)Au [⊕] -Cl-Au(PPh ₃) 4.5	30.7	28.5
Ph ₃ P-Au [⊕] -PPh ₃ 4.6	45.5	41.8

Perhaps best characterized of these triphenylphosphine gold π -complexes is the 4-methylstyrene complex [(PPh₃)Au(η^2 -H₂C=C(H)-4-C₆H₄CH₃)]⁺ BF₄⁻ (**4.7**·BF₄), which was

interrogated by variable-temperature, multinuclear, one- and two-dimensional NMR analysis.⁴¹ However, significant broadening of the reported ³¹P NMR resonance of $4.7 \cdot \text{BF}_4^-$ ($\delta = 37.6$ ppm, $\nu_{1/2} \approx 250$ Hz at -20 °C) suggested that a rapidly equilibrating mixture of complexes is actually present in solution.

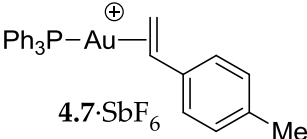
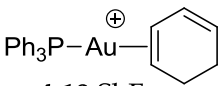
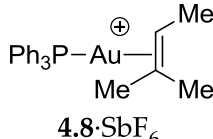
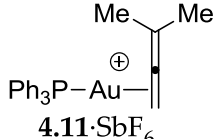
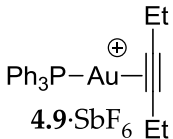
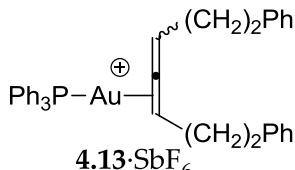
4.1.3 Project goals and scope

Due to the apparent inconsistencies and discrepancies in the extant reports of two-coordinate triphenylphosphine gold π -complexes, we sought to develop a more detailed understanding of the spectroscopy and solution behavior of these complexes. We hoped to establish a well-defined set of solution characteristics and spectroscopic handles for identification of these complexes. Further, we sought to understand more about the ligand-exchange and decomposition behavior of the complexes and the influence of the complex counterion.

To this end, a family of gold complexes of the form $[(\text{PPh}_3)_3\text{Au}(\pi\text{-ligand})]^+$ (π -ligand = alkene, vinyl arene, alkyne, conjugated diene, allene) was generated and characterized without isolation, employing low-temperature, multinuclear NMR spectroscopy (Table 12). Key observations made in the course of our investigation include the following: 1) the π -ligands of cationic triphenylphosphine gold π -complexes are considerably more labile than the π -ligands of related gold NHC and *o*-biphenylphosphine π -complexes; 2) careful control of reaction stoichiometry and employment of a weakly coordinating counterion, such as SbF_6^- , was required to

generate solutions of cationic triphenylphosphine gold π -complexes free from byproducts; 3) all of the gold π -complexes generated in this study are thermally unstable and decompose above $-20\text{ }^{\circ}\text{C}$ to form the bis(triphenylphosphine) gold cation $[(\text{PPh}_3)_2\text{Au}]^+$ (**4.6**); and 4) the ^{31}P NMR resonances of these complexes fall within the range of $\delta = 37.1 \pm 1.7$ ppm.

Table 12: ^{31}P NMR chemical shifts of the synthesized triphenylphosphine gold π -complexes in CD_2Cl_2 .

π -complex	^{31}P δ (ppm)	π -complex	^{31}P δ (ppm)
 4.7 ·SbF ₆	38.8 ($-90\text{ }^{\circ}\text{C}$)	 4.10 ·SbF ₆	37.2 ($-90\text{ }^{\circ}\text{C}$)
 4.8 ·SbF ₆	36.8 ($-85\text{ }^{\circ}\text{C}$)	 4.11 ·SbF ₆	36.3 ($-90\text{ }^{\circ}\text{C}$)
 4.9 ·SbF ₆	36.1 ($-70\text{ }^{\circ}\text{C}$)	 4.13 ·SbF ₆	36.5, 35.4 ($\sim 1:2.5$, $-90\text{ }^{\circ}\text{C}$)

4.2 Results and discussion

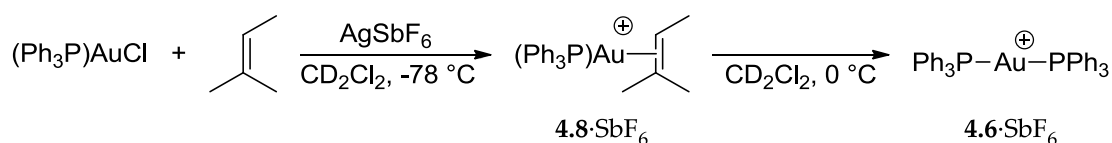
4.2.1 Triphenylphosphine gold π -alkene complexes

4.2.1.1 Synthesis and characterization of $[(\text{PPh}_3)\text{Au}(\eta^2\text{-Me(H)C=CMe}_2)]^+\text{SbF}_6^-$ (**4.8**·SbF₆)

Addition of 2-methyl-2-butene (1 equiv.) to a 1:1 mixture of $[(\text{PPh}_3)\text{AuCl}]$ and AgSbF_6 in CD_2Cl_2 at $-78\text{ }^{\circ}\text{C}$ for 5 min led to formation of thermally unstable $[(\text{PPh}_3)\text{Au}(\eta^2\text{-Me(H)C=CMe}_2)]^+\text{SbF}_6^-$ (**4.8**·SbF₆; Table 12 and Scheme 13). Complex

4.8·SbF₆ was characterized without isolation by low temperature NMR spectroscopy. The ³¹P NMR spectrum of **4.8**·SbF₆ at -85 °C displayed a single sharp resonance at δ = 36.8 ppm consistent with complete conversion of the starting [(PPh₃)AuCl] to a new organometallic complex.

Scheme 13: Low temperature generation of triphenylphosphine gold π-alkene complex **4.8·SbF₆ and its decomposition to **4.6**·SbF₆.**



Complexation of the alkene to gold was established by the downfield shift of the C2 alkene carbon resonance (δ = 145.4 ppm) and the upfield shift of the C3 alkene carbon resonance (δ = 111.8 ppm, d, J_{CP} = 10.5 Hz) relative to free 2-methyl-2-butene (C2, δ = 132.0; C3, δ = 118.0 ppm) in the ¹³C NMR spectrum of **4.8**·SbF₆ at -85 °C. The ¹³C NMR chemical shifts of the alkenyl carbon atoms of **4.8**·SbF₆ are similar to those observed for [(P1)Au(η²-Me(H)C=CMe₂)]⁺SbF₆⁻ (**4.9**·SbF₆, δ = 146.1, 111.4 ppm),⁴⁶ corroborating formation of a single gold(I) π-alkene complex in solution. Unlike **4.9**·SbF₆, with a vinyl proton resonance (δ = 4.20 ppm) that was shifted upfield relative to free alkene (δ = 5.12 ppm), the vinyl proton of **4.8**·SbF₆ (δ = 5.96) was shifted strongly downfield relative to free alkene. Rather, the downfield shift of the vinyl protons was consistently observed for π-alkene complexes bearing the ^tBu₃P ligand.³⁶

Warming a CD₂Cl₂ solution of **4.8**·SbF₆ at 0 °C led to decomposition (t_{1/2} ≈ 90 min) with concomitant formation of a sharp resonance at δ = 43.8 ppm in the ³¹P NMR

spectrum of the mixture as well as precipitation of black material and/or plating of metallic gold from the solution (Scheme 13). The resonance at δ 43.8 ppm was confidently attributed to $[(PPh_3)_2Au]^+ SbF_6^-$ (**4.6** \cdot SbF_6) by comparison to an authentic sample prepared by treatment of a 1:1 mixture of $[(Ph_3P)AuCl]$ and $AgSbF_6$ with 1 equiv. triphenylphosphine in CD_2Cl_2 .

4.2.1.2 Effect of stoichiometry on the synthesis of **4.8** \cdot SbF_6

To explore the effect of reaction stoichiometry on the composition and solution behavior of **4.8**, complex **4.8** was generated and studied *in situ* with equimolar $[(Ph_3P)AuCl]/AgSbF_6$ and a deficiency of 2-methyl-2-butene and with equimolar $[(Ph_3P)AuCl]/2$ -methyl-2-butene and a deficiency of $AgSbF_6$. When a 2:2:1 mixture of $[(PPh_3)AuCl]$, $AgSbF_6$ and 2-methyl-2-butene in CD_2Cl_2 reacted at -78 °C, the ^{31}P NMR spectrum of the resulting solution at -94 °C displayed an approximately 2:1 ratio of sharp resonances at $\delta = 36.8$ and 28.2 ppm (Figure 37). Although the resonance at $\delta = 36.8$ ppm can be confidently assigned to **4.8** \cdot SbF_6 , which was also observed in the 1H NMR spectrum of the mixture, the composition of the complex (**A** \cdot SbF_6) that gives rise to the $\delta = 28.2$ ppm resonance remains unclear. Possible structures of complex **A** \cdot SbF_6 include the free gold cation $[(PPh_3)Au]^+ SbF_6^-$, the solvated cation $[(PPh_3)Au(CD_2Cl_2)]^+ SbF_6^-$, or the gold/silver heterobimetallic complex $[(PPh_3)Au(\mu-Cl)Ag]^+ SbF_6^-$. In any case, reaction of a 1:1 mixture of $[(PPh_3)AuCl]$ and $AgSbF_6$ at -78 °C in the absence of alkene or

other π -ligand likewise displays a broad resonance at $\delta \approx 28$ ppm, indicating that 2-methyl-2-butene is unlikely to be a component of $\mathbf{A}\cdot\text{SbF}_6$.

Warming the aforementioned solution of $\mathbf{4.8}\cdot\text{SbF}_6$ and $\mathbf{A}\cdot\text{SbF}_6$ above -50 °C resulted in broadening of the resonance of $\mathbf{A}\cdot\text{SbF}_6$ at $\delta \approx 28$ ppm without detectable broadening of the phosphorous resonance of $\mathbf{4.8}\cdot\text{SbF}_6$ below the onset of decomposition at -20 °C (Figure 37), which argues against intermolecular alkene exchange between $\mathbf{4.8}\cdot\text{SbF}_6$ and $\mathbf{A}\cdot\text{SbF}_6$. Supporting this contention, the ^1H NMR spectrum of this 2:1 mixture of $\mathbf{4.8}\cdot\text{SbF}_6$ and $\mathbf{A}\cdot\text{SbF}_6$ displayed only a single set of alkene resonances, corresponding to the bound 2-methyl-2-butene ligand of $\mathbf{4.8}\cdot\text{SbF}_6$ which did not broaden or shift over the temperature range -94 to 0 °C. Qualitatively, the presence of $\mathbf{A}\cdot\text{SbF}_6$ did not have an effect on the decomposition of $\mathbf{4.8}\cdot\text{SbF}_6$.

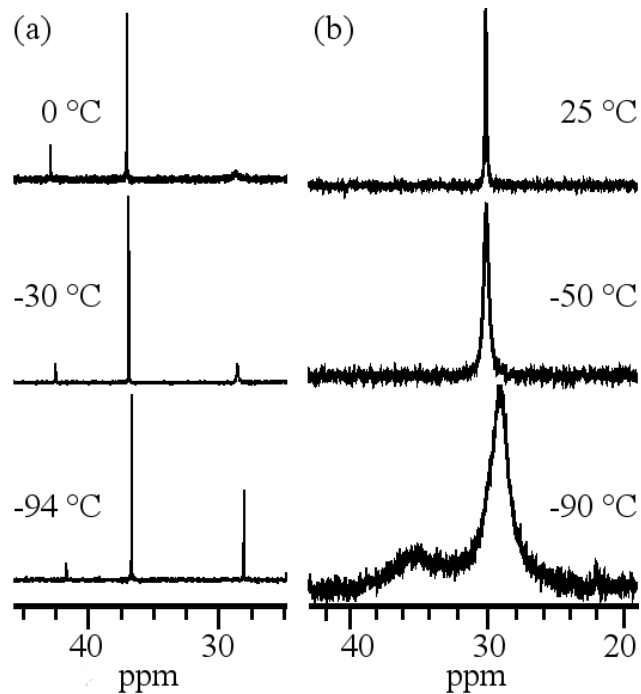


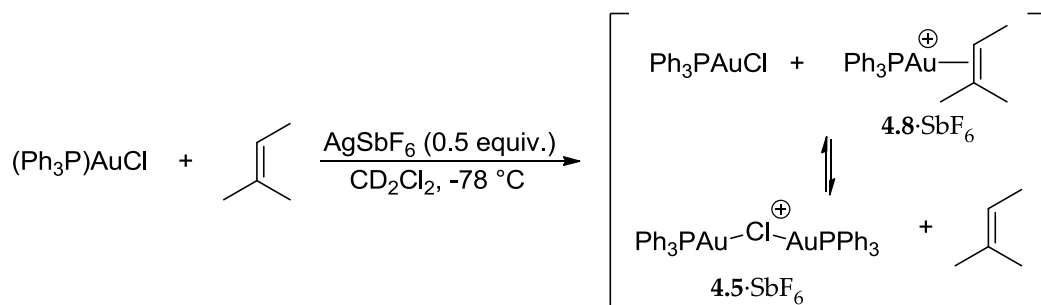
Figure 37: Variable-temperature ^{31}P NMR spectra of the solutions generated from reaction of (a) a 2:2:1 mixture of $[(\text{PPh}_3)\text{AuCl}]$, AgSbF_6 , and 2-methyl-2-butene in CD_2Cl_2 at $-78\text{ }^\circ\text{C}$ (left); and (b) a 2:1:2 mixture of $[(\text{PPh}_3)\text{AuCl}]$, AgSbF_6 , and 2-methyl-2-butene in CD_2Cl_2 at $-78\text{ }^\circ\text{C}$ (right). Vertical amplitude is not consistent between spectra.

To evaluate the effect of a deficiency of silver salt on the formation of **4.8**· SbF_6 , a 2:1:2 mixture of $[(\text{PPh}_3)\text{AuCl}]$, AgSbF_6 , and 2-methyl-2-butene was combined in CD_2Cl_2 at $-78\text{ }^\circ\text{C}$. The ^{31}P NMR spectrum of this mixture at $-90\text{ }^\circ\text{C}$ displayed a large broad resonance at $\delta = 29$ and a small broad peak at $\delta \approx 35$ ppm (Figure 37). When the temperature of the solution was raised, these resonances coalesced to form a single peak at $\delta = 30.6$ ppm ($\nu_{1/2} = 84$ Hz) at $-50\text{ }^\circ\text{C}$, which sharpened further upon warming the solution to $25\text{ }^\circ\text{C}$ ($\delta = 30.0$ ppm ($\nu_{1/2} = 11$ Hz); Figure 37). No decomposition or formation of **4.6** was detected after 5 h at this temperature. Likewise, the ^1H NMR spectrum of the

same mixture at -90 °C revealed extremely broad resonances in the vinylic ($\delta = 5.7 - 4.7$ ppm) and aliphatic ($\delta = 2.4 - 0.9$ ppm) regions, which sharpened upon warming to -50 °C, forming one vinylic resonance at $\delta = 5.27$ and three methyl resonances at $\delta = 1.75$, 1.68, and 1.60 ppm.

Treatment of [(PPh₃)AuCl] with a sub-stoichiometric amount of an activating silver salt is known to result in formation of the bis(gold) chloronium species [(PPh₃)Au]₂(μ -Cl)]⁺ (**4.5**).¹⁴⁴ Spectroscopic analysis of **4.5**·SbF₆ in CD₂Cl₂, generated by reacting a 2:1 mixture of [(PPh₃)AuCl] and AgSbF₆ at 25 °C, revealed a single resonance at δ 28.5 ppm at -90 °C and δ 30.7 ppm at 25 °C. Based on this and the spectra of independently generated **4.8**·SbF₆, it was concluded that the reaction of [(PPh₃)AuCl], AgSbF₆, and 2-methyl-2-butene in a 2:1:2 ratio results in a rapidly interconverting mixture of π -alkene complex **4.8**·SbF₆ ($\delta = 36.8$ ppm), [(PPh₃)AuCl] ($\delta = 30.6$ ppm), the chloride-bridged bis(gold) cation [(PPh₃)Au]₂(μ -Cl)]⁺ SbF₆⁻ (**4.5**·SbF₆) ($\delta = 28.5$ ppm), and free 2-methyl-2-butene that favors **4.8**·SbF₆ and free alkene (Scheme 14). The thermal stability of the mixture presumably reflects the low equilibrium concentration of **4.8**·SbF₆ present under these conditions.

Scheme 14: Reaction of an equimolar mixture of [(PPh₃)AuCl] and 2-methyl-2-butene with a deficiency of AgSbF₆ to form an equilibrating mixture of 4.8·SbF₆ and 4.5·SbF₆.

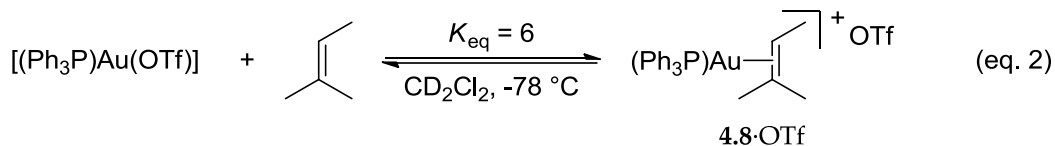
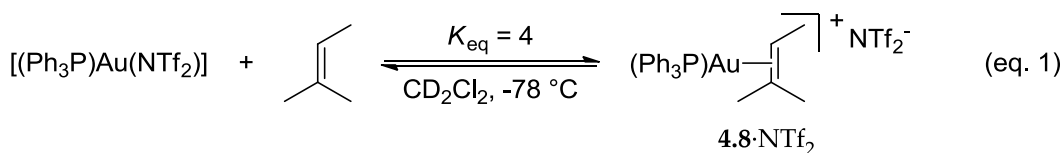


4.2.1.3 Effect of counterion on the synthesis of 4.8·SbF₆

The bistriflimide (NTf₂⁻) and triflate (OTf⁻) anions are common counterions used in gold(I) π-activation catalysis as they coordinate very weakly to the [(L)Au]⁺ cation. On the other hand, they are more coordinating than the SbF₆⁻ commonly used in synthesis and isolation of cationic gold π-complexes. To evaluate the effect of counterion on the formation and solution behavior of alkene complex **4.8**, formation of the complex was attempted with both the NTf₂⁻ and OTf⁻ counterions. When an equimolar mixture of Ph₃PAuNTf₂ and 2-methyl-2-butene (73 mM) was combined in CD₂Cl₂ at -78 °C (Scheme 15, eq. 2), the ³¹P NMR spectrum of the resulting mixture at -90 °C displayed a ~4:1 ratio of broad resonances at δ = 37 (ν_{1/2} = 105 Hz) and δ = 28 (ν_{1/2} = 38 Hz), consistent with an equilibrating mixture of π-alkene complex **4.8**·NTf₂ and gold bistriflimide complex Ph₃PAuNTf₂. Both the ¹H and ¹³C NMR spectra of the solution at -90 °C displayed broad, time-averaged resonances for bound and free alkene, consistent with rapid exchange of alkene and bistriflimide on the NMR time scale. Similarly, when an equimolar mixture

of Ph_3PAuCl , AgOTf , and 2-methyl-2-butene was combined in CD_2Cl_2 at $-78\text{ }^\circ\text{C}$ (Scheme 15, eq. 2), the ^{31}P NMR spectrum at $-90\text{ }^\circ\text{C}$ displayed a ~6:1 ratio of broad resonances at $\delta = 38$ ($\nu_{1/2} \approx 100\text{ Hz}$) and $\delta = 30$ ($\nu_{1/2} \approx 400\text{ Hz}$), consistent with an equilibrating mixture of $4.8\cdot\text{OTf}$ and Ph_3PAuOTf .

Scheme 15: Competitive binding of 2-methyl-2-butene and the NTf_2^- (eq. 1) and OTf^- (eq. 2) counterions for $[(\text{PPh}_3)\text{Au}]^+$.



4.2.2 Triphenylphosphine gold π -(vinyl arene) complex 4.7

As previously introduced, broadening in the ^{31}P NMR spectrum ($-20\text{ }^\circ\text{C}$) of what was assumed to be a solution of $4.7\cdot\text{BF}_4$ suggested the presence of a mixture of complexes.⁴¹ On the other hand, the significant perturbation of the vinylic proton resonances present in this solution relative to free 4-methylstyrene leaves little doubt that complex $4.7\cdot\text{BF}_4$ is generated in solution from mixtures of $[(\text{PPh}_3)\text{AuCl}]$, AgBF_4 , and 4-methylstyrene. Comparison of the reported spectra to those obtained in the generation of $4.8\cdot\text{SbF}_6$ with a deficiency of alkene implicate $\text{A}\cdot\text{BF}_4$ as a likely byproduct. Furthermore, $\text{A}\cdot\text{BF}_4$ may be more prevalent in this case than was $\text{A}\cdot\text{SbF}_6$ in the formation of $4.8\cdot\text{SbF}_6$ owing both to the weaker ligating ability of 4-methylstyrene relative to 2-

methyl-2-butene for $[(L)Au]^+$, as was demonstrated for π -alkene complexes in which $L = IPr^{42}$ and $P1$,⁴⁶ and the stronger coordination of BF_4^- relative to SbF_6^- .

We sought to investigate the possibility of the formation of byproducts such as $A \cdot SbF_6^-$ in the generation of $4.7 \cdot SbF_6^-$ by replicating the synthesis under carefully controlled conditions and analyzing the mixture using variable temperature NMR spectroscopy. Indeed, the ^{31}P NMR spectrum of a 1:1:1.15 mixture of $[(PPh_3)AuCl]$, $AgBF_4$, and 4-methylstyrene in CD_2Cl_2 at $-20^\circ C$ displayed a single broad resonance at $\delta = 33.9$ ppm ($\nu_{1/2} = 112$ Hz) (Table 12). Although a slight discrepancy is observed between the ^{31}P chemical shift for $4.7 \cdot BF_4^-$ reported by Macchoni ($\delta = 37.8$ ppm) and in this work ($\delta = 34.3$ ppm), this can be attributed to the different referencing systems employed in the two studies (85% H_3PO_4 versus $(PPh_3)O$ in CD_2Cl_2). When the solution of $4.7 \cdot BF_4^-$ was cooled to $-90^\circ C$, the observed ^{31}P resonance broadened significantly ($\nu_{1/2} > 1000$ Hz; Figure 38), further indicating the presence of a mixture of complexes in solution.

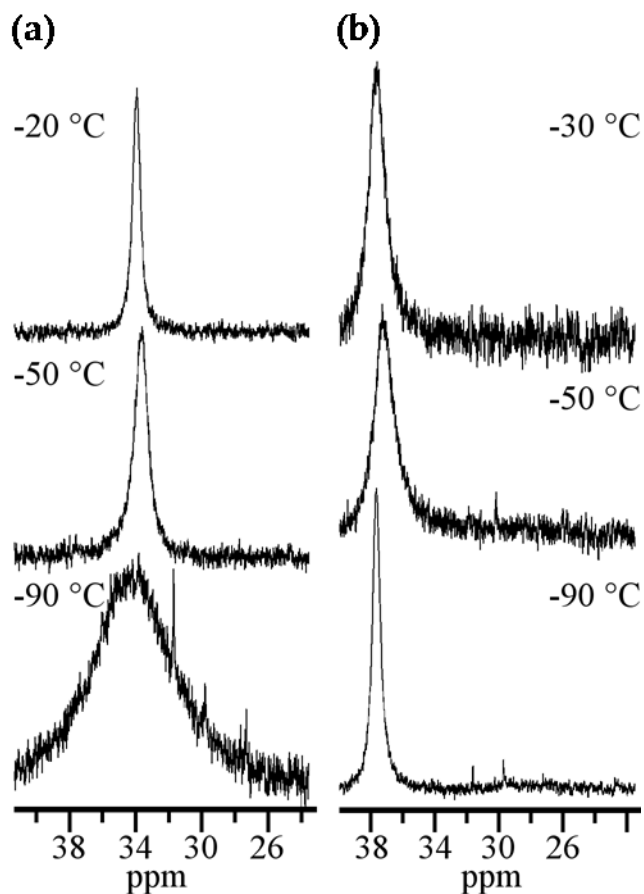


Figure 38: Variable-temperature ^{31}P NMR spectra of the solutions generated from reaction of (a) a 1:1:1.15 mixture of $[(\text{PPh}_3)\text{AuCl}]$, AgBF_4 , and 4-methylstyrene in CD_2Cl_2 at $-78\text{ }^\circ\text{C}$ (left); and (b) a 1:1:1 mixture of $[(\text{PPh}_3)\text{AuCl}]$, AgSbF_6 , and 4-methylstyrene in CD_2Cl_2 at $-78\text{ }^\circ\text{C}$ (right). Vertical amplitude is not consistent among the spectra.

Given that one of the possible byproducts contributing to the broad ^{31}P resonance observed in the experiment above is the gold counterion complex $[(\text{Ph}_3\text{P})\text{Au}(\text{BF}_4)]$, a similar experiment employing the less coordinating SbF_6^- counterion was performed in an effort to minimize the contribution of this possible byproduct. An equimolar mixture of $[(\text{PPh}_3)\text{AuCl}]$, AgSbF_6 , and 4-methylstyrene in CD_2Cl_2 was mixed at $-78\text{ }^\circ\text{C}$ for

5 min. The ^1H NMR spectrum of the resultant solution at $-70\text{ }^\circ\text{C}$ displayed a 1:1 ratio of doublets at $\delta = 5.84$ and 5.51 ppm, corresponding to the terminal vinylic protons of bound 4-methylstyrene; the internal vinylic proton was shifted downfield to the extent that it was obscured by the aromatic resonances. As in the previous experiment, the ^{31}P NMR spectrum of this solution at $-30\text{ }^\circ\text{C}$ displayed a broad resonance at $\delta = 38.0$ ppm ($\nu_{1/2} = 260$ Hz), which broadened further upon cooling to $-50\text{ }^\circ\text{C}$ ($\nu_{1/2} = 310$ Hz). However, as the temperature was lowered further to $-90\text{ }^\circ\text{C}$, the resonance sharpened and shifted downfield slightly to $\delta = 38.8$ ppm ($\nu_{1/2} = 120$ Hz), and a second broad resonance appeared at $\delta = 33\text{--}25$ ppm, just visible above the baseline. These spectra are consistent with a mixture of **4.7**· SbF_6^- and **A**· SbF_6^- that favors formation of **4.7** to a greater extent than did the reaction of $[(\text{PPh}_3)\text{AuCl}]$ and 4-methylstyrene with AgBF_4 (Figure 38).

4.2.3 Triphenylphosphine gold π -(3-hexyne) complex **4.9**

In an effort to form the thermally sensitive 3-hexyne complex $[(\text{PPh}_3)\text{Au}(\eta^2\text{-CH}_3\text{CH}_2\text{C}\equiv\text{CCH}_2\text{CH}_3)]^+\text{SbF}_6^-$, an equimolar mixture of $[(\text{PPh}_3)\text{AuCl}]$, AgSbF_6 , and 3-hexyne was reacted at $-78\text{ }^\circ\text{C}$. The ^{31}P NMR spectrum of the mixture at $-70\text{ }^\circ\text{C}$ displayed a single sharp resonance at $\delta = 36.1$ ppm ($\nu_{1/2} = 5.7$ Hz), indicating the presence of a single organometallic complex (Table 12). Coordination of 3-hexyne to gold to form (**4.9**· SbF_6^-) was established by the presence of a sp-carbon resonance that displayed carbon–phosphorous coupling at $\delta = 91.9$ ppm (d, $J_{\text{CP}} = 8.6$ Hz) downfield relative to free 1-hexyne ($\delta = 81.7$ ppm) in the ^{13}C NMR spectrum at $-90\text{ }^\circ\text{C}$. Similarly, the ^1H NMR

spectrum of **4.9**·SbF₆ at -85 °C displayed a quartet at $\delta = 2.79$ and a triplet at $\delta = 1.26$ ppm corresponding to the methylene and methyl protons, respectively, of equivalent ethyl groups of the 3-hexyne ligand; both resonances were shifted to higher frequency relative to free 3-hexyne ($\delta = 2.29$ and 1.12 ppm, respectively, at -90 °C). Warming a CD₂Cl₂ solution of **4.9**·SbF₆ at -20 °C for 20 min led to approximately 15 % decomposition to form **4.6**·SbF₆.

Mixtures of **4.9**·SbF₆ and free 3-hexyne displayed well-resolved resonances for free ($\delta = 2.79$ ppm) and bound ($\delta = 2.24$ ppm) 3-hexyne in the ¹H NMR spectrum at -85 °C. This peak separation was exploited to analyze the kinetics of intermolecular ligand exchange employing spin-saturation techniques. To this end, the rate of intermolecular 3-hexyne exchange with **4.9**·SbF₆ (80 mM) was recorded as a function of [3-hexyne] from 18 to 60 mM in CD₂Cl₂ at -85 °C (Table 13). Further experimental details are included in section 4.4.3. A plot of k_{obs} versus [3-hexyne] was linear, which established the second-order rate law for intermolecular 3-hexyne exchange with **4.9**·SbF₆ of rate = $k_2[\text{4.9}\cdot\text{SbF}_6][\text{3-hexyne}]$, in which $k_2 = 100 \pm 14 \text{ m}^{-1} \text{ s}^{-1}$ ($\Delta G^\ddagger_{188\text{K}} = 9.10 \pm 0.05 \text{ kcal mol}^{-1}$; Figure 39).

Table 13: Observed rate constants for the intermolecular exchange of 3-hexyne with complex 4.9.

[3-hexyne] _{free} (mM)	K_{obs} (s ⁻¹)
16	0.89
38	2.9
46	4.5
60	5.2

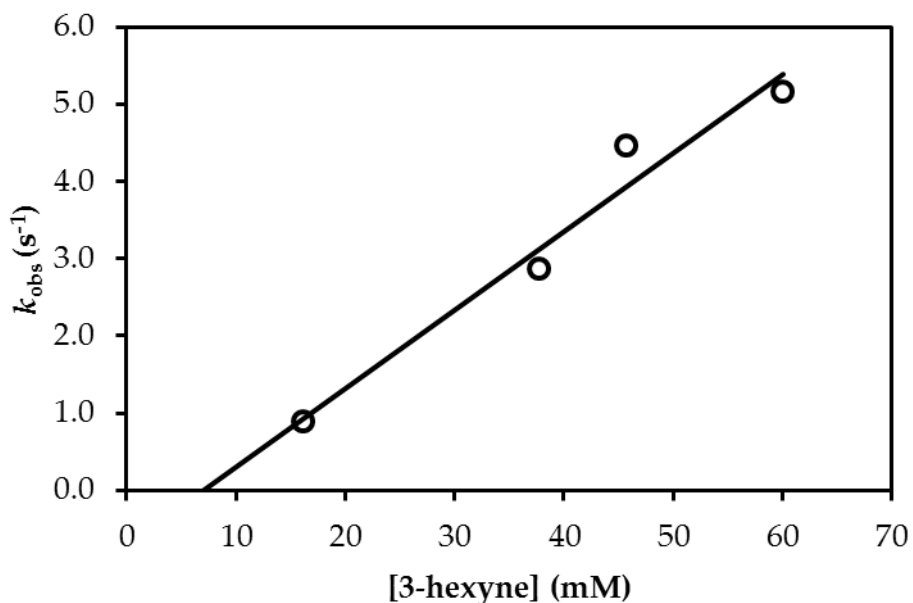


Figure 39: Plot of k_{obs} versus [3-hexyne] for the intermolecular exchange of the 3-hexyne ligand of 4.9-SbF_6 ($[4.9\text{-SbF}_6] = 80 \text{ mM}$) from 18 to 60 mM at $-85 \text{ }^\circ\text{C}$ in CD_2Cl_2 .

The dependence of the rate of exchange on [3-hexyne] supports an associative pathway for 3-hexyne exchange via the cationic bis(alkyne) intermediate $[(\text{PPh}_3)\text{Au}(\eta^2\text{-CH}_3\text{CH}_2\text{C}\equiv\text{CCH}_2\text{CH}_3)_2]^+\text{SbF}_6^-$. The energy barrier for intermolecular 3-hexyne exchange with 4.9-SbF_6 is $\geq 6 \text{ kcal mol}^{-1}$ lower than the energy barriers determined for the intermolecular, associative π -ligand exchange with $[(\text{P1})\text{Au}(\pi\text{-ligand})]$ complexes.^{46, 122, 130, 146} This difference presumably reflects both the diminished steric environment about gold and the weaker gold-(π -ligand) bond of 4.9-SbF_6 relative to that of the gold π -complexes bearing the bulky, electron rich P1 ligand.

The effect of a deficiency of alkyne on the formation and solution behavior of **4.9**·SbF₆ was analogous to the effect of a deficiency of 2-methyl-2-butene on the formation of **4.8**·SbF₆. [(PPh₃)AuCl], AgSbF₆, and 3-hexyne were mixed in a 2:2:1 ratio in CD₂Cl₂ at -78 °C, and subsequent ³¹P NMR analysis at -90 °C revealed a 1.5:1 ratio of sharp resonances at δ = 35.1 and 28.2 ppm corresponding to **4.9**·SbF₆ and **A**·SbF₆, respectively. When the solution was warmed above -50 °C, the ³¹P NMR resonance corresponding to **A**·SbF₆ broadened without detectable broadening of the resonance corresponding to **6**·SbF₆. Warming the solution above -20 °C led to rapid decomposition of **4.9**·SbF₆ (ca. 30 % decomposition after 25 min) with concomitant formation of bis(phosphine) complex **4.6**·SbF₆.

4.2.4 Triphenylphosphine gold π-(1,3-cyclohexadiene) complex 4.10

The reaction of an equimolar mixture of [(PPh₃)AuCl], AgSbF₆, and 1,3-cyclohexadiene in CD₂Cl₂ at -78 °C led to formation of the thermally unstable η²-diene complex **4.10**·SbF₆, as evidenced by the single sharp resonance at δ = 36.3 ppm in the ³¹P NMR spectrum of the reaction mixture at -90 °C (Table 12). Binding of gold to one of the two C=C bonds of the cyclohexadiene ligand was established by low-temperature ¹³C and ¹H NMR analysis. Specifically, the ¹³C NMR spectrum of **4.10**·SbF₆ at -90 °C displayed four alkenyl resonances (δ = 137.9, 121.7, 119.8, 117.9 ppm) and two aliphatic resonances (δ = 25.0, 22.2 ppm), corresponding to the six chemically inequivalent carbon atoms of the cyclohexadiene ligand. Furthermore, the sp²-carbon resonances of **4.10**

closely match those of [(P1)Au(η^2 -(1,3-cyclohexadiene))]⁺ SbF₆⁻ at -70 °C (δ = 136.4, 121.1, 117.4, and 114.7 ppm).¹²²

As was seen for the corresponding P1 complex, complex **4.10**·SbF₆ displayed fluxional behavior consistent with facile interconversion of the complexed and uncomplexed C=C bonds of the cyclohexadiene ligand. The ¹H NMR spectrum of **4.10**·SbF₆ at -94 °C displayed a 1:1:1:1 ratio of four broad vinylic resonances at δ = 6.89, 6.50, 6.41, and 6.31 and a broad multiplet at 2.8–2.3 ppm, corresponding to the allylic protons (Figure 40). When the temperature was raised, the pairs of resonances at δ = 6.50 and 6.41 and at δ = 6.89 and 6.31 ppm broadened and coalesced independently forming a 1:1 ratio of resonances at δ = 6.48 and 6.62 ppm at -25 °C (Figure 40). Over the same temperature range, the broad allylic multiplet collapsed to form a single sharp peak at δ = 2.65 ppm at -25 °C. Breadth of the vinyl proton resonances even at -90 °C precluded precise calculation of the energy barrier for π -face exchange in **4.10**·SbF₆; however, line-shape analysis of the vinyl resonances at δ = 6.50 and 6.41 ppm near the coalescence temperature estimated the upper-limit for the energy barrier for exchange of the complexed and uncomplexed C=C bonds of the 1,3-cyclohexadiene ligand of **10**·SbF₆ of $\Delta G^{\ddagger}_{185\text{K}} \leq 9.0 \text{ kcal mol}^{-1}$.

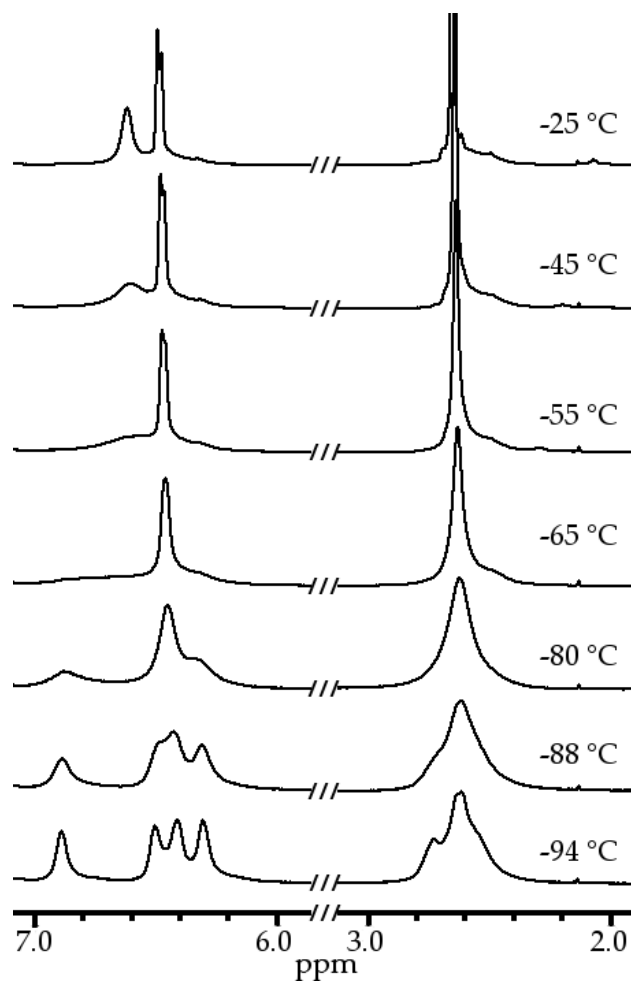


Figure 40: Temperature dependence of the alkenyl (left) and aliphatic (right) ^1H NMR resonances of $4.10 \cdot \text{SbF}_6^-$ from -94 to -25 °C in CD_2Cl_2 .

We have previously established that the lowest energy pathway for interconversion of the complexed and uncomplexed C=C bonds of $[(\text{P}1)\text{Au}(\eta^2\text{-}1,3\text{-cyclohexadiene})]^+ \text{SbF}_6^-$ is intramolecular and occurs with an energy barrier of $\Delta G^\ddagger_{233\text{K}} = 10.4 \text{ kcal mol}^{-1}$.¹²² The intramolecular pathway was confirmed by the presence of two distinct resonances for the pairs of time-averaged allylic protons positioned *cis* and *trans* to the $[(\text{PPh}_3)\text{Au}]$ -moiety. Conversely, an intermolecular pathway for exchange

would necessarily occur with concomitant exchange of the two faces of the 1,3-cyclohexadiene ligand, producing a single, time-averaged allylic resonance in the fast-exchange spectrum, as was observed for **4.10**·SbF₆. While the presence of a single resonance can also be attributed to accidental equivalence of the *cis*- and *trans*-allylic protons, the observation that the ¹H NMR spectrum of a solution of **4.10**·SbF₆ (42 mM) that contained a trace of free 1,3-cyclohexadiene (ca. 4 mM) at -90 °C displayed only two alkenyl (δ = 6.56 and 6.42 ppm) and one allylic-proton resonance (δ = 2.61 ppm) confirmed that **4.10**·SbF₆ can undergo rapid, intermolecular exchange of bound and free 1,3-cyclohexadiene.

4.2.5 Triphenylphosphine gold π-allene complexes

4.2.5.1 Synthesis, characterization, and fluxional behavior of 1,1-dimethylallene complex **4.11**

Building on previous studies of the gold π-allene complexes of the form [(P1)Au(π-allene)]⁺ SbF₆⁻,¹³⁰⁻¹³¹ we extended our analysis of triphenylphosphine gold π-complexes to include π-allene complexes. In one experiment, reaction of an equimolar mixture of [(PPh₃)AuCl], AgSbF₆, and 3-methyl-1,2-butadiene in CD₂Cl₂ at -78 °C for 5 min generated the complex [(PPh₃)Au(η²-H₂C=C=C=CMe₂)]⁺ SbF₆⁻ (**4.11**·SbF₆), which displayed a single sharp resonance at δ = 36.3 ppm in the ³¹P NMR at -90 °C (Table 12). π-Complexation of 3-methyl-1,2-butadiene to gold was established by ¹H and ¹³C NMR spectroscopy at -90 °C. The ¹³C NMR chemical shifts of the allenyl carbon atoms of **4.11**·SbF₆ [δ=105.3 (CMe₂), 198.2 (=C=), 62.6 ppm (CH₂)] were shifted significantly from

those of free 3-methyl-1,2-butadiene [$\delta = 94.4, 205, 72.6$ ppm] and were similar to those observed for the related π -allene complex [(P1)Au(η^2 -H₂C=C=C(CH₃)₂)]⁺SbF₆⁻ (**4.12**·SbF₆) [$\delta=105.6$ (CMe₂), 197.0 (=C=), 63.1 ppm (CH₂)]. In comparison, the allenyl proton of **4.11**·SbF₆ ($\delta = 5.23$ ppm) was shifted downfield relative to the allenyl resonance of both free 3-methyl-1,2-butadiene ($\delta = 4.46$ ppm) and **4.12**·SbF₆ ($\delta = 4.07$ ppm).¹³⁰⁻¹³¹

Selective binding of the 3-methyl-1,2-butadiene ligand of **4.11**·SbF₆ through the less substituted allenyl C=C bond was established by the presence of a pair of diastereotopic allenyl methyl resonances in both the ¹³C ($\delta = 21.4, 20.2$ ppm) and the ¹H NMR spectrum ($\delta = 1.93, 1.87$ ppm) of **4.11**·SbF₆ at -90 °C (Figure 41). When the temperature was raised, the proton resonances broadened and coalesced, forming a single resonance at $\delta = 1.93$ ppm at -30 °C. Line-shape analysis of these resonances near the coalescence point provided an energy barrier for this exchange of $\Delta G^{\ddagger}_{215\text{K}} = 10.9$ kcal mol⁻¹. Although this value is similar to the energy barrier determined for intramolecular π -face exchange of the 3-methyl-1,2-butadiene ligand of **4.12**·SbF₆ ($\Delta G^{\ddagger}_{220\text{K}} = 11.0$ kcal mol⁻¹),¹³⁰⁻¹³¹ we could not distinguish between intra- and intermolecular pathways for interconversion of the diastereotopic methyl groups of **4.11**·SbF₆. Warming a solution of **4.11**·SbF₆ at 0 °C for 1.5 h led to 90 % decomposition to form the bis(triphenylphosphine) gold cation **4.6**·SbF₆.

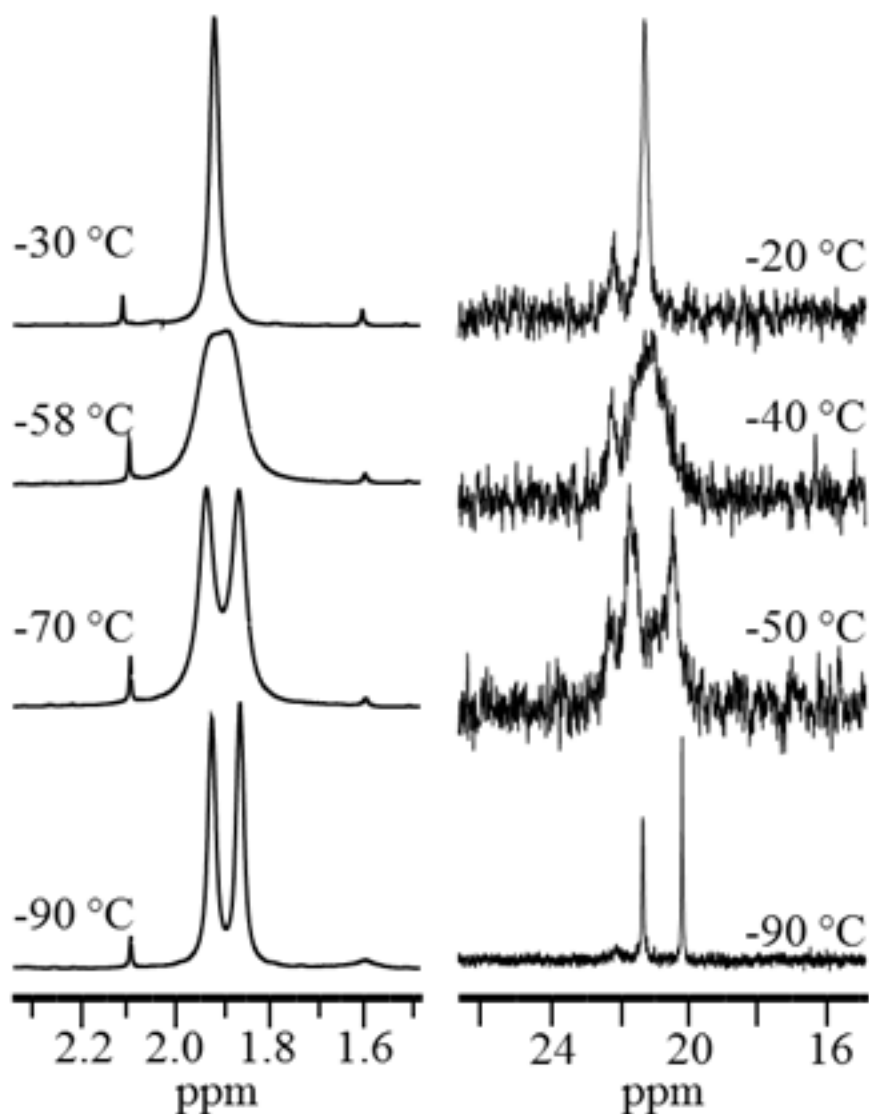
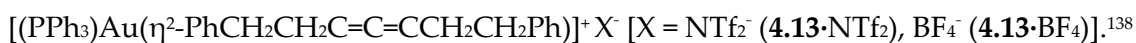


Figure 41: Temperature dependence of the allenyl methyl ^1H (left) and ^{13}C (right) NMR resonances of $4.11 \cdot \text{SbF}_6$ in CD_2Cl_2 . Amplitude is not consistent between spectra.

4.2.5.2 Synthesis, characterization, and fluxional behavior of 1,3-disubstituted allene complex 4.13

Both the ^{31}P NMR chemical shift and thermal instability of $4.11 \cdot \text{SbF}_6$ appeared incongruent with the data reported for the related gold π -allene complexes



Complex **4.13** was reportedly generated *in situ* from reaction of 1,7-diphenylhepta-3,4-diene with either [(PPh₃)AuNTf₂] or a mixture of [(PPh₃)AuCl] and AgBF₄ in CD₃NO₂ and/or CD₂Cl₂, but it was characterized by the presence of a sharp resonance at $\delta = 45.2$ ppm in CD₃NO₂ (44.8 ppm in CD₂Cl₂) in the ³¹P NMR spectrum at 25–45 °C. The ³¹P chemical shift reported for **4.13** is not only outside of the narrow range defined by triphenylphosphine gold π -complexes described in previous sections ($\delta = 36.1$ –38.1 ppm), it is near the value expected for the bis(triphenylphosphine) gold cation **4.6**, and the rapid decomposition of **4.13** to form **4.6** at or above room temperature is in accord with the observed thermal stability of **4.11**.

To gain insight into the spectroscopy and solution behavior of gold π -allene complex **4.13**, the reaction of an equimolar mixture of [(PPh₃)AuCl], AgSbF₆, and 1,7-diphenyl-3,4-heptadiene was investigated by NMR spectroscopy in CD₂Cl₂ at -78 °C. Low-temperature one- and two-dimensional NMR analysis of the resulting solution was most consistent with an equilibrating approximately 1:2.5 mixture of diastereomeric η^2 -allene complexes, presumably *cis*-**4.13**·SbF₆ and *trans*-**4.13**·SbF₆, although we have no information that would allow assignment of the major and minor isomers and little information regarding the structure of the minor isomer. The ³¹P NMR spectrum of **4.13**·SbF₆ at -89 °C displayed an approximately 1:2.5 ratio of resonances at $\delta = 36.5$ and 35.4 ppm (Table 12 and Figure 42), and the ¹H NMR spectrum of **4.13**·SbF₆ at -89 °C displayed an approximately 1:2.5 ratio of broad allenyl resonances at $\delta = 6.14$ and

6.03 ppm (Figure 42). Assignment of the 6.03 ppm resonance to both allenyl protons (time-averaged or coincidental) of the major diastereomer was further supported by ^1H - ^1H COSY and heteronuclear multiple-quantum-coherence (HMQC) analysis at $-90\text{ }^\circ\text{C}$ (see below and section 4.4.2). When the temperature was raised, the approximately 1:2.5 ratio of ^1H and ^{31}P NMR resonances broadened and coalesced, forming single resonances in both the ^{31}P ($\delta = 36.6\text{ ppm}$ at $-50\text{ }^\circ\text{C}$) and ^1H ($\delta = 6.06\text{ ppm}$ at $-60\text{ }^\circ\text{C}$) NMR spectra, with an energy barrier for interconversion of the major and minor diastereomers of **4.13**· SbF_6 of $\Delta G^\ddagger_{215\text{K}} = 9.5\text{ kcal mol}^{-1}$, as was determined from ^{31}P NMR line-shape analysis (Figure 42).

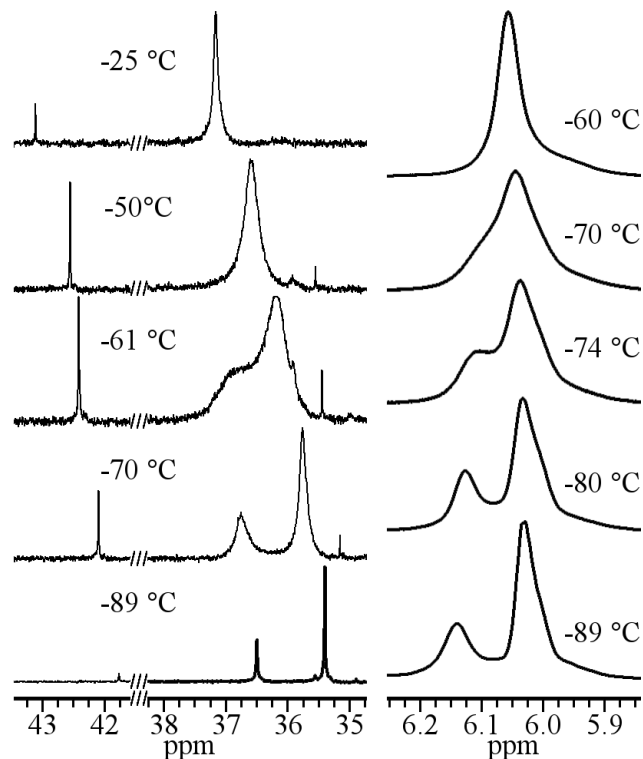


Figure 42: Temperature dependence of the ³¹P resonances (left) and allenyl ¹H resonances (right) of 4.13·SbF₆ in CD₂Cl₂. Amplitude is not consistent between spectra.

Assignment of the major diastereomer of 4.13·SbF₆ as an η²-allene complex was further supported by low-temperature ¹³C NMR analysis. The ¹³C NMR spectrum of 4.13·SbF₆ at -90 °C displayed a resonance at δ = 190.2 ppm (d, J_{CP} = 6.9 Hz), an approximately 1:1 ratio of resonances at δ = 100.0 and 86.0 ppm (d, J_{CP} = 6.7 Hz), and an approximately 1:1:1:1 ratio of resonances at δ = 34.8, 33.7, 32.5, and 31.8 ppm, assigned to the allenyl sp-carbon atom, the allenyl sp²-carbon atoms, and the methylene-carbon atoms, respectively, of the allene ligand of the major diastereomer of 4.13 under conditions of slow exchange. The corresponding ¹³C NMR resonances for free

1,7-diphenyl-3,4-heptadiene (-90 °C, CD₂Cl₂) were displayed at $\delta = 202.6$ (sp), 90.6 (allenyl sp²), and 34.3 and 30.6 ppm (sp³). Corroborating this assignment, HMQC analysis of **4.13**·SbF₆ at -90 °C revealed a strong correlation between the allenyl sp²-carbon resonances at $\delta = 100.0$ and 86.0 with the ¹H NMR resonance at $\delta = 6.03$ ppm assigned to the allenyl protons of the major diastereomer (Figure 43).

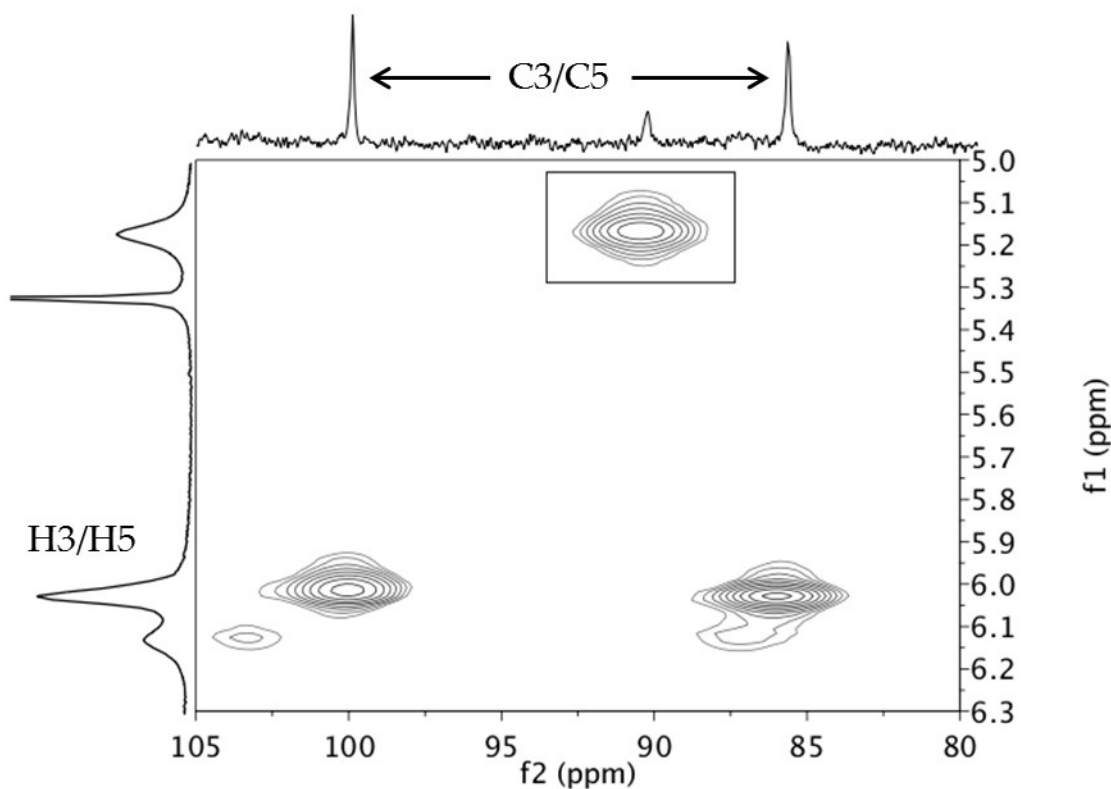


Figure 43: Partial ¹H–¹³C HMQC spectrum of **4.13·SbF₆ in CD₂Cl₂ at -90 °C. The cross-peak at $\delta 5.2 \times \delta 90.6$ (indicated with a box) corresponds to equivalent sp² allenyl protons/carbons of free 1,7-diphenyl-3,4-heptadiene.**

In addition to the resonances attributed to the major diastereomer of **4.13**, the ¹³C NMR spectrum of **4.13**·SbF₆ at -90 °C displayed a resonance at $\delta = 188.6$ ppm, which was approximately half the intensity of the 190.2 ppm resonance and was assigned to

the allenyl sp²-carbon atom of the minor diastereomer. The associated allenyl sp²-carbon resonances and methylene-carbon resonances of the minor diastereomer were not observed, presumably due to more facile π -face exchange of this diastereomer and failure to realize the slow-exchange regime in the ¹³C NMR spectrum at -90 °C. Warming a solution of **4.13**·SbF₆ at 0 °C for 75 min led to 37 % decomposition to form **4.6**·SbF₆.

4.2.5.3 Effect of counterion and solvent on the synthesis and reactivity of **4.13**

As a basis for comparison to the observed behavior of triphenylphosphine gold π -alkene complexes **4.7** and **4.8** and literature reports of complex **4.13**, we performed some additional experiments that evaluated the spectroscopy and solution behavior of **4.13** as a function of counterion and solvent. In one experiment, an equimolar mixture of [(PPh₃)AuNTf₂] and 1,7-diphenyl-3,4-heptadiene was mixed at -78 °C in CD₂Cl₂ for 5 min. The ³¹P NMR spectrum of the resulting solution at -90 °C displayed an approximately 2.5:1 ratio of resonances at δ = 35.2 and 27.8 ppm, assigned to the time-averaged resonance of *cis*- and *trans*-**4.13**·NTf₂ and [(PPh₃)AuNTf₂], respectively. When the temperature was raised, these resonances collapsed to form a single resonance at δ = 28.4 ppm at -30 °C. In contrast to **4.13**·SbF₆, warming this solution to 25 °C led to only 9 % conversion to the bis(triphenylphosphine) cation **4.6**·NTf₂ after 12 h, which is perhaps due to the low concentration of **4.13**·NTf₂ in solution.

In comparison, when an equimolar mixture of [(PPh₃)AuNTf₂] and 1,7-diphenyl-3,4-heptadiene was combined in CD₃NO₂ at -25 °C, the ³¹P NMR spectrum obtained

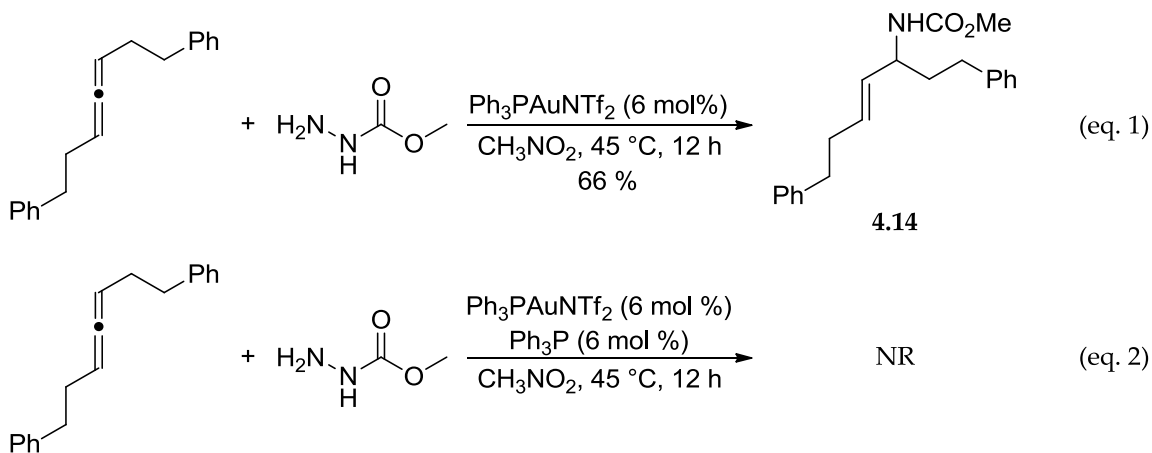
within 10 min of mixing displayed an approximately 1:5 ratio of a sharp resonance at $\delta = 42.4$ ppm, corresponding to **4.6**·NTf₂, and a broad resonance at $\delta = 36.1$ ppm ($\nu_{1/2} = 150$ Hz), corresponding either to **4.13**·NTf₂ or to an equilibrating mixture of **4.13**·NTf₂ and [(PPh₃)AuNTf₂]. Warming this mixture above -20 °C resulted in rapid disappearance of the $\delta = 36.1$ ppm resonance with concomitant increase in the 42.4 ppm resonance of **4.6**·NTf₂. From these experiments, we conclude that the spectroscopy and solution behavior previously attributed to **4.13** correspond instead to the bis(triphenylphosphine) gold complex **4.6** generated through decomposition of **4.13** under the conditions employed for its synthesis and spectroscopic analysis.¹³⁸

4.2.5.4 The role of 4.13 in the hydroamination of 1,7-diphenyl-3,4-heptadiene with methyl carbazate

With our new understanding of complex **4.13**, we sought to gain further insight into the gold-catalyzed hydroamination of 1,7-diphenyl-3,4-heptadiene with methyl carbazate (Scheme 16, eq. 1) Previous studies of the mechanism concluded that the gold π -allene complex **4.13** is the catalyst resting state based on the observation of the resonance at $\delta 45.2$ ppm in the ³¹P NMR spectrum of the reaction mixture in CD₃NO₂. Based on the hypothesis that this species is actually **4.6** formed *in situ*, we sought to evaluate the catalytic activity of **4.6** for the given reaction. Treatment of a 1:2.5 mixture of 1,7-diphenyl-3,4-heptadiene and methyl carbazate with 6 mol% Ph₃PAuNTf₂ in nitromethane for 12 h at 45 °C following the published procedure afforded carbazate **4.14** in 61% yield as a single diastereomer (Scheme 16, eq. 1). However, repeating this

procedure with the addition of 6 mol% PPh₃ to the initial reaction mixture resulted in the complete inhibition of catalysis, with no evidence of product formation after 12 h at 45 °C (Scheme 16, eq. 2). This confirmed that complex **4.6**, which is formed rapidly from a Ph₃PAu⁺ species with a weakly coordinating ligand or counterion in the presence of free Ph₃P, is catalytically inactive in this system.

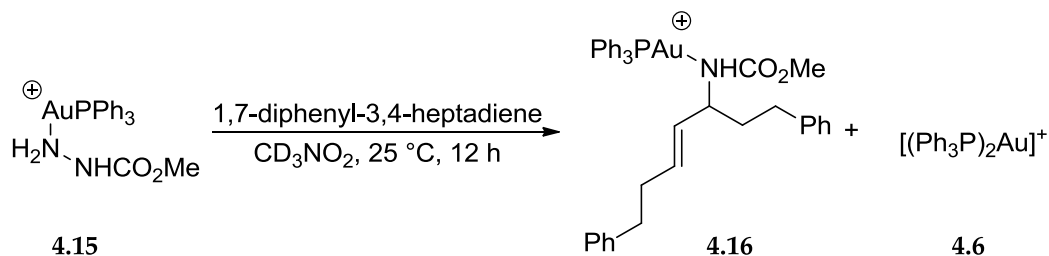
Scheme 16: Hydroamination of 1,7-diphenyl-3,4-heptadiene with methyl carbazate catalyzed by [(PPh₃)AuNTf₂] in CH₃NO₂ in the absence (eq. 1) and the presence (eq. 2) of PPh₃.



³¹P NMR analysis of a 1:1 mixture of methyl carbazate and Ph₃PAuNTf₂ in CD₃NO₂ at -25 °C revealed a sharp resonance at δ = 28.8 ppm, presumably corresponding to the Ph₃PAu⁺ carbazate complex **4.15**·NTf₂; warming this solution to 25 °C revealed no evidence of decomposition or formation of **4.6** (Figure 44a). Addition of one equivalent of 1,7-diphenyl-3,4-heptadiene to the solution of **4.15**·NTf₂ at -25 °C causes no apparent change to the ³¹P spectrum, and the ¹H spectrum of this mixture shows only **4.15**·NTf₂ and free 1,7-diphenyl-3,4-heptadiene. Warming the mixture to 25 °C resulted in

hydroamination of 1,7-diphenyl-3,4-heptadiene with methyl carbazate, which could be monitored by ^1H and ^{31}P NMR. The ^{31}P resonance corresponding to **4.15**·NTf₂ ($\delta = 30$ ppm at 25 °C) persisted early in the reaction, but formation of a small amount of **4.13**·NTf₂ was suggested by the emergence of a small, broad resonance at $\delta = 36$ ppm (Figure 44b). As the reaction progressed, the $\delta = 36$ ppm disappeared and a sharp resonance corresponding to **4.6**·NTf₂ at $\delta = 45$ ppm grew in; the resonance corresponding to **4.15**·NTf₂ broadened and shifted slightly to higher frequency, presumably representing a dynamic equilibrium between **4.15**·NTf₂ and the complex of product **4.14** to $[\text{Ph}_3\text{PAu}]^+$ (**4.16**·NTf₂) (Scheme 17 and Figure 44c). Upon completion of the reaction, the $\delta = 45$ ppm resonance persisted, signifying no regeneration of an active catalytic species from **4.6**·NTf₂, and the resonance representing gold-carbazate complexes **4.15/4.16**·NTf₂ sharpened at $\delta = 29$ ppm (Figure 44d), which corresponds to the ^{31}P resonance observed in a sample of **4.16**·NTf₂ generated independently (Figure 44e).

Scheme 17: Hydroamination of 1,7-diphenyl-3,4-heptadiene by stoichiometric gold carbazate complex 4.15 (1 equiv.) to give gold bound product 4.16 with concomitant generation of decomposition product 4.6.



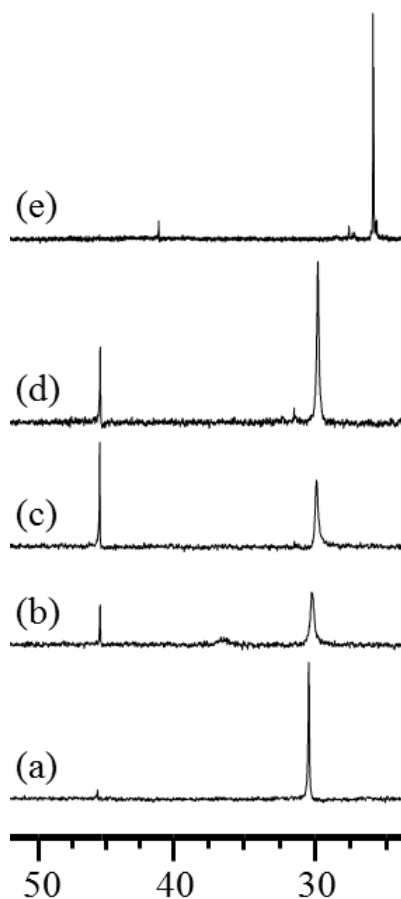


Figure 44: ^{31}P NMR resonances of: (a) a 1:1 mixture of $\text{Ph}_3\text{PAuNTf}_2$ and methyl carbazate in CD_3NO_2 at 25°C ; (b) sample from (a) plus 1 equiv. 1,7-diphenyl-3,4-heptadiene after 10 minutes at 25°C ; (c) sample from (b) after 1 h at 25°C ; (d) sample from (b) after 12 h at 25°C ; (e) a 1:1 mixture of $\text{Ph}_3\text{PAuNTf}_2$ and carbazate 4.14 in CD_3NO_2 at -20°C .

4.3 Summary of conclusions

Monomeric, cationic triphenylphosphine gold(I) complexes that contain a π -alkene, vinyl arene, internal alkyne, conjugated diene, or allene ligand were synthesized and characterized without isolation by low-temperature NMR spectroscopy. Each of these triphenylphosphine gold(I) π -complexes is thermally unstable and decomposes above -20°C in CD_2Cl_2 to form the bis(triphenylphosphine) gold cation

$[(\text{Ph}_3\text{P})_2\text{Au}]^+$ (**4.6**). The π ligands of these complexes undergo rapid intermolecular exchange with free ligand and are competitively displaced by weak σ -donors, such as OTf. One of the key ramifications of the weak gold– π -ligand interaction of these complexes is that careful control of reaction stoichiometry and employment of a weakly coordinating counterion, such as SbF_6^- , is required to generate pure triphenylphosphine gold π -complexes. In many cases, the presence of rapidly equilibrating impurities was revealed only by low-temperature ^{31}P NMR spectroscopy ($\leq -80^\circ\text{C}$). The ^{31}P NMR resonance of these triphenylphosphine gold π -complexes was diagnostic and fell within the range $\delta = 37.1 \pm 1.7$ ppm.

4.4 Experimental

4.4.1 General methods

Reactions were performed under a nitrogen atmosphere employing standard Schlenk and glovebox techniques unless specified otherwise. NMR spectra were obtained on a Varian spectrometer operating at 500 MHz for ^1H NMR, 125 MHz for ^{13}C NMR, and 202 MHz for ^{31}P NMR in CD_2Cl_2 unless noted otherwise; ^{13}C NMR was referenced relative to CD_2Cl_2 ($\delta = 53.8$), ^1H NMR was referenced relative to residual CH_2Cl_2 ($\delta = 5.32$), and ^{31}P spectra was referenced to an external solution of triphenylphosphine oxide in CD_2Cl_2 ($\delta = 26.9$). NMR probe temperatures were calibrated using a neat methanol thermometer. CD_2Cl_2 was dried over CaH_2 prior to use. $\text{Ph}_3\text{PAuNTf}_2$ ¹⁴², 1,7-diphenyl-3,4-heptadiene,¹³⁸ and **4.14**¹³⁸ were synthesized employing

published procedures. [(PPh₃)AuCl], AgSbF₆, AgOTf, 2-methyl-2-butene, 4-methylstyrene, 3-hexyne, 1,3-cyclohexadiene, 3-methyl-1,2-butadiene, nitromethane, and CD₃NO₂ were purchased from major chemical suppliers and used as received. Line shape analysis was performed using WINDNMR-Pro.⁹⁸

4.4.2 Complex synthesis and characterization

[(Ph₃PAu)₂Cl]⁺ SbF₆⁻ (4.5·SbF₆).¹⁴⁴ A mixture of Ph₃PAuCl (40 mg, 8.0 × 10⁻² mmol) and AgSbF₆ (14 mg, 4.0 × 10⁻² mmol) was dissolved in CD₂Cl₂ (0.60 mL) in an NMR tube. The tube was inverted several times to mix the contents, which formed a white precipitate that was allowed to settle to the bottom of the tube. ³¹P NMR analysis of the resulting colorless solution revealed complete conversion of starting materials to 4.5·SbF₆. ¹H NMR (-90 °C): δ 7.83– 6.93 (m, 30 H). ³¹P{¹H} NMR (25 °C): δ 30.7. ³¹P{¹H} NMR (-90 °C): δ 28.5.

[(Ph₃P)₂Au]⁺ SbF₆⁻ (4.6·SbF₆).¹⁴⁵ An equimolar mixture of Ph₃PAuCl (49 mg, 8.1 × 10⁻² mmol), AgSbF₆ (28 mg, 8.1 × 10⁻² mmol), and PPh₃ (21 mg, 8.1 × 10⁻² mmol) was dissolved in CD₂Cl₂ (0.60 mL) in an NMR tube. The tube was inverted several times to mix the contents, which formed a white precipitate that was allowed to settle to the bottom of the NMR tube. ³¹P NMR analysis of the resulting colorless solution revealed complete conversion of starting materials to 4.6·SbF₆. ¹H NMR (25 °C): δ 7.73-7.67 (m, 6H), 7.66 - 7.48 (m, 24 H). ¹³C{¹H} NMR (25 °C): δ 134.5, 133.2, 130.3, 127.5 (t, J = 29.9 Hz). ³¹P{¹H} NMR (25 °C): δ 44.5. ³¹P{¹H} NMR (-90 °C): δ 41.8.

$[(PPh_3)Au(\eta^2-Me(H)C=CMe_2)]^+ SbF_6^-$ (4.8·SbF₆) A solution of $[(PPh_3)AuCl]$ (22 mg, 4.4×10^{-2} mmol) in CD_2Cl_2 (0.50 mL) was added to an NMR tube containing $AgSbF_6$ (15 mg, 4.4×10^{-2} mmol); the mixture was shaken vigorously, and the resultant suspension was cooled to -78 °C. To this suspension was added 2-methyl-2-butene (3.1 mg, 4.4×10^{-2} mmol) at -78 °C. The contents of the tube were thoroughly mixed by inverting the tube repeatedly over about 2 min period while maintaining temperature at -78 °C, causing a fine white powder to precipitate from solution. Low-temperature 1H and ^{31}P NMR analyses of the resulting solution revealed complete conversion of the starting materials to 4.8·SbF₆. 1H NMR (500 MHz, -85 °C): δ = 7.68–7.24 (m, 15 H), 5.98–5.90 (m, 1 H), 2.32 (s, 3 H), 2.27 (s, 3 H), 2.03 ppm (d, J = 1.5 Hz, 3 H); $^{13}C\{^1H\}$ NMR (125 MHz, -85 °C): δ = 145.4, 133.5 (d, J = 13.4 Hz), 132.4, 129.2 (d, J = 11.7 Hz), 125.1 (d, J = 62.7 Hz), 111.8 (d, J = 10.5 Hz), 28.5, 21.5, 16.0 ppm; $^{31}P\{^1H\}$ NMR (202 MHz, -70 °C): δ = 36.8 ppm.

Complexes 4.7·SbF₆, 4.9·SbF₆–4.11·SbF₆, and 4.13·SbF₆ were generated in solution by employing a procedure similar to that used to generate 4.8·SbF₆.

$[(PPh_3)Au(\eta^2-CH_3CH_2C \equiv CCH_2CH_3)]^+ SbF_6^-$ (4.9·SbF₆): 1H NMR (500 MHz, -70 °C): δ = 7.65 (t, J = 7.4 Hz, 3 H), 7.57 (dt, J = 1.5, 7.1 Hz, 6 H), 7.48–7.40 (m, 6 H), 2.80 (q, J = 7.0 Hz, 4 H), 1.27 ppm (t, J = 7.2 Hz, 6 H); $^{13}C\{^1H\}$ NMR (125 MHz, -90 °C): δ = 133.4 (d, J = 13.6 Hz), 132.4 (d, J = 2 Hz), 129.2 (d, J = 12.2 Hz), 125.0 (d, J = 63.7 Hz), 91.9 (d, J = 8.6), 15.0, 14.0 ppm; $^{31}P\{^1H\}$ NMR (202 MHz, -70 °C): δ = 36.1 ppm.

[(PPh₃)Au(η^2 -1,3-cyclohexadiene)]⁺SbF₆⁻ (4.10·SbF₆): ¹H NMR (500 MHz, -94 °C): δ = 7.62 (t, J = 7.5 Hz, 3 H), 7.54 (dt, J = 1.4, 7.2 Hz, 6 H), 7.43–7.36 (m, 6 H), 6.89 (br s, 1 H), 6.50 (br s, 1 H), 6.41 (br s, 1 H), 6.31 (br s, 1 H), 2.82–2.32 ppm (m, 4 H); ¹³C{¹H} NMR (125 MHz, -90 °C): δ = 137.9 (br), 133.5 (br), 132.4, 129.2 (d, J = 12.1 Hz), 125.2 (d, J = 62.0 Hz), 121.7 (br), 119.8 (br), 117.9 (br), 25.0 (br), 22.2 ppm (br); ³¹P{¹H} NMR (202 MHz, -90 °C): δ = 36.3 ppm.

[(PPh₃)Au(η^2 -H₂C=C=CMe₂)]⁺SbF₆⁻ (4.11·SbF₆): ¹H NMR (500 MHz, -90 °C): δ = 7.64 (t, J = 7.1 Hz, 3 H), 7.59–7.52 (m, 6 H), 7.49–7.40 (m, 6 H), 5.23 (br s, 2 H), 1.93 (s, 3 H), 1.87 ppm (s, 3 H); ¹³C{¹H} NMR (125 MHz, -90 °C): δ = 198.2, 133.5 (d, J = 13.3 Hz), 132.4, 129.3 (d, J = 11.9 Hz), 125.0 (d, J = 62.6 Hz), 105.3, 62.6 (d, J = 10.4 Hz), 21.4, 20.2 ppm; ³¹P{¹H} NMR (202 MHz, -90 °C): δ = 36.3 ppm.

[(PPh₃)Au(η^2 -PhCH₂CH₂(H)C=C(H)CH₂CH₂Ph)]⁺SbF₆⁻ (4.13·SbF₆):
Approximately 2.5:1 mixture of diastereomers; ¹H NMR (500 MHz, -89 °C): δ = 7.75–7.36 (m, 29 H), 7.36–6.86 (m, 45 H), 6.78 (br s, 9 H), 6.42 (br d, J = 7.4 Hz, 4 H), [6.14 (br s), 6.03 (br s), ca. 1:2.5, 2 H] 3.15–2.16 ppm (m, 26 H); ¹³C{¹H} NMR (125 MHz, -85 °C): δ = [190.2 (d, J = 6.9 Hz), 187.8 (d, J = 7.2 Hz), ca. 2.5:1], 139.4, 139.0, 133.5 (d, J = 13.5 Hz), 132.5 (m), 129.1 (d, J = 12.0 Hz), 128.5, 128.1, 127.9, 126.0, 125.7, [124.8 (d, J = 62.5 Hz), 124.5 (d, J = 62.5 Hz), 1:2.5], 100.0, 86.0 (d, J = 6.7 Hz), 34.0, 32.9, 31.6, 31.4 ppm; ³¹P{¹H} NMR (202 MHz, -89 °C): δ = 36.5, 35.4 ppm (ca. 1:2.5).

The ^1H - ^1H COSY spectrum of **4.13**· SbF_6 in CD_2Cl_2 at $-90\text{ }^\circ\text{C}$ shows a correlation between the resonance at $\delta = 6.03$ to two allenyl methylene resonances. This observation indicates that the resonance at $\delta = 6.03$ corresponds to both allenyl protons (time averaged or coincidental) of the major diastereomer of **4.13**· SbF_6 .

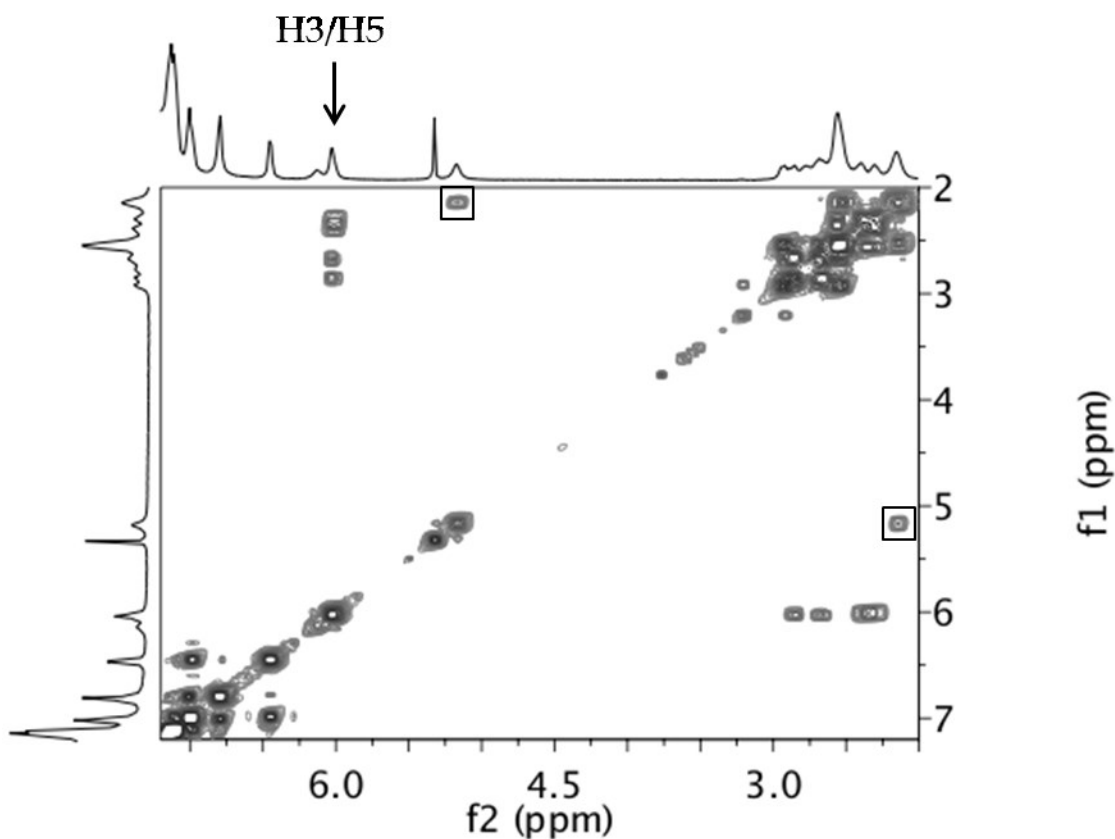


Figure 45: Partial ^1H - ^1H COSY spectrum of **4.13**· SbF_6 in CD_2Cl_2 at $-90\text{ }^\circ\text{C}$. The cross-peaks at $\delta = 5.2 \times \delta = 2.1$ (indicated with boxes) corresponds to protons of free 1,7-diphenyl-3,4-heptadiene.

$[(\text{PPh}_3)\text{Au}(\text{NH}_2\text{NHCO}_2\text{Me})]^+ \text{NTf}_2^-$ (**4.15**) A mixture of $[(\text{PPh}_3)\text{AuNTf}_2]$ and methyl carbazate were dissolved in CD_3NO_2 at $-25\text{ }^\circ\text{C}$ in an NMR tube. The resultant colorless solution was analyzed by ^1H and ^{31}P NMR analysis from $-29\text{ }^\circ\text{C}$ to $25\text{ }^\circ\text{C}$. ^1H

NMR (500 MHz, -29 °C, CD₃NO₂): δ = 7.82–7.50 (m, 15 H), 6.95–6.20 (br s, 3 H), 3.74 (s, 3 H); ¹³C{¹H} NMR (125 MHz, -29 °C, CD₃NO₂): δ = 153.9, 129.9 (d, *J* = 13.6 Hz), 128.4 (d, *J* = 2.4 Hz), 123.1 (d, *J* = 64.9 Hz), 115.4 (q, *J* = 318 Hz), 48.8 ppm; ³¹P{¹H} NMR (202 MHz, -29 °C): δ = 28.8 ppm.

[(PPH₃)Au((E)-N'-(1,7-diphenylhept-4-en-3-yl)methyl carbazate)]⁺ NTf₂⁻

(4.16·NTf₂) Complex **4.16·NTf₂** was generated as a mixture of isomers using a procedure similar to that employed to synthesize **4.15·NTf₂**. ¹H NMR (500 MHz, -25 °C, CD₃NO₂): δ = 7.80–6.80 (m, 27 H), 6.18–5.98 (m, 1 H), 5.70–5.61 (m, 1 H), 3.99 (br s, 1 H), 3.74 (s, 3 H), 2.75–1.95 (m, 8 H) ppm; ¹³C{¹H} NMR (125 MHz, -25 °C, CD₃NO₂): δ = 152.9, 152.8, 137.4, 137.1, 136.8, 136.0, 129.8 (d, *J* = 13.6 Hz), 128.4, 125.3 (d, *J* = 12.0 Hz), 124.4–124.0 (m), 123.0 (d, *J* = 64.6 Hz), 115.4 (q, *J* = 318 Hz), 64.9, 64.2, 48.9, 30.6, 30.0, 29.9, 29.7, 27.0, 26.9 ppm; ³¹P{¹H} NMR (202 MHz, -29 °C): δ = 26.05, 26.00 ppm.

4.4.3 Kinetics of intermolecular 3-alkyne exchange with 4.9

3-Hexyne (0.9 μL, 8.1 × 10⁻³ mmol, 16 mM) was added via syringe to a solution of **4.9·SbF₆** (4.0 × 10⁻² mmol) and 1,3-dimethoxybenzene (internal standard, 1.5 × 10⁻² mmol) in CD₂Cl₂ (0.50 mL) at -78 °C in an NMR tube sealed with a rubber septum. The tube was shaken vigorously at -78 °C, placed in an NMR probe precooled at -85 °C, and analyzed employing ¹H NMR spin saturation techniques. The propargylic resonance of the 3-hexyne ligand of **4.9·SbF₆** (δ = 2.79) was integrated relative to the methoxy resonance of 1,3-dimethoxybenzene (δ = 3.71) both without (S₀) and with (S) saturation

($\delta = -1358.1$ Hz at -8 dB for 5 sec) of the propargylic resonance of free 3-hexyne ($\delta = 2.13$). From these values and from the independent determination of the spin-lattice relaxation times (T_1) of the propargylic protons of the 3-hexyne ligand of **4.9**·SbF₆ (0.70 s) and of free 3-hexyne (0.66 s), an observed rate constant for intermolecular 3-hexyne exchange with **4.9**·SbF₆ of $k_{\text{obs}} = (1/T_{1,\text{free}})[(S_0/S)-1] = 0.9 \text{ s}^{-1}$ was determined. Observed rate constants for intermolecular exchange of 3-hexyne with **4.9**·SbF₆ were likewise determined at [3-hexyne] = 38 mM ($k_{\text{obs}} = 2.9 \text{ s}^{-1}$), 46 mM ($k_{\text{obs}} = 4.5 \text{ s}^{-1}$), and 60 mM ($k_{\text{obs}} = 5.2 \text{ s}^{-1}$) through successive iterations of the above procedure. A plot of k_{obs} versus [3-hexyne] was linear (Figure 39), which established the second-order rate law for intermolecular alkyne exchange with **4.9**·SbF₆ of rate = $k_2[\text{4.9}\cdot\text{SbF}_6][\text{3-hexyne}]$ where $k_2 = 100 \pm 14 \text{ M}^{-1} \text{ s}^{-1}$ ($\Delta G^\ddagger_{188\text{K}} = 9.10 \pm 0.05 \text{ kcal mol}^{-1}$).

4.4.4 Kinetics of π -face exchange in complexes **4.10**, **4.11**, and **4.13**

An NMR tube containing a solution of **4.10**·SbF₆ (0.044 mmol) in CD₂Cl₂ (0.6 mL) was placed in the probe of an NMR spectrometer precooled at -94 °C, allowed to equilibrate for 10 min, and analyzed by ¹H NMR spectroscopy. The solution was warmed incrementally, equilibrated at -88, -80, -65, -45, and -25 °C, and analyzed at each temperature by ¹H NMR spectroscopy. Simulation of the ¹H NMR resonances at $\delta = 6.50$ and 6.41 (-94 °C) near the coalescence temperature (-88 °C) employing the parameters $\Delta\omega = 44 \text{ Hz}$, $\omega_\alpha = 26 \text{ Hz}$, $\omega_\beta = 30 \text{ Hz}$ gave a best fit with an exchange rate of $k_{\text{ex}} = 96 \pm 3 \text{ s}^{-1}$ (Figure 46), which corresponds to an apparent energy barrier of $\Delta G^\ddagger_{185} = 9.0 \text{ kcal mol}^{-1}$.

Peak separations ($\Delta\omega$) were obtained directly from the $-94\text{ }^{\circ}\text{C}$ ^1H NMR spectrum of $4.10\cdot\text{SbF}_6$. Natural peak widths (ω) were measured as upper limits from the ^1H NMR spectrum ($-94\text{ }^{\circ}\text{C}$) of $4.10\cdot\text{SbF}_6$ as these peaks appeared significantly broadened, presumably due to C=C bond exchange.

The energy barrier for interconversion of diastereotopic methyl resonances of $4.11\cdot\text{SbF}_6$ (Figure 47) and phosphorus resonances of $4.13\cdot\text{SbF}_6$ (Figure 48) were determined using a similar analysis.

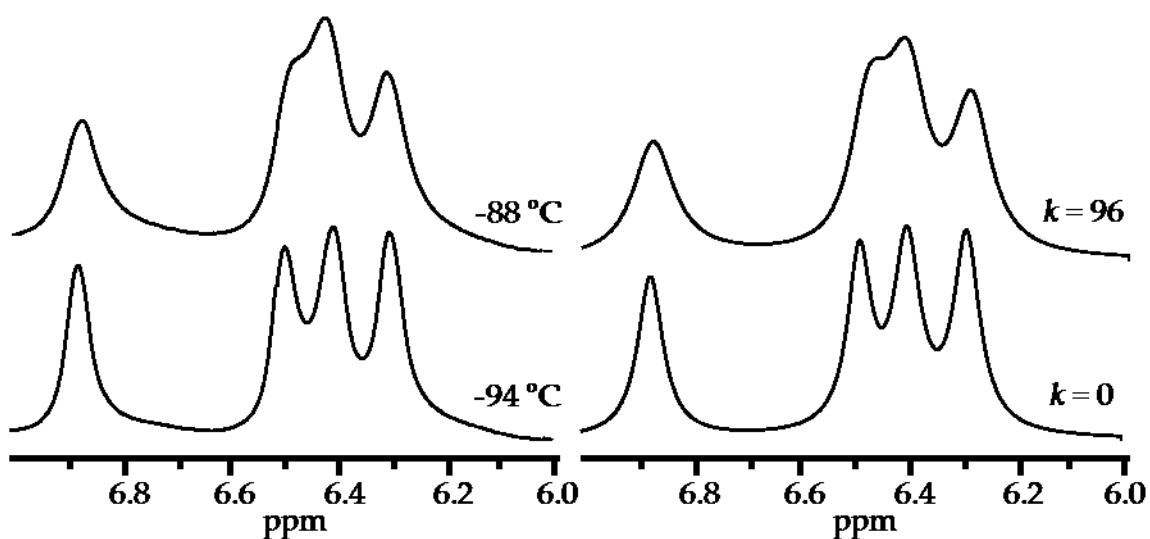


Figure 46: Experimental (left) and simulated (right) ^1H NMR spectra of the vinyl protons used to approximate the rate constant and free energy of activation for the intramolecular alkene exchange in $4.10\cdot\text{SbF}_6$.

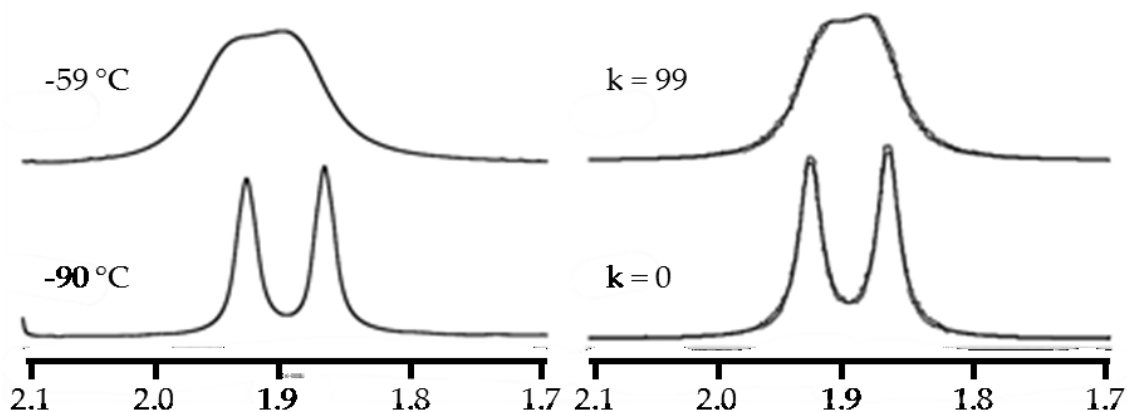


Figure 47: Experimental (left) and simulated (right) ^1H NMR spectra of the diastereotopic methyl groups used to approximate the rate constant and free energy of activation for the intramolecular alkene exchange in $4.11\cdot\text{SbF}_6$.

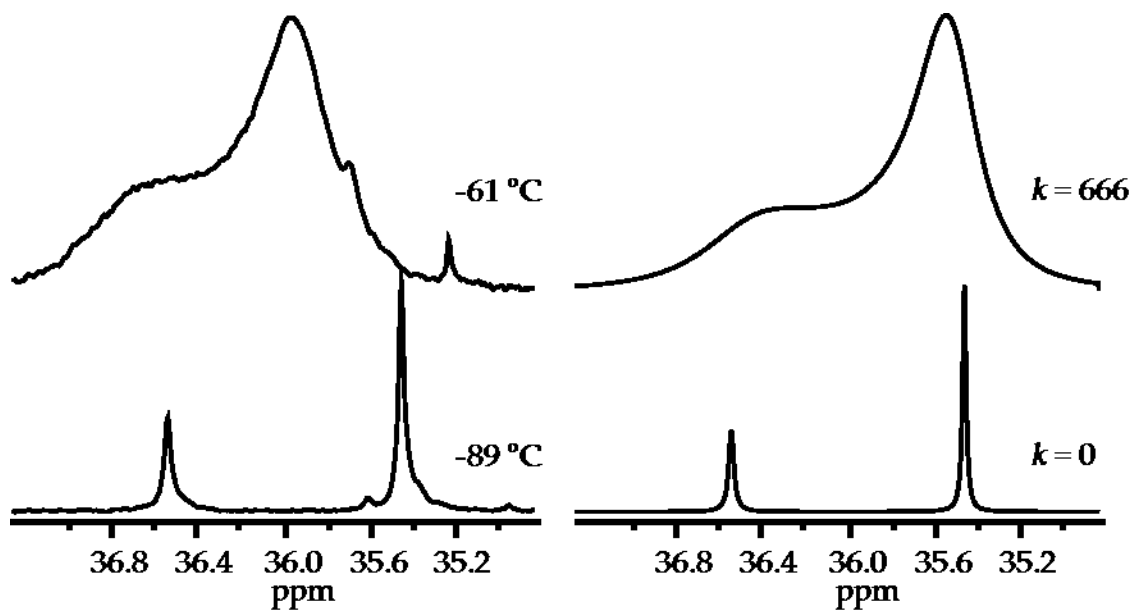


Figure 48: Experimental (left) and simulated (right) ^{31}P NMR spectra of the phosphorus resonances used to approximate the rate constant and free energy of activation for the intramolecular alkene exchange in $4.13\cdot\text{SbF}_6$.

5. Mechanistic studies of the gold-catalyzed intramolecular cycloisomerizations of 1,6-enynes

Portions of this chapter have been published: Brooner, R. E. M.; Brown, T. J.; Widenhoefer, R. A. *Angew. Chem. Int. Ed.* **2013**, *52*, 6259. Initial syntheses and characterization of **5.9**, **5.9-¹³C₁**, **5.9-¹³C₃**, **5.9-*d*₂** and **5.10**, and **5.10-¹³C₃** were performed by Dr. T. J. Brown.

5.1 Introduction

5.1.1 Gold(I) catalyzed cycloisomerization of 1,6-enynes

The cycloisomerization of enynes catalyzed by electrophilic noble-metal complexes, in particular Au and Pt, has attracted considerable attention because of its ability to form skeletal rearrangement products.^{9-11, 147-153} Gold(I)-catalyzed cycloisomerizations of 1,6-enynes to give a variety of rearranged carbon skeletons have been reported, and the selectivity of these reactions has been shown to rely heavily on the substitution of the starting enyne and the structure of the catalyst. For example, Echavarren and coworkers have shown that by changing the substitution at the C1 and C6 carbons or incorporating a heteroatom along the backbone of a 1,6-enyne, vinylcyclopentenes, bicyclo[4.1.0]heptenes, or bicyclo[3.2.0]heptenes can be formed selectively upon treatment with a cationic gold(I) catalyst (Figure 49).¹⁵⁴⁻¹⁵⁸

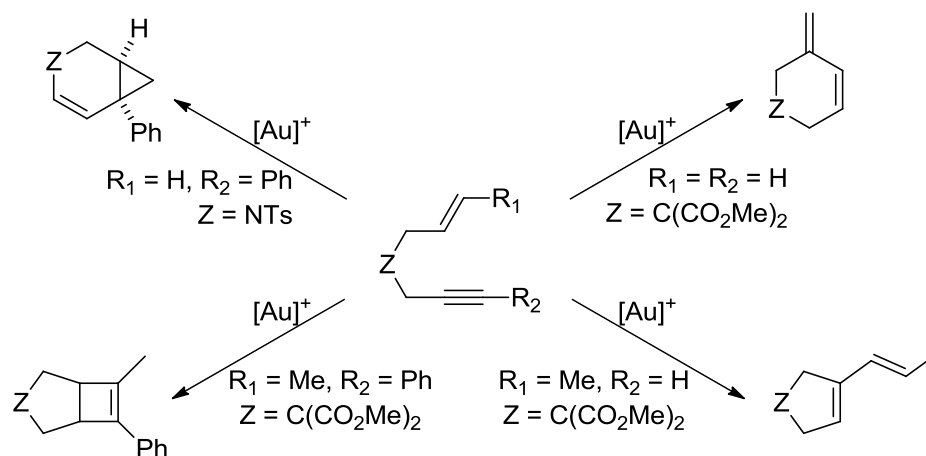


Figure 49: Skeletal rearrangements in the gold-catalyzed cycloisomerizations of 1,6-enynes.

5.1.2 Proposed mechanism(s) of gold(I) catalyzed enyne cycloisomerization

Fürstner first posited that the products of electrophilic transition metal enyne cycloisomerizations were consistent with the intermediacy of metal-stabilized nonclassical cyclopropylmethyl-, cyclobutyl-, and homoallylic carbocations/carbenes accessed via attack of the C=C moiety on a metal-complexed C≡C bond (Figure 50),¹⁵⁹ and mechanistic thought in this area has evolved largely within this conceptual framework.

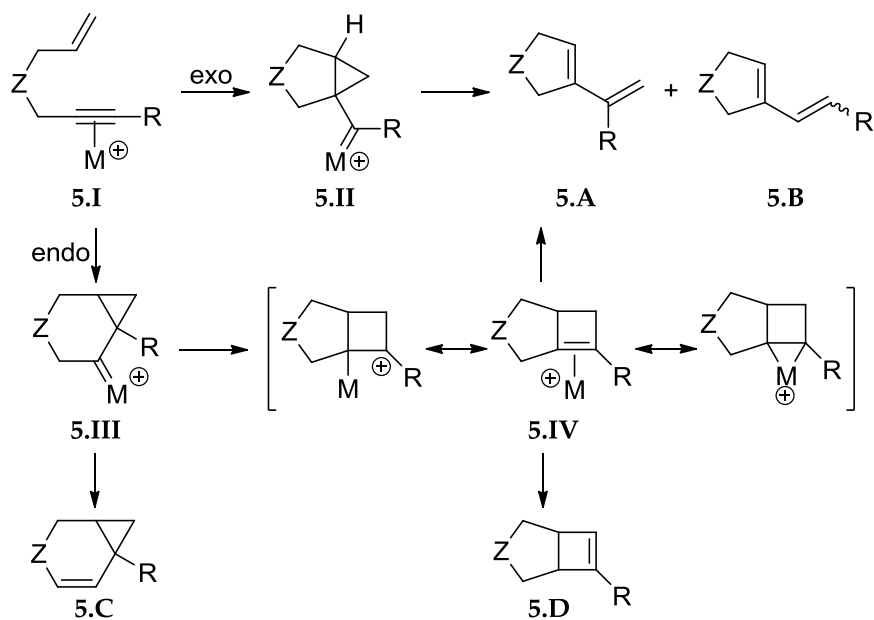
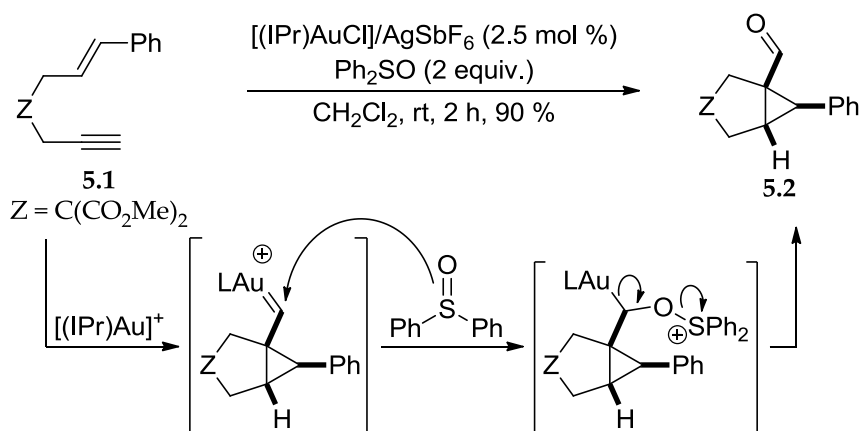


Figure 50: Possible cationic intermediates in the ligand- and substrate-dependent pathways for enyne cycloaddition catalyzed by electrophilic noble metal complexes.

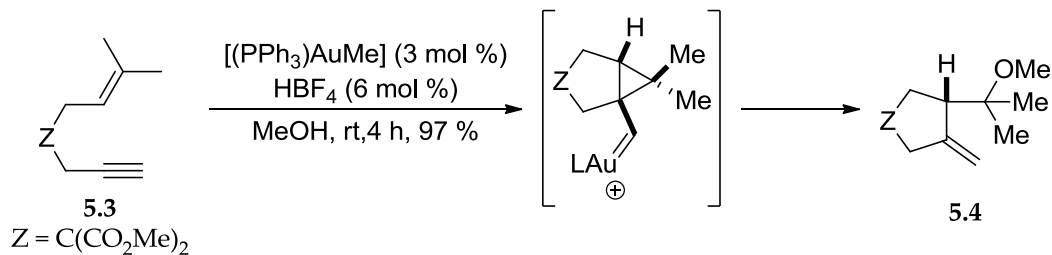
The intermediacy of non-classical carbocations/carbenes is supported indirectly by experiments that invoke trapping this reactive species. For example, the gold-catalyzed cycloisomerization of enyne **5.1** in the presence of excess Ph₂SO resulted in exclusive formation of the cyclopropyl aldehyde complex **5.2**, presumably through trapping of a gold-carbene intermediate of type **5.I** (Scheme 18).¹⁶⁰ Carbene/carbocationic intermediates can also be trapped with neutral nucleophiles such as methanol. Cyclization of **5.3** in MeOH with [(PPh₃)AuMe] (3 mol %) and HBF₄ (6 mol %) results in formation of ether **5.4** in 97 % yield (Scheme 19).¹⁵⁴ A wealth of other trapping experiments and indirect experimental evidence including isotopic labeling studies and stereochemical analyses have been cited in support of the involvement of gold carbene or carbene-like intermediates, as have numerous computational studies.^{9-11, 147-153}

However, direct experimental evidence regarding the structure and reactivity of these cationic intermediate(s) is absent, as no organometallic intermediate has been observed spectroscopically in any of these transformations.¹⁷

Scheme 18: Trapping of a gold cyclopropyl carbene complex by oxidation with Ph₂SO.¹⁶⁰



Scheme 19: Trapping of a gold cyclopropyl carbene complex with methanol.¹⁵⁴

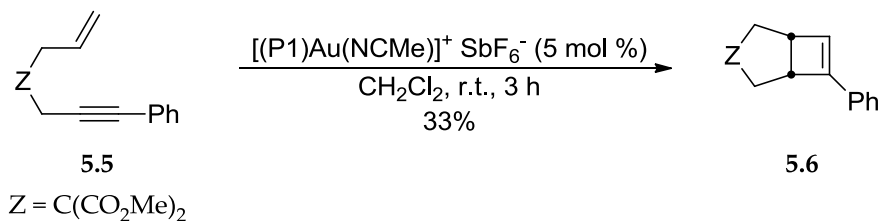


5.1.3 Project goals and scope

Gold is known to catalyze the cycloisomerization of 7-aryl-1,6-enynes (**A**, R=Ar) to give vinylcyclopentenenes **5.A** and/or bicyclo[3.2.0]hept-6-enes **5.D**.^{155, 161-162} Directly implicated in these transformations is the strained bicyclo[3.2.0]hept-1(7)-ene species **5.IV** (Figure 50). Intermediate **5.IV** is presumably generated through 6-*endo*-

cyclization followed by 1,2-alkyl migration from cyclopropyl carbene **5.III** and consumed either by ring opening to form **5.A** and/or 1,3-hydrogen migration to form **5.D** (Figure 50).^{155, 161-165} Given that a number of stable gold(I) π -alkene complexes are known while cationic gold carbene complexes remain elusive, it appeared likely that **5.IV** might represent a local minimum on the reaction coordinate, making it an ideal target for initial investigations. Toward detection of the first organometallic complex intermediating the cycloisomerization of an enyne, we chose to investigate the cyclization of the 7-phenyl-1,6-enyne **5.5** to the 6-phenylbicyclo[3.2.0]hept-6-ene **5.6** originally reported by Echavarren (Scheme 20).^{155, 161}

Scheme 20: Cycloisomerization of 7-phenyl-1,6-enyne **5.1 to the 6-phenylbicyclo[3.2.0]hept-6-ene **5.2** catalyzed by [(P1)Au(NCMe)]⁺ SbF₆⁻.**



Indeed, here we report the selective generation, spectroscopic characterization, and trapping of a gold-bicyclo[3.2.0]hept-1(7)-ene complex of the type **5.IV** that is formed in the gold-catalyzed cycloisomerization of **5.5** to give **5.6**. A detailed study of the complex (**5.9**, see below) is presented in four parts. First, the generation and structural characterization of the intermediate is discussed, including observations regarding the gold π -enyne complexes and detailed insight into the electronic structure of the gold π -bicycloheptene complex. As an extension of the characterization, the

reactivity of the complex has been probed with emphasis on ligand displacement and reactivity with nucleophiles. Next, details regarding the conversion of the bicyclo[3.2.0]hept-1(7)-ene complex to bicyclo[3.2.0]hept-6-ene are presented, and a plausible mechanism for this transformation is proposed. Finally, the findings of this investigation were applied to the modification of the reported conditions for the conversion of 5.5 to 5.6, resulting in an increase in reaction efficiency.

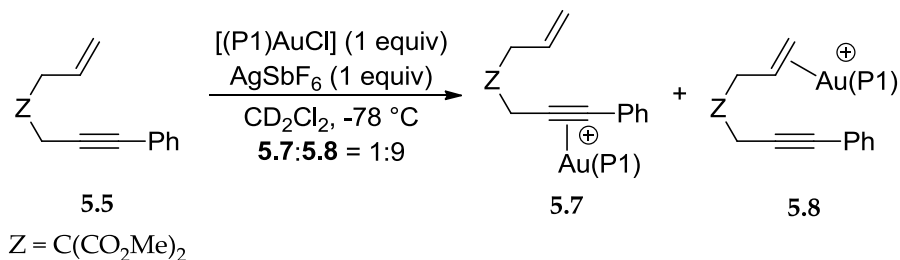
5.2 Results and discussion

5.2.1 Generation and characterization of gold π -(bicyclo[3.2.0]hept-1(7)-ene) complex 5.9

5.2.1.1 Stoichiometric generation of gold π -enyne complexes 5.7 and 5.8 and their conversion to π -(Bicyclo[3.2.0]hept-1(7)-ene) complex 5.9

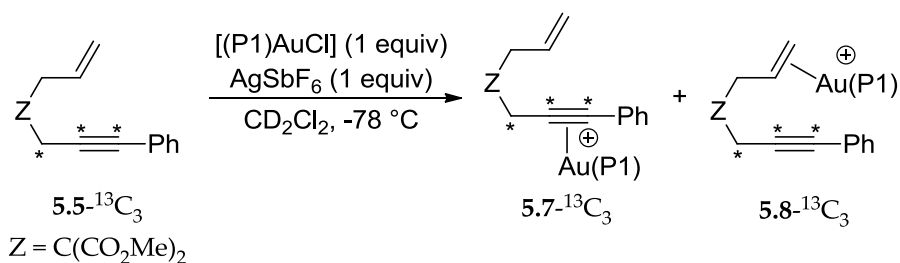
In an initial attempt to observe an organometallic complex relevant to the gold(I)-catalyzed cycloisomerization of 1,6-enynes, a 1:1:1 mixture of [(P1)AuCl], AgSbF₆, and enyne 5.9 were combined in CD₂Cl₂ in an NMR tube at -78 °C (Scheme 21). ³¹P NMR analysis of the mixture at -80 °C showed formation of a pair of new complexes in an approximately 1:9 ratio with resonances at δ = 62.6 and 62.2 ppm, respectively, which together constituted ~90 % of the reaction mixture.

Scheme 21: Formation of gold π -alkyne complex 5.7 and gold π -alkene complex 5.8



The major species **5.8** (^{31}P δ = 62.2) was identified as a π -alkene complex by the presence of resonances in the ^1H NMR spectrum at δ = 4.27 (dd, J = 2.8, 16.4 Hz, 1 H) and 4.13 (dd, J = 3.6, 8.8 Hz, 1 H), which were assigned to the terminal vinylic protons of **5.8** and shifted upfield by \sim 1 ppm relative to the terminal vinylic protons of **5.5**. Strong upfield shifts of terminal vinyl protons is characteristic of $[(\text{P1})\text{Au}(\eta^2\text{-alkene})]^+$ complexes.⁴⁶ In comparison, the terminal vinylic protons of the minor π -alkyne complex **5.7** appeared as a multiplet at δ = 5.2, which was shifted only \sim 0.05 ppm downfield from the terminal vinylic protons of **5.5**. The minor species **5.7** was identified as a π -alkyne complex on the basis of ^{31}P NMR analysis of the corresponding ^{13}C isotopomer **5.7- $^{13}\text{C}_3$** , generated along with **5.8- $^{13}\text{C}_3$** from reaction of **5.5- $^{13}\text{C}_3$** with $[(\text{P1})\text{AuCl}]$ and AgSbF_6 at -78 °C (Scheme 22). The ^{31}P NMR resonance for **5.7- $^{13}\text{C}_3$** appeared as a doublet of doublets [δ = 62.6 (dd, J_{CP} = 4.9, 27.5 Hz)] owing to the presence of carbon-phosphorous coupling, which could only result from binding of the ^{13}C -labelled alkyne moiety to gold. Conversely, the ^{31}P NMR resonance for **5.8- $^{13}\text{C}_3$** was indistinguishable from that of unlabeled **5.8**.

Scheme 22: Formation of isotopically labeled gold π -alkyne complex **5.7- $^{13}\text{C}_3$ and gold π -alkene complex **5.8- $^{13}\text{C}_3$** .**

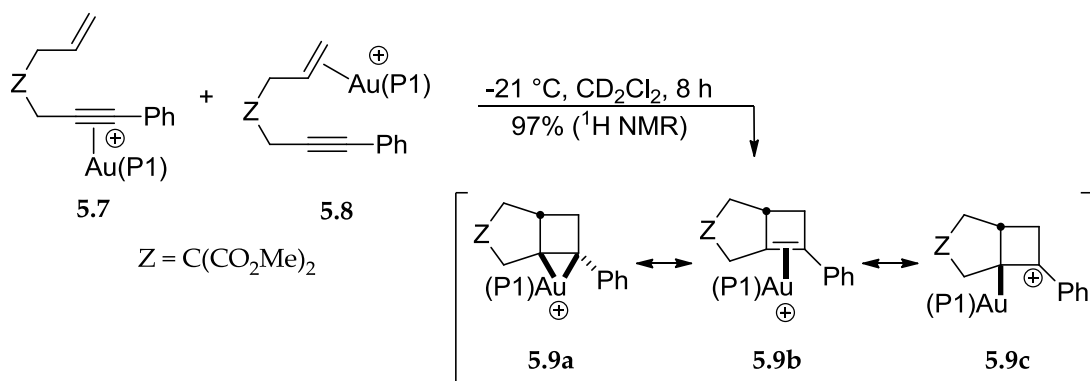


Although the gold π -alkyne species is thought to be the catalytically active species in gold-catalyzed 1,n-enyne cycloisomerizations, selective binding to the alkene does not preclude the proposed mechanism, as gold π -complexes have been shown to undergo facile intra- and intermolecular π -ligand exchange.^{46, 49, 122, 130-131} In fact, warming this solution to -21 °C results in broadening and partial coalescence of the ³¹P resonance corresponding to **5.7** and **5.8**, indicating exchange of the alkene and alkyne π -ligands on the NMR time-scale. Further, preferential coordination of the alkene is not surprising. Widehiefer and coworkers have previously demonstrated that terminal alkenes have a higher equilibrium binding affinity for [(P1)Au]⁺ than aryl alkynes,^{46, 49} and this observation is corroborated by computational studies that show that a gold-alkene π -bond is slightly stronger than a gold-alkyne π -bond.^{31, 37}

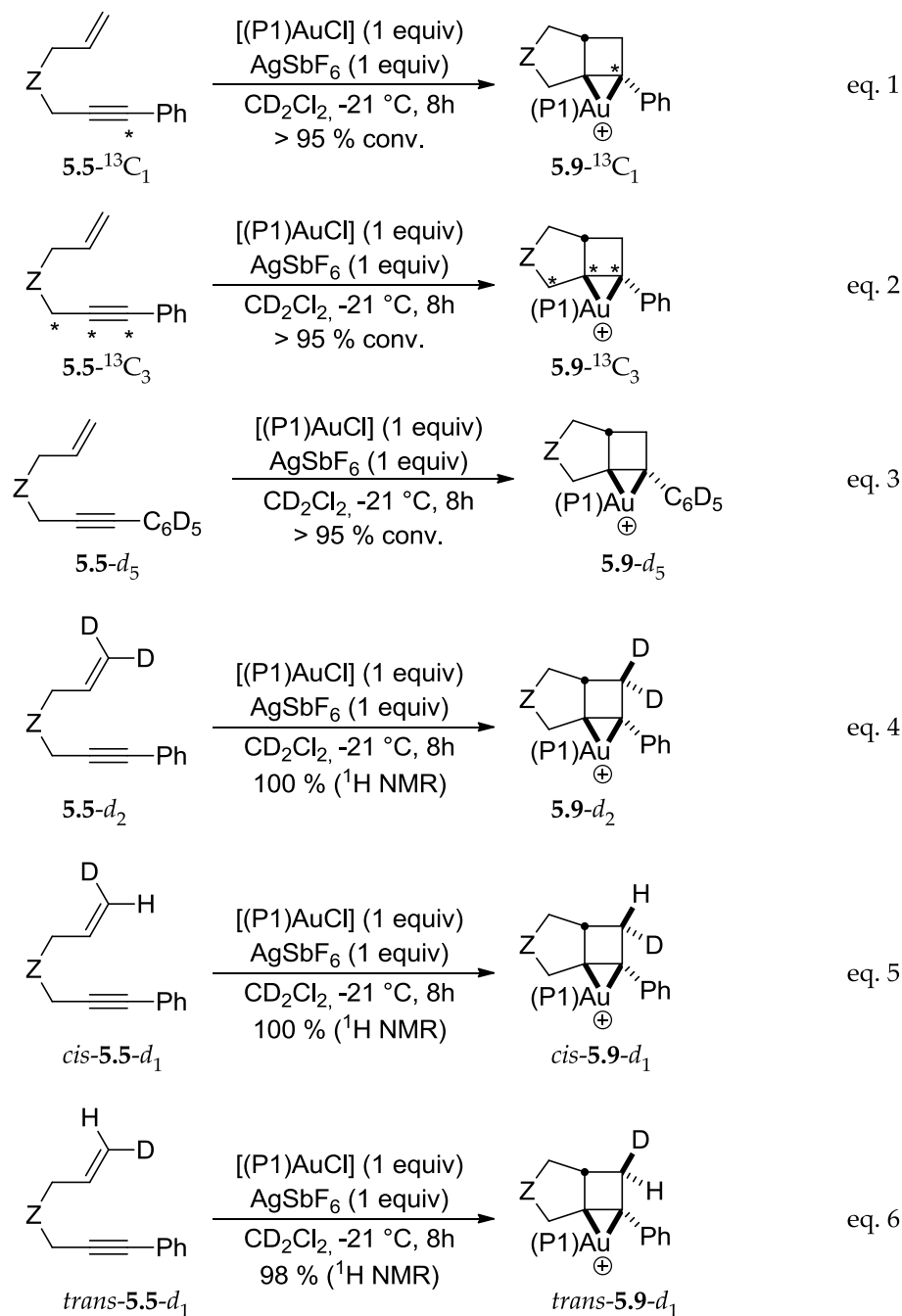
Warming a solution of **5.7** and **5.8** at -20 °C for 8 h led to consumption of the gold π -alkene and π -alkyne complexes and formation of the gold π -(bicyclo[3.2.0]hept-1(7)-ene) complex **5.5** in 97 % yield (¹H NMR), as indicated by ¹H, ³¹P, and ¹³C NMR spectroscopy (Scheme 23). Following a similar procedure, isotopomers **5.9-¹³C₁**, **5.9-¹³C₃**, and **5.9-*d*₅** were generated from the corresponding enyne isotopomers **5.5-¹³C₁**, **5.5-¹³C₃**, **5.5-*d*₅**, respectively, in > 95 % conversion as determined by ¹H NMR analysis (Scheme 24, eq. 1 – 3). Furthermore, terminally-deuterated enynes **5.5-*d*₂**, *cis*-**5.5-*d*₁**, and *trans*-**5.5-*d*₁** cyclized under the same conditions to **5.9-*d*₂**, *cis*-**5.9-*d*₁**, and *trans*-**5.9-*d*₁** in 98 – 100 % yield and no loss or scrambling of deuterium as determined by ¹H NMR

analysis (Scheme 24, eq. 4 – 6). Notably, the stereospecificity of the cyclizations of *cis*- and *trans*-5.5-*d*₁ suggests that minimal carbocation character develops on C1 in the conversion of 5.7/5.8 to 5.9.

Scheme 23: Conversion of 5.7 and 5.8 to 5.9 at -20 °C in CD₂Cl₂. Three canonical structures of 5.9 are shown.



Scheme 24: Conversion of enyne isotopomers 5.5-¹³C₁, 5.5-¹³C₃, 5.5-*d*₅, 5.5-*d*₂, *cis*-5.5-*d*₁, and *trans*-5.5-*d*₁ to gold bicyclo[3.2.0]heptene isotopomers 5.9-¹³C₁, 5.9-¹³C₃, 5.9-*d*₅, 5.9-*d*₂, *cis*-5.9-*d*₁, and *trans*-5.9-*d*₁.



5.2.1.2 Characterization of 5.9 and isotopomers

Complex **5.9** was reasonably stable in solution at -20 °C, with no observed decomposition or isomerization over ~12 h in CD₂Cl₂, but decomposed upon attempted isolation at or below room temperature. Characterization of **5.9** was aided by comparison to **5.6**, the free bicyclo[3.2.0]hept-1(7)-ene **5.10** (see section 5.2.2.1) and the gold bicyclo[3.2.0]hept-6-ene π -complex **5.11**, which was generated upon warming a solution of **5.9** at or above 0 °C (Figure 51). The details of the latter transformation are discussed at length in section 5.2.3.

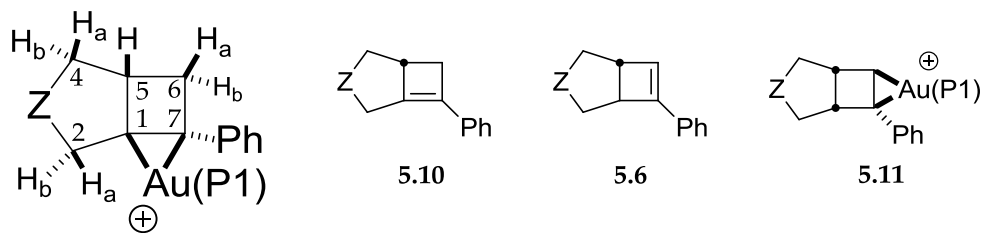


Figure 51: Partial atom numbering scheme of **5.9 and complexes which aided in the characterization of **5.9**.**

The hydrocarbon ring structure of complex **5.9** and the corresponding free bicyclo[3.2.0]heptene **5.10** were fully characterized in solution at or below -20 °C using one- and two-dimensional NMR spectroscopy (Figure 51). Coordination of gold to the C1–C7 bond of the bicyclo[3.2.0]heptene ligand was established by the large upfield shift ($\Delta\delta = -20$) of the C1 carbon resonance of **5.9** relative to that of **5.10** and by the presence of phosphorus coupling to both the C1 [$\delta = 126.9$ ($J_{CP} = 13.8$ Hz)] and C7 carbon atom [$\delta = 141.2$ ($J_{CP} = 7.5$ Hz)] of the bicycloheptene ligand of **5.9** in the ¹³C NMR spectrum. ¹H-¹H NOESY analysis established binding of the LAu⁺ fragment to the convex face of the

bicycloheptene ligand by the presence of NOE cross peaks between the ligand *tert*-butyl proton resonances at δ 1.35 and 1.24 and the H_{2a} (δ 3.24), H₅ (δ 2.84), and H_{6a} (δ 3.07) bicycloheptene proton resonances (See section 5.4.2.3, Figures 58 and 60).

Three possible canonical forms exist which could explain the nature of the gold–alkene bond in **5.9**: the metalocyclopropane structure **5.9a**, the gold π -alkene complex **5.9b**, and the cyclobutyl cation structure **5.9c** (Scheme 23). Because complex **5.9** could not be structurally characterized in the solid state, the relative importance of each of the possible contributors was probed spectroscopically; thus, NMR techniques were used to elucidate the electronic structure of **5.9** and isotopomers. For example, the C7 (δ = 141.2) and C7-phenyl resonances (δ = 131.8, 129.1, 127.2) of **5.9**, which were identified by comparison of the ¹³C NMR spectra of **5.9** and **5.9-d₅**, were shifted downfield only slightly relative to those of free **5.10** [δ = 137.59 (C7), 128.6, 127.7, 125.0 (*Ph*)] in the ¹³C NMR spectrum. This observation points to modest accumulation of positive charge at the C7 carbon atom of **5.9** and, hence, nominal contribution of the cyclobutyl cation structure **5.9c**.

The one-bond C–C coupling constants of the metal-bound carbon atoms in metal π -complexes are a sensitive measure of the hybridization of the bound carbon atoms.¹⁶⁶⁻

¹⁶⁹ The C1–C7 coupling constant of **5.9** (¹J_{C1C7} = 33 Hz), measured from the ¹³C NMR of **5.9-¹³C₃**, was diminished significantly relative to that of **5.9** (¹J_{C1C7} = 61 Hz), consistent with ~sp³ hybridization of the C1 and C7 carbon atoms of the bicycloheptene ligand of

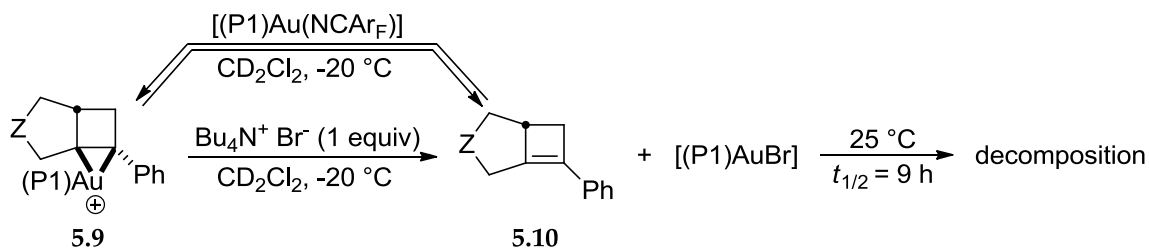
5.9. This observation reveals significant $d \rightarrow \pi^*$ back-bonding and the predomination of the metallacyclopropane structure **5.9a** (Scheme 23).¹⁶⁶⁻¹⁶⁹ The metallacyclopropane character of **5.9** stands in sharp contrast to the predominant σ -bonding character of extant gold π -alkene complexes,^{42, 46} but this discrepancy can be attributed to the significant strain of the bicyclo[3.2.0]hept-1-ene ring system.¹⁷⁰⁻¹⁷²

5.2.2 Reactivity of gold π -(bicyclo[3.2.0]hept-1(7)-ene) complex **5.9**

5.2.2.1 Generation of free bicyclo[3.2.0]hept-1(7)-ene **5.10**

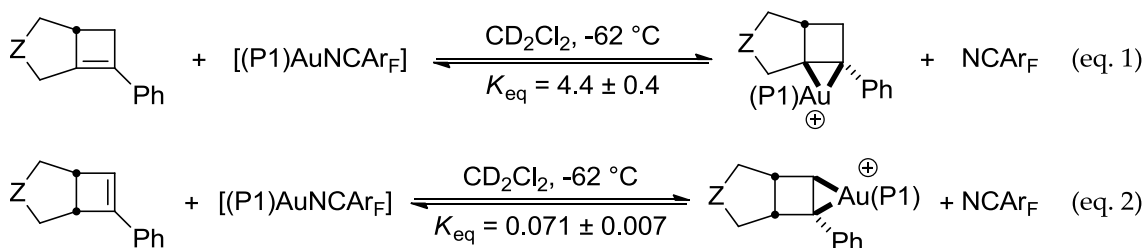
Treatment of **5.10** with the σ -donor ligands pyridine or n -Bu₄N⁺ Br⁻ (1 equiv) at -20 °C led to quantitative formation of free **5.10** and [(P1)Au(pyr)]⁺ SbF₆⁻ or [(P1)AuBr], respectively (Scheme 25). Likewise, **5.9** was partially regenerated from **5.10** by the addition of [(P1)Au(NCAr_F)] [NCAr_F = 3,5-bis(trifluoromethyl)benzonitrile] (**5.12**), supporting our characterization of **5.9** as the gold π -complex of **5.10**. Warming a solution of **5.10** and [(P1)AuBr] at 25 °C led to the slow ($t_{1/2} \approx 9$ h) decomposition of **5.10** without detectable formation of **5.6**, **5.11**, or vinylcyclopentenes.

Scheme 25: Generation of the thermally sensitive bicyclo[3.2.0]hept-1(7)-ene **5.10 from **5.9** and regeneration of **5.9** from **5.10**.**



The ligand displacement reactivity of **5.9** was exploited to further probe the nature of the gold–bicyclo[3.2.0]heptene bond through an equilibrium binding affinity study. To this end, NCAR_F was added to a solution of **5.9** at -62 °C, partially displacing **5.10** from [(P1)Au]⁺ and forming **5.12**. The relative equilibrium concentrations of **5.9**, **5.10**, **5.12**, and NCAR_F were determined from the ¹H NMR spectrum of the mixture and used to calculate an equilibrium constant for the displacement of NCAR_F from **5.12** by **5.10** of $K_{\text{eq}} = 4.4 \pm 0.4$ (Scheme 26, eq. 1). The binding affinity of **5.10** to gold was ~60 fold higher than the binding affinity of **5.6**, which was found to displace NCAR_F from **5.12** with an equilibrium constant of $K_{\text{eq}} = 0.071 \pm 0.007$ (Scheme 26, eq. 2). The higher binding affinity of **5.9** relative to **5.6** is significant considering that the binding affinity of the trisubstituted alkene 2-methyl-2-butene to (P1)Au⁺ is ~350 times greater than is that of the tetrasubstituted alkene 2,3-dimethyl-2-butene.⁴⁶ Presumably, this difference reflects the increased strain of **5.9** relative to **5.6** which is relieved upon formation of **5.9**, further corroborating the predominance of the metallacyclopropane binding structure **5.9a**.¹⁷³

Scheme 26: Equilibrium binding affinities of 5.9 (eq. 1) and 5.6 (eq. 2) to [(P1)Au]⁺ relative to NCAR_F [NCAR_F = 3,5-bis(trifluoromethyl)benzotrile].

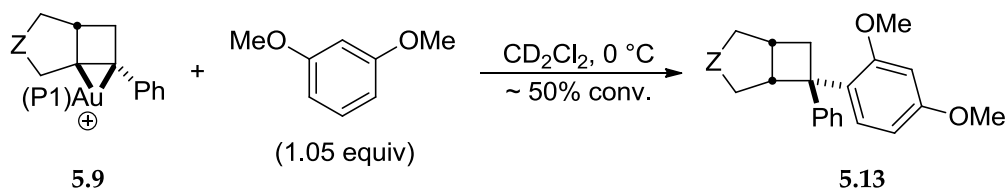


5.2.2.2 Hydroarylation of **5.9** with 1,3-dimethoxybenzene

In a further effort to evaluate the electronic structure of **5.9**, we sought to probe the reactivity of the gold π -complex with nucleophiles. π -Complexation of an alkene to an electrophilic metal for which the bonding interaction is dominated by σ -donation from the ligand to the metal results in increased electrophilicity of the alkene and, therefore, enhanced reactivity toward nucleophiles; however, π -backdonation from the metal to the alkene should attenuate this effect. Thus, the reactivity of **5.9** with nucleophiles is indicative of the nature of the gold–alkene bond.

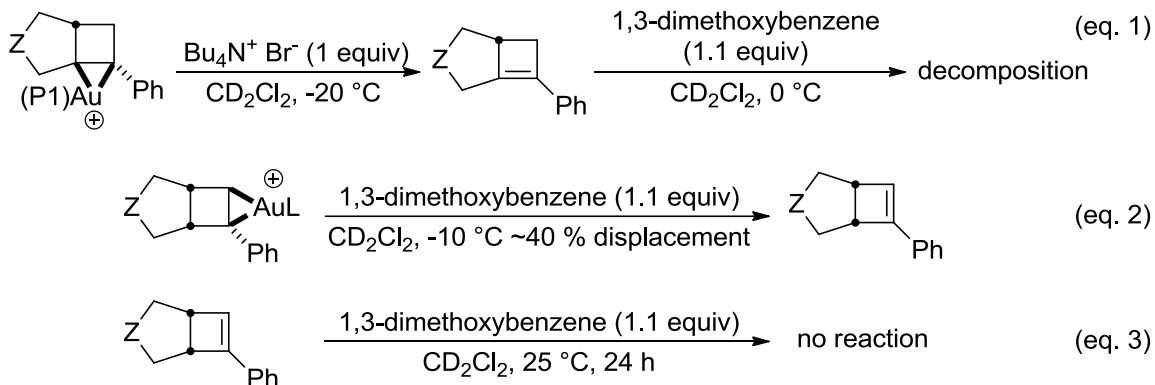
Initial experiments involved treatment of complex **5.9** with methanol, as this nucleophile has been shown to react with cationic/carbene-like intermediates of enyne cycloisomerization.^{154, 156} No reaction was observed upon treatment of a CD₂Cl₂ solution of **5.9** with 1 equiv. MeOH at -20 °C, and warming the reaction mixture resulted only in isomerization of **5.9** to **5.11**. Increasing the loading of MeOH to 10 equiv. resulted in partial generation of **5.10** and, eventually, sample decomposition. Conversely, the addition of 1.1 equiv. of the non-coordinating, electron rich arene 1,3-dimethoxybenzene to a CD₂Cl₂ solution of **5.9** and reaction at 0 °C for 2 h resulted in ~50 % conversion to give the 6,6-diarylbicyclo[3.2.0]heptane **5.13** (¹H NMR). Longer reaction times resulted in degradation of **5.9** and **5.13**, possibly due to the build-up of reactive [(P1)Au]⁺ species.

Scheme 27: Hydroarylation of 5.9 with 1,3-dimethoxybenzene to give 5.13.



The observed hydroarylation is not surprising, as a number of examples of gold(I)-catalyzed hydroarylations have been reported,¹⁷⁴⁻¹⁷⁸ but it is significant in the context of this study. A solution of free **5.10**, generated from the reaction of **5.9** and tetra-*n*-butylammonium bromide as described above, does not react with 1.1 equiv. 1,3-dimethoxybenzene at 0 °C before the onset of significant decomposition, suggesting that the strain of the molecule alone does not induce the observed reactivity (Scheme 28, eq. 1). Likewise, gold bicyclohept-6-ene complex **5.11** does not undergo hydroarylation with 1,3-dimethoxybenzene at -10 °C; rather, the addition of the arene results in formation of an ~2:3 mixture of **5.6** and **5.11** that does not yield any hydroarylation product after 100 min at 0 °C (Scheme 28, eq. 2). Treatment of an independently generated solution of **5.11** with 1.1 equiv. 1,3-dimethoxybenzene does not result in hydroarylation after 24 h at 25 °C (Scheme 28, eq. 3). These observations suggest that the unique combination of strain and coordination-induced electrophilicity are necessary for the hydroarylation of **5.9**.

Scheme 28: Control reactions showing that 5.10 (eq. 1), 5.11 (eq. 2), and 5.6 (eq. 3) do not undergo hydroarylation with 1,3-dimethoxybenzene.



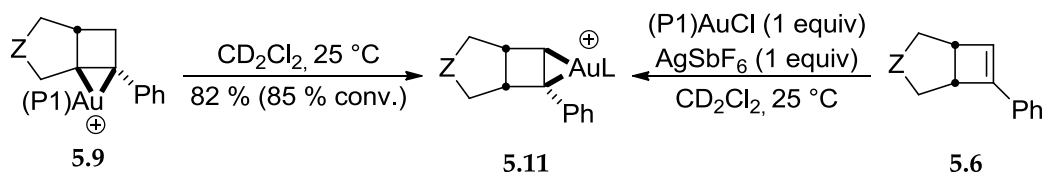
As an additional point of significance, the hydroarylation of **5.9** represents the first known example of the direct observation of a nucleophile to a gold π -complex. To date, no reports of this type of reactivity exist in the literature, despite its frequent invocation. Mechanistic studies of this important transformation are ongoing.

5.2.3 Conversion of **5.9** to **5.11**

5.2.3.1 Characterization of gold 6-phenylbicyclo-[3.2.0]-hept-6-ene complex **5.11**

Warming a solution of **5.9** at 25 °C led to rapid ($t_{1/2} \approx 16$ min) 1,3-hydrogen migration to form **5.11** in $82 \pm 5\%$ yield at 85% conversion ($96 \pm 5\%$ selectivity) (Scheme 29). Conversion continued past 85%, but resonances corresponding to **5.11** broadened and became slightly obscured, precluding quantification. Identification of **5.11** as the gold bicyclo-[3,2,0]-hept-6-ene complex was corroborated by independent synthesis from the reaction of **5.6** (1 equiv.) with a 1:1 mixture of [(P1)AuCl] and AgSbF₆ in CD₂Cl₂ at 25 °C (Scheme 29).

Scheme 29: The conversion of 5.9 to 5.11, and independent synthesis of 5.11 from 5.6.



Complex **5.11** was thermally sensitive and decomposed in solution with a half-life of ~12 h at 25 °C. The bicyclo[3.2.0]hept-6-ene ligand of **5.11** is weakly bound to gold and undergoes “on-off” fluxionality which results in broadening of some resonances in the ¹H and ¹³C NMR spectra of **5.11**. For this reason, complex characterization was carried out in solution at -40 °C. All attempts at obtaining X-ray quality crystals of **5.11** failed, presumably due to the lability of the π-ligand.

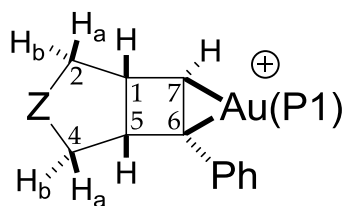
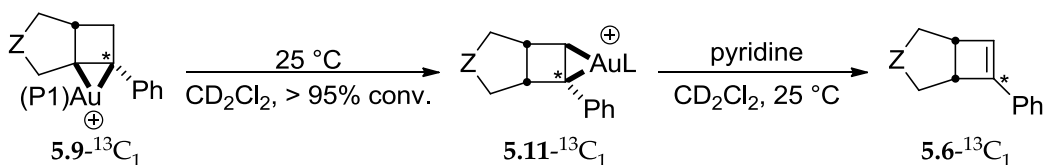


Figure 52: Partial atom numbering scheme for 5.11.

The presence of a single, sharp resonance in the ³¹P spectrum of **5.11** suggests formation of the complex as a single diastereomer. Complexation of the alkene to gold was confirmed by the downfield shift of C6 resonance ($\Delta\delta = 8.2$ ppm) and upfield shift of the C7 resonance ($\Delta\delta = -17.7$ ppm) relative to **5.6** (Figure 52), as well as the presence of phosphorus coupling in both of these resonance ($J_{CP} = 4.4$ and 15.9 Hz, respectively) in the ¹³C NMR spectrum of **5.11** at -40 °C. The ¹³C NMR spectrum of **5.11**-¹³C₁, generated by warming a solution of **5.9**-¹³C₁ at 25 °C, revealed a ¹J_{C6C7} coupling constant of ¹J_{C6C7} = 35

Hz. This was diminished significantly relative to that of free **5.6**- $^{13}\text{C}_1$ ($^1J_{\text{C6C7}} = 63$ Hz), which was isolated from the reaction of **5.11**- $^{13}\text{C}_1$ with excess pyridine followed by column chromatography (Scheme 30). The strain of **5.11**, although attenuated relative to **5.9**, is apparently sufficient to significantly bias the gold alkene bond of **5.11** toward the metallacyclopropane structure, but the significantly lower binding affinity of **5.6** for $[(\text{P1})\text{Au}]^+$ relative to **5.10** suggests that π -backbonding is stronger in complex **5.9** relative to complex **5.11**.

Scheme 30: Thermal rearrangement of **5.9- $^{13}\text{C}_1$ to **5.11**- $^{13}\text{C}_1$ and displacement of gold to form **5.6**- $^{13}\text{C}_1$.**



5.2.3.2 Kinetics of the conversion of **5.9 to **5.11****

To better understand the mechanism of the conversion of **5.9** to **5.11**, we sought to determine the rate law for this transformation. To this end, a solution of **5.9** was warmed at 25 °C and monitored periodically by ^1H NMR spectroscopy. A plot of $\ln[\mathbf{5.9}]$ versus time was linear to ~ 3 half-lives and gave a first order rate constant for the disappearance of **5.9** of $k_{\text{obs}} = 7.41 \pm 0.05 \times 10^{-4} \text{ s}^{-1}$ (Figure 53). In comparison, warming a solution of the deuterated isotopomer **5.9**- d_2 ($d_2:d_1 \approx 90:10$) at 25 °C led to first-order isomerization ($k = 1.92 \pm 0.03 \times 10^{-4} \text{ s}^{-1}$; $k_{\text{H}}/k_{\text{D}} = 3.86 \pm 0.06$) to form **5.11**- d_x with $\geq 95\%$ deuterium incorporation at the vinylic H_7 position and with $\leq 10\%$ deuterium

incorporation at the bridgehead H_5 position as determined by ^1H NMR and MS analysis (Scheme 31). Periodic analysis of the reaction mixture by ^1H NMR spectroscopy indicated that the loss of deuterium occurred upon conversion from 5.9 to 5.11 with no loss of deuterium in unreacted 5.9.

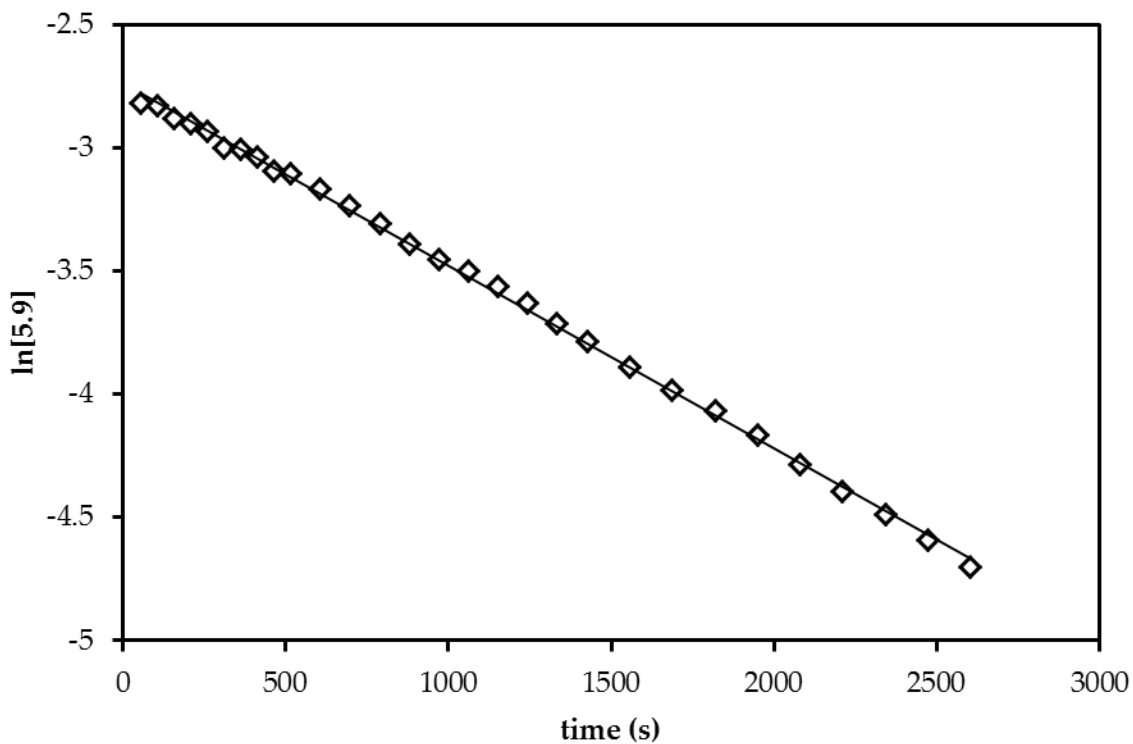
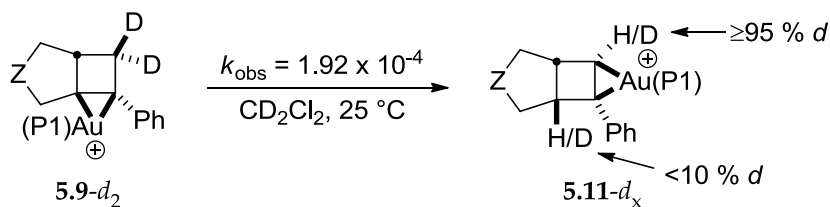


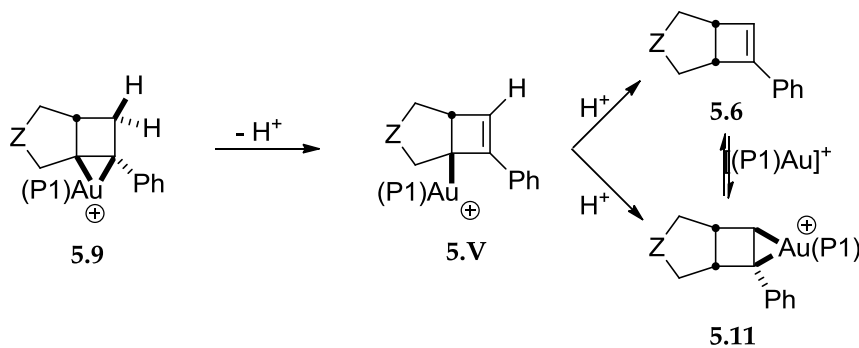
Figure 53: First order plot of the conversion of 5.9 to 5.11 ($[\text{5.9}]_0 = 0.076 \text{ M}$) in CD_2Cl_2 at 25°C .

Scheme 31: Conversion of 5.9- d_2 to 5.11- d_x .



The large primary kinetic isotope observed for the conversion of **5.9** to **5.11** resulting from deuteration of C6 points to rate-limiting cleavage of the C6–H/D bond.¹⁷⁹ In addition, the significant loss of deuterium in the isomerization of **5.5-*d*₂** points to an intermolecular pathway for deuterium migration and argues against a pathway involving a gold-hydride intermediate. Initial interpretation of these kinetic data suggested a mechanism for the conversion of **5.9** to **5.11** involving rate-limiting deprotonation of the C6–H atom of **5.9** in an E₂-like process followed by rapid protodeauration of the resultant gold σ-allyl intermediate **5.V** to initially form either **5.6** or **5.10** depending on the timing of π-complexation (Scheme 32).

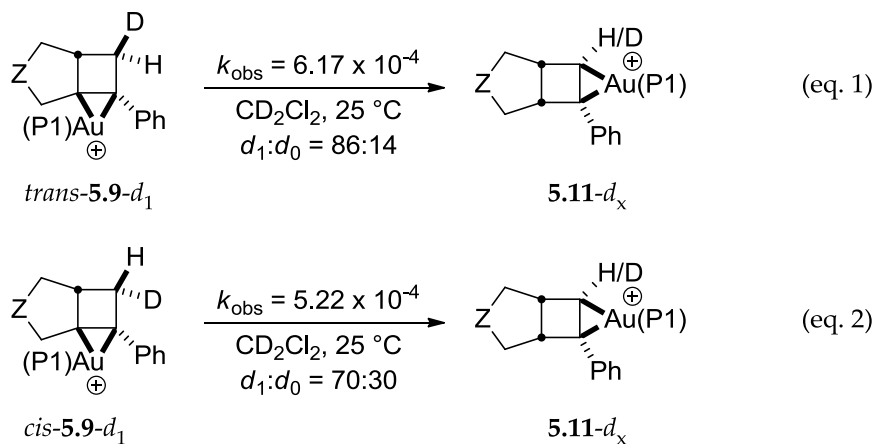
Scheme 32: E₂-like mechanism for conversion of **5.9 to **5.11** through gold σ-alkyl species **5.V**.**



Although the E₂-mechanism fit our initial kinetic data and observations well, further investigation led to a number of observations that were inconsistent with the initially proposed mechanism. For example, periodic ¹H NMR analysis of the conversion of *trans*-**5.9-*d*₁** to **5.11-*d*_x** revealed a rate constant for the consumption of *trans*-**5.9-*d*₁** of $k = 6.17 \pm 0.08 \times 10^{-4} \text{ s}^{-1}$ ($k_{\text{H}}/k_{\text{D}} = 1.20 \pm 0.02$) and an 86% incorporation of deuterium at the *H*₇

position of **5.11-*d_x*** (Scheme 33, eq. 1). Using the same procedure, *cis*-**5.9-*d₁*** was found to cyclize with a first-order rate constant of $k = 5.22 \pm 0.03 \times 10^{-4} \text{ s}^{-1}$ ($k_{\text{H}}/k_{\text{D}} = 1.42 \pm 0.01$) and ~70% deuteration at the *H₇*-position of **5.11-*d_x*** (Scheme 33, eq. 2). An E₂-like mechanism should favor, if not require, elimination of the proton/deuteron *anti* to gold (H_{6b}); thus, isomerization of *trans*-**5.11-*d₁*** should occur with a minimal KIE relative to **5.9** and maintain high deuterium incorporation at the *H₇* position of **5.7-*d_x***, while *cis*-**5.9-*d₁*** should isomerize slowly and with low deuterium incorporation at the vinylic site.

Scheme 33: Conversion of *trans*-5.9-*d₁* (eq. 1) and *cis*-5.9-*d₁* (eq. 2) to 5.11-*d_x*.



In addition to the low stereoselectivity of the isomerization of **5.9** to **5.11**, significant variation was observed in the rate of isomerization upon small changes in reaction conditions. Most notably, solutions of **5.9** generated employing AgSbF₆ from different lots exhibited an ~5-fold rate difference for isomerization to **5.11**. However, warming a CD₂Cl₂ solution of **5.9** (0.076 M), generated as described above, in the presence of excess AgSbF₆ (1 equiv.) resulted in conversion to **5.11** at approximately the

same rate as a sample of **5.9** with no additional silver. Furthermore, reacting a 1:1 mixture of AgSbF₆ and **5.10**, generated *in situ* by reaction of **5.9** with *n*-Bu₄N⁺ Br⁻, at 25 °C in CD₂Cl₂ resulted in decomposition of **5.10** at a rate similar to that observed for the decomposition of **5.10** with no excess silver. The absence of an observable effect of [silver] on the rate of conversion of **5.9** to **5.11** suggests that silver is not involved in the isomerization.

Recent reports suggest that strong Brønsted-acids generated *in situ* in transformations catalyzed by electrophilic transition metal salts may have a significant effect on the transformation or, potentially, be responsible for all activity.¹⁸⁰⁻¹⁸⁴ To probe the effect of Brønsted-acid on the conversion of **5.9** to **5.11**, triflic acid (HOTf, 25 mol %) was added to a solution of **5.9** at -78 °C and the rate of isomerization to **5.11** was monitored at -21 °C by ¹H NMR. With an observed rate constant of $k_{\text{obs}} = 6.98 \pm 0.05 \times 10^{-4} \text{ s}^{-1}$ at -21 °C, this reaction was significantly faster than the conversion of **5.9** to **5.11** without added acid, which proceeded with a rate constant of $k = 7.41 \pm 0.05 \times 10^{-4} \text{ s}^{-1}$ at 25 °C. Likewise, the conversions of **5.9-d₂**, *trans*-**5.9-d₁**, and *cis*-**5.9-d₁** to **5.11-d_x** occurred with similar kinetic isotope effects and selectivities as the corresponding transformations without added acid (Table 14), suggesting that similar pathways are operative under both sets of conditions.

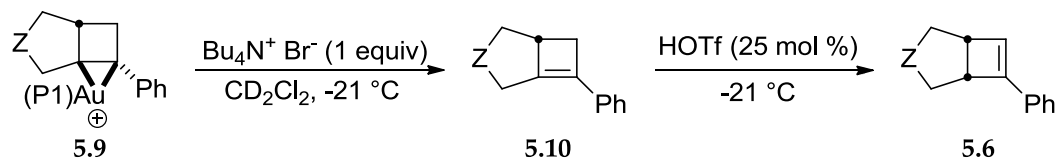
Table 14: Observed rate constants and selectivities for the conversions of 5.9 ([5.9]₀ = 0.76 M) and isotopomers to 5.11 or 5.11-*d_x* in CD₂Cl₂ without added acid and with [HOTf] = 0.019 M.

	without added acid			with [HOTf] (0.019 M)		
	T (°C)	<i>k</i> _{obs} × 10 ⁴ (s ⁻¹)	% <i>d</i> ₁ ^a	T (°C)	<i>k</i> _{obs} × 10 ⁴ (s ⁻¹)	% <i>d</i> ₁ ^a
5.9	25	7.41 ± 0.05	--	-21	6.98 ± 0.05	--
5.9-<i>d</i>₂	25	1.92 ± 0.03	> 95 %	-21	1.39 ± 0.03	97 %
<i>trans</i> - 5.9-<i>d</i>₁	25	6.17 ± 0.08	86 %	-21	3.34 ± 0.02	85 %
<i>cis</i> - 5.9-<i>d</i>₁	25	5.22 ± 0.03	~70 % ^b	-21	2.51 ± .01	75 %

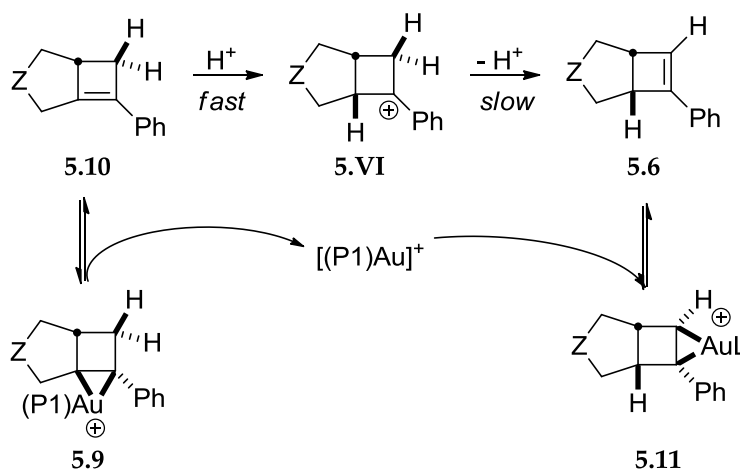
^a%-*d*₁ refers to the percent deuterium incorporation in the *H7*-position at in 5.11-*d_x*. ^bBredth and partial occlusion of resonance precluded precise integration .

As an acid-catalyzed pathway for the direct conversion of the electrophilic gold π -complex **5.9** to either **5.11** or **5.6** seemed unlikely, we expanded our investigation to study the reactivity of free bicyclo[3.2.0]heptene **5.10** in the presence of HOTf. To this end, a solution of **5.10** in CD₂Cl₂ was generated *in situ* through the reaction of **5.9** with 1 equiv. Bu₄N⁺ Br⁻ and treated with HOTf (25 mol %) at -21 °C (Scheme 34). ¹H NMR analysis of the mixture within one minute of the addition revealed complete consumption of **5.10** and formation of **5.6**. Together with the kinetic data presented above, this analysis points to a mechanism for the conversion of **5.9** to **5.11** that proceeds by initial dissociation of [(P1)Au]⁺ from **5.9** to give **5.10** followed by rapid protonation of **5.10** by a strong acid (either added or generated *in situ*) yielding unobserved cationic intermediate **5.VI**. Rate-limiting elimination from **5.VI** regenerates H⁺ and forms **5.6**, which rapidly complexes with [(P1)Au]⁺ to ultimately yield **5.11** (Scheme 35). Assignment of the elimination step as rate-limiting is based on the primary kinetic isotope effect observed between the rates of conversion of **5.9** and **5.9-*d_x***.

Scheme 34: Conversion of 5.10 to 5.6 with HOTf (25 mol %).



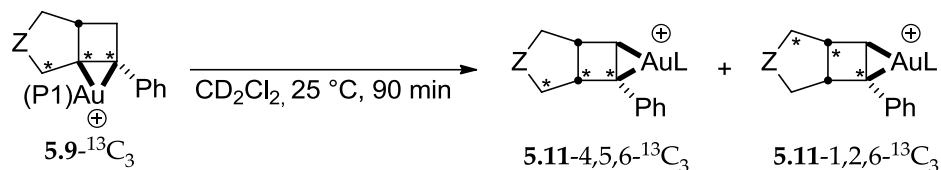
Scheme 35: Mechanism of the conversion of 5.9 to 5.11 by the acid-catalyzed isomerization of 5.10 to 5.6 through intermediate 5.VI.



5.2.3.3 Skeletal rearrangement of 5.11- $^{13}\text{C}_3$

While all observations regarding the conversion of 5.9, 5.9- $^{13}\text{C}_1$, and 5.9- d_x to 5.11 and isotopomers are consistent with the proposed acid-catalyzed mechanism for this isomerization, observation of the isomerization of 5.9- $^{13}\text{C}_3$ to 5.11- $^{13}\text{C}_3$ revealed an added level of complexity unknown to that point. Warming a CD_2Cl_2 solution of 5.9- $^{13}\text{C}_3$, generated from 5.5- $^{13}\text{C}_3$, $[(\text{P}1)\text{AuCl}]$ and AgSbF_6 as described previously, at 25°C for 90 min resulted in formation of an ~1:1 ratio of two isotopomers of 5.7- $^{13}\text{C}_3$, the expected isotopomer 5.7-4,5,6- $^{13}\text{C}_3$ and the skeletally-rearranged isotopomer 5.7-1,2,6- $^{13}\text{C}_3$ (Scheme 36).

Scheme 36: Conversion of 5.9-¹³C₃ to 5.11-4,5,6-¹³C₃ and 5.11-1,2,6-¹³C₃.



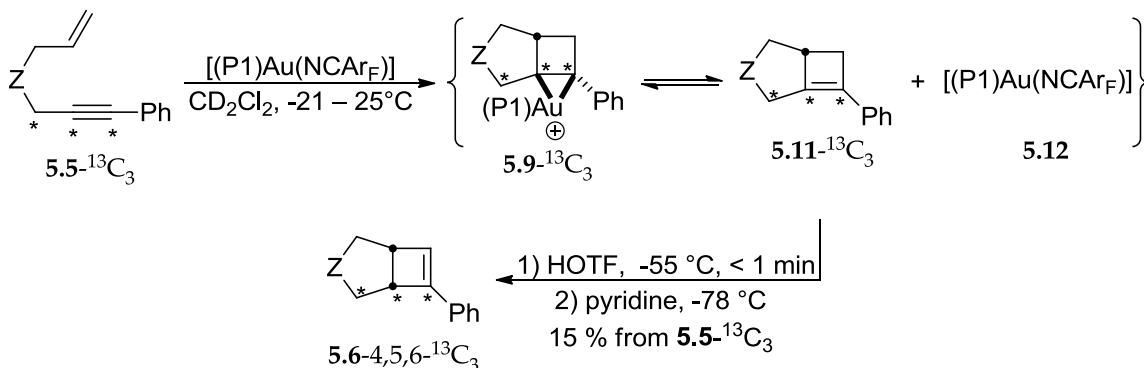
Three scenarios can be envisioned for the formation of the two isotopomers of 5.11-¹³C₃ as a statistical mixture. The two isotopomers could be formed reversibly from 5.9 and/or 5.10 or a common intermediate in the conversion to 5.11; alternatively, the isotopomers could be formed irreversibly but at the same rate from an intermediate in which C4 and C5 are equivalent to C2 and C1, respectively. On the other hand, isomerization of 5.9 could lead to selective formation of 5.11-4,5,6-¹³C₃, which then isomerizes to a statistical mixture of the two isotopomers.

Towards identifying the operative scenario, the conversion of 5.9-¹³C₃ to 5.11-¹³C₃ at 25 °C was monitored periodically by ¹³C and ¹H NMR at -40 °C. At ~15 % conversion, the reaction mixture contained a 1:1.3 ratio of 5.11-1,2,6-¹³C₃ and 5.11-4,5,6-¹³C₃; as the reaction progressed, the ratio of the two isotopomers approached 1:1 with no isotopic scrambling of 5.9-¹³C₃. These observations argue against a mechanism for the conversion of 5.9-¹³C₃ to 5.11-¹³C₃ in which the two isotopomers are formed at the same rate and establish the irreversibility of the overall conversion of 5.9 to 5.11.

As it is known that highly strained carbocycles undergo isomerization in the presence of Ag⁺,¹⁸⁵⁻¹⁹⁰ we next sought to investigate the potential role of silver in the formation/isomerization of 5.11-¹³C₃. To this end, labelled enyne 5.5-¹³C₃ was treated

with **5.12** under silver free conditions in CD₂Cl₂ for 105 min at -21 °C then 55 min at 25 °C; analysis of this reaction mixture at -65 °C by ¹³C and ³¹P NMR revealed complete consumption of **5.5**-¹³C₃ and formation of a 2.9:1 mixture of **5.9**-¹³C₃ and **5.12** as well as corresponding organic compound **5.10**-¹³C₃ and NCAr_F (Scheme 37). Surprisingly, maintaining this solution at 25 °C for an additional 150 min resulted in no change to the reaction mixture. In contrast, addition of HOTf (31 mol %) to the reaction mixture at -55 °C resulted in immediate consumption of **5.9** and **5.10**, and formation of a complex mixture of **5.11**-4,5,6-¹³C₃, **5.6**-4,5,6-¹³C₃, **5.12**, NCAr_F, and decomposition products. The mixture was treated with pyridine and chromatographed to afford **5.2**-4,5,6-¹³C₃ as a single isotopomer in 15 % yield.

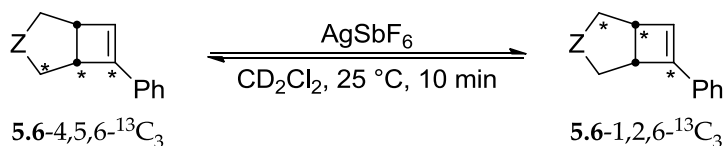
Scheme 37: Synthesis of 5.6-4,5,6-¹³C₃ from the [(P1)Au(NCAr_F)] (5.12**) catalyzed cyclization of 5.5-¹³C₃ to 5.9-¹³C₃ and 5.10-¹³C₃ followed by H⁺ catalyzed isomerization.**



The isotopically-pure **5.6-4,5,6-¹³C₃** was used to probe the mechanism and timing of the skeletal rearrangement. Reaction of a suspension of **5.6-4,5,6-¹³C₃** and AgSbF₆ in CD₂Cl₂ at 25 °C led to isomerization of **5.6-4,5,6-¹³C₃** to form a 1:1 mixture of **5.6-4,5,6-¹³C₃** and **5.2-1,2,6-¹³C₃** within 10 min at 25 °C (Scheme 38), clearly showing that **5.6** undergoes

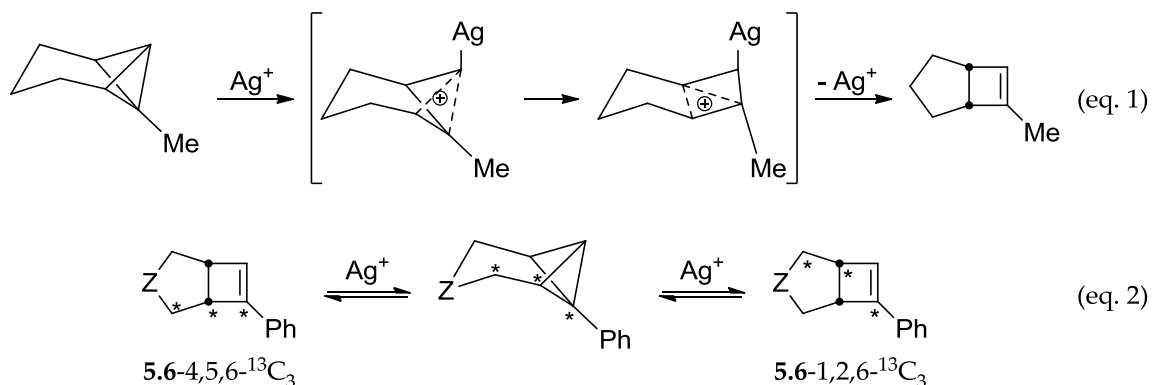
a skeletal isomerization in the presence of Ag^+ and that Au^+ is neither required nor sufficient for induction of the observed isomerization. Together, the results also suggest that H^+ is required for the conversion of **5.5/5.6** to **5.7/5.2**, which occurs without a skeletal rearrangement, and they further implicate the silver salt as the source or precursor of H^+ in the reaction mixture.

Scheme 38: Silver catalyzed isomerization of $5.6-4,5,6-^{13}\text{C}_3$ to $5.6-1,2,6-^{13}\text{C}_3$.



Interestingly, Paquette and co-workers observed the formation of bicyclo[3.2.0]hept-6-enes from the reaction of tricyclo[4.1.0.0]heptanes with silver salts, presumably through so-called argento-carbonium ion intermediates or transition states (Scheme 39, eq. 1); however, these isomerizations were irreversible and the *cis*-bicyclo[3.2.0]hept-6-enes were unreactive in the presence of Ag^+ salts.¹⁸⁶⁻¹⁸⁸ On the other hand, the C6-phenyl substituent on **5.6** could be sufficiently stabilizing to render the transformation reversible and account for the observed isomerization (Scheme 39, eq. 2). Mechanistic studies are ongoing to probe this form of reactivity.

Scheme 39: The Ag⁺ catalyzed isomerization of tricyclo[4.1.0.0]heptanes to bicyclo[3.2.0]hept-6-enes (eq. 1)¹⁸⁶⁻¹⁸⁸, and the proposed mechanism for the Ag⁺ catalyzed isomerization of 5.6-4,5,6-¹³C₃ to 5.6-1,2,6-¹³C₃ (eq. 2).



5.2.4 Catalytic enyne cycloisomerizations

5.2.4.1 Mechanistic studies of the catalytic conversion of 5.5 to 5.6

With new insight provided by our stoichiometric studies of the cyclization of 5.5 to 5.9 and 5.10 and conversion of 5.6/5.10 to 5.11/5.6, we sought to further examine the catalytic transformation of 5.5 to 5.6. To this end, the reaction of 5.5 with [(P1)AuCl] (5 mol %) and AgSbF₆ (5 mol %) in CD₂Cl₂ at 25 °C was monitored periodically by ¹H and ³¹P NMR. The presence of a single ³¹P resonance corresponding to 5.9 over the course of the reaction established this species as the catalyst resting state. Furthermore, ¹H NMR analysis of the reaction within one minute of mixing revealed ~20 % conversion of 5.5 to 5.10, which was slowly depleted over ~90 min by competing conversion to 5.6 and decomposition (Figure 54).

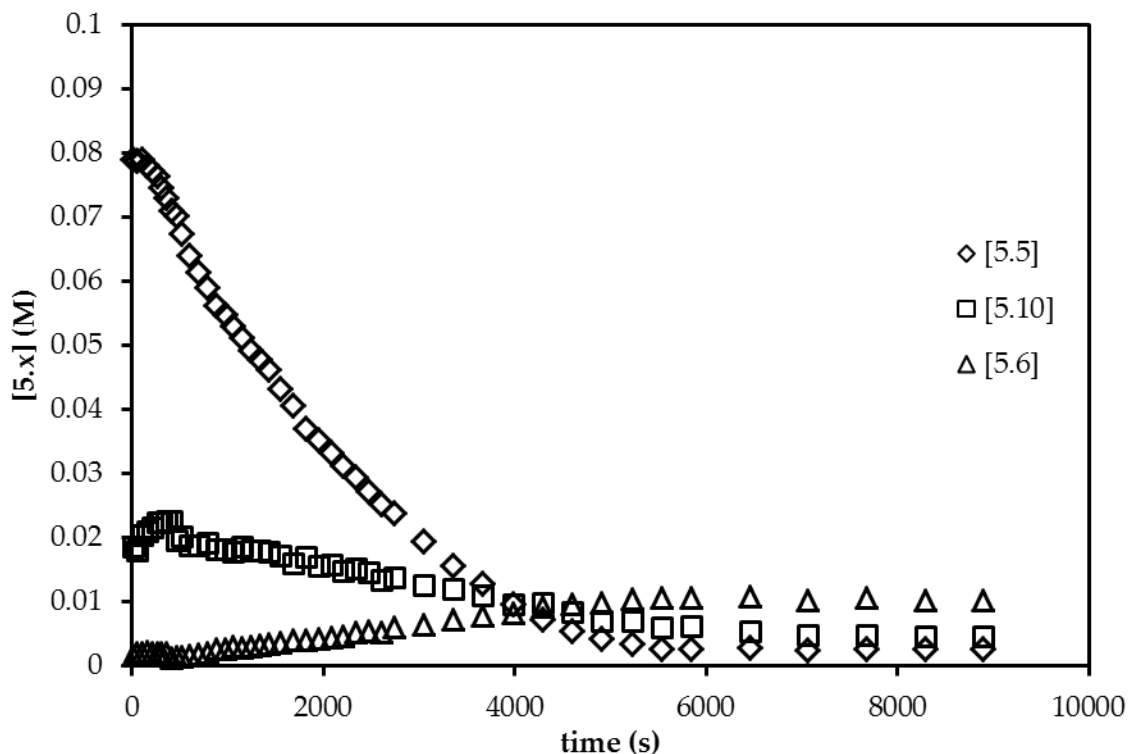
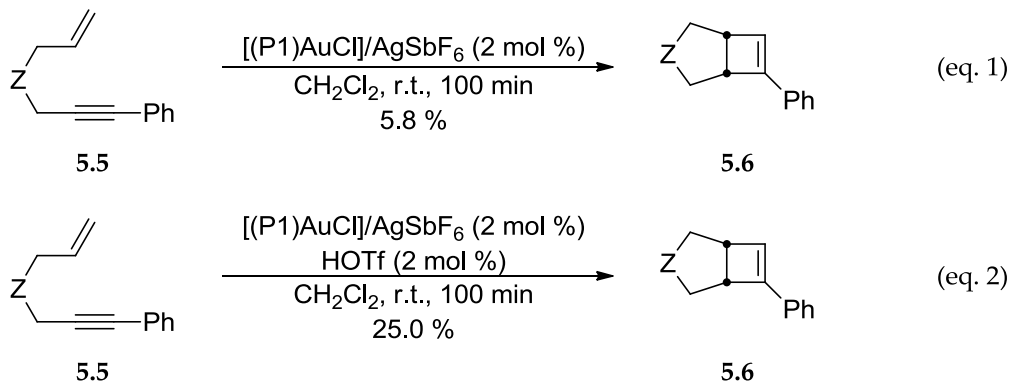


Figure 54: Analysis of the cycloisomerization of 5.5 ($[5.5]_0 = 0.10$ M) to 5.6 via 5.10 catalyzed by a mixture of [(P1)AuCl] (5 mol %) and AgSbF₆ (5 mol %) in CD₂Cl₂ at 25 °C.

Based on the observation that H⁺ is required for the conversion of 5.5 to 5.6 and the assumption that very low [H⁺] is generated *in situ*, we postulated that addition of catalytic HOTf to the reaction mixture would increase the reaction efficiency. Indeed, the reaction of 5.1 with [(P1)AuCl] (2 mol %) and AgSbF₆ (2 mol %) with no added acid in CH₂Cl₂ for 100 min resulted in complete consumption of 5.5 but only a 5.8 % yield of 5.6 (Scheme 40, eq. 1). Conversely, addition of HOTf (2 mol %) to a reaction similar to that described above resulted in consumption of 5.5 with the same efficiency but formation of 5.6 in a significantly higher 25.0 % yield (Scheme 40, eq 2). Notably, neither HOTf (2

mol %) nor AgSbF₆ (2 mol %) alone were sufficient for effecting the cycloisomerization of 5.5 to 5.6.

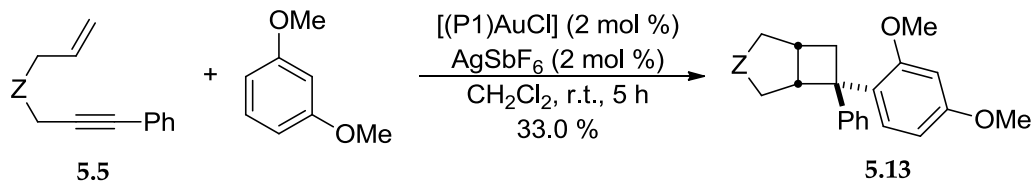
Scheme 40: The cycloisomerization of 5.5 to 5.6 catalyzed by [(P1)Au]⁺ without (eq. 1) and with (eq. 2) added HOTf.



5.2.4.2 Catalytic tandem cyclization/hydroarylation of 5.5 and 1,3-dimethoxybenzene

Stemming from the observed stoichiometric reactivity of gold bicyclo-3.2.0]heptene complex **5.9** with 1,3-dimethoxybenzene and the establishment of **5.9** as the catalyst resting state of the conversion of **5.5** to **5.6**, we sought to develop a gold-catalyzed tandem cyclization/hydroarylation protocol for the conversion of **5.5** and 1,3-dimethoxybenzene to **5.13**. Gratifyingly, reaction of a 1:2 mixture of **5.5** and 1,3-dimethoxybenzene in the presence of catalytic [(P1)AuCl] (2 mol %) and AgSbF₆ (2 mol %) for 5 h resulted in formation of **5.13** in 33 % yield (Scheme 41). Development and expansion of this new methodology is ongoing.

Scheme 41: Gold-catalyzed tandem cyclization/hydroarylation protocol for the conversion of 5.5 and 1,3-dimethoxybenzene to 5.13.



5.3 Summary and conclusions

The stoichiometric conversion of 1,6-enyne **5.5** to **5.11** with $[(P1)AuCl]/AgSbF_6$ in CD_2Cl_2 was found to be a complex process that can be summarized in four observable “steps” (Figure 55, $^{13}C_3$ -series depicted). The reaction is initiated by complexation of gold to enyne **5.5** at $-78\text{ }^\circ C$ to give an observed 1:9 mixture of enyne π -complexes **5.7** and **5.8** (step one). Reaction of the enyne π -complexes at $-20\text{ }^\circ C$ led to selective ($97 \pm 5\%$) formation of the gold bicyclo[3.2.0]hept-1(7)-ene complex **5.9**, either directly or through conversion to free bicyclo[3.2.0]hept-1(7)-ene complex **5.10** followed by complexation to $[(P1)Au]^+$ (step two). Complex **5.9** is the catalyst resting state for the gold-catalyzed conversion of **5.5** to **5.6** and exhibits dominant metallacyclopropane character, which differs markedly from the predominant σ -donating character of known cationic, two-coordinate gold π -alkene complexes.^{42, 46, 128}

Complex **5.9** undergoes rapid 1,3-hydrogen migration at room temperature ($t_{1/2} \approx 16\text{ min}$) to form the gold bicyclo-[3.2.0]-hept-6-ene complex **5.11** with 90% selectivity (steps three and four). This step likely proceeds via initial dissociation of $[(P1)Au]^+$ from **5.9** to form **5.10** followed by acid catalysed isomerization to form **5.6** (step three).

Bicycloheptene **5.6** undergoes rapid complexation/dissociation with $[(P1)Au]^+$ to give **5.11** as well as a silver-catalyzed skeletal rearrangement resulting in isomerized **5.6/5.11**, but the latter processes is only observable in the isotopically labelled **5.6/5.11**- $^{13}C_3$ system.

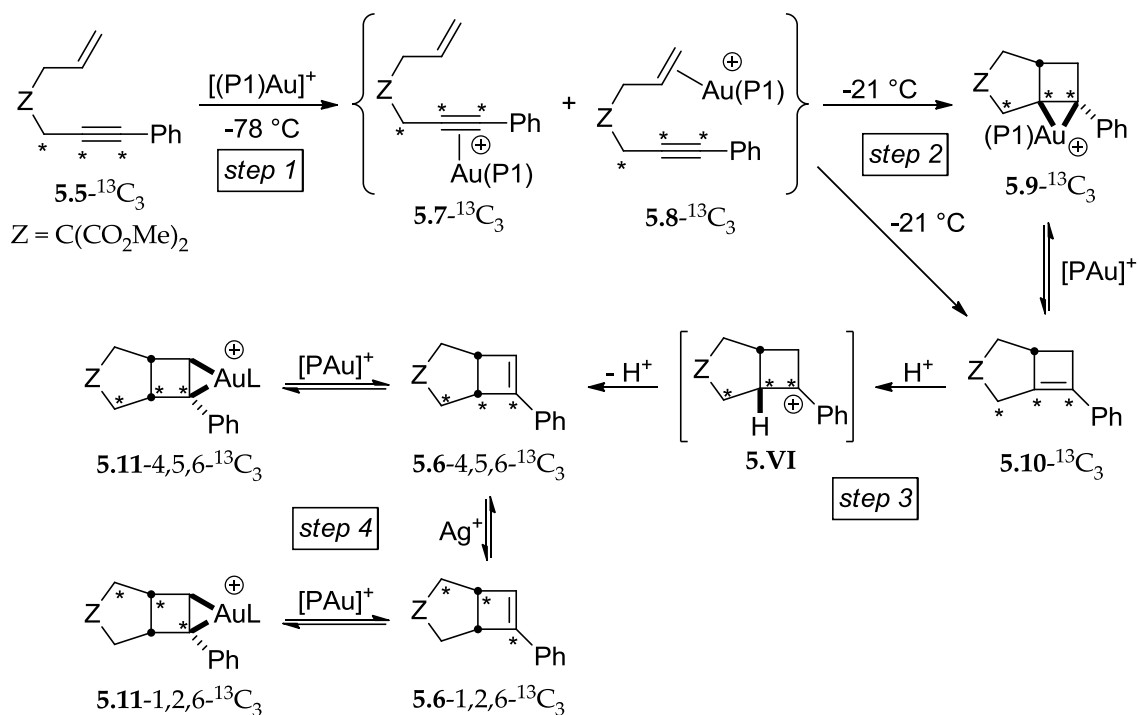


Figure 55: The overall conversion of 5.5- $^{13}C_3$ to 5.11-4,5,6- $^{13}C_3$ and 5.11-1,2,6- $^{13}C_3$ in the presence of $[(P1)Au]^+$, Ag^+ , and H^+ .

Investigation of the catalytic conversion of **5.5** to **5.6** revealed **5.9** as the catalyst resting state and identified a significant improvement in product yield when a catalytic amount of HOTf was introduced to the reaction mixture. Furthermore, complex **5.9**, generated either stoichiometrically or in the course of the catalytic reaction, could be intercepted in the presence of 1,3-dimethoxybenzene to afford the tandem

cyclization/hydroarylation product **5.13**. The scope of this novel methodology is currently being explored.

5.4 Experimental

5.4.1 General methods

Reactions were performed under a nitrogen atmosphere employing standard Schlenk and glovebox techniques unless specified otherwise. NMR spectra were obtained on a Varian spectrometer operating at 500 MHz for ^1H NMR, 125 MHz for ^{13}C NMR, and 202 MHz for ^{31}P NMR in CD_2Cl_2 unless noted otherwise; ^{13}C NMR was referenced relative to CD_2Cl_2 ($\delta = 53.8$), ^1H NMR was referenced relative to residual CH_2Cl_2 ($\delta = 5.32$), and ^{31}P spectra was referenced to an external solution of triphenylphosphine oxide in CD_2Cl_2 ($\delta = 26.9$). NMR Probe temperatures were calibrated using a neat methanol thermometer. LCMS was performed on an Agilent Technologies 1100 Series LC/MSD-Trap SL equipped with an Agilent Zorbax C-18 with 3.5 μm particle 1×150 mm column. Flash column chromatography was performed employing 200-400 mesh silica gel (EM). Thin layer chromatography (TLC) was performed on silica gel 60 F254. CD_2Cl_2 was dried over CaH_2 prior to use. Ether, methylene chloride, and THF were purified by passage through columns of activated alumina under nitrogen. LAuCl , [L = $P(t\text{-Bu}_2)O\text{-biphenyl}$], AgSbF_6 , 1,3-dimethoxybenzene, nitromethane, and reagents for enyne synthesis were obtained through major chemical suppliers and used as received.

Authentic sample of **5.6** was synthesized from **5.5** employing the method of Echavarren.¹⁵⁵

5.4.2 Syntheses and characterization of complexes

5.4.2.1 Syntheses and characterization of enyne **5.5** and isotopomers

7-Phenyl-4,4-bis(methoxycarbonyl)-1,6-enyne (5.5) Enyne **5.5** was synthesized according to a published procedure.¹⁹¹ ¹H NMR (-80 °C): δ = 7.40 – 7.22 (m, 5 H), 5.58 (br qd, J = 7.6, 17.2 Hz, 1 H), 5.19 (d, J = 16.6 Hz, 1 H), 5.13 (d, J = 9.9 Hz, 1 H), 3.68 (s, 6 H), 2.91 (s, 2 H), 2.75 (d, J = 7.3 Hz, 2 H).

7-Pentadeuteriophenyl-4,4-bis(methoxycarbonyl)-1,6-enyne (5.5-*d*₅).

Iodobenzene-*d*₅ (418 mg, 2.00 mmol) and propargyl alcohol (123 mg, 2.20 mmol) were added to a stirred suspension of (PPh₃)₂PdCl₂ (15 mg, 0.020 mmol) and copper(I) iodide (8 mg, 0.04 mmol) in triethylamine (8 mL) at room temperature. The reaction mixture was stirred at room temperature for 5 h and treated with saturated aqueous NH₄Cl. The resulting mixture was extracted with CH₂Cl₂ (3 × 20 mL) and the combined organic extracts were dried (MgSO₄), filtered, and concentrated. The resulting oily residue was chromatographed (SiO₂; hexanes–EtOAc = 9:1 → 7:3) to give 3-pentadeuteriophenylprop-2-yn-1-ol (**5.14-*d*₅**) as a pale yellow oil (274 mg, 100 % yield).

Phosphorus tribromide (271 mg, 1.00 mmol) was added to a vigorously stirred solution of **5.14-*d*₅** (274 mg, 2.00 mmol) and pyridine (54 mg, 0.69 mmol) in diethyl ether (2 mL) at 0 °C. The reaction mixture was stirred at 0 °C for 2 h and quenched by addition

of cold deionized water (3 mL). The resulting mixture was extracted with diethyl ether (20 mL) and the organic extract was washed with NaHCO₃ (aq) (10 mL), dried (MgSO₄), filtered, and concentrated under vacuum. Chromatography of the oily residue (SiO₂; hexanes) gave 1-(3-bromoprop-1-yn-1-yl)-pentadeuteriobenzene (**5.15-*d*₅**) as a yellow oil (203 mg, 51 %).

A solution of dimethyl allylmalonate (174 mg, 1.01 mmol) in THF (1 mL) was added to a suspension of sodium hydride (25 mg, 1.06 mmol) in THF (1 mL) at 0 °C. The resultant suspension was stirred for 1 h at 0 °C and treated with a solution of **5.15-*d*₅** (203 mg, 1.01 mmol) in THF (1 mL). The resulting mixture was warmed to room temperature, stirred for 14 h, quenched with saturated aqueous NH₄Cl (5 mL) and extracted with ether (2 × 10 mL). The combined organic extracts were dried (MgSO₄), filtered, concentrated under vacuum, and chromatographed (SiO₂; hexanes–EtOAc = 19:1 → 9:1) to give **5.5-*d*₅** and a colorless, viscous oil (263 mg, 90 %).

For 5.14-*d*₅: ¹H NMR (CDCl₃, 25 °C, 400 MHz): δ 4.50 (s, 2 H), 2.09 (br s, 1 H).

¹³C{¹H} NMR (CDCl₃, 25 °C): δ 131.4 (t, *J* = 24.7 Hz), 128.6 – 127.4 (m), 122.4, 87.4, 85.7, 51.7.

For 5.15-*d*₅: ¹H NMR (CDCl₃, 25 °C, 400 MHz): δ 4.17 (s, 2 H).

For 5.5-*d*₅: ¹H NMR (CDCl₃, 25 °C): δ 5.68 (br qd, *J* = 7.8, 17.3 Hz, 1 H), 5.21 (d, *J* = 17.0 Hz, 1 H), 5.15 (d, *J* = 10.1 Hz, 1 H), 3.76 (s, 6 H), 3.02 (s, 2 H), 2.88 (d, *J* = 7.5 Hz, 2 H).

7-Phenyl-4,4-bis(methoxycarbonyl)-1,6-enyne-7-¹³C₁ (5.5-¹³C₁)

3-Phenylprop-2-yn-1-ol-3-¹³C₁ (**5.14-¹³C₁**) was synthesized employing a published procedure¹⁹² and was converted to **5.5-¹³C₁** in two steps employing a procedure similar to that used to synthesize **5.5-*d*₅** from **5.14-*d*₅**.

For 5.14-¹³C₁: ¹³C{¹H} NMR (CDCl₃, 25 °C, enriched resonance only): δ 83.6.

For 5.5-¹³C₁: ¹³C{¹H} NMR (CDCl₃, 25 °C, enriched resonance only): δ 83.8.

7-Phenyl-4,4-bis(methoxycarbonyl)-1,6-enyne-5,6,7-¹³C₃ (5.5-¹³C₃)

3-phenylprop-2-yn-1-ol-¹³C₃ (**5.14-¹³C₃**) was synthesized from reaction of iodobenzene with propargyl alcohol-¹³C₃ following a procedure analogous to that used to synthesize **5.14-*d*₅** and was converted to **5.5-¹³C₃** in two steps employing a procedure similar to that used to synthesize **5.5-*d*₅** from **5.14-*d*₅**. The labeled carbon atoms of **5.5-¹³C₃** comprised an ABX spin system in the ¹³C{¹H} NMR spectrum (CDCl₃, 25 °C) with δ_X = 22.4 (C5) and *J*_{AB} (*J*_{C6C7}) = 179.7 Hz (Figure 56).

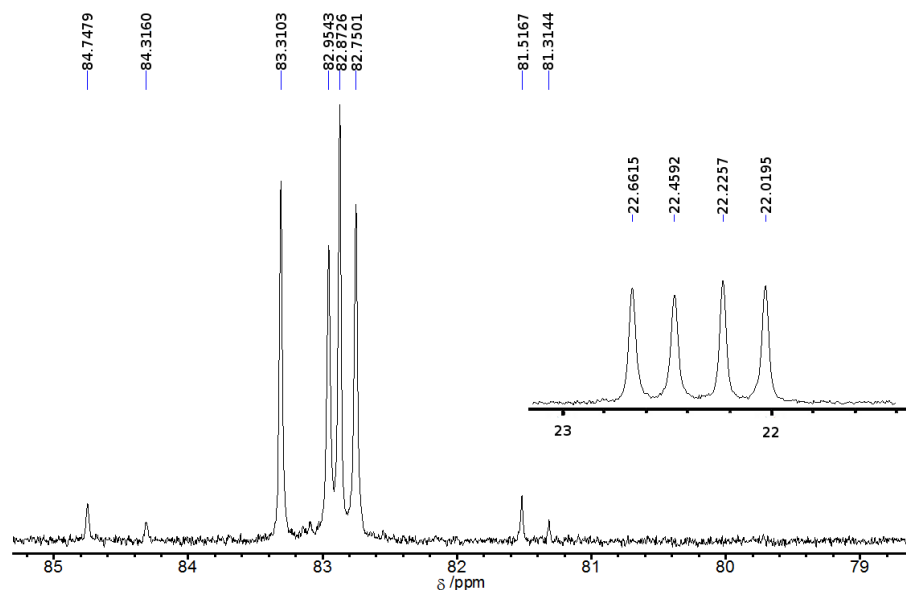


Figure 56: Partial $^{13}\text{C}\{^1\text{H}\}$ NMR spectrum of $5.5\text{-}^{13}\text{C}_3$ showing resonances corresponding to the labeled carbon atoms (CDCl_3 , 25°C).

1,1-Dideuterio-7-phenyl-4,4-bis(methoxycarbonyl)-1,6-enyne (5.5- d_2) (3-Bromo-1-propyn-1-yl)benzene (**5.16**) was synthesized employing a published procedure.¹⁹³ 4,4-Bis(methoxycarbonyl-1-phenyl-1,6-heptadiyne (**5.17**) was synthesized from reaction of dimethyl propargylmalonate with **5.16** employing a procedure analogous to that used to synthesize **5.5- d_5** from **5.15- d_5** .

A solution of **5.17** (865 mg, 3.04 mmol) in methanol- $O\text{-}d$ (4 mL) was added to a stirred suspension of NaOMe (33 mg, 0.61 mmol) in methanol- $O\text{-}d$ (4 mL) at room temperature. The resultant suspension was stirred at room temperature for 45 min, concentrated to 2 mL, and diluted with fresh methanol- $O\text{-}d$ (8 mL). The cycle was repeated three times and the resulting suspension was treated with D_2O (4 mL) and extracted with CH_2Cl_2 (2 x 10 mL). The combined organic extracts were dried (MgSO_4)

and concentrated to give 1,1-dideuterio-7-phenyl-4,4-bis(methoxycarbonyl)-1,6-enyne (**5.16-*d*₁**) (862 mg, 99%) which was used in the subsequent step without further purification.

Cp₂ZrHCl (284 mg, 1.10 mmol) was added in one portion to a solution of **5.16-*d*₁** (285 mg, 1.00 mmol) in CH₂Cl₂ (8 mL) at 0 °C. The resultant suspension was stirred for 80 min, over which time all solids dissolved, and quenched by the addition of D₂O (2 mL). The resulting biphasic mixture was stirred vigorously at 0 °C for 10 min and warmed to room temperature stirred for 10 min. The reaction mixture was filtered through a pad of silica gel, eluted further with CH₂Cl₂, and the filtrate was concentrated and chromatographed (SiO₂, hexanes–EtOAc = 95:5) to give **5.5-*d*₂** (155 mg, 54%) as a colorless oil.

For 5.17: ¹H NMR (CDCl₃, 25 °C, 400 MHz): δ 7.39 – 7.35 (m, 2 H), 7.31 – 7.26 (m, 3 H), 3.79 (s, 6 H), 3.21 (s, 2 H), 3.06 (d, *J* = 2.6 Hz, 2 H), 2.06 (t, *J* = 2.6 Hz, 1 H).

For 5.17-*d*₁: ¹H NMR (CDCl₃, 25 °C, 400 MHz): δ 7.39 – 7.35 (m, 2 H), 7.30 – 7.26 (m, 3 H), 3.79 (s, 6 H), 3.21 (s, 2 H), 3.06 (s, 2 H).

For 5.5-*d*₂: Spectroscopic analysis revealed ~85% deuterium incorporation, with < 5% of the residual proton *cis*- to the alkyl substituent on the alkene and the remainder *trans*- to the alkyl substituent. ¹H NMR: (CDCl₃, 25 °C, 400 MHz): δ 7.40 – 7.35 (m, 2 H), 7.30 – 7.25 (m, 3 H), 5.67 (br t, *J* = 7.0 Hz, 1 H), 5.14 (d, *J* = 10.2 Hz, ~0.1 H), 3.76 (s, 6 H),

3.02 (s, 2 H), 2.87 (d, $J = 7.5$ Hz, 2 H). MS [ESI (M + Na)⁺]: 311.1 (82.4 %), 310.1 (14.7 %), 309.1 (3.0 %).

1-(*E*)-deuterio-7-phenyl-4,4-bis(methoxycarbonyl)-1,6-enyne (*trans*-5.5-*d*₁)

Dimethyl [4-(*E*)-²H₁]but-3-ene-1,1-dicarboxylate was synthesized according to published procedure in 45 % yield and ≥ 95 % deuterium incorporation at the indicated position.¹⁹² *trans*-5.5-*d*₁ was synthesized from dimethyl [4-(*E*)-²H₁]but-3-ene-1,1-dicarboxylate and phenylpropargyl bromide using a procedure analogous to that used to synthesize 5.5-*d*₅ from 5.15-*d*₅. ¹H NMR (CDCl₃, 400 MHz, 25 °C): δ 7.40-7.35 (m, 2H), 7.31-7.27 (m, 3H), 5.68 (td, $J = 7.6, 16.8$ Hz, 1 H), 5.20 (td, $J = 1.2, 16.8$ Hz, 1 H), 3.76 (s, 6 H), 3.02 (s, 2 H), 2.87 (dd, $J = 1.2, 7.6$ Hz, 2 H). MS [ESI (M + Na)⁺]: 310.1 (97.4 %), 309.1 (2.6 %).

1-(*Z*)-deuterio-7-phenyl-4,4-bis(methoxycarbonyl)-1,6-enyne (*cis*-5.5-*d*₁)

cis-5.5-*d*₁ was synthesized from 5.17-*d*₁ employing a procedure similar to the one used to prepare 5.5-*d*₂ from 5.17-*d*₂, but the hydrozirconation was quenched by the addition of H₂O. *cis*-5.5-*d*₁ (155 mg, 54.0 %) was isolated as colorless oil. Spectroscopic analysis revealed > 95 % deuteration at the indicated site. ¹H NMR (CDCl₃, 400 MHz, 25 °C): δ 7.40-7.35 (m, 2H), 7.31-7.26 (m, 3H), 5.72-5.63 (m, 1 H), 5.13 (d, $J = 10.1$ Hz, 1 H), 3.76 (s, 6 H), 3.02 (s, 2 H), 2.87 (d, $J = 1.2, 7.5$ Hz, 2 H). MS [ESI (M + Na)⁺]: 310.1 (97.5 %), 309.1 (2.5 %).

5.4.2.2 Syntheses and characterization of gold π -enyne complexes 5.7 and 5.8 and isotopomers

A suspension of [(P1)AuCl] (24 mg, 4.5×10^{-2} mmol) and AgSbF₆ (16 mg, 4.7×10^{-2} mmol) in CD₂Cl₂ (0.3 mL) was mixed at -78 °C for 10 min in an NMR tube. The resulting suspension was treated with a solution of 5.5 (13 mg, 4.5×10^{-2} mmol) in CD₂Cl₂ (0.3 mL) at -78 °C and mixed thoroughly by shaking the NMR tube at -78 °C, which formed a flaky white precipitate that settled to the bottom of the tube. The tube was placed in the probe of an NMR spectrometer precooled at -80 °C and analyzed by ¹H and ³¹P NMR spectroscopy.

For 5.7: ³¹P{¹H} NMR (-80 °C): δ 62.6.

For 5.8: ¹H NMR (-80 °C, selected resonances): δ 6.04 – 5.94 (m, 1 H), 4.27 (dd, $J = 2.8, 16.4$ Hz, 1 H), 4.13 (dd, $J = 3.6, 8.8$ Hz, 1 H). ³¹P{¹H} NMR (-80 °C): δ 62.8.

For 5.7-¹³C₃: Synthesized along with 5.8-¹³C₃ from 5.5-¹³C₃ employing the procedure used to synthesize 5.7 and 5.8 from 5.5. ³¹P{¹H} NMR (-80 °C): δ 62.6 (dd, $J_{CP} = 4.9, 27.5$ Hz).

5.4.2.3 Syntheses and characterization of gold η^2 -bicyclo-[3.2.0]-hept-1(7)ene 5.9 and isotopomers

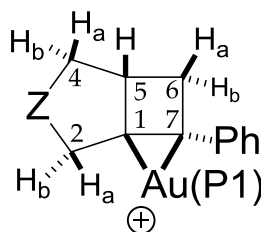
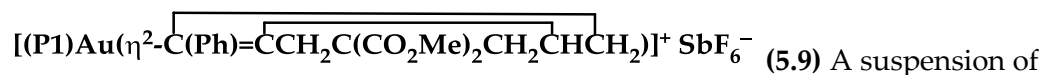


Figure 57: Partial atom numbering scheme for 5.9.



A suspension of [(P1)AuCl] (24 mg, 4.5×10^{-2} mmol) and AgSbF₆ (16 mg, 4.7×10^{-2} mmol) in CD₂Cl₂ (0.3 mL) was mixed at -78 °C for 10 min in an NMR tube. The resulting suspension was treated with a solution of **5.5** (13 mg, 4.5×10^{-2} mmol) in CD₂Cl₂ (0.3 mL) at -78 °C and mixed thoroughly by shaking the NMR tube at -78 °C, forming a flaky white precipitate that was allowed to settle. The NMR tube was maintained at -20 °C for 8 h, treated with nitrobenzene (4.6 μL, 4.5×10^{-2} mmol, internal standard), and analyzed by ¹H NMR spectroscopy, which revealed formation of **5.9** in $97 \pm 5\%$ yield as determined by integration of the proton resonances of **5.9** at δ 2.51 (*H*_{4a}) and 2.22 ppm (*H*_{4b}) relative to the resonance corresponding to the *ortho*-protons of the nitrobenzene (δ 8.21). The aliphatic ¹H NMR resonances of **5.9** were unambiguously assigned by comparison to spectra of isotopically labeled **5.9** and from the 2D ¹H-¹H COSY and NOESY spectra of **5.9** (Figures 57–60). In addition, the selective binding of gold to the convex face of the bicycloheptene ring was established by the presence of NOE cross peaks between the ligand *tert*-butyl proton resonances at δ 1.35 and 1.24 and the H_{2a} (δ 3.24), H₅ (δ 2.84), and H_{6a} (δ 3.07) bicycloheptene proton resonances (Figures 58 and 60).

For 5.9: ¹H NMR (-21 °C): δ = 7.88 – 7.83 (m, 1 H), 7.61 (dt, *J* = 1.0, 7.4 Hz, 1 H), 7.59-7.55 (m, 2 H), 7.52 (tt, *J* = 1.3, 7.8 Hz, 1 H), 7.49 – 7.41 (m, 3 H), 7.20 (td, *J* = 1.2, 7.8 Hz, 1 H), 7.17 – 7.13 (m, 3 H), 6.96 (td, *J* = 1.4, 7.8 Hz, 1 H), 6.92 (t, *J* = 7.2 Hz, 1 H), 3.74 (s, 3 H, OCH₃), 3.28 (s, 3 H, OCH₃), 3.24 (d, *J* = 14.9 Hz, 1 H, *H*_{2a}), 3.12 (d, *J* = 14.9 Hz, 1 H,

H_{2b}), 3.07 (dtd, $J = 1.5, 4.3, 15$ Hz, 1 H, H_{6a}), 2.84 (ddd, $J = 4.0, 5.2, 9.4$ Hz, 1 H, H_5), 2.77 (dd, $J = 3.2, 14.9$ Hz, 1 H, H_{6b}), 2.51 (dd, $J = 9, 14.2$ Hz, 1 H, H_{4a}), 2.22 (dd, $J = 5.8, 14.2$ Hz, 1 H, H_{4b}), 1.35 (d, $J = 16.2$ Hz, 9 H), 1.24 (d, $J = 16.2$ Hz, 9 H). $^{13}\text{C}\{^1\text{H}\}$ NMR (-20 °C, 150.8 MHz): $\delta = 170.7, 170.5, 148.0$ (d, $J_{\text{CP}} = 13.6$ Hz), 143.1 (d, $J_{\text{CP}} = 7.8$ Hz), 141.1 (d, $J_{\text{CP}} = 10$ Hz, C7), 134.4 (d, $J_{\text{CP}} = 2.7$ Hz), 133.3 (d, $J_{\text{CP}} = 7$ Hz), 133.0 (d, $J_{\text{CP}} = 2$ Hz, C_{ipso}), 131.9 (d, $J_{\text{CP}} = 5.9$ Hz), 131.8 (C_{Ph}), 130.4, 129.8 (d, $J_{\text{CP}} = 5.6$ Hz), 129.1 (C_{Ph}), 128.7, 128.3, 128.2, 127.9, 127.2 (C_{Ph}), 126.9 (d, $J_{\text{CP}} = 14.0$ Hz, C1), 124.5 (d, $J = 44.9$ Hz), 63.8, 53.6, 53.0, 41.2 (C5), 37.8, 37.4 (d, $J_{\text{CP}} = 20.5$ Hz), 37.3 (d, $J_{\text{CP}} = 20.1$ Hz), 36.4, 34.7 (C6), 30.5 (d, $J_{\text{CP}} = 6.0$ Hz), 30.2 (d, $J = 5.6$ Hz). $^{31}\text{P}\{^1\text{H}\}$ NMR (-20 °C): δ 65.4.

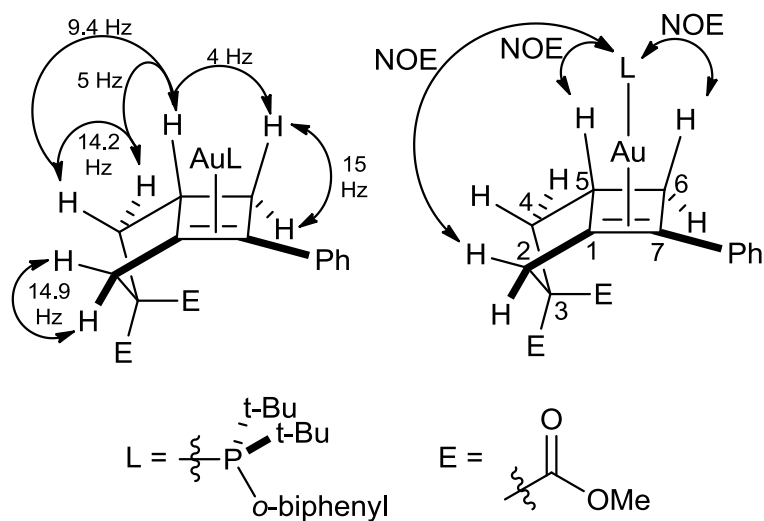


Figure 58: Selected coupling constants (left) and NOE enhancements observed in NMR spectra of 5.9.

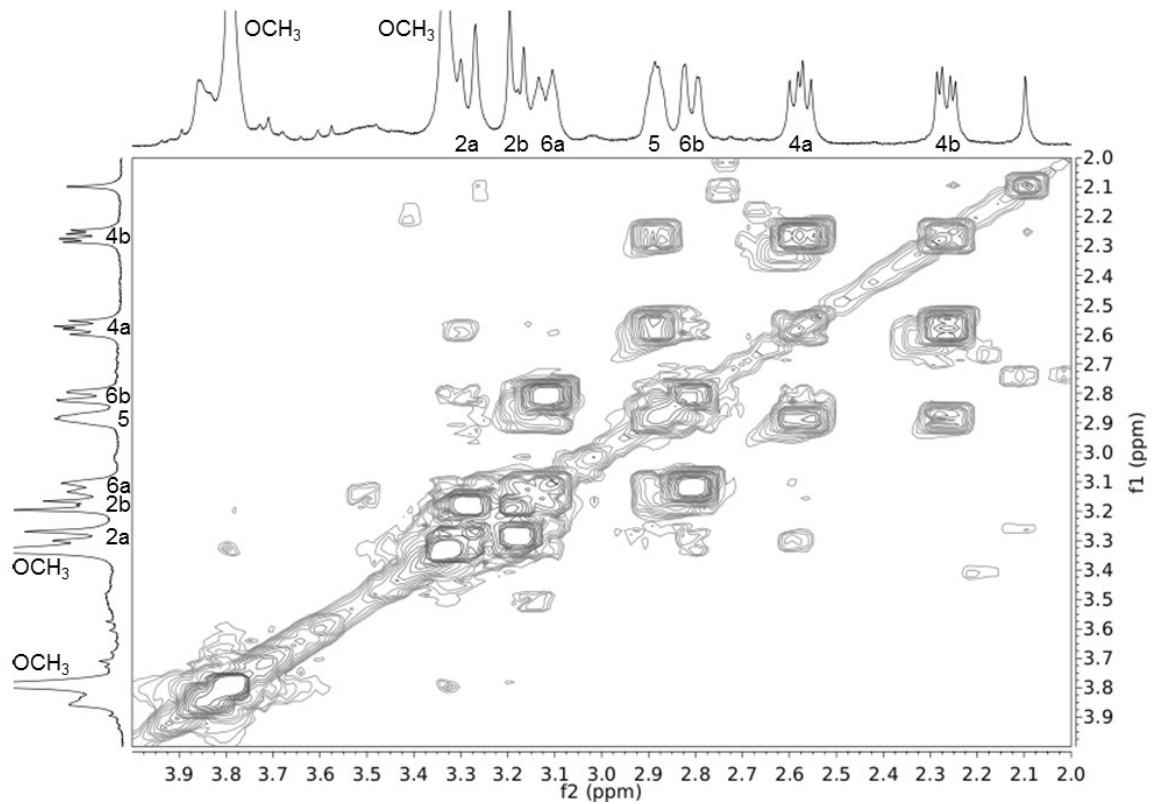


Figure 59: Partial ^1H - ^1H COSY spectrum of 5.9 in CD_2Cl_2 at $-20\text{ }^\circ\text{C}$. Resonances are labeled in accord with the numbering scheme depicted in Figure 57.

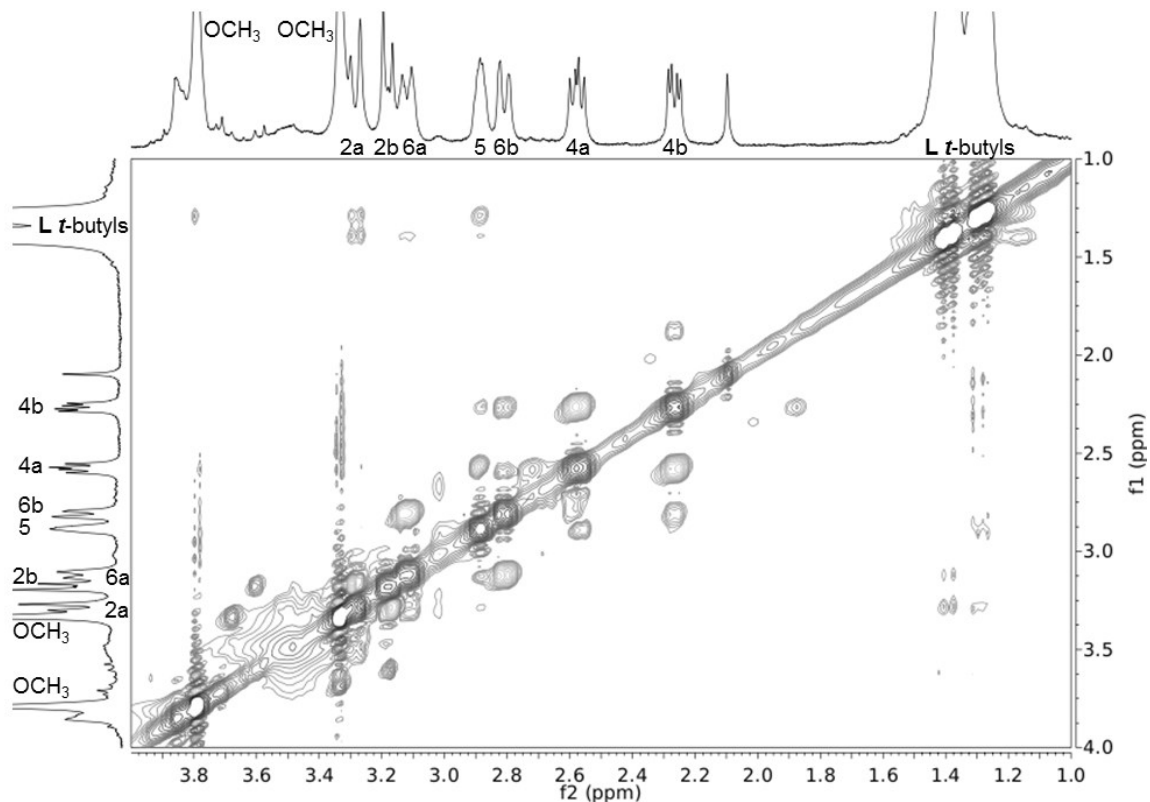
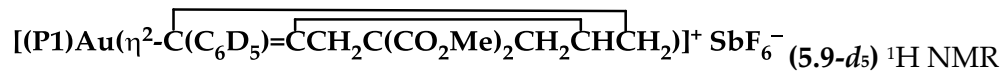


Figure 60: Partial ^1H - ^1H NOESY spectrum of 5.9 in CD_2Cl_2 at $-20\text{ }^\circ\text{C}$. Resonances are labeled in accord with the numbering scheme depicted in Figure 57.

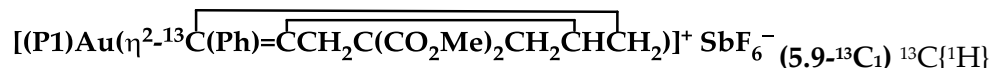
Isotopically labeled substrates $5.9\text{-}d_5$, $5.9\text{-}^{13}\text{C}_1$, $5.9\text{-}^{13}\text{C}_3$, $5.9\text{-}d_2$, *trans*- $5.9\text{-}d_1$, and *cis*- $5.9\text{-}d_1$ were synthesized from isotopically labeled enynes $5.5\text{-}d_5$, $5.5\text{-}^{13}\text{C}_1$, $5.5\text{-}^{13}\text{C}_3$, $5.5\text{-}d_2$, *trans*- $5.5\text{-}d_1$, and *cis*- $5.5\text{-}d_1$ respectively, employing procedures similar to that used to generate 5.9 from 5.5.



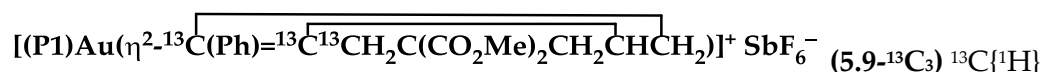
($-21\text{ }^\circ\text{C}$, aromatic resonances only): δ 7.88 – 7.83 (m, 1 H), 7.61 (dt, $J = 1.0, 7.4$ Hz, 1H), 7.59-7.55 (m, 2 H), 7.52 (tt, $J = 1.3, 7.4$ Hz, 1 H), 7.20 (td, $J = 1.3, 7.5$ Hz, 1 H), 7.17 – 7.13 (m, 1 H), 6.96 (td, $J = 1.3, 7.6$ Hz, 1 H), 6.92 (dt, $J = 0.8, 7.5$ Hz, 1 H). ^{13}C NMR ($-21\text{ }^\circ\text{C}$,

select resonances only): δ 132.8 (d, $J_{CP} = 2.5$ Hz, C_{ipso} , isotopic shift = -184 ppb).

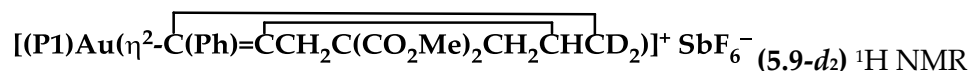
Resonances at 131.8 (C_{Ph}), 129.1 (C_{Ph}), and 127.2 (C_{Ph}) were not observed.



NMR (-40 °C, enriched resonance only): δ 140.2 (d, $J_{CP} = 8.1$ Hz, C7). $^{31}P\{^1H\}$ NMR (-40 °C): δ 65.3 (d, $J_{CP} = 10.0$ Hz).



NMR (-21 °C, enriched resonances only): δ 141.2 (dd, $J_{CP} = 8.9$, $J_{C7C1} = 33.5$ Hz, C7), 126.9 (ddd, $J_{CP} = 13.8$, $J_{C1C7} = 33.4$, $J_{C1C2} = 39.4$ Hz, C1), 37.7 (d, $J_{C2C1} = 39.4$ Hz, C2). $^{31}P\{^1H\}$ NMR (-21 °C): 65.9 (dd, $J_{CP} = 9.9$, 13.5 Hz).



(-21 °C, 500 MHz) analysis revealed ≥ 95 % deuteration at the H_{6b} position and ~15 % deuteration at the H_{6a} position, consistent with cyclization with retention of deuterium from the labeled enyne 5.5- d_2 (83% d_2 , 15% d_1). 1H NMR (-21 °C, 500 MHz, aliphatic region only): δ 3.78 (s, 3 H, OCH₃), 3.28 (s, 3 H, OCH₃), 3.25 (d, $J = 14.9$ Hz, 1 H, H_{2a}), 3.13 (d, $J = 14.9$ Hz, 1 H, H_{2b}), 2.83 (dd, $J = 5.6$, 8.9 Hz, 1 H, H_5), 2.51 (dd, $J = 9.0$, 14.1 Hz, 1 H, H_{4a}), 2.22 (dd, $J = 5.8$, 14.1 Hz, 1 H, H_{4b}), 1.35 (d, $J = 16.4$ Hz, 9 H), 1.24 (d, $J = 16.4$ Hz, 9 H). $^{13}C\{^1H\}$ NMR (-20 °C, 125 MHz, select resonances only): δ 127.2 (d, $J = 14.0$ Hz, C1, isotopic shift = 68 ppb), 41.0 (C5, isotopic shift = -56 ppb). The resonance corresponding to C6 was not observed.



5.5-*d*₁) ¹H NMR (-21 °C, 500 MHz) analysis revealed ≥ 95 % deuteration at the *H*_{6a} position, consistent with cyclization with retention of deuterium from the labeled enyne *trans*-**5.5-*d*₁** (97.4 % *d*₁). ¹H NMR (-21 °C, 500 MHz, aliphatic region only): δ 3.74 (s, 3 H, OCH₃), 3.28 (s, 3 H, OCH₃), 3.25 (d, *J* = 14.9 Hz, 1 H, *H*_{2a}), 3.12 (d, *J* = 14.9 Hz, 1 H, *H*_{2b}), 2.83 (dd, *J* = 5.9, 8.7 Hz, 1 H, *H*₅), 2.75 (d, *J* = 3.1 Hz *H*_{6b}), 2.51 (dd, *J* = 9.0, 14.1 Hz, 1 H, *H*_{4a}), 2.21 (dd, *J* = 5.8, 14.2 Hz, 1 H, *H*_{4b}), 1.35 (d, *J* = 16.4 Hz, 9 H), 1.24 (d, *J* = 16.4 Hz, 9 H).



***d*₁)** ¹H NMR (-21 °C, 500 MHz) analysis revealed ≥ 95 % deuteration at the *H*_{6b} position, consistent with cyclization with retention of deuterium from the labeled enyne *cis*-**5.5-*d*₁** (97.5 % *d*₁). ¹H NMR (-21 °C, 500 MHz, aliphatic region only): δ 3.74 (s, 3 H, OCH₃), 3.27 (s, 3 H, OCH₃), 3.25 (d, *J* = 14.4 Hz, 1 H, *H*_{2a}), 3.12 (d, *J* = 14.9 Hz, 1 H, *H*_{2b}), 3.05 (dt, *J* = 1.6, 4.3 Hz, *H*_{6a}), 2.83 (ddd, *J* = 4.0, 5.2, 9.4 Hz, 1 H, *H*₅), 2.50 (dd, *J* = 9.0, 14.1 Hz, 1 H, *H*_{4a}), 2.22 (dd, *J* = 5.8, 14.1 Hz, 1 H, *H*_{4b}), 1.35 (d, *J* = 16.4 Hz, 9 H), 1.24 (d, *J* = 16.4 Hz, 9 H).

5.4.2.4 Syntheses and characterization of free bicyclo-[3.2.0]-hept-1(7)ene **5.10** and isotopomers

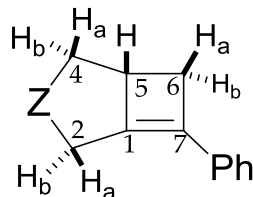


Figure 61: Partial atom numbering scheme for **5.6**.

Reaction of **5.9 with pyridine.** An NMR tube containing a CD_2Cl_2 (0.6 mL) solution of **5.9** (3.8×10^{-2} mmol) at -78°C was treated with pyridine (3 mg, $3 \mu\text{L}$, 4×10^{-2} mmol). The contents of the tube were thoroughly mixed by shaking the NMR tube at -78°C and the tube was then placed in the probe of an NMR spectrometer precooled at -20°C . Subsequent ^1H , ^{31}P and ^{13}C NMR analysis within 5 min revealed complete consumption of **5.9** to form 3,3-dimethoxycarbonyl-7-phenylbicyclo[3.2.0]hept-1(7)-ene (**5.10**) and $[\text{LAu}(\text{Py})]^+ \text{SbF}_6^-$ (**5.18**) as determined by the appearance of (1) a single resonance in the ^{31}P NMR spectrum at $\delta = 55$ corresponding to **5.18**, (2) a new alkene ^{13}C NMR resonances at $\delta 144.9$ and 138.9 which did not display J_{CP} , and (3) ^1H NMR resonances attributed to **5.10**.

For **5.10:** ^1H NMR (-20°C , 600 MHz): δ 7.33 (t, $J = 7.8$ Hz, 2 H), 7.26 – 7.18 (m, 3 H), 3.73 (s, 3 H), 3.64 (s, 3 H), 3.19 (tdd, $J = 2.9, 5.4, 16.5$ Hz, 1 H), 2.99 (br d, $J = 16.5$ Hz, 1 H), 2.85 (td, $J = 3.5, 12.5$ Hz, 1 H), 2.80 – 2.74 (m, 1 H), 2.58 (dd, $J = 6.7, 12.8$ Hz, 1 H), 2.32 (br d, $J = 12.7$ Hz, 1 H), 1.68 (dd, $J = 10.0, 12.8$ Hz, 1 H). $^{13}\text{C}\{^1\text{H}\}$ NMR (-20°C , 150.8 MHz):

δ 172.7, 171.5, 144.9 (C1), 138.9 (C7), 134.7 (C_{ipso}), 128.6 (C_{Ph}), 127.8 (C_{Ph}), 125.1 (C_{Ph}), 66.1, 53.1, 52.9, 39.1, 35.4, 30.7.

For 5.18. ^1H NMR (-20 °C, 600 MHz): δ 8.08 (t, $J = 7.8$ Hz, 1 H), 7.96 (d, $J = 4.8$ Hz, 2 H), 7.95 – 7.88 (m, 1 H), 7.66 (t, $J = 6.6$ Hz, 2 H), 7.60 (m, 2 H), 7.32 – 7.26 (m, 1 H), 7.23–7.20 (m, 4 H), 6.76 (m, 1 H), 1.45 (d, $J = 16.2$ Hz, 18 H). $^{13}\text{C}\{^1\text{H}\}$ NMR (-20 °C, 150.8 MHz): δ 150.5 (d, $J_{\text{CP}} = 20.8$ Hz), 148.8 (d, $J_{\text{CP}} = 12.1$ Hz), 143.3, 141.5 (d, $J_{\text{CP}} = 13.7$ Hz), 133.5 (d, $J_{\text{CP}} = 18.4$ Hz), 133.2, 131.3 (d, $J_{\text{CP}} = 31.7$ Hz), 129.7 (d, $J_{\text{CP}} = 23.5$ Hz), 128.5, 127.7, 127.5, 126.5 (d, $J_{\text{CP}} = 29.4$), 124.0 (d, $J_{\text{CP}} = 49.6$ Hz), 40.4 (d, $J_{\text{CP}} = 19.6$ Hz), 37.7 (d, $J_{\text{CP}} = 26.5$ Hz). $^{31}\text{P}\{^1\text{H}\}$ NMR (-20 °C): δ 55.5.

Reaction of 5.9 with tetrabutylammonium bromide. An NMR tube containing a CD_2Cl_2 (0.6 mL) solution of **5.9** (3.8×10^{-2} mmol) at -78 °C was treated with tetra-*n*-butylammonium bromide (16.1 mg, 5×10^{-2} mmol, 1.3 equiv). The contents of the tube were thoroughly mixed by shaking the tube at -78 °C and the tube was then placed in the probe of an NMR spectrometer maintained at -20 °C. ^1H NMR analysis within 5 min revealed complete consumption of **5.9** to form **5.10** and [(P1)AuBr]. Warming this solution at 25 °C led to decomposition of **5.10** with a half-life of ~9 h.

Isotopomers **5.10- d_5** and **5.10- $^{13}\text{C}_3$** were generated from the corresponding labeled gold cyclobutene complexes **5.9- d_5** and **5.9- $^{13}\text{C}_3$** using a procedure analogous to that used to generate **5.10** from **5.9**.

For 5.10-ds: $^{13}\text{C}\{^1\text{H}\}$ NMR (-21 °C, selected resonances): δ 135.0 (C_{ipso} , isotopic shift = -216 ppb). Resonances at 128.6 (C_{Ph}), 127.8 (C_{Ph}), 125.1 (C_{Ph}) were not observed.

For 5.10- $^{13}\text{C}_3$: $^{13}\text{C}\{^1\text{H}\}$ NMR (-20 °C, 150.8 MHz, labeled resonances only): δ 146.9 (dd, $J_{\text{C1C2}} = 42.0$, $J_{\text{C1C7}} = 61.5$ Hz, C1), 137.6 (d, $J_{\text{C1C7}} = 61.5$, C7), 34.7 (d, $J_{\text{CC}} = 42$ Hz, C2).

5.4.2.5 Syntheses and characterization of gold bicyclo-[3.2.0]-hept-6-ene 5.11 and isotopomers

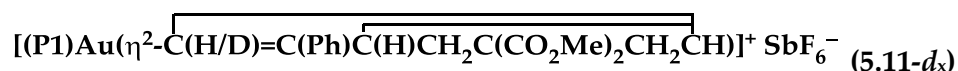
Generation of 5.11 from 5.6. A mixture of [(P1)AuCl] (24 mg, 4.5×10^{-2} mmol) and AgSbF₆ (16 mg, 4.7×10^{-2} mmol) in CD₂Cl₂ (0.3 mL) was combined in an NMR tube at -78 °C and maintained at this temperature for 10 min. To this suspension was added a solution of 5.6 (13 mg, 4.5×10^{-2} mmol) in CD₂Cl₂ (0.3 mL) at -78 °C and the contents of the tube were mixed thoroughly at -78 °C forming a flaky white precipitate that settled to the bottom of the tube upon standing at -78 °C for 10 min. Analysis at this time by ^1H , ^{31}P , and ^{13}C NMR at or below -21 °C revealed complete formation of 5.11.



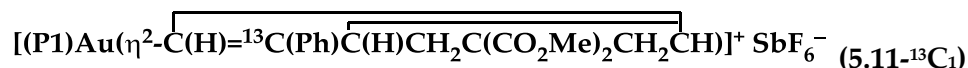
(-21 °C): δ 7.74 (t, $J = 7.5$ Hz, 1 H), 7.70 – 7.60 (m, 3 H), 7.60 – 7.45 (m, 3 H), 7.43 (m, 3 H), 7.32 – 7.08 (m, 4 H), 4.66 (d, $J = 4.8$ Hz, 1 H), 3.99 (dd, $J = 2.9, 7.9$ Hz, 1 H), 3.67 (s, 3 H), 3.21 (ddd, $J = 1.4, 3.0, 7.6$ Hz, 1 H), 3.15 (s, 3 H), 2.69 (d, $J = 14.0$ Hz, 1 H), 2.55 (d, $J = 14.4$ Hz, 1 H), 2.29 (dd, $J = 8.2, 14.4$ Hz, 1 H), 2.08 (dd, $J = 7.8, 14.0$ Hz, 1 H), 1.30 (d, $J = 16.6$ Hz, 9 H), 0.86 (d, $J = 16.6$ Hz, 9 H). $^{13}\text{C}\{^1\text{H}\}$ NMR (-40 °C): δ 171.1, 171.4, 154.7 (d, $J_{\text{CP}} = 4.4$ Hz), 147.8 (d, $J_{\text{CP}} = 13.6$ Hz), 143.4 (d, $J_{\text{CP}} = 7.4$ Hz), 133.8, 133.2 (d, $J_{\text{CP}} = 7.4$ Hz), 132.5,

131.6, 130.3, 129.8, 129.7, 129.5, 129.2, 128.0, 127.8, 123.9 (d, $J_{CP} = 46.9$ Hz), 112.0 ($J_{CP} = 15.9$ Hz), 59.6, 53.7, 53.5, 50.3, 48.2, 37.0 (d, $J_{CP} = 15.5$ Hz), 36.8 (d, $J_{CP} = 15.0$ Hz), 34.2, 33.1, 30.4 (d, $J_{CP} = 6.1$ Hz), 29.2 (d, $J_{CP} = 3.9$ Hz). $^{31}\text{P}\{^1\text{H}\}$ NMR (-21 °C): δ 65.0.

Conversion of 5.9 to 5.11 In a separate experiment, a solution of **5.9** (4.5×10^{-2} mmol) in CD_2Cl_2 (0.60 mL) was generated in an NMR tube as described in section 5.4.2.3. The solution was cooled at -78 °C and nitrobenzene (internal standard, 5.5 mg, 4.5×10^{-2} mmol) was added via syringe; the contents of the tube were mixed quickly and thoroughly and the tube was returned to -78 °C for 15 minutes to allow the solid precipitate to settle. The tube was then placed in the probe of an NMR spectrometer regulated at 25 °C and monitored periodically by ^1H NMR spectroscopy. The concentrations of **5.9** and **5.11** were determined from the integration of the methyl ester resonances at δ 3.81 and 3.73, respectively, relative to the resonance corresponding to the *ortho*-protons of the nitrobenzene internal standard (δ 8.23). ^1H NMR analysis after 39 min revealed 85% conversion to form **5.11** in $82 \pm 5\%$ yield, which corresponds to $96 \pm 5\%$ selectivity for the conversion of **5.9** to **5.11**.

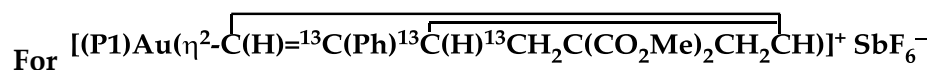


Isotopomer **5.11-d_x** was generated from **5.9-d_x** using a procedure analogous to that used to generate **5.11** from **5.9**. ^1H NMR analysis (-40 °C) was used to determine the deuterium incorporation at the H_5 and H_7 sites by integration of the residual proton resonances at δ 3.99 and 4.64, respectively.

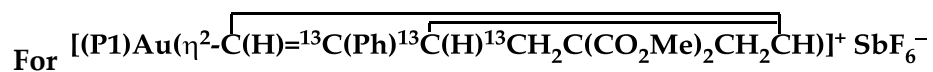


Isotopomer **5.11-¹³C₁** was generated from **5.9-¹³C₁** using a procedure analogous to that used to generate **5.11** from **5.9**. ¹³C{¹H} NMR (-40 °C select resonances only): δ 155.0 (d, *J*_{CP} = 4.3 Hz, C6), 112.2 (dd, *J*_{CP} = 15.6, *J*_{CC} = 34.8 Hz, C7). ³¹P{¹H} NMR (-40 °C): δ 64.9 (d, *J*_{CP} = 4.2 Hz).

Conversion of 5.9-¹³C₃ to 5.11-¹³C₃ Attempts to generate isotopomer **5.11-¹³C₃** from **5.9-¹³C₃** using a procedure analogous to that used to generate **5.11** from **5.9** resulted in formation of a 1:1 mix of isotopomers **5.11-4,5,6-¹³C₃** and **5.11-1,2,6-¹³C₃**.



(5.11-4,5,6-¹³C₃) ¹³C{¹H} NMR (-40 °C select resonances only): δ 155.0 (dd, *J* = 3.5, 30.9 Hz, C6), 50.5 (t, *J* = 31.8 Hz, C5), 33.1 (d, *J* = 33.0 Hz, C4).



(5.11-1,2,6-¹³C₃) ¹³C{¹H} NMR (-40 °C select resonances only): δ 155.0 (br s, C6), 48.2 (dd, *J* = 3.1, 33.3 Hz, C1), 34.1 (d, *J* = 33.1 Hz, C2).

5.4.2.6 Syntheses and characterization of free bicyclo-[3.2.0]-hept-6-ene isotopomers **5.6-¹³C₁** and **5.6-*d*_x**

3,3-Bis(methoxycarbonyl)-6-phenylbicyclo-[3.2.0]-hept-6-ene (5.6-¹³C₁)

Isotopomer **5.6-¹³C₁** was generated from the reaction of **5.11-¹³C₁** with pyridine at -78 °C and isolated as a white solid (9.8 mg, 75 %) by column chromatography at room temperature (SiO₂; hexanes–EtOAc = 19:1). ¹³C{¹H} NMR (25 °C, CDCl₃): δ 172.7, 172.1,

146.8 (C6) 133.4 (d, $^2J_{CC} = 56$ Hz, C_{ipso}), 129.9 (d, $^2J_{C6C7} = 63$ Hz, C7), 128.5, 128.4, 127.9, 124.7 (d, $^3J_{CC} = 2.9$ Hz), 61.0, 53.0, 51.9, 45.9 (d, $^2J_{C5C6} = 33$ Hz, C5), 43.6, 35.5, 34.2.

5,7-*d*_x-3,3-Bis(methoxycarbonyl)-6-phenylbicyclo-[3.2.0]-hept-6-ene (5.6-*d*_x)

Isotopomer **5.6-*d*_x** was generated from the reaction of **5.11-*d*_x** with pyridine at -78 °C and isolated as a white solid (7.1 mg, 54 %) by column chromatography at room temperature (SiO₂; hexanes–EtOAc = 19:1). ¹H NMR (25 °C, CDCl₃): δ 7.32 – 7.22 (m, 5 H), 6.08 (s, ~0.1 H), 3.69 (s, 3 H), 3.65-3.61 (m, ~0.75 H), 3.33 (dd, $J = 3, 7$ Hz, 1 H), 3.22 (s, 3 H), 2.81 (d, $J = 13.5$ Hz, 1 H), 2.69 (d, $J = 13.5$ Hz, 1 H), 2.06 – 1.95 (m, 2 H).

5.4.3 Determination of equilibrium binding affinities of 5.10 and 5.6 for [(P1)Au]⁺

Binding affinity of 5.10 relative to NCAR_F. 3,5-Bistrifluoromethylbenzotrile (NCAR_F; 11 mg, 4.6×10^{-2} mmol) was added via syringe to an NMR tube containing a solution of **5.9** (4.5×10^{-2} mmol) in CD₂Cl₂ (0.6 mL) at -78 °C. The tube was placed into the probe of an NMR spectrometer pre-cooled at -62 °C and was analyzed by ¹H NMR spectroscopy. The relative concentrations of **5.9**, **5.10**, **5.12**, and NCAR_F were determined by integrating the resonances corresponding to the methyl ester groups of **5.9** (δ 3.70) and **5.10** (δ 3.62) and the aromatic protons of bound (δ 8.38) and free NCAR_F (δ 8.26-8.14). These values were used to calculate an equilibrium constant for the displacement of NCAR_F from **5.12** with **5.10** of $K_{eq} = \frac{[5.9][NCAR_F]}{[5.10][5.12]} = 4.4 \pm 0.4$. The error value refers to the propagated error assuming an error in each NMR integration of ± 5%.

Binding affinity of 5.6 relative to NCAR_F. 3,5-Bistrifluoromethylbenzonitrile (NCAR_F; 11 mg, 4.6×10^{-2} mmol) was added via syringe to an NMR tube containing a solution of **5.11** (3.7×10^{-2} mmol) in CD₂Cl₂ (0.6 mL) at -78 °C. The tube was placed into the probe of an NMR spectrometer pre-cooled at -62 °C and was analyzed by ¹H NMR spectroscopy. The relative concentrations of **5.11**, **5.6**, **5.12**, and NCAR_F were determined by integrating the resonances corresponding to the vinyl protons of **5.11** (δ 4.58) and **5.6** (δ 6.06) and the aromatic protons of bound (δ 8.38) and free NCAR_F (δ 8.26-8.14). These values were used to calculate an equilibrium constant for the displacement of NCAR_F from **5.12** with **5.6** of $K_{eq} = \frac{[\mathbf{5.11}][\text{NCAR}_F]}{[\mathbf{5.6}][\mathbf{5.12}]} = 0.71 \pm 0.007$. The error value refers to the propagated error assuming an error in each NMR integration of $\pm 5\%$.

5.4.4 Kinetics of the conversion of 5.9 and isotopomers to 5.11 and isotopomers

5.4.4.1 Kinetic analyses of the conversions of 5.9 and isotopomers to 5.11 without added acid

Conversion of 5.9 to 5.11 A solution of **5.9** (4.5×10^{-2} mmol) in CD₂Cl₂ (0.60 mL) was generated in an NMR tube as described in section 5.4.2.3. The solution was cooled at -78 °C and nitrobenzene (internal standard, 5.5 mg, 4.5×10^{-2} mmol) was added via syringe; the contents of the tube were mixed quickly and thoroughly and the tube was returned to -78 °C for 15 minutes to allow the solid precipitate to settle. The tube was then placed in the probe of an NMR spectrometer regulated at 25 °C and monitored periodically by ¹H NMR spectroscopy. The concentrations of **5.9** and **5.11** were

determined from the integration of the methyl ester resonances at δ 3.81 and 3.73, respectively, relative to the resonance corresponding to the *ortho*-protons of the nitrobenzene internal standard (δ 8.23). A plot of $\ln[5.9]$ versus time was linear to ~ 3 half-lives and gave a first order rate constant for the disappearance of **5.9** of $k_{\text{obs}} = (7.41 \pm 0.05) \times 10^{-4} \text{ s}^{-1}$ (Figure 53).

The kinetics of the conversions of **5.9-*d*₂**, *trans*-**5.9-*d*₁**, and *cis*-**5.9-*d*₁** to **5.9-*d*_x** were analyzed using a similar procedure.

Conversion of 5.9-*d*₂ to 5.11-*d*_x A plot of $\ln[5.9-*d*₂]$ versus time was linear to ~ 3 half-lives and gave a first order rate constant for the disappearance of **5.9-*d*₂** of $k_{\text{obs}} = (1.92 \pm 0.03) \times 10^{-4} \text{ s}^{-1}$ (Figure 62).

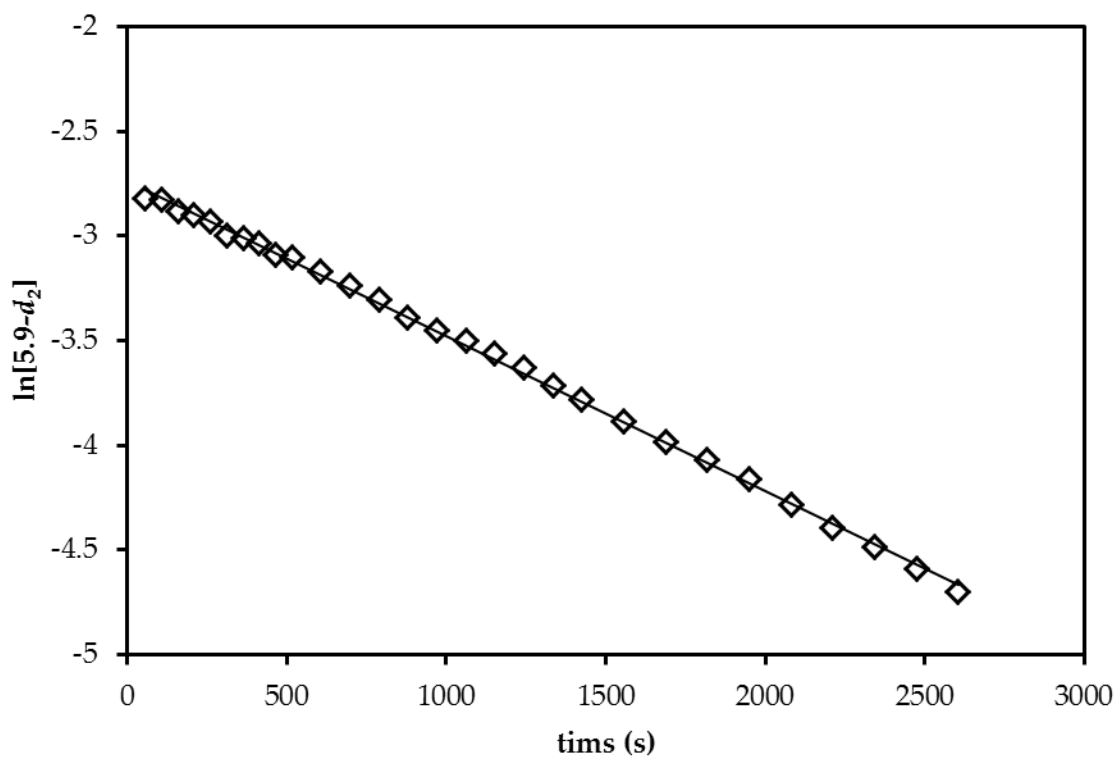


Figure 62: First order plot of the conversion of 5.9- d_2 to 5.11- d_x ($[5.9-d_2]_0 = 0.076$ M) in CD_2Cl_2 at 25 °C.

Conversion of *trans*-5.9- d_1 to 5.11- d_x A plot of $\ln[trans\text{-}5.9\text{-}d_1]$ versus time was linear to ~ 3 half-lives and gave a first order rate constant for the disappearance of *trans*-5.9- d_1 of $k_{obs} = (6.17 \pm 0.08) \times 10^{-4} \text{ s}^{-1}$ (Figure 63).

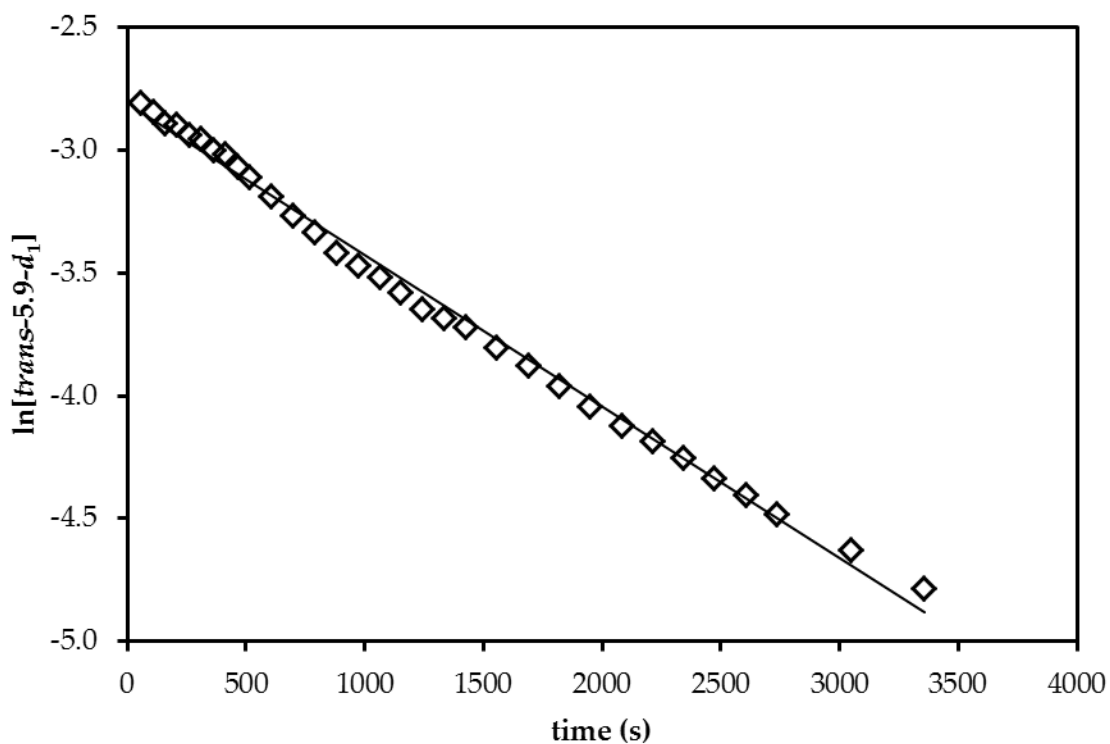


Figure 63: First order plot of the conversion of *trans*-5.9-*d*₁ to 5.11-*d*_x ($[trans-5.9-d_1]_0 = 0.073$ M) in CD₂Cl₂ at 25 °C.

Conversion of *cis*-5.9-*d*₁ to 5.11-*d*_x A plot of $\ln[cis-5.9-d_1]$ versus time was linear to ~3 half-lives and gave a first order rate constant for the disappearance of *cis*-5.9-*d*₁ of $k_{obs} = (5.22 \pm 0.03) \times 10^{-4} \text{ s}^{-1}$ (Figure 64).

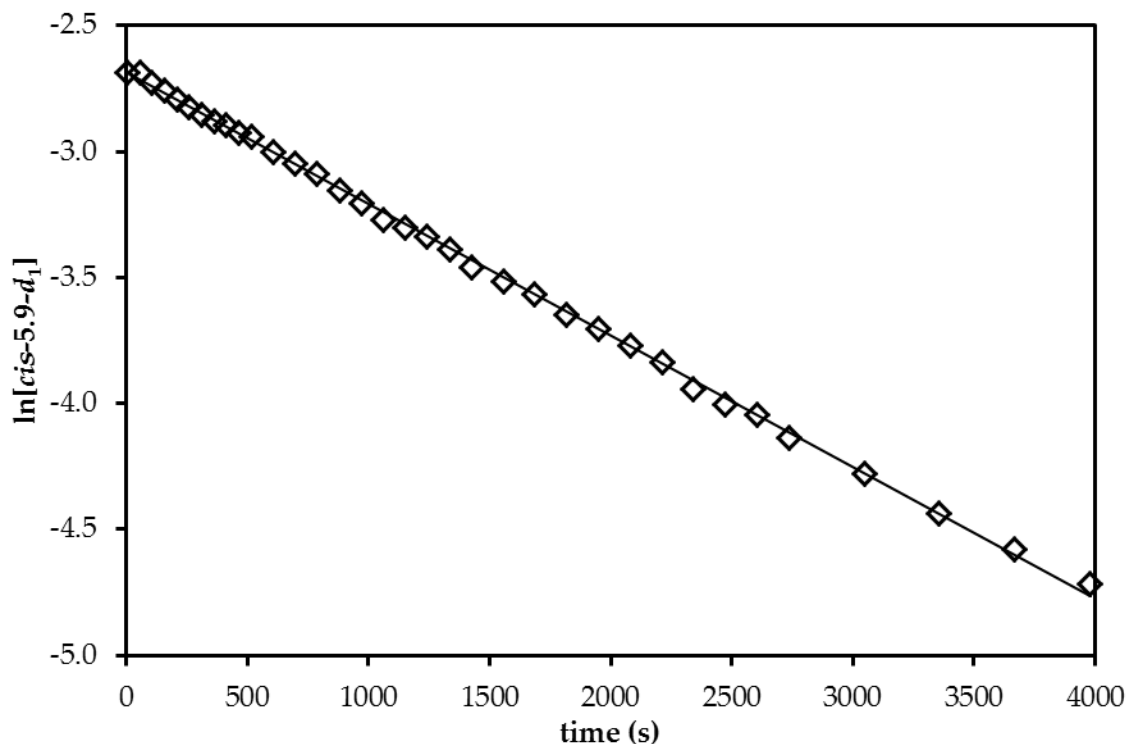


Figure 64: First order plot of the conversion of *cis*-5.9-*d*₁ to 5.11-*d*_x ($[cis-5.9-d_1]_0 = 0.076$ M) in CD₂Cl₂ at 25 °C.

5.4.4.2 Kinetic analyses of the conversions of 5.9 and isotopomers to 5.11 with added acid

Conversion of 5.9 to 5.11 A solution of 5.9 (4.5×10^{-2} mmol) in CD₂Cl₂ (0.60 mL) was generated in an NMR tube as described in section 5.4.2.3. The solution was cooled at -78 °C and nitrobenzene (internal standard, 5.5 mg, 4.5×10^{-2} mmol) and HOTf (1.0 μL, 1.1×10^{-2} mmol) was added via syringe; the contents of the tube were mixed quickly and thoroughly and the tube was placed in the probe of an NMR spectrometer regulated at -21 °C and monitored periodically by ¹H NMR spectroscopy. The concentrations of 5.9 and 5.11 were determined from the integration of the methyl ester resonances at δ 3.81

and 3.73, respectively, relative to the resonance corresponding to the *ortho*-protons of the nitrobenzene internal standard (δ 8.23). A plot of $\ln[5.9]$ versus time was linear to ~ 3 half-lives and gave a first order rate constant for the disappearance of **5.9** of $k_{\text{obs}} = (6.98 \pm 0.05) \times 10^{-4} \text{ s}^{-1}$ (Figure 65).

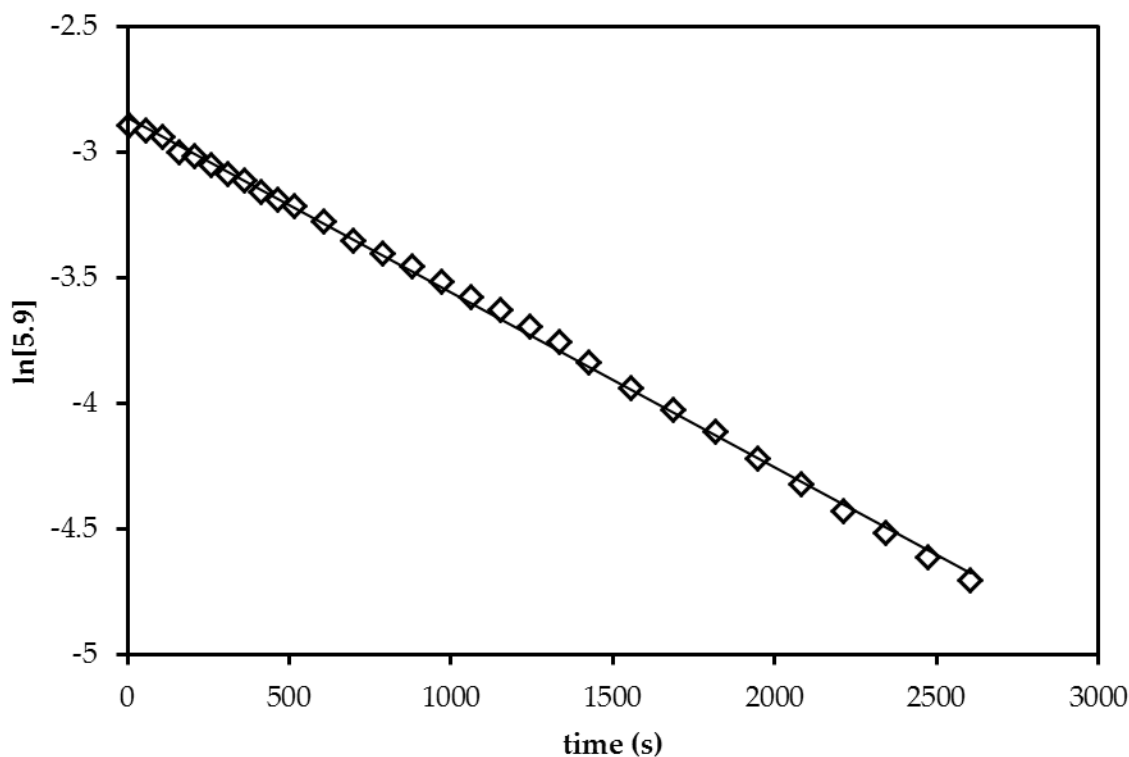


Figure 65: First order plot of the conversion of 5.9 to 5.11 ($[5.9]_0 = 0.076 \text{ M}$) with HOTf ($[\text{HOTf}] = 0.019 \text{ M}$) in CD_2Cl_2 at $-21 \text{ }^\circ\text{C}$.

The kinetics of the conversions of **5.9- d_2** , *trans*-**5.9- d_1** , and *cis*-**5.9- d_1** to **5.11- d_x** in the presence of HOTf were analyzed using a similar procedure.

Conversion of 5.9- d_2 to 5.11- d_x A plot of $\ln[5.9-d_2]$ versus time was linear to ~ 3 half-lives and gave a first order rate constant for the disappearance of **5.9- d_2** of $k_{\text{obs}} = (1.39 \pm 0.03) \times 10^{-4} \text{ s}^{-1}$ (Figure 66).

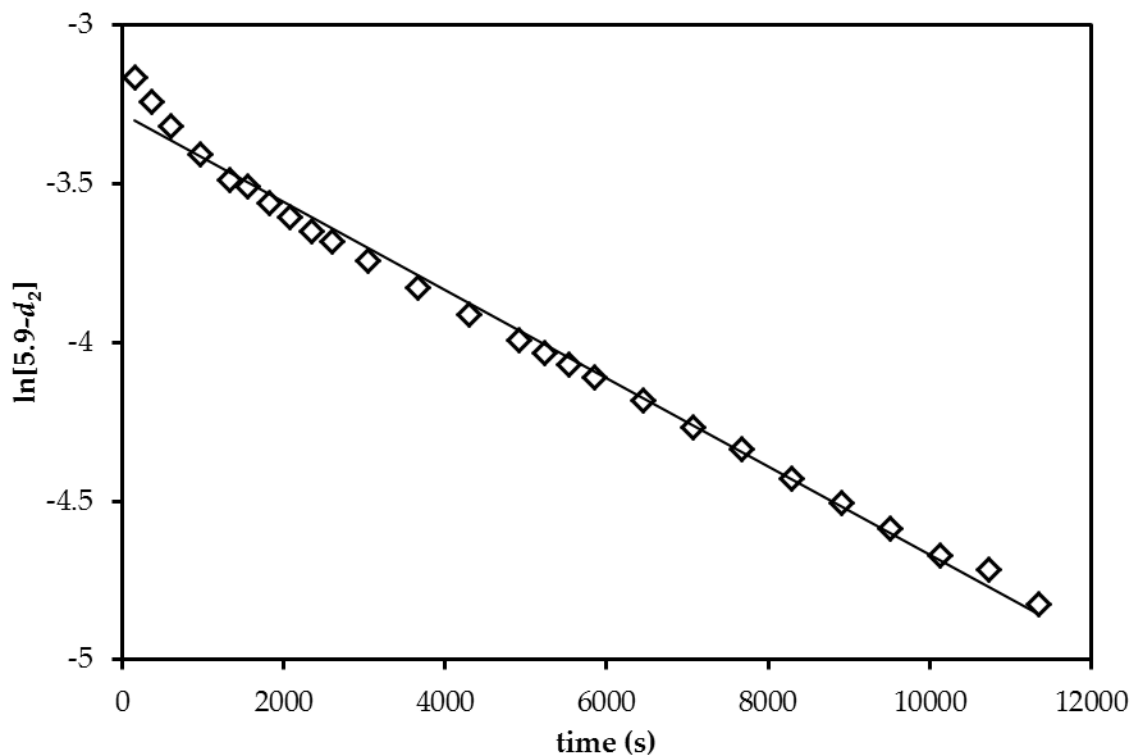


Figure 66: First order plot of the conversion of 5.9- d_2 to 5.11- d_x ($[5.9-d_2]_0 = 0.076$ M) with HOTf ($[HOTf] = 0.019$ M) in CD_2Cl_2 at -21 °C.

Conversion of *trans*-5.9- d_1 to 5.11- d_x A plot of $\ln[trans-5.9-d_1]$ versus time was linear to ~ 3 half-lives and gave a first order rate constant for the disappearance of *trans*-5.9- d_1 of $k_{obs} = (3.34 \pm 0.02) \times 10^{-4} \text{ s}^{-1}$ (Figure 67).

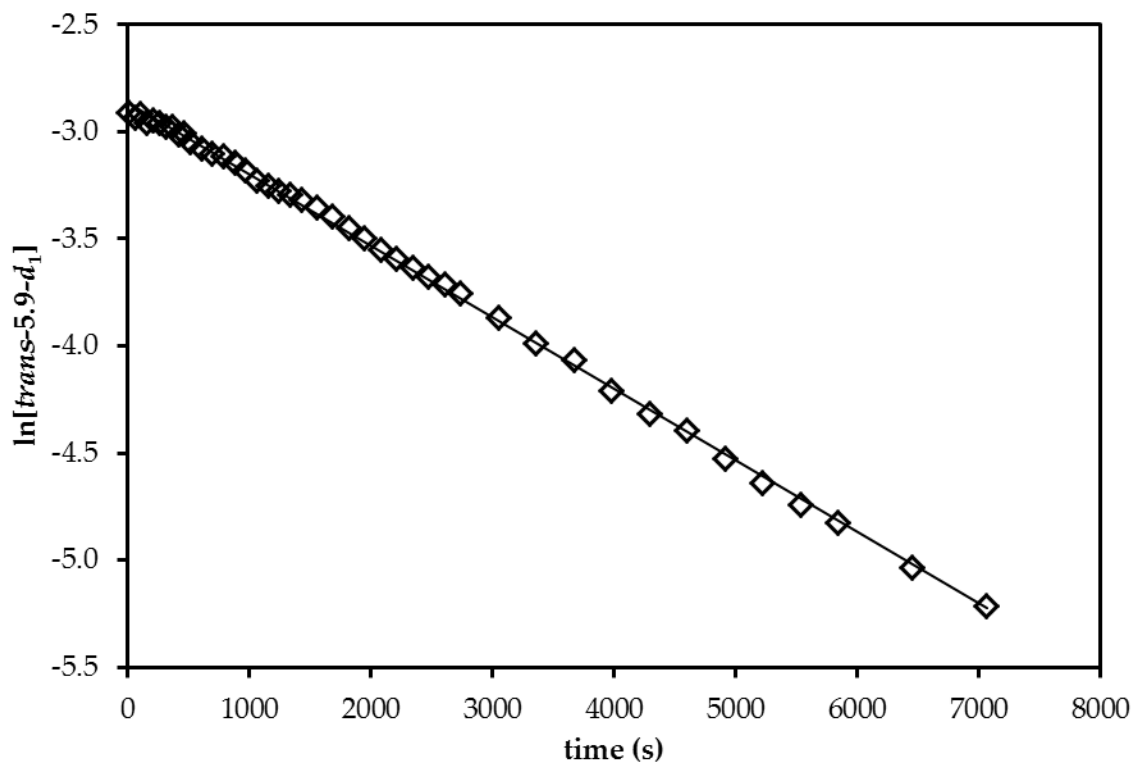


Figure 67: First order plot of the conversion of *trans*-5.9-*d*₁ to 5.11-*d*_x ($[trans-5.9-d_1]_0 = 0.070$ M) with HOTf ($[HOTf] = 0.019$ M) in CD₂Cl₂ at -21 °C.

Conversion of *cis*-5.9-*d*₁ to 5.11-*d*_x A plot of $\ln[cis-5.9-d_1]$ versus time was linear to ~3 half-lives and gave a first order rate constant for the disappearance of *cis*-5.9-*d*₁ of $k_{obs} = (2.51 \pm 0.01) \times 10^{-4} \text{ s}^{-1}$ (Figure 68).

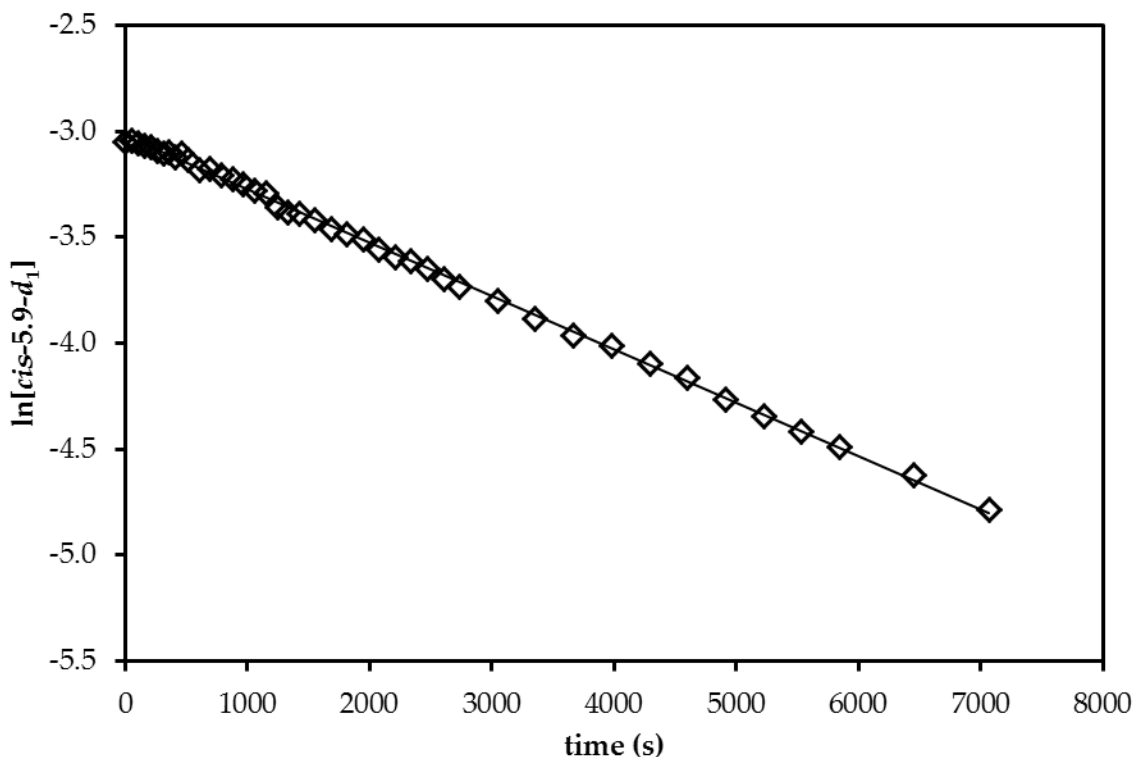


Figure 68: First order plot of the conversion of *cis*-5.9-*d*₁ to 5.11-*d*_x ($[cis-5.9-d_1]_0 = 0.076$ M) with HOTf ($[HOTf] = 0.019$ M) in CD₂Cl₂ at 25 °C.

5.4.5 “Gold-free” and silver-free stoichiometric transformations

5.4.5.1 Reaction of 5.10 with HOTf

An NMR tube containing a solution of **5.9** (3.7×10^{-2} mmol) and nitrobenzene (internal standard, 5.5 mg, 4.5×10^{-2} mmol) in CD₂Cl₂ (0.60 mL), generated as described in section 5.4.2.3, was treated with a solution of tetra-*n*-butylammonium bromide (4.5×10^{-2} mmol) in CD₂Cl₂ (80 μL) at -78 °C to generate **5.10** *in situ*. The contents of the tube were thoroughly and quickly mixed, and the tube was returned to -78 °C for 5 min. HOTf (1 μL, 1.1×10^{-2} mmol) was added to the tube via syringe at -78 °C and the contents were quickly mixed and allowed to sit at -78 °C for 5 min. The tube was placed

in the probe of an NMR spectrometer precooled at -21 °C. Subsequent ¹H NMR analysis within 5 min revealed complete consumption of **5.10** to form **5.6** in 30 % yield as determined by integration of the H₇ proton resonance of **5.6** (δ 6.06) relative to the *ortho*-proton resonance of the nitrobenzene (δ 8.23). In addition, much decomposition and/or polymerization was observed.

5.4.5.2 Generation and isomerization of **5.2-4,5,6-¹³C₃**

A solution of [(P1)Au(NCAr_F)] (**5.12**)(35 mg, 3.6 × 10⁻² mmol) in CD₂Cl₂ (0.3 mL) was cooled to -78 °C and treated with a solution of **5.5-¹³C₃** (10 mg, 3.6 × 10⁻² mmol) in CD₂Cl₂ (0.3 mL). The NMR tube was shaken at -78 °C to mix the contents, maintained at -21 °C for 105 min., then warmed to 25 °C and allowed to react at 55 °C. ¹H and ³¹P NMR analysis (-65 °C) revealed a mixture of **5.9**, **5.10**, **5.12**, and NCAr_F which did not react further upon maintaining the tube at 25 °C for an additional 150 min. The NMR tube was cooled to -78 °C and HOTf (1 μL, 1.1 × 10⁻² mmol) was added via syringe. The contents of the tube were mixed quickly and placed in the probe of an NMR spectrometer precooled to -55 °C. Subsequent ¹H, ³¹P, and ¹³C analysis revealed within 5 min of HOTf addition revealed complete consumption of **5.9-¹³C₃**/**5.10-¹³C₃** to give a mixture of **5.11-¹³C₃**/**5.6-¹³C₃** and decomposition/polymerization products. The reaction mixture was cooled to -78 °C, treated with pyridine (6 μL), warmed to 25 °C and filtered through SiO₂. **5.6-4,5,6-¹³C₃** was isolated as a white solid (1.6 mg, 15 %) by column chromatography (SiO₂; hexanes–EtOAc = 9:1) and determined to be a single isotopomer

by ^{13}C NMR. $^{13}\text{C}\{^1\text{H}\}$ NMR (25 °C, CDCl_3 , select resonance only): δ 146.7 (dd, $J = 2.6, 33.3$ Hz, C6), 45.8 (t, $J = 34.3$ Hz, C5), 34.1 (dd, $J = 3.0, 34.8$ Hz, C4).

A solution of **5.6-4,5,6- $^{13}\text{C}_3$** (1.6 mg, 5.5×10^{-3} mmol) in CD_2Cl_2 (0.60 mL) was added to AgSbF_6 (1.9 mg, 5.5×10^{-3} mmol) in an NMR tube at 25 °C. Subsequent ^{13}C NMR analysis of the mixture within 10 minutes revealed isomerization of **5.6-4,5,6- $^{13}\text{C}_3$** to a ~1:1 mix of **5.6-4,5,6- $^{13}\text{C}_3$** and **5.6-1,2,6- $^{13}\text{C}_3$** .

5.4.6 Catalytic Reactions

5.4.6.1 Gold-catalyzed enyne cycloisomerization

***In situ* analysis of the gold-catalyzed conversion of 5.5 to 5.6** A suspension of [(P1)AuCl] (2.7 mg, 5.1×10^{-3} mmol) and AgSbF_6 (1.7 mg, 5.1×10^{-3} mmol) in CD_2Cl_2 (0.5 mL) was mixed at -78 °C for 10 min in an NMR tube. The resulting suspension was treated with a solution of **5.5** (28.6 mg, 0.100 mmol) and nitrobenzene (4.6 μL , 4.5×10^{-2} mmol, internal standard) at -78 °C and mixed thoroughly by shaking the NMR tube at -78 °C. The NMR tube was maintained at room temperature and monitored periodically by ^1H NMR and ^{31}P spectroscopy. The catalyst resting state was assigned as **5.9** based on the presence of a single resonance at δ 65.4 in the ^{31}P spectrum of the reaction mixture. The concentrations of reaction components were calculated from integration of the resonances corresponding to H_2 of **5.5** (δ 5.72), one H_4 of **5.10** (δ 1.70, dd), and H_7 of **5.6** (δ 6.08) relative to the *ortho*-protons of nitrobenzene (δ 8.22) in the ^1H NMR spectrum of the reaction mixture. Initial analysis within one minute of mixing revealed ~20 %

conversion of **5.5** to **5.10**, which was slowly depleted along with **5.5** over ~90 min by competing conversion to **5.6** and decomposition (Figure 54).

General procedure for benchtop catalytic reactions A solution of **5.5** (57.3 mg, 0.200 mmol) in CH₂Cl₂ (0.5 mL) was added to a stirred suspension of catalyst mixture in CH₂Cl₂ (0.5 mL) at room temperature. The reaction was stirred at room temperature until all **5.1** was consumed, as determined by TLC, or for 18 h. **5.6** was isolated by column chromatography of the crude reaction mixture (SiO₂, 19:1 hexanes:EtOAc to 9:1 hexanes:EtOAc).

For [(P1)AuCl]/AgSbF₆ Enyne **5.5** underwent cycloisomerization in the presence of [(P1)AuCl] (2.1 mg, 4.0 × 10⁻³ mmol) and AgSbF₆ (2.1 mg, 4.0 × 10⁻³ mmol) according to the general procedure in 100 min to give **5.6** (3.3 mg, 5.8 % yield) and polymerized/decomposed material.

For [(P1)AuCl]/AgSbF₆/HOTf Enyne **5.5** underwent cycloisomerization in the presence of [(P1)AuCl] (2.1 mg, 4.0 × 10⁻³ mmol), AgSbF₆ (2.1 mg, 4.0 × 10⁻³ mmol), and HOTf (0.4 μL, 4.0 × 10⁻³ mmol) according to the general procedure in 100 min to give **5.6** (14.3 mg, 25.0 % yield) and polymerized/decomposed material.

For HOTf Enyne **5.5** did not undergo cycloisomerization in the presence of HOTf (0.4 μL, 4.0 × 10⁻³ mmol) according to the general procedure after 18 h. ¹H NMR analysis of the crude reaction mixture revealed ~5 % decomposition of **5.5**.

For AgSbF_6 Enyne **5.5** did not undergo cycloisomerization in the presence of AgSbF_6 (2.1 mg, 4.0×10^{-3} mmol) according to the general procedure after 18 h. ^1H NMR analysis of the crude reaction no reaction or decomposition of **5.5**.

5.4.6.2 Gold catalyzed tandem cyclization/hydroarylation of **5.5** and 1,3-dimethoxybenzene

A solution of **5.5** (250 mg, 0.870 mmol) and 1,3-dimethoxybenzene (241 mg, 1.70 mmol) in CH_2Cl_2 (2.5 mL) was added to a stirred suspension of $[(\text{P}1)\text{AuCl}]$ (9.3 mg, 1.7×10^{-2} mmol) and AgSbF_6 (6.0 mg, 1.7×10^{-2} mmol) in CH_2Cl_2 (2.5 mL) at room temperature and allowed to stir 5 h. Chromatography of the crude reaction mixture (SiO_2 , 19:1 hexanes:EtOAc to 9:1 hexanes to EtOAc) afforded **5.13** (124 mg, 33.0 %) as a white solid. ^1H NMR (CDCl_3 , 25 °C) δ 7.49 (d, $J = 8.7$ Hz, 1 H), 7.21 – 7.15 (m, 2 H), 7.14 – 7.10 (m, 2 H), 7.08 -7.01 (m, 1 H), 6.47 (dd, $J = 2.5, 8.5$ Hz, 1 H), 6.33 (d, $J = 2.5$ Hz, 1 H), 3.73 (s, 3 H), 3.67 (s, 3 H), 3.58 (m, 4 H), 3.55 (s, 3 H), 2.89 – 2.82 (m, 1 H), 2.68 – 2.58 (m, 2 H), 2.49 (dd, $J = 7.7, 13.8$ Hz, 1 H), 2.45 (dd, $J = 8.2, 13.7$), 2.38 (m, 2 H), 2.09 (dd, $J = 3.5, 13.8$ Hz, 1 H), 1.95 (dd, $J = 9.1, 13.7$ Hz, 1 H). $^{13}\text{C}\{^1\text{H}\}$ NMR (CDCl_3 , 25 °C): δ 173.0, 172.3, 159.5, 158.8, 146.9, 129.1, 127.5, 127.3, 126.5, 124.9, 103.5, 99.9, 64.3, 55.4, 55.0, 55.8, 52.6, 47.8, 47.0, 41.1, 38.7, 38.1, 33.3.

6. Synthesis and Characterization of a Gold Cyclopropyl Carbene Compound

6.1 Introduction

6.1.1 Questions on the electronic structure of gold carbenes

Nonstabilized gold carbenes are highly implicated as key intermediates in the gold-catalyzed cycloaddition/cycloisomerization of enynes and π -systems, olefin cyclopropanation, cyclopropene ring opening, and a variety of other transformations. Despite the great interest in studying the mechanism of gold-catalyzed enyne cycloisomerizations, no direct evidence for the intermediacy or existence of gold cyclopropyl carbenes has been reported. While the gold-carbene complex **6.1** has been detected in the gas-phase (Scheme 42),¹⁹⁴ reports of nonstabilized gold carbenes observed in solution or the solid-state are absent. As such, the electronic structure of these complexes is highly debated, with proposed structures ranging from a “true” gold carbene (**6.I**) to a stabilized carbocation (**6.II**) (Figure 70).^{17, 195-196} In the absence of experimental data, information regarding the structure and binding in gold carbene complexes is derived from computational studies,¹⁹⁷ trapping experiments,¹⁹⁸ and structural analyses of stabilized gold carbenes and carbenoids.¹⁹⁹⁻²⁰⁰

Scheme 42: Gas phase synthesis of gold carbene complex 6.1 employing collision-induced dissociation (CID). Mes = 2,4,6-trimethylphenyl

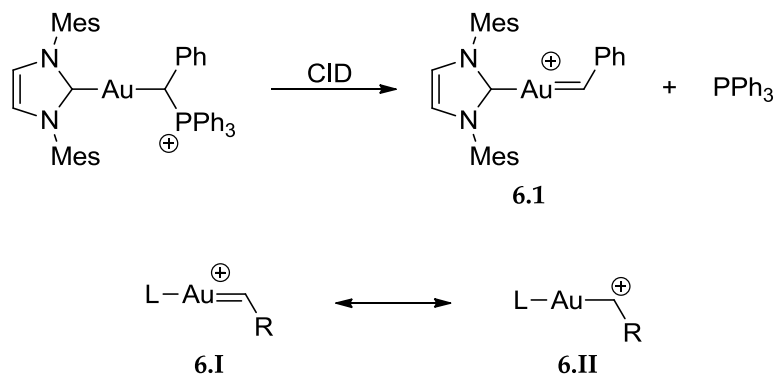


Figure 69: Possible canonical forms for the structure of [(L)Au–C(H)R]⁺, including the carbene form (6.I) and the stabilized carbocation form (6.II).

6.1.2 Synthesis and structure of stabilized gold carbenes

Fischer-type carbenes are stabilized by donation of electron density from an α -heteroatom to the carbene carbon. Despite their enhanced stability relative to the cyclopropyl carbenes implicated in enyne cycloisomerizations, only a few examples of gold Fischer carbenes are known and no cyclopropyl carbenes have been reported. The neutral chlorogold carbene **6.2** has been isolated and structurally characterized, although the structure more resembles the α -aurated imine ion (**6.2'**) (Figure 71). The Au–C₁ bond length (2.02(3) Å) is typical of that of a Au–C σ -bond, while the C₁–N (1.262 Å) bond is shorter than that of a typical imine.²⁰¹⁻²⁰²

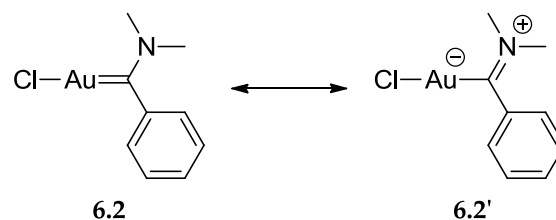
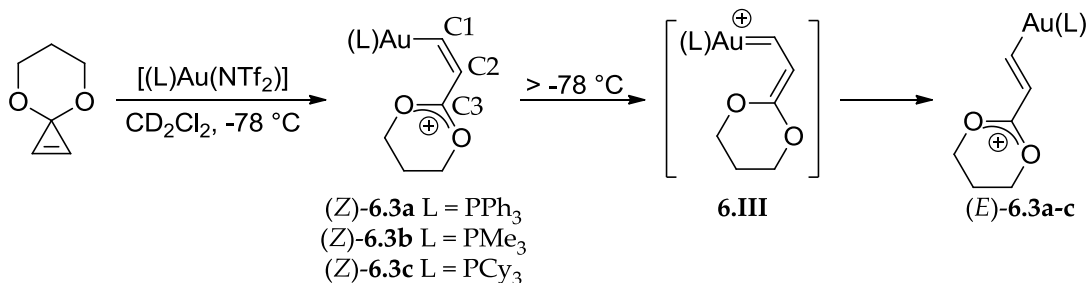


Figure 70: Structurally characterized neutral Fischer-type gold carbene.²⁰¹

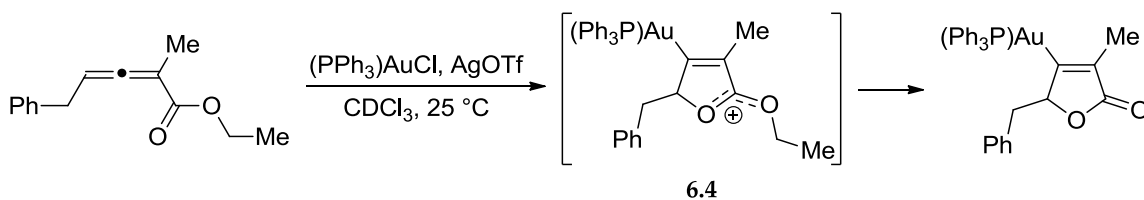
Although the anionic chloride ligand is predicted to stabilize gold carbene complexes,¹⁹⁷ most catalytic methodology of interest employs gold catalysts bearing NHC or phosphine ligands. In an effort to understand the structure of the latter class of complexes, Fürstner and coworkers synthesized a family of cationic, heteroatom-stabilized gold carbenoids **6.3a-c** via the [(L)Au(NTf₂)] mediated ring opening of 4,8-dioxaspiro[2.5]oct-1-ene (Scheme 43). Spectroscopic analysis revealed strong contribution of an oxocarbenium ion structure with a *cis*-arrangement about C1–C2 bond ((*Z*)-**6.3**). This characterization was based on the deshielding of both the C1 ($\delta = 212.9 - 219.3$) and C3 ($\delta = 172.3 - 173.0$) carbon resonances in the ¹³C NMR of **6.3**, suggesting accumulation of positive charge at these sites, and the presence of a single set of sharp resonances for the two –O–CH₂– groups, which equilibrate by rotation about the C2–C3 bond. Complexes (*Z*)-**6.3** isomerized in solution above -78 °C to give mixtures of (*Z*)- and (*E*)-**6.3**, presumably through gold carbene **6.III** or the corresponding gold-coordinated carbocation.

Scheme 43: Gold-mediated rearrangement of dioxaspiro[2.5]oct-1-ene to form stabilized gold carbenoids 6.3.



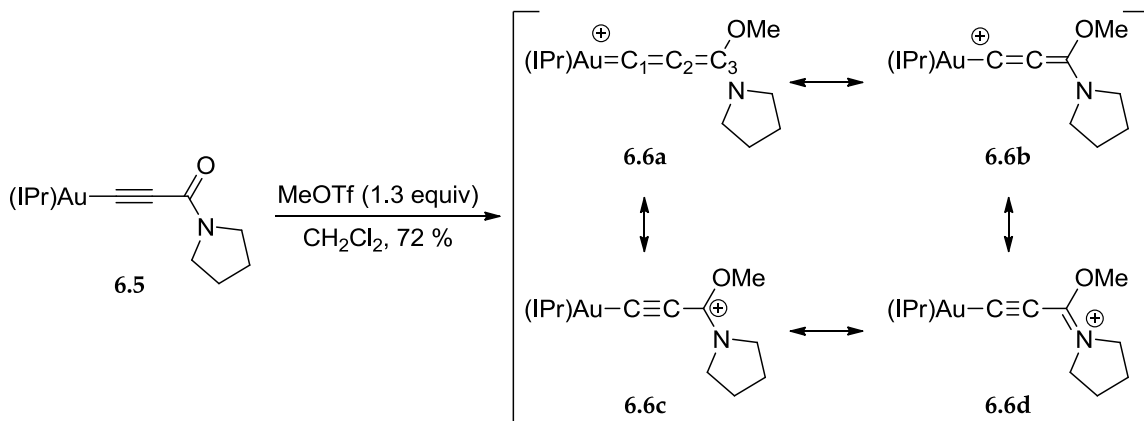
Although information regarding the nature of the stabilization of positive charge by gold can be gained from analyses of complexes **6.3**, the relevance of these analyses to the reactive gold-carbene species though to intermediate cycloisomerizations and cyclopropanation is questioned. In a combined experimental/DFT study, Toste, *et al* note that 4,8-dioxaspiro[2.5]oct-1-ene does not undergo cyclopropanation with *trans*-stilbene in the presence of LAu⁺, suggesting that the Au-C binding mode observed in these complexes is not reflective the binding in less-stabilized gold-carbene species.¹⁹⁷ Furthermore, a similar cationic species (**6.4**) was observed *in situ* by ¹H and ³¹P NMR in the course of the gold catalyzed cyclization of ethyl 2-methyl-5-phenyl-2,3-pentadienoate (Scheme 44), a reaction which does not display characteristics consistent with reactive gold-carbene intermediates.²⁰³⁻²⁰⁴

Scheme 44: Observation of a cationic intermediate in the course of the gold catalyzed cyclization of 2-methyl-5-phenyl-2,3-pentadienoate.



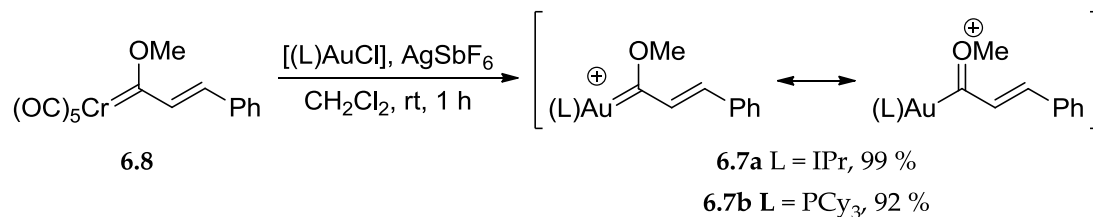
In another example of a highly γ -stabilized gold-carbenoid, Hasmi *et al* have reported the synthesis and characterization of cationic gold allenylidene **6.6** by methylation of the corresponding gold-acetylide **6.5** (Scheme 45).²⁰⁵ Possible contributors to the electronic structure of complex **6.6** include a gold allenylidene (**6.6a**), a gold-stabilized allenyl cation (**6.6b**), or a stabilized propargyl cation (**6.6c** and **6.6d**). In the solid state, the Au–C1 bond of **6.6** (1.978(4) Å) is slightly shorter than that of **6.5** (1.996(4) Å), and the C1–C2 bond (1.196(5) Å) is elongated slightly relative to **6.5** (1.919(6) Å), representing a minor perturbation of the hybridization of the C1 and C2 carbon atoms in the transformation of **6.5** to **6.6**. In contrast, the C3–O bond of **6.6** (1.321(2) Å) is elongated and the C3–N bond (1.28(1) Å) shortened significantly relative to **6.5** (1.225(5) Å and 1.337(5) Å, respectively). These data point to significant contribution from the γ -aurated imminium ion form **6.6d**. This conclusion is corroborated by solution spectroscopic data, which indicate a modest accumulation of positive charge at C1, marginal reduction of the bond order of the C1–C2 bond relative to **6.5**, and a high energy barrier for rotation about the C3–N bond.²⁰⁵

Scheme 45: Generation of gold allenylidene 6.6 from gold acetylide 6.5, and four possible canonical forms of 6.6.



A similar σ -alkyl binding mode was observed in the thermally- and air-stable gold Fischer-type vinylidene carbene complexes **6.7**, which were synthesized by carbene transfer from the corresponding chromium carbene complex **6.8** (Scheme 46).¹⁹⁹ The complexes were characterized spectroscopically and, in the case of **6.7a**, in the solid state by X-ray diffractometry. The C1 carbon resonances were shifted farther downfield in the ¹³C NMR spectra of **6.7a** ($\delta = 281.5$) and **6.7b** ($\delta = 287.4$) than in carbenoids **6.3** and **6.6**, suggesting an electronic structure more typical of a Fischer-type carbene. As was the case for **6.2**, the Au-C1 distance (2.010(10) Å) is typical of Au-C bond lengths in gold σ -arene complexes²⁰⁶ or Au-NHC complexes.²⁰⁷ The C1-O bond (1.316 Å) is shorter than that of an average enol ether (1.354 Å) but not as short as the C=O bond of a ketone (1.210 Å),²⁰² suggesting significant contribution of the metalated oxocarbenium ion form.

Scheme 46: Synthesis of gold Fischer-carbene complexes 6.7.¹⁹⁹



6.1.3 Project goals and scope

As a first step toward understanding the structure and reactivity of cyclopropyl gold carbenes/carbocations, we sought to synthesize a stabilized Fischer-type gold cyclopropyl carbene complex. With slight modifications to the method used to synthesize 6.7, we were able to synthesize the first example of a gold cyclopropyl carbene complex and characterize it in solution and in the solid state.

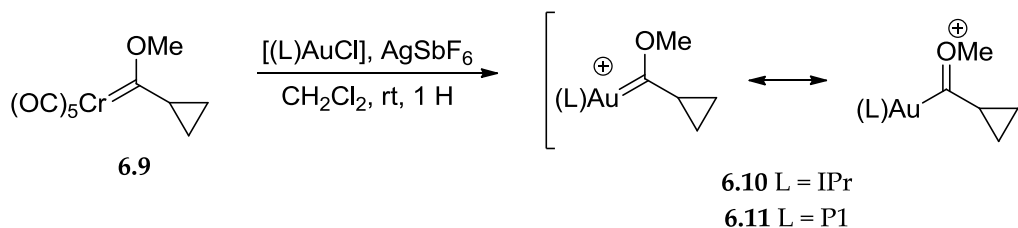
6.2 Results and discussion

6.2.1 Synthesis of gold cyclopropyl Fischer-carbene 6.11

Initial attempts to synthesize a gold cyclopropyl carbene complex by carbene transfer from chromium carbene 6.9 targeted the IPr-gold complex 6.10 (Scheme 47), as the strongly σ -donating and weakly π -accepting NHC ligands are thought to stabilize *trans*-carbene ligands.¹⁹⁷ Treatment of a 1:1 suspension of [(IPr)AuCl] and AgSbF₆ in CH₂Cl₂ with 6.9 (1 equiv.) for 1 hour according to the published procedure for the synthesis of 6.7 undoubtedly resulted in generation of gold carbene 6.10, as evidenced by the presence of a diagnostic carbene carbon resonance at δ 299.3 ppm in the ¹³C NMR of the crude reaction mixture; however, further characterization of complex 6.10 was

precluded by the presence of an unidentified impurity or impurities, and all attempts to purify **6.10** resulted in sample degradation.

Scheme 47: Synthesis of gold cyclopropyl carbene complexes 6.10 and 6.11.



Substituting the bulky, electron-rich phosphine ligand for IPr increased the yield of the desired gold carbene product **6.11** relative to impurities but did not allow for isolation of clean **6.11** employing a procedure analogous to that published for the synthesis of **6.7**. Treatment of a 1:1 suspension of [(P1)AuCl] and AgSbF₆ in CH₂Cl₂ with **6.9** (1 equiv.) for 1 hour followed by filtration resulted in formation of two ³¹P-containing compounds in varying ratios as evidenced by two sharp resonances at δ 62.1 (major) and 61.7 ppm (minor). The major ³¹P resonance was assigned to the desired product **6.11** based on the presence of characteristic resonances in the ¹H and ¹³C spectra of the mixture (see below). Additionally, the ¹H spectrum of the mixture contained aromatic resonances and a large doublet (δ 1.39, *J* = 16 Hz) corresponding to the P1 ligand of a distinct compound but no other aliphatic proton resonances. While the identity of the minor impurity was never confirmed, the cationic species [(P1)₂Au]⁺ or [(P1)Au]₂Cl⁺ remain likely candidates.

Key to the isolation of pure **6.11** was the observation that the product purity was sensitive to the stoichiometry of the carbene transfer reaction; specifically, reactions run with an excess of [(P1)Au]⁺ produced more impurities, while reactions with excess **6.9** produced less impurities. Furthermore, reversing the order of reagent addition such that a suspension of [(P1)AuCl]/AgSbF₆ was added dropwise to a solution of **6.9** resulted in a decreased presence of impurities in the crude reaction mixture. In a final iteration, a 1:1 suspension of [(P1)AuCl] and AgSbF₆ in CD₂Cl₂ was added dropwise to a solution of **6.9** (3 equiv.). The resulting suspension was stirred for 1 h at room temperature, then filtered through Celite. The filtrate was concentrated to a yellow, wet solid residue, which was washed with pentane until rinses eluted colorless. This procedure afforded the desired cyclopropyl gold carbene complex **6.10** as a white solid in 65.7 % yield and > 95 % purity by ¹H, ¹³C, and ³¹P NMR.

6.2.2 Solution characterization of **6.11**

The Fischer-type carbene structure of **6.11** was confirmed by the presence of a diagnostic resonance at δ 303.9, corresponding to gold-bound carbene carbon C1, which displayed carbon-phosphorus coupling ($J_{CP} = 99$ Hz). The C1 resonance of **6.11** appeared downfield of those of complexes **6.7**, perhaps suggesting greater deshielding due to accumulation of positive charge on C1 in **6.11** relative to **6.7**. Formation of complex **6.11** as a single diastereomer or rapidly equilibrating mix of diastereomers was confirmed by the presence of a single, sharp resonance in ³¹P NMR spectrum of **6.11** at 25 °C. In

contrast, a single set of ligand *tert*-butyl resonances in the ^1H NMR ($\delta = 1.42$) and ^{13}C NMR ($\delta = 38.3, 31.1$) spectra of **6.11** suggests the equivalence of these groups, due either to inherent symmetry in the solution structure of the complex or fast rotation about the Au-C1 bond.

It is known that the cyclopropyl group can delocalize positive charge from an α -carbocation with efficiency similar to that of a phenyl substituent and that ^{13}C NMR is a sensitive probe of the extent to which positive charge is accumulating within the cyclopropyl ring.²⁰⁸⁻²¹² The chemical shift of the resonances for the cyclopropyl C2 (δ 35.6) and C3/C4 (δ 19.2) carbons are shifted downfield relative to neutral monosubstituted cyclopropanes such as 1-cycloproylethanol (**6.12**) and acetylcyclopropane (**6.13**) (Figure 71), suggesting a modest accumulation of positive charge in the cyclopropane ring. Interestingly, the cyclopropyl resonances of corresponding iron (**6.14**) and ruthenium (**6.15**) cyclopropyl carbene Fischer carbenes were deshielded relative to those of **6.11**.²¹³ The increased charge density on the cyclopropyl groups in **6.14** and **6.15** relative to **6.11** indicates greater cationic character of the metal bound carbene carbon, presumably due to decreased donation of electron density from the methoxy substituent or decreased π -backbonding from the metal relative to **6.11**. The latter possibility represents a departure from general speculation regarding gold carbenes, which are thought to have very little π -backbonding character owing to the difference in size of the frontier orbitals of gold and carbon.²⁰⁰

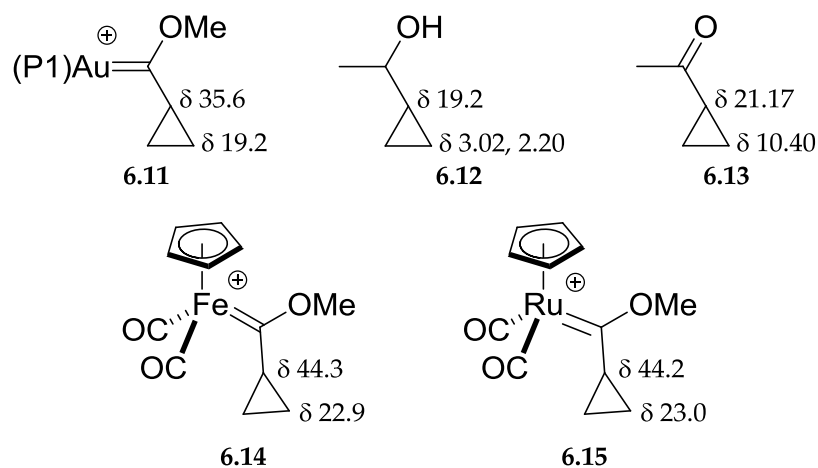


Figure 71: ^{13}C chemical shifts of cyclopropyl carbons of cationic metal carbenes and neutral organic cyclopropanes.

6.2.3 X-ray crystal structure of 6.11

Slow diffusion of hexanes into a CH_2Cl_2 solution of **6.11** at 4°C gave colorless crystals of **6.11** suitable for single-crystal X-ray analysis (Figure 72). The crystal structure of **6.11** established it as a monomeric complex with complexation of the methoxy cyclopropyl carbene group to gold through the C1 carbon atom. Complex **6.11** adopts a linear conformation in the solid state, with a P-Au-C1 angle of $177.64(10)^\circ$ and with the carbene ligand bound such that the methoxy and cyclopropyl substituents are directed roughly perpendicular to the P1-Au1-C1 plane.

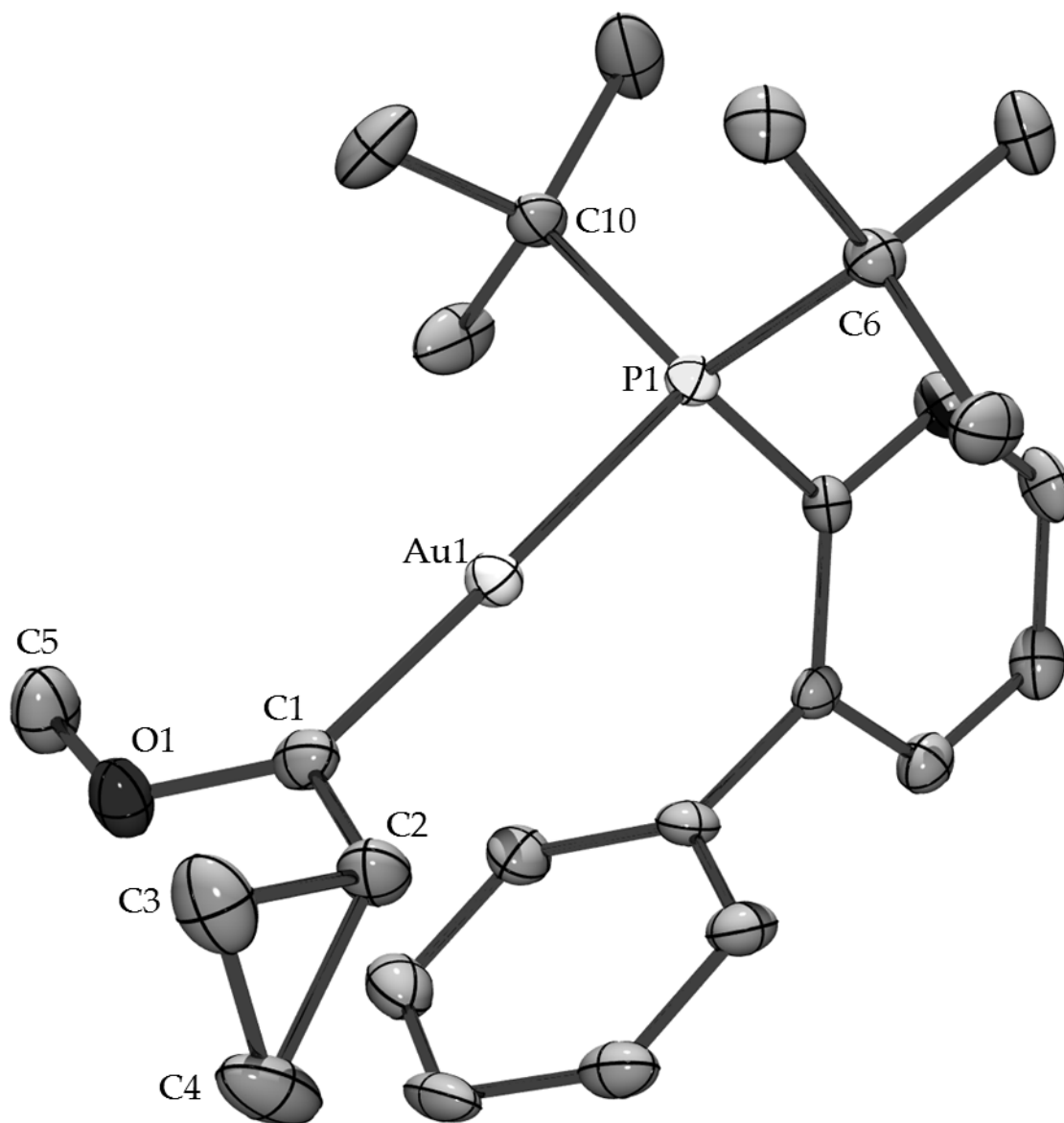


Figure 72: ORTEP diagram of 6.11 showing partial atom numbering scheme. Ellipsoids are shown at the 50% probability level. Hydrogen atoms and counterion have been removed for clarity.

The C1 atom of **6.11** exhibits the expected planar, distorted sp^2 geometry with the methoxy and cyclopropyl substituents bent slightly away from the [(P1)Au] moiety at an O1–C1–C2 bond angle of $113.2(3)^\circ$. The Au–C1 bond length of $2.032(4) \text{ \AA}$ is slightly

longer than that of gold Fischer carbene complex **6.7a** but still within the range of typical gold–arene σ -bonds.²⁰⁶ Additionally, the C1–O1 bond (1.285(4) Å) is shorter than that of **6.7a** and more comparable to that of a ketone.²⁰² These observations support the contention that complex **6.11** exhibits greater donation of electron density from the methoxy substituent to the C1 carbene carbon relative to other known Fischer-carbene complexes.

6.3 Summary and conclusions

Here we report the synthesis and characterization of the first example of a gold cyclopropyl carbene complex. Complex **6.11** was synthesized via carbene transfer from the corresponding chromium carbene complex. Characterization of **6.11** in solution and in the solid state reveals dominance of the metalated oxocarbenium ion form, with a short C1–O bond and a long Au–C1 bond resembling a Au–C σ -bond. Reactivity studies on **6.11** are ongoing.

6.4 Experimental

6.4.1 General methods

Reactions were performed under a nitrogen atmosphere employing standard Schlenk and glovebox techniques unless specified otherwise. NMR spectra were obtained on a Varian spectrometer operating at 400 MHz for ^1H NMR, 101 MHz for ^{13}C NMR, and 161 MHz for ^{31}P NMR in CD_2Cl_2 at room temperature. Methylene chloride and diethylether were purified by passage through columns of activated alumina under

nitrogen. CD_2Cl_2 was dried over CaH_2 prior to use. Chromium hexacarbonyl, bromocyclopropane, *tert*-butyllithium, [(P1)AuCl], AgSbF_6 , hexanes, and pentane were purchased from major chemical suppliers and used as received.

6.4.2 Synthesis and characterization of carbene complexes

Pentacarbonyl[cyclopropyl(methoxy)carbene]chromium (6.9) Chromium complex **6.9** was synthesized using slightly modified published procedures.²¹⁴⁻²¹⁵ To a stirred solution of cyclopropylbromide (121 mg, 1.00 mmol) in Et_2O (2 mL) at $-78\text{ }^\circ\text{C}$ was added *tert*-butyllithium (1.2 mL of a 1.7 M solution in hexane, 2.00 mmol) dropwise. The mixture was stirred at $-78\text{ }^\circ\text{C}$ for 30 min then transferred via canulae over 10 min to a suspension of chromium hexacarbonyl (220 mg, 1.00 mmol) in Et_2O (4 mL) at $0\text{ }^\circ\text{C}$. The resulting brown solution was warmed to room temperature and stirred for 2 h. The crude reaction mixture was concentrated under vacuum, and the residue was dissolved in ice-cold DI H_2O and cooled in an ice bath. Trimethyloxonium tetrafluoroborate (296 mg, 2.00 mmol) was added to the reaction at $0\text{ }^\circ\text{C}$, and the resultant solution was warmed to room temperature over 15 minutes. The crude reaction mixture was extracted with pentane (4 x 30 mL), and the combined organic fractions were dried over Na_2SO_4 , filtered, and concentrated to give a yellow solid. Column chromatography (SiO_2 , pentane) of the crude residue afforded **6.9** as a yellow solid (158 mg, 57.2 %).

P1[cyclopropyl(methoxy)carbene]gold (6.11) To a stirred solution of **6.11** (51.3 mg, 0.186 mmol) in CH_2Cl_2 (1 mL) was added a suspension of [(P1)AuCl] (32.9 mg, 6.20

$\times 10^{-2}$ mmol) and AgSbF_6 (21.3 mg, 6.20×10^{-2} mmol) in CH_2Cl_2 (1 mL) at room temperature. The resultant solution was stirred 1 h at room temperature then filtered through Celite, eluting with CH_2Cl_2 . The filtrate was concentrated and dried to give a solid yellow residue which was rinsed with pentane to yield **6.11** as a white solid (50.5 mg, 65.7). ^1H NMR (CD_2Cl_2 , 25 °C, 400 MHz): δ 7.91 (dt, $J = 2.4, 7.2$ 1 H), 7.54 – 7.56 (m, 2 H), 7.53 (t, $J = 7.6$ Hz, 2 H), 7.34 (t, $J = 7.6$ Hz, 1 H), 7.30 – 7.25 (m, 2H), 4.53 (s, 3 H), 2.46 (tdd, $J = 4.0, 8.4, 11.6$ Hz, 1 H), 1.89 – 1.81 (m, 2 H), 1.80 – 1.76 (m, 2 H), 1.42 (d, $J = 15.6$ Hz, 18 H). ^{13}C NMR: δ 303.9 (d, $J = 99.0$ Hz), 149.1 (d, $J = 14.6$ Hz), 143.9 (d, $J = 5.8$ Hz), 134.9, 133.5 (d, $J = 7.5$ Hz), 130.1, 129.8, 128.2 (d, $J = 6.3$ Hz), 128.0, 125.5 (d, $J = 42.3$ Hz), 71.5, 38.3 (d, $J = 22.4$ Hz), 35.6 (d, $J = 5.6$ Hz), 31.1 (d, $J = 4.8$ Hz), 19.2. $^{31}\text{P}\{^1\text{H}\}$ NMR (CD_2Cl_2 , 25 °C, 161 MHz): δ 62.2. Anal. Calcd (found) for $\text{C}_{25}\text{H}_{35}\text{AuF}_6\text{PSb}$: H, 4.32 (4.41); C, 37.46 (37.57).

6.4.3 X-ray crystal structure determination

The sample was mounted on a Mitegen polyimide micromount with a small amount of Paratone N oil. All X-ray measurements were made on a Bruker-Nonius Kappa Axis X8 Apex2 diffractometer at a temperature of 110 K. The unit cell dimensions were determined from a symmetry constrained fit of 9918 reflections with $4.74^\circ < 2\theta < 58.42^\circ$. The data collection strategy was a number of ω and ϕ scans which collected data up to 73.98° (2θ). The frame integration was performed using SAINT.⁹⁹ The resulting

raw data was scaled and absorption corrected using a multi-scan averaging of symmetry equivalent data using SADABS.¹⁰⁰

The structure was solved by direct methods using the XS program.¹⁰¹ All non-hydrogen atoms were obtained from the initial solution. The hydrogen atoms were introduced at idealized positions and were allowed to ride on the parent atom. The structural model was fit to the data using full matrix least-squares based on F². The calculated structure factors included corrections for anomalous dispersion from the usual tabulation. The structure was refined using the XL program from SHELXTL,¹⁰³ graphic plots were produced using the NRCVAX crystallographic program suite.

Table 15: Crystal and structure refinement data for complex 6.11

Formula	C ₂₅ H ₃₅ AuF ₆ OPSb
Formula Weight (<i>g/mol</i>)	815.22
Crystal Dimensions (<i>mm</i>)	0.21 × 0.07 × 0.05
Crystal Color and Habit	colourless needle
Crystal System	monoclinic
Space Group	P 21/c
Temperature, K	110
<i>a</i> , Å	12.132(5)
<i>b</i> , Å	9.596(4)
<i>c</i> , Å	23.868(7)
<i>a</i> , °	90.00
<i>b</i> , °	91.292(7)
<i>g</i> , °	90.00
<i>V</i> , Å ³	2777.8(17)
Number of reflections to determine final unit cell	9918
Min and Max 2 θ for cell determination, °	4.74, 58.42
<i>Z</i>	4
F(000)	1568
ρ (<i>g/cm</i> ³)	1.949
<i>l</i> , Å, (MoKa)	0.71073
<i>m</i> , (<i>cm</i> ⁻¹)	6.362
Diffractometer Type	Bruker-Nonius Kappa Axis X8 Apex2
Scan Type(s)	omega and phi scans
Max 2 θ for data collection, °	73.98
Measured fraction of data	0.991
Number of reflections measured	101264
Unique reflections measured	13422
Rmerge	0.0807
Number of reflections included in refinement	13422
Cut off Threshold Expression	>2 σ (I)
Structure refined using	full matrix least-squares using F2
Weighting Scheme	calc w=1/[σ^2 (F _o ²)+(0.0474P) ² +0.0000P] where P=(F _o ² +2F _c ²)/3
Number of parameters in least-squares	323
R1	0.0424
wR2	0.0913
R1 (all data)	0.0746
wR2 (all data)	0.1026
GOF	1.040
Maximum shift/error	0.001
Min & Max peak heights on final DF Map (<i>e</i> ⁻ /Å)	-2.110, 3.867

7. Stereochemistry and Mechanism of the Brønsted Acid Catalyzed Intramolecular Hydrofunctionalization of an Unactivated Cyclic Alkene

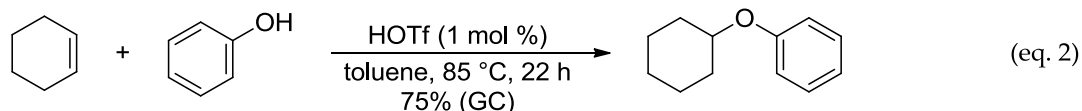
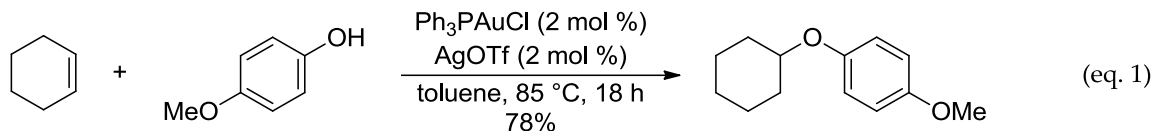
Portions of this chapter have been published: Brooner, R. E. M.; Widenhoefer, R. A. *Chem.-Eur. J.* **2011**, *17*, 6170. The X-ray crystal structure of **7.2** was solved and refined by Dr. Marina G. D. Leed.

7.1 Introduction

7.1.1 Transition metal- and acid-catalyzed hydrofunctionalizations

The catalytic, intramolecular addition of the X–H (X = O, N) bond of a nitrogen or oxygen nucleophile across the C=C bond of an electronically unactivated alkene (hydrofunctionalization) represents an attractive and atom economical approach to the synthesis of oxygen and nitrogen heterocycles^{59, 216-218} Although much of the effort in the area of catalytic alkene hydrofunctionalization has been focused on transition metal-based processes, Brønsted acids also catalyze the hydrofunctionalization of C=C bonds, oftentimes with rates and selectivities comparable to transition-metal-catalyzed methods.^{180-181, 183, 219-242} For example, a mixture of [(PPh₃)AuCl] and AgOTf (1:1, 2 mol %) is reported to catalyze the hydroalkoylation of cyclohexene with *para*-methoxyphenol in to yield 1-(cyclohexyloxy)-4-methoxybenzene in 78 % yield after 18 h in toluene at 85 °C (Scheme 48, eq. 1).²⁴³ Similarly, the hydroalkoxylation of cyclohexene with phenol is also catalyzed by HOTf (1 mol %) in toluene at 85 °C to (cyclohexyloxy)benzene in 75 % yield (GC) after 22 h (Scheme 48, eq. 2).¹⁸¹

Scheme 48: Gold(I)- and HOTf-catalyzed hydroalkoxylation of cyclohexene with phenols.^{181, 243}



For this reason, there is growing concern that a number of metal-based hydrofunctionalization processes, particularly those that employ electrophilic metal complexes or metal triflates in combination with modestly basic nucleophiles, may be catalyzed by a Brønsted acid generated under reaction conditions.^{181-182, 242, 244-249}

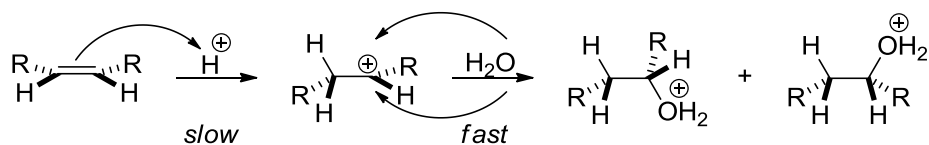
Distinguishing between transition metal and Brønsted acid catalyzed pathways for intramolecular alkene hydrofunctionalization is complicated by our limited understanding of the mechanisms of Brønsted acid-catalyzed alkene hydrofunctionalization. Whereas the mechanisms of Brønsted acid mediated intermolecular alkene hydrofunctionalization have been studied for decades,²⁵⁰⁻²⁹⁹ mechanistic information regarding the corresponding intramolecular processes is scarce, and none of the available data pertains to electronically unactivated alkenes.

7.1.2 Mechanism of the intermolecular acid-catalyzed alkene hydrofunctionalization

7.1.2.1 Alkene hydration

Extensive kinetic analyses of the Brønsted acid catalyzed hydration and intermolecular hydroalkoxylation of conjugated and nonconjugated alkenes reveal that, with few exceptions, these transformations occur through irreversible, turnover-limiting protonation of the C=C bond followed by nucleophilic trapping of a solvated carbenium ion intermediate (Scheme 49).²⁵⁰⁻²⁵⁵ Although early work by Taft et al. suggested that the proton transfer was preceded by reversible formation of a π -protonium complex,²⁵⁶⁻²⁵⁸ this hypothesis has been largely discounted.^{250-255 259-260} Deviations from the general hydration mechanism are rare but may occur in the cases of particularly long-lived or short-lived carbenium ions. For example, mechanisms involving rapid and reversible C=C bond protonation followed by rate-limiting nucleophilic addition to the resulting carbenium ion have been documented in the cases of highly stabilized carbenium ions.²⁶¹⁻²⁶⁴

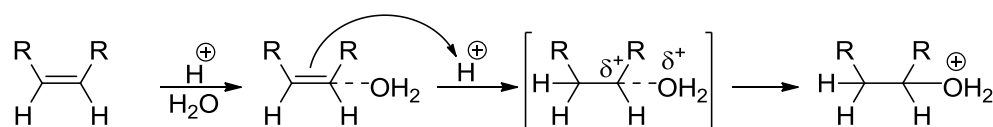
Scheme 49: General mechanism for the acid-catalyzed hydration of alkenes.



Drawing from the analyses of Jencks,²⁶⁵⁻²⁶⁷ Kresge et al. posited that preassociation or concerted mechanisms for alkene hydration may be enforced by short carbenium ion lifetimes.²⁶⁸ For example, Kresge et al. considered a preassociation

pathway for the acid-catalyzed hydration of *trans*-cyclooctene, but this hypothesis was ultimately discounted; however, they maintained that preassociation pathways may be operative for the hydration of unstrained olefins that generate secondary carbocations under dilute acidic conditions (Scheme 50).²⁶⁸ Similarly, consideration of carbocation lifetimes led Jencks et al.²⁶⁹ and Herlihy²⁷⁰ to propose concerted pathways for the hydration of monosubstituted alkenes under dilute acidic conditions, although in neither case were these pathways rigorously established.

Scheme 50: Proposed preassociation mechanism for the acid-catalyzed hydration of alkenes.

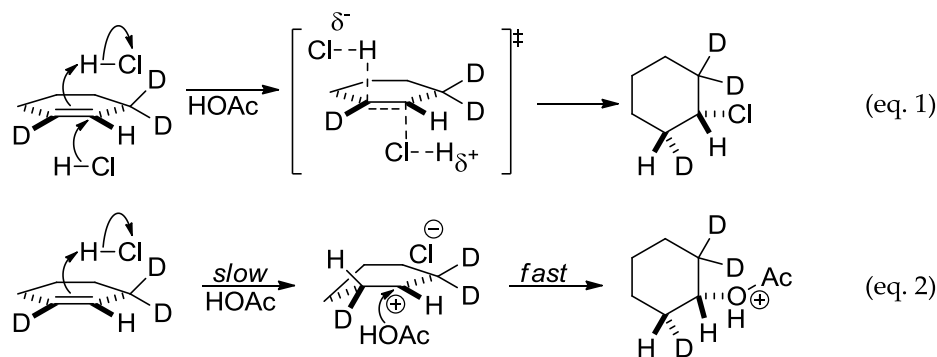


7.1.2.2 Addition of hydrogen halides to alkenes

The mechanisms of the addition of hydrogen halides to alkenes and the addition of acetic acid to nonconjugated alkenes catalyzed by hydrogen halides and related Brønsted acids have also been investigated.²⁷¹⁻²⁹⁷ These transformations typically occur with about 85 % *anti* selectivity in the case of nonconjugated acyclic alkenes and with >95 % *anti* selectivity in the case of nonconjugated cyclic alkenes.^{272-283, 285} Hydrogen halide addition typically obeys the ternary rate law: $\text{rate} = k[\text{alkene}][\text{HX}]^2$, whereas the acid-catalyzed hydroacetoxylation typically obeys the binary rate law: $\text{rate} = k[\text{alkene}][\text{HX}]$.^{274-277, 284-288} Both A_{de}3 pathways involving concerted C–H and C–X (X = halide or OAc) addition across the C=C bond of the alkene (Scheme 51, eq. 1)^{272-273, 276-}

^{277, 280-281, 283, 285-286} and/or stepwise Ad_E2 pathways involving rate-limiting, halide-assisted protonation of the alkene followed by rapid trapping of a tight carbenium ion pair (Scheme 51, eq. 2) have been proposed to account for these observations.^{274-276, 280, 283-284, 287-}
²⁸⁸ Initial formation of a π -protonium complex has also been invoked,^{272-273, 282-283} but, as was the case for alkene hydration, little direct evidence supports these hypotheses.²⁸⁹

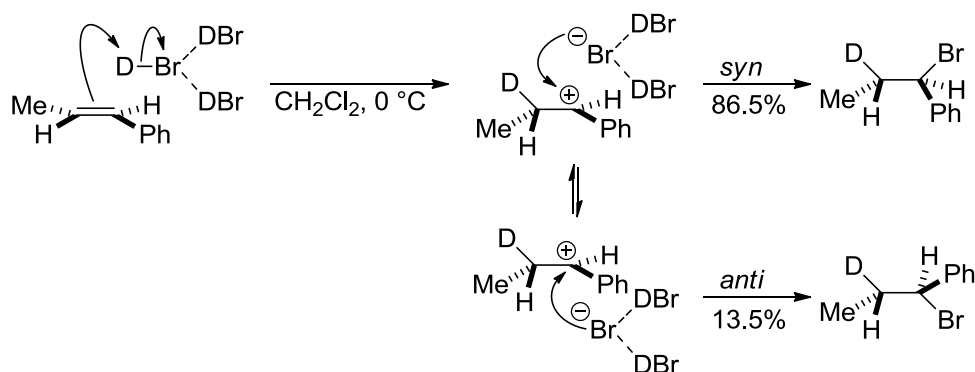
Scheme 51: The HCl-catalyzed addition of HCl to 1,3,3-trideuteriocyclohexene via an Ad_E3 mechanism (eq. 1), and the HCl-catalyzed addition of HOAc to 1,3,3-trideuteriocyclohexene via an Ad_E2 mechanism (eq.2).²⁸⁰



In contrast to the behavior of weaker Brønsted acids, Roberts reported that the HOTf-catalyzed addition of [*O*-D₁]acetic acid to cyclopentene was non-stereoselective.²⁹⁰ In a separate study, Pasto et al. reported that the HOTf-catalyzed addition of [*O*-D₁]acetic acid to 2-butene occurred with modest (57–72 %) *anti* stereoselectivity and was accompanied by alkene isomerization and H/D exchange.²⁸¹ The latter transformation was proposed to occur through an Ad_E2 pathway involving reversible formation of a carbenium ion pair that was trapped by acetic acid. The slight preference for the *anti* addition was attributed to steric shielding of

the *syn* face of the carbenium ion in the tight ion pair. In comparison, the addition of hydrogen halides to cyclic and acyclic vinyl arenes occurs with up to 90 % *syn* selectivity in low-polarity solvents.²⁹¹⁻²⁹⁷ For example, the addition of DBr to *trans*-1-phenylpropene in dichloromethane at 0 °C occurs with 86.5% *syn* selectivity (Scheme 52).²⁹² This behavior is in accord with a stepwise Ad_E2 pathway involving turnover-limiting protonation to form a tight ion pair that undergoes rapid collapse (*syn* addition) or rearrangement followed by collapse (nonselective).

Scheme 52: The *syn* selective addition of DBr to *trans*-1-phenylpropene in dichloromethane via an Ad_E2 mechanism.²⁹²

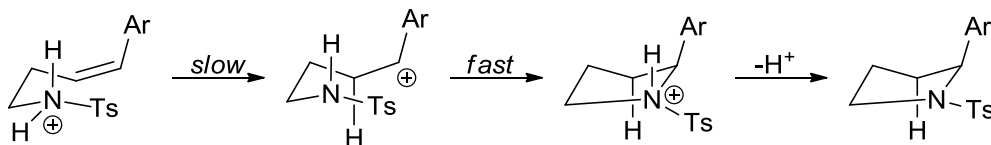


Recently, the mechanisms of triflic acid catalyzed intermolecular alkene hydrofunctionalization with phenols and protected amines has been investigated by a pair of DFT studies.²⁹⁸⁻²⁹⁹ In both cases, calculations predict a concerted, *syn* addition of the H-X (X = N, O) bond of the nucleophile across the C=C bond of the alkene through an eight-membered cyclic transition state in which triflic acid interacts with both the alkene and the nucleophile.²⁹⁸⁻²⁹⁹

7.1.3 Mechanism of the intramolecular acid-catalyzed alkene hydrofunctionalizations

Unlike intermolecular variants, information regarding the mechanisms of intramolecular additions of nucleophiles to alkenes is scarce. Hosomi et al. have reported that the intramolecular hydroalkoxylation and hydroamination of vinylsilanes with alcohols and sulfonamides occur with around 85 % *syn* stereoselectivity, which was attributed to an intramolecular proton transfer from a protonated nucleophile to the C=C bond of the alkene followed by stereoselective trapping of the more stable β -silylcarbenium rotamer.³⁰⁰⁻³⁰¹ Hartwig and Schlummer proposed a similar mechanism for the triflic acid (HOTf) catalyzed intramolecular hydroamination of vinylarenes with sulfonamides involving intramolecular proton transfer from the protonated sulfonamide to the alkene followed by trapping of the resulting benzylic carbenium ion (Scheme 53). However, this latter study included neither stereochemical nor kinetic data.¹⁸⁰

Scheme 53: Proposed mechanism for the acid-catalyzed intramolecular addition of sulfonamides across vinyl arenes.¹⁸⁰

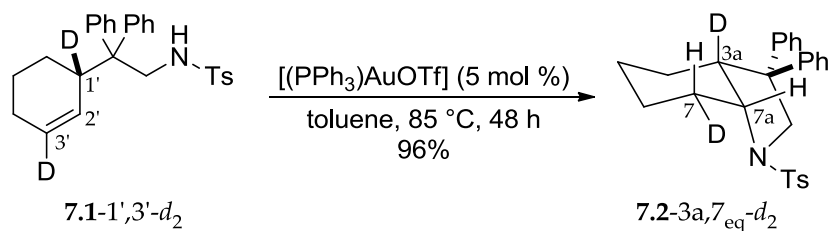


7.1.4 Project goals and scope

Owing to the considerable current interest in the catalytic intramolecular hydrofunctionalization of electronically unactivated alkenes,^{59, 216-218} we sought to gain information regarding the mechanisms of the Brønsted acid catalyzed intramolecular

hydrofunctionalization of unactivated alkenes. Initial mechanistic studies focused on the acid-catalyzed hydroamination of doubly deuterium-labeled γ -alkenyl sulfonamide *N*-(2-1',3'-dideuteriocyclohex-2'-enyl-2,2-diphenylethyl)-*p*-toluenesulfonamide (**7.1-1',3'-d₂**), as this species has previously been employed to evaluate the stereoselectivity of gold(I)-catalyzed alkene hydroamination (Scheme 54).¹⁴⁰ Here, we report the stereochemical analysis of the Brønsted acid-catalyzed intramolecular hydrofunctionalization of **7.1** and a corresponding alcohol and carboxylic acid, supported by the kinetic analysis of Brønsted acid catalyzed intramolecular hydroamination. The results of these studies, particularly in the case of intramolecular hydroamination, support a mechanism involving concerted, intermolecular protonation of the alkene coupled with intramolecular *anti* addition of the pendant nucleophile.

Scheme 54: Gold-catalyzed intramolecular *syn*-hydroamination of doubly deuterated γ -cyclohexenyl sulfonamide **7.1-1',3'-d₂.¹⁴⁰**



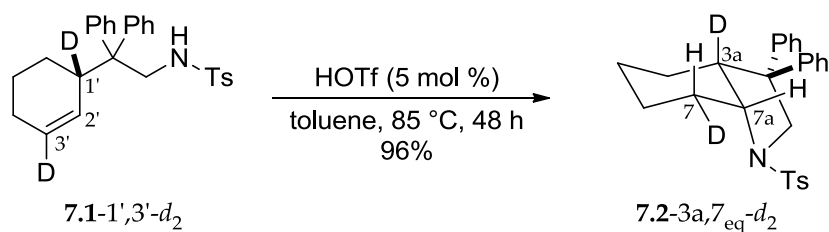
7.2 Results and discussion

7.2.1 Stereochemistry of intramolecular hydrofunctionalization

7.2.1.1 Intramolecular hydroamination

To evaluate the stereoselectivity of Brønsted acid-catalyzed intramolecular alkene hydroamination, we sought to evaluate the stereoselectivity of the triflic acid (HOTf) catalyzed intramolecular alkene hydroamination of **7.1-1',3'-d₂**. Treatment of **7.1-1',3'-d₂** [(83 ± 1) % *d₂*, 17 % *d₁* by MS, ≈ 85 % deuterated at C3' by ¹H NMR spectroscopy] with a catalytic amount of triflic acid (5 mol %) in toluene at 85 °C for 48 h led to 5-*exo* hydroamination with isolation of **7.2-3a,7_{eq}-d₂** [(83 ± 1) % *d₂*, 16 % *d₁* by MS) as the exclusive dideuterated isotopomer in 96 % yield without loss of deuterium (Scheme 55). Subsequent experimentation revealed that the triflic acid catalyzed cyclization of **7.1** occurs at lower temperature and with shorter reaction time (60 °C, 3 h) with the same stereochemical outcome.

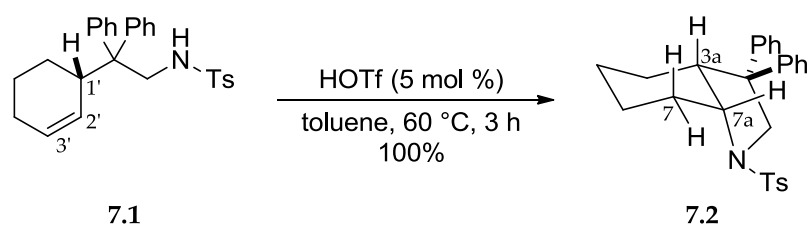
Scheme 55: HOTf-catalyzed intramolecular *syn*-hydroamination of doubly deuterated γ -cyclohexenyl sulfonamide **7.1-1',3'-d₂.**



In order to confidently assign the configuration of **7.2-3a,7_{eq}-d₂** using ¹H and ²H NMR spectroscopy, the structure and relevant ¹H NMR resonances of the protio isotopomer **7.2** were confidently established. Compound **7.2** was obtained quantitatively

from the reaction of **7.1** with HOTf (5 mol %) in toluene at 60 °C for 3 h (Scheme 56), and crystals suitable for single-crystal X-ray analysis were obtained from slow evaporation of a solution of **7.2**. In the solid state, **7.2** adopts a *cis*-fused chair cyclohexane with an equatorial diphenylalkyl substituent and an axial sulfonamide substituent (Figure 73).

Scheme 56: HOTf-catalyzed intramolecular hydroamination of γ -cyclohexenyl sulfonamide **7.1.**



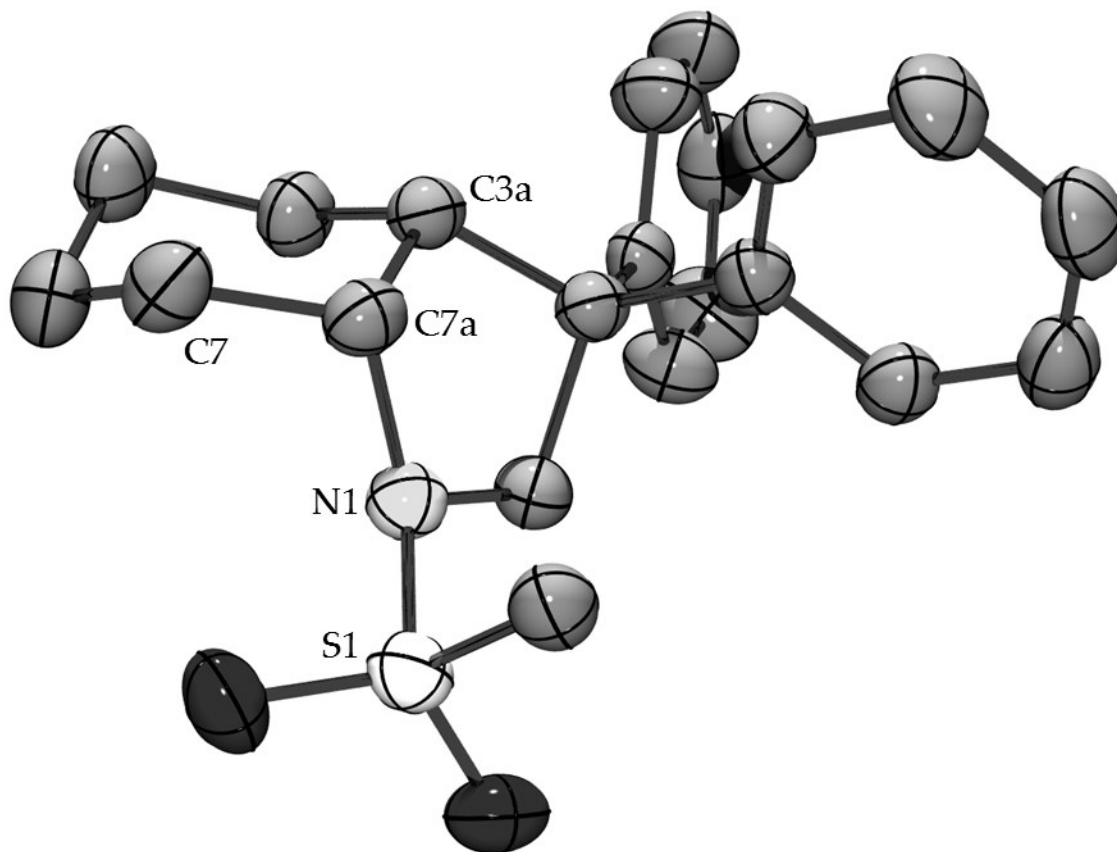


Figure 73: ORTEP diagram of 7.2 showing partial atom numbering scheme. Ellipsoids are shown at the 50% probability level. Hydrogen atoms and aromatic portion of tosyl group removed for clarity.

High-field ^1H NMR spectroscopy (Figure 74a), ^1H - ^1H COSY (Figures 82 and 83, section 7.4.3.1), and ^1H - ^1H NOESY (Figures 82 and 84, section 7.4.3.1) analysis confirmed that the solid-state conformation of 7.2 was preserved in solution and allowed unambiguous assignment of all aliphatic proton resonances. The H7_{ax} and H7_{eq} ^1H NMR resonances could not be assigned on the basis of the three bond coupling $\text{H7}_{\text{ax}}\text{-H7a}$ and $\text{H7}_{\text{eq}}\text{-H7a}$ constants as previously reported because the equatorial confirmation of H7a leads to similar dihedral angles for $\text{H7a-C7a-C7-H7}_{\text{eq}}$ and $\text{H7a-C7a-C7-H7}_{\text{ax}}$ ¹⁴⁰ As a

result, protons H7_{eq} and H7_{ax} display similar three-bond coupling constants to H7a of 4.8 and 3.5 Hz, respectively, and both H7_{eq} and H7_{ax} display strong cross peaks to H7a in the ¹H-¹H NOESY spectrum of **7.2**. Key to the assignment of the resonances corresponding to H7_{ax} and H7_{eq} was the presence of a cross peak between H3 and H7_{ax} and the absence of a cross peak between H3 and H7_{eq} in the ¹H-¹H NOESY spectrum of **7.2** (Figure 82 and 84, section 7.4.3.1).

Integration of the H7_{eq} resonance at $\delta = 2.49$ ppm in the ¹H NMR spectrum of **7.2-3a,7_{eq}-d₂** revealed ~85 % deuteration at this position (Figure 74b). More importantly, ²H NMR analysis of **7.2-3a,7_{eq}-d₂** displayed an approximate 1:1 ratio of resonances at $\delta = 2.95$ (H3a) and 2.49 ppm (H7_{eq}) with no detectable deuteration at either the H7_{ax} ($\delta \approx 1.58$ ppm) or H7a ($\delta \approx 3.73$ ppm) positions (Figure 74c). Taken together, these observations established the net *anti* addition of the N-H bond across the pendant C=C bond of **7.1-1',3'-d₂** without loss or scrambling of deuterium.

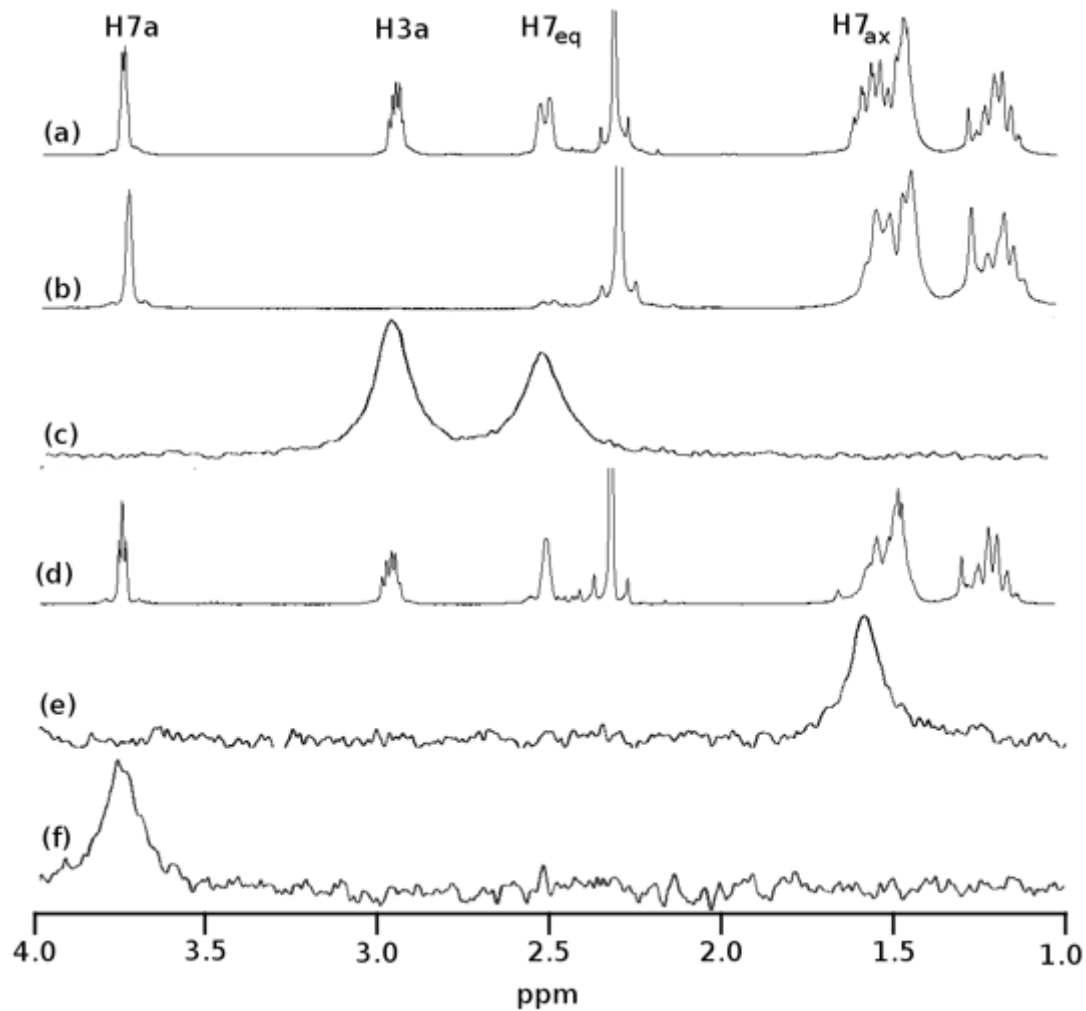
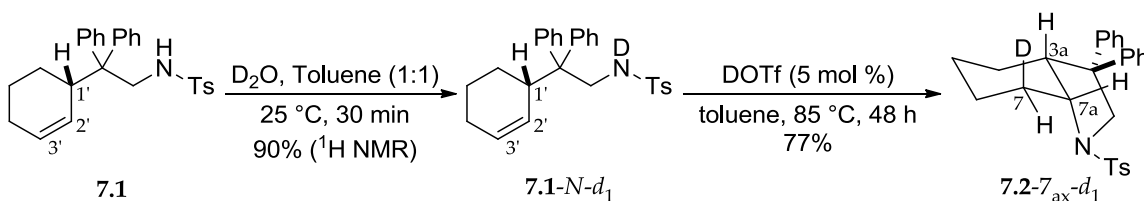


Figure 74: (a) Partial ^1H NMR spectrum of 7.2; (b),(c) Partial ^1H and ^2H NMR spectra of 7.2-3a,7_{eq}-d₂; (d),(e) Partial ^1H and ^2H NMR spectra of 7.2-7_{ax}-d₁; (f) Partial ^2H NMR spectrum of 7.2-7_a-d₁.

To corroborate the findings outlined in the preceding paragraph, we evaluated the stereoselectivity of the acid-catalyzed intramolecular deuteroamination of the *N*-deuterated isotopomer 7.1-*N*-d₁. Isotopomer 7.1-*N*-d₁ (~90 % d₁ by ^1H NMR) was generated *in situ* by stirring a toluene solution of purified 7.1 with D₂O at room temperature followed removal of the toluene solution by using a syringe (Scheme 57);

attempted isolation or purification of **7.1-*N-d*₁** led to significant loss of deuterium. Treatment of **7.1-*N-d*₁** with a catalytic amount of deuterated triflic acid (DOTf) (5 mol %) at 85 °C in toluene for 48 h led to isolation of **7.2-7_{ax-d}₁** [(90 ± 1) % *d*₁ by MS] as the exclusive deuterated isotopomer in 77 % yield (Scheme 57). Integration of the H7_{eq} resonance at δ = 2.49 ppm in the ¹H NMR spectrum of **7.2-7_{ax-d}₁** revealed no significant deuteration at this position (Figure 74d), whereas ²H NMR analysis displayed a single resonance at δ = 1.58 ppm corresponding to deuteration of the C7_{ax} position with no detectable deuteration at either the C7_{eq} (δ = 2.49 ppm) or the C7a (δ = 3.73 ppm) positions (Figure 74e).

Scheme 57: Generation and DOTf-catalyzed cyclization of 7.1-*N-d*₁ to 7.2-7_{ax-d}₁.



The absence of deuterium incorporation at the C7a and the C7_{eq} positions of **7.2-7_{ax-d}₁** in the DOTf-catalyzed cyclization of **7.1-*N-d*₁** argues against reversible deuteration of the C2' or C3' carbon atoms of the cyclohexenyl moiety prior to cyclization. To further probe for reversible protonation/deuteration of the alkene prior to cyclization, the reaction of **7.1-*N-d*₁** (≈ 90 % *d*₁) and a catalytic amount of DOTf (5 mol %) at 60 °C in toluene was monitored periodically by ²H NMR spectroscopy and quenched at about 50 % conversion by addition of triethylamine. A similar experiment

utilizing ^1H NMR analysis of a mixture of $7.1\text{-}N\text{-}d_1$ ($\approx 90\%$ d_1) and DOTf (5 mol %) in toluene- d_8 was run concurrently. ^1H and ^2H NMR analysis of the respective solutions revealed no positional isomerization and no detectable incorporation of deuterium into the C2' or the C3' positions ($\delta = 5.68$ and 5.58 ppm) of $7.1\text{-}N\text{-}d_1$ (Figure 75). These observations, together with those outlined above, argue strongly against a reversible deuteration of either the cyclohexene C2' or C3' carbon atoms prior to cyclization.

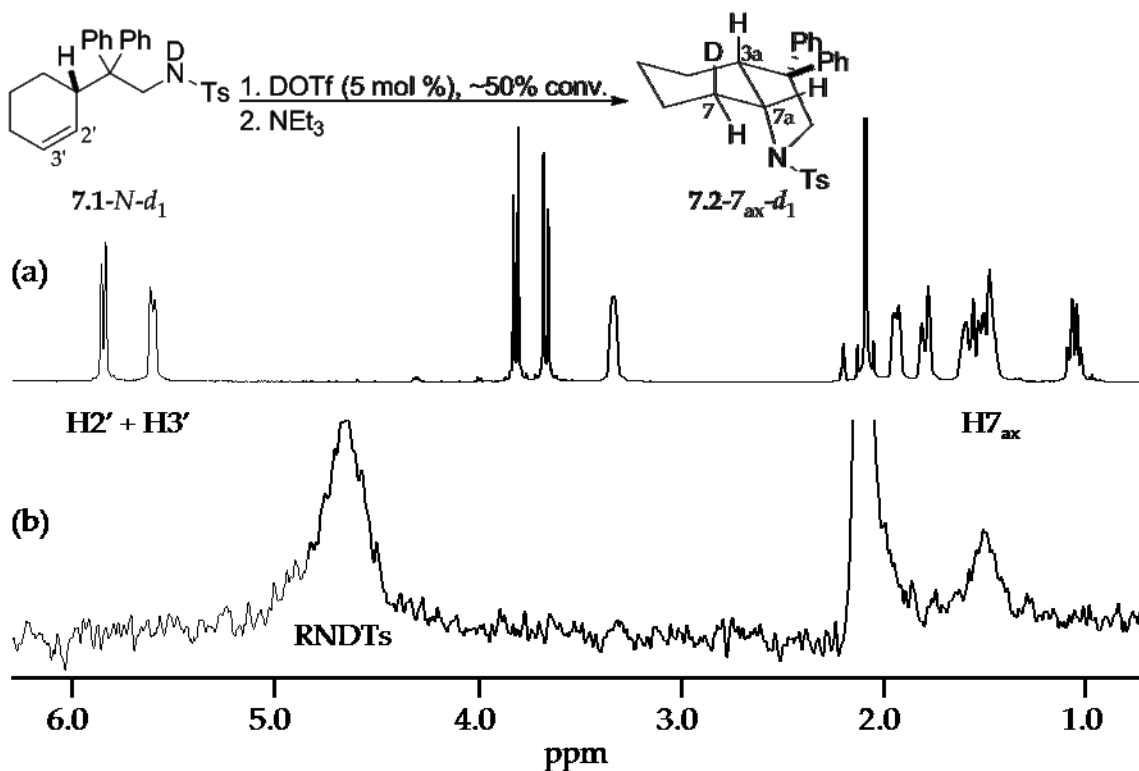


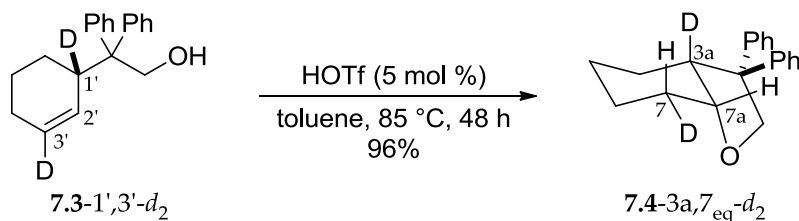
Figure 75: ^1H (a) and ^2H NMR analysis of the DOTf-catalyzed conversion of $7.1\text{-}N\text{-}d_1$ to $7.2\text{-}7_{\text{ax}}\text{-}d_1$ quenched at $\sim 50\%$ conversion with NEt_3 .

7.2.1.2 Intramolecular hydroalkoxylation and hydroacyloxylation:

We extended our stereochemical analysis of acid-catalyzed alkene hydrofunctionalization to include catalytic hydroalkoxylation and hydroacyloxylation

employing an approach similar to that employed for the intramolecular hydroamination. In one experiment, treatment of the γ -alkenyl alcohol **7.3-1',3'-d₂** (96 % *d₂* by MS) with a catalytic amount of triflic acid (5 mol %) led to 5-*exo* hydroalkoxylation to form **7.4-3a,7_{eq}-d₂** in 96 % yield as the exclusive dideuterated isotopomer with no loss or scrambling of deuterium (95 % *d₂* by MS) (Scheme 58). ¹H and ²H NMR analysis of **7.4-3a,7_{eq}-d₂** revealed ≥ 95 % deuteration of the C7_{eq} ($\delta = 1.89$ ppm) and the C3a ($\delta = 2.71$ ppm) positions with no detectable deuteration at the C7_{ax} ($\delta = 1.34$ ppm) or the C7a ($\delta = 4.12$ ppm) positions (Figure 76).

Scheme 58: HOTf-catalyzed intramolecular *syn*-hydroalkoxylation of doubly deuterated γ -cyclohexenyl alcohol **7.3-1',3'-d₂.**



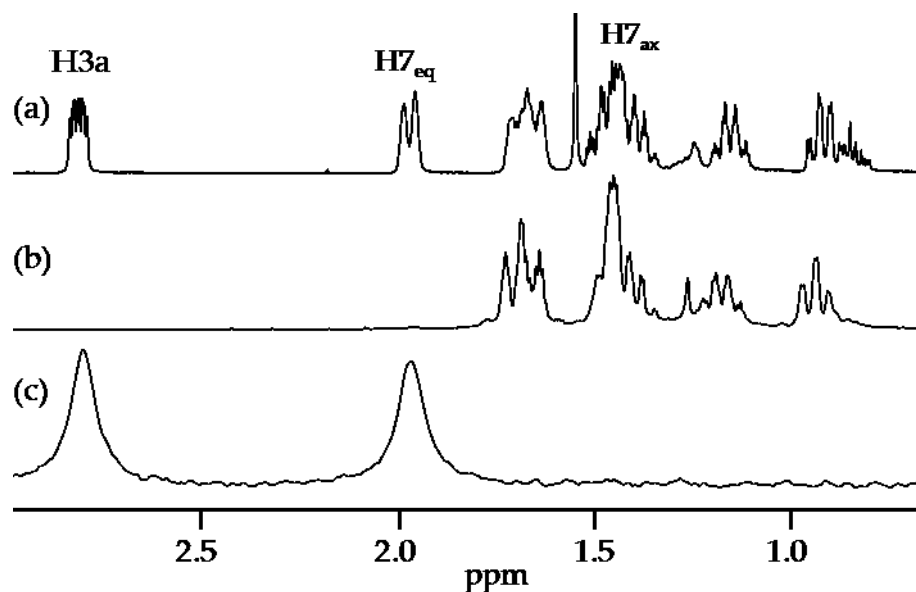


Figure 76: (a) Partial ^1H NMR spectrum of 7.4; (b),(c) Partial ^1H and ^2H NMR spectra of 7.4-3a,7_{eq}-d₂.

Similarly, treatment of β -alkenyl carboxylic acid 7.5-1',3'-d₂ (> 99 % d₂ by MS) with a catalytic amount of triflic acid (5 mol %) led to 5-*exo* hydroacyloxylation to form 7.6-3a,7_{eq}-d₂ as the exclusive dideuterated isotopomer (> 98 % d₂ by MS) in quantitative yield (Scheme 59). ^1H and ^2H NMR analysis of 7.6-3a,7_{eq}-d₂ revealed ≥ 95 % deuteration of the C7_{eq} ($\delta = 2.16$ ppm) and the C3a ($\delta = 3.07$ ppm) positions with no detectable deuteration at the C7_{ax} ($\delta = 1.55$ ppm) or the C7a ($\delta = 4.61$ ppm) positions (Figure 77). In both cases, these results established the net *anti* addition of the O-H bond across the C=C bond of the cyclohexene moiety.

Scheme 59: HOTf-catalyzed intramolecular *syn*-hydroacyloxylation of doubly deuterated γ -cyclohexenyl carboxylic acid 7.5-1',3'- d_2 .

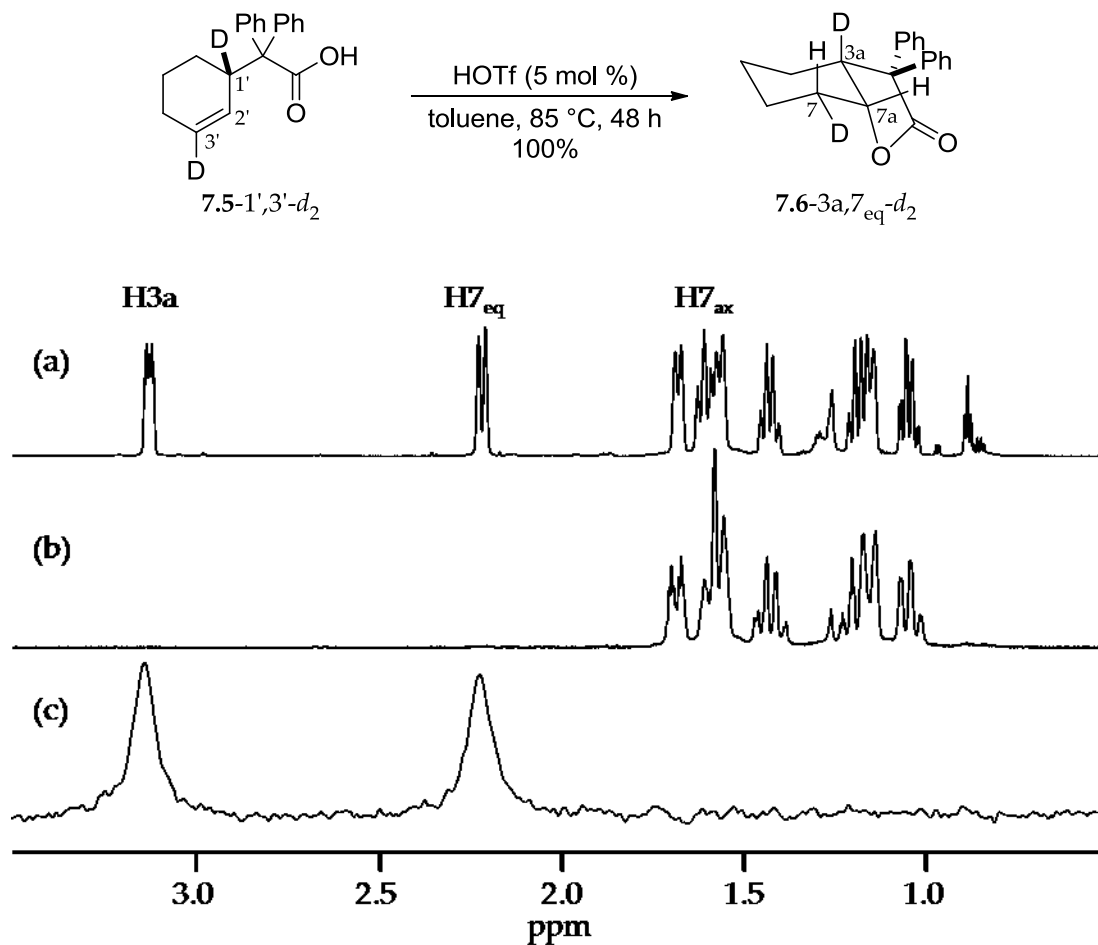


Figure 77: (a) Partial ^1H NMR spectrum of 7.6; (b),(c) Partial ^1H and ^2H NMR spectra of 7.6-3a,7_{eq}- d_2

7.2.1.3 Effect of solvent and acid on hydrofunctionalization

The efficiency and stereoselectivity of the Brønsted acid-catalyzed intramolecular hydrofunctionalization of 7.1-1',3'- d_2 , 7.3-1',3'- d_2 , and 7.5-1',3'- d_2 were evaluated as a function of the acid catalyst and the solvent at 85 °C (Table 16). Treatment of each of the substrates with a catalytic amount of triflic acid (5 mol %) in diglyme at 85 °C for 48 h

led, in each case, to complete consumption of starting material to form the 5-*exo* hydrofunctionalization products **7.2-3a**,_{7_{eq}-d₂}, **7.4-3a**,_{7_{eq}-d₂}, and **7.6-3a**,_{7_{eq}-d₂} as the exclusive dideuterated isotopomers (Table 16, entries 1–3). In comparison, reaction of substrates with triflic acid in acetonitrile effected a significant decrease in reaction rate but led, in each case, to formation of the 5-*exo* hydrofunctionalization products as the exclusive isotopomers (Table 16, entries 4–6). Attempts to cyclize the substrates with weaker acids such as HCl or trifluoroacetic acid (TFA) in toluene at 85 °C for 48 h gave low conversions (Table 16, entries 7–12).

The high stereoselectivity of hydrofunctionalization of **7.2-3a**,_{7_{eq}-d₂}, **7.4-3a**,_{7_{eq}-d₂}, and **7.6-3a**,_{7_{eq}-d₂} in increasingly polar solvents argues against a mechanism for these transformations that invokes formation of a tight ion pair to block *syn*-addition, such as the one proposed for the intermolecular *anti*-addition of HOAc across cyclohexene (Scheme 51, eq. 2).²⁸⁰ In such a mechanism, increasing solvent polarity should lead to decreased stereoselectivity owing to disruption of the tight-ion pair through solvation.

Table 16: Brønsted acid-catalyzed intramolecular hydrofunctionalization of substrates 7.1-1',3'-d₂, 7.3-1',3'-d₂, and 7.5-1',3'-d₂ at 85 °C for 48 h as a function of the solvent and the acid (5 mol %).

Entry	Substrate	Solvent	Acid	Product ^{a,b}	Conversion (%) ^b
1	7.1-1',3'-d ₂	diglyme	HOTf	7.2-3a,7 _{eq} -d ₂	≥ 95
2	7.3-1',3'-d ₂	diglyme	HOTf	7.4-3a,7 _{eq} -d ₂	≥ 95
3	7.5-1',3'-d ₂	diglyme	HOTf	7.6-3a,7 _{eq} -d ₂	≥ 95
4	7.1-1',3'-d ₂	CH ₃ CN	HOTf	7.2-3a,7 _{eq} -d ₂	54
5	7.3-1',3'-d ₂	CH ₃ CN	HOTf	7.4-3a,7 _{eq} -d ₂	36
6	7.5-1',3'-d ₂	CH ₃ CN	HOTf	7.6-3a,7 _{eq} -d ₂	43
7	7.1-1',3'-d ₂	toluene	HCl	7.2-3a,7 _{eq} -d ₂	11
8	7.3-1',3'-d ₂	toluene	HCl	7.4-3a,7 _{eq} -d ₂	≤ 5
9	7.5-1',3'-d ₂	toluene	HCl	7.6-3a,7 _{eq} -d ₂	≤ 5
10	7.1-1',3'-d ₂	toluene	TFA	7.2-3a,7 _{eq} -d ₂	12
11	7.3-1',3'-d ₂	toluene	TFA	7.4-3a,7 _{eq} -d ₂	22
12	7.5-1',3'-d ₂	toluene	TFA	7.6-3a,7 _{eq} -d ₂	≤ 5

^aStereoselectivity was >90% in all cases. ^bConversion and stereoselectivity were determined by ¹H NMR of the purified reaction mixture.

7.2.2 Kinetics of the hydroamination

7.2.2.1 Conversion of 7.1 to 7.2

We sought to gain additional information regarding the mechanism of Brønsted acid catalyzed hydroamination through kinetic analysis of the triflic acid catalyzed conversion of 7.1 to 7.2. To this end, reaction of 7.5 (0.50 M) with a catalytic amount of HOTf (25 mM) in toluene at 62 °C was analyzed periodically by liquid chromatography. A plot of ln[7.1] versus time was linear to about three half-lives with an observed rate

constant of $k_{\text{obs}} = (4.2 \pm 0.1) \times 10^{-3} \text{ s}^{-1}$, which established the first-order dependence of the rate on [7.1] (Figure 78; Table 17, entry 1).

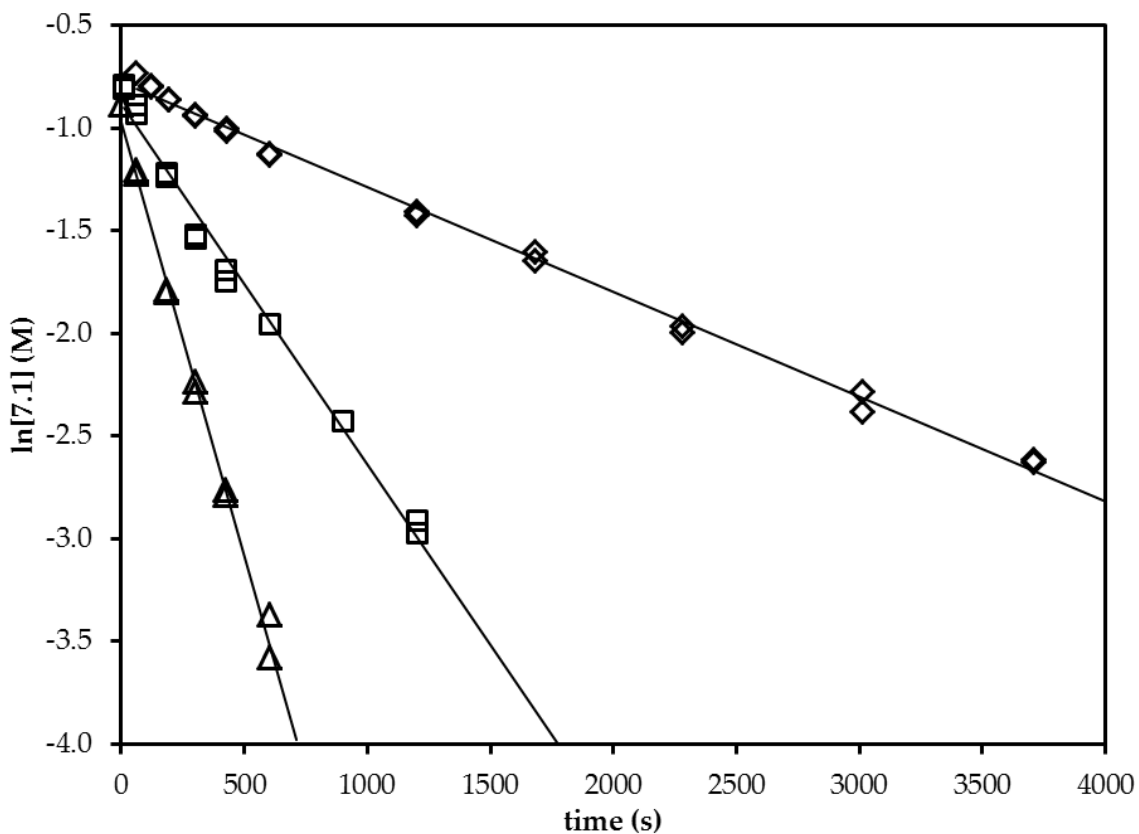


Figure 78: First-order plots for the conversion of 7.1 ($[7.1]_0 = 0.50 \text{ M}$) to 7.2 catalyzed by triflic acid ($[\text{HOTf}] = 5.0$ (◇), 12.6 (□), and 25.2 (△) mM) in toluene at $62 \text{ }^\circ\text{C}$.

To determine the dependence of the rate on the concentration of the triflic acid, observed rate constants for the conversion of 7.1 to 7.2 were also determined at $[\text{HOTf}] = 5.0$ and 12.6 mM (Figure 78; Table 17, entries 2 and 3). A plot of k_{obs} versus $[\text{HOTf}]$ was linear (Figure 79), which established the first-order dependence of the rate on $[\text{HOTf}]$ and the second-order rate law: $\text{rate} = k_2[7.1][\text{HOTf}]$ where

$$k_2 = (1.37 \pm 0.04) \times 10^{-1} \text{ m}^{-1} \text{ s}^{-1} (\Delta G^\ddagger_{336\text{K}} = (21.2 \pm 0.1) \text{ kcal mol}^{-1}).$$

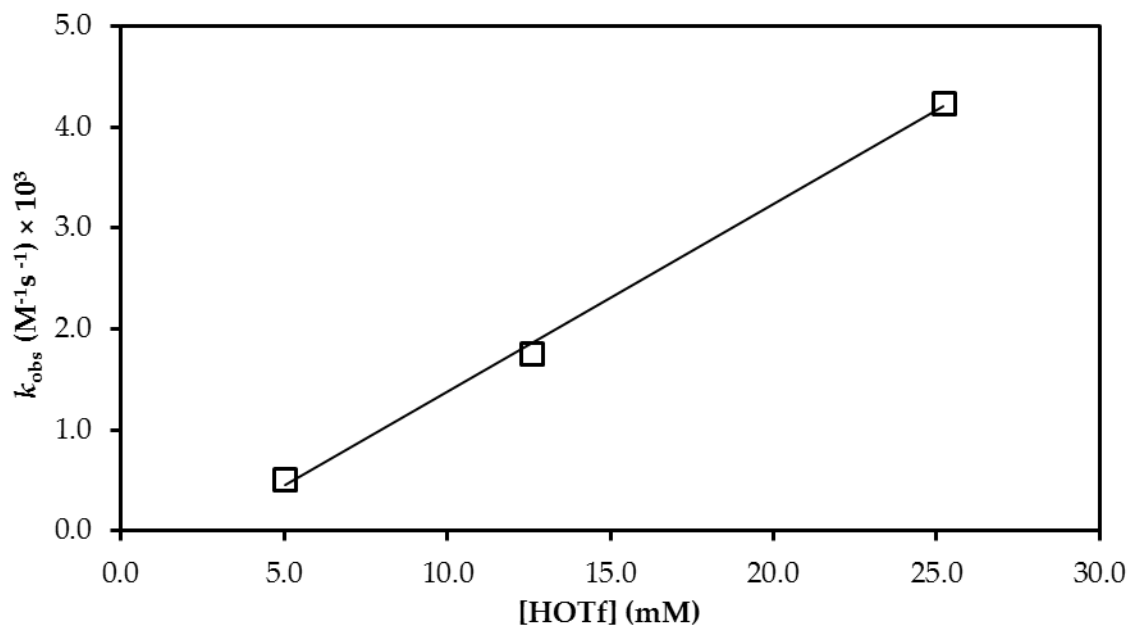


Figure 79: Plot of k_{obs} versus the concentration of triflic acid for the conversion of 7.1 ($[\text{7.1}]_0 = 0.50 \text{ M}$) to 7.2 in toluene at 62 °C.

To determine the activation parameters for the triflic-acid-catalyzed conversion of 7.1 to 7.2, second-order rate constants for the conversion of 7.1 to 7.2 were determined as a function of the temperature from 39 °C to 72 °C (Table 17, entries 4 – 7). An Eyring plot of these data provided the activation parameters: $\Delta H^\ddagger = (9.7 \pm 0.5) \text{ kcal mol}^{-1}$ and $\Delta S^\ddagger = (-34 \pm 5) \text{ cal K}^{-1} \text{ mol}^{-1}$ (Figure 80).

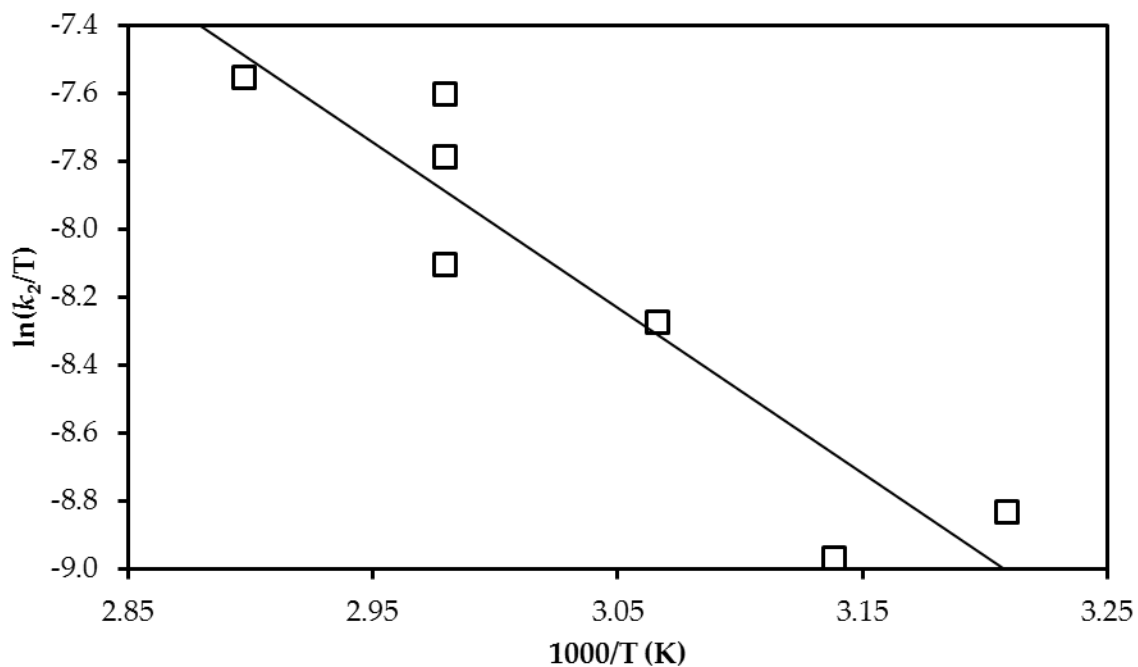


Figure 80: Eyring plot for the conversion of 7.1 ($[7.1]_0 = 0.50 \text{ M}$) to 7.2, catalyzed by HOTf (25 mM) in toluene over the temperature range 39 °C – 72 °C.

Table 17: Observed rate constants for the conversion of 7.1 ($[7.1]_0 = 0.5 \text{ M}$) to 7.2 catalyzed by HOTf in toluene as a function of temperature and [HOTf].

Entry	[HOTf] (mM)	T [°C]	$k_{\text{obs}} (\times 10^3 \text{ m}^{-1} \text{ s}^{-1})$
1	25	62.5	4.2 ± 0.1
2	12.6	62.5	1.54 ± 0.07
3	5.0	62.5	0.511 ± 0.007
4	25	38.5	1.15 ± 0.04
5	25	45.5	1.02 ± 0.03
6	25	53.0	2.10 ± 0.08
7	25	72.0	2.29 ± 0.07

Hartwig and Schlummer have shown that *N*-alkyl-*p*-toluenesulfonamides are quantitatively protonated by triflic acid,¹⁸⁰ consistent with the significantly greater

acidity of HOTf ($pK_a \approx -15$) relative to a protonated sulfonamide ($pK_a \approx -5$);³⁰²⁻³⁰⁴ it is also known that sulfonamides are protonated at nitrogen rather than at oxygen.³⁰⁵⁻

³⁰⁶ Therefore, the active catalytic species in the conversion of **7.1** to **7.2** is most likely an *N*-protonated sulfonamide. Laughlin³⁰³ and Olavi et al.³⁰⁴ have shown that the conjugate acids of *N*-alkyl sulfonamides are more acidic than the conjugate acids of *N,N*-dialkyl sulfonamides by ≈ 0.5 pK_a (H_0) units. However, if **7.1**·HOTf were more acidic than **7.2**·HOTf, deviation from first-order behavior in the conversion of **7.1** to **7.2** would be observed due to the changing composition of the acidic species with increasing conversion. Because no significant deviation from linearity was observed in any of the pseudo first-order plots for the conversion of **7.1** to **7.2** (Figure 78), it appears that the acidity and/or the reactivity of **7.1**·HOTf and **7.2**·HOTf are not significantly different. For these reasons, the rate law for the conversion of **7.1** to **7.2** of $k_2[\mathbf{7.1}][\text{HOTf}]$ is more appropriately described as $\text{rate} = k_2[\mathbf{7.1}][\text{R}_2\text{NTs}\cdot\text{HOTf}]$ ($\text{R}_2\text{NTs} = \mathbf{7.1}$ and $\mathbf{7.2}$).

7.2.2.2 α -Secondary kinetic isotope effect

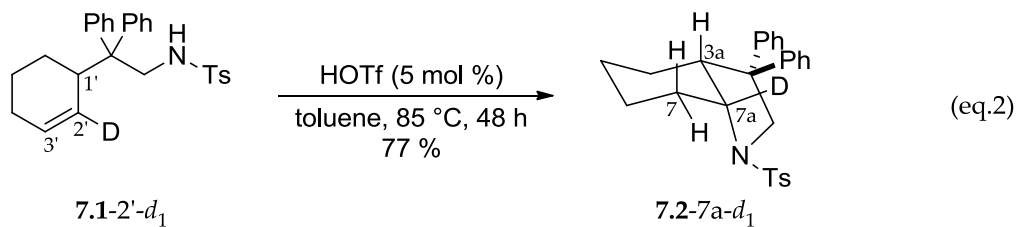
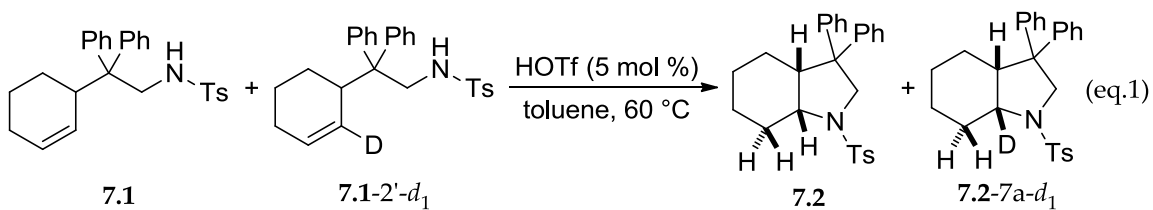
α -Secondary kinetic isotope effects (KIEs) have been utilized to probe for transition-state rehybridization in the elucidation of a range of organic reaction mechanisms.³⁰⁷⁻³¹⁰ As was outlined by Steitwieser et al.,³¹¹ α -secondary KIEs are typically attributed to changes in the stretching and bending frequencies of a C–H bond undergoing ground-state to transition-state rehybridization, although alternative explanations have been presented.³¹²⁻³¹⁴ Because C–H stretching and in-plane bending

frequencies differ little between sp^3 and sp^2 centers, α -KIEs arise primarily from the significantly higher out-of-plane bending frequency of an sp^3 C–H bond ($\approx 1340\text{ cm}^{-1}$) relative to an sp^2 C–H bond ($\approx 800\text{ cm}^{-1}$), which produces a normal KIE in the case of $sp^3 \rightarrow sp^2$ rehybridization and an inverse KIE in the case of $sp^2 \rightarrow sp^3$ rehybridization.

To probe for rehybridization of the C2' carbon atom of the cyclohexenyl moiety in the transition state of the turnover-limiting step of the triflic-acid-catalyzed hydroamination of **7.1**, we determined the α -secondary KIE resulting from deuteration of the C2' carbon atom of the cyclohexenyl moiety employing deuterated isotopomer **7.1-2'-d₁**. Owing to the small magnitude of secondary KIEs³⁰⁷⁻³¹⁰ and to avoid errors associated with variations in catalyst concentration and temperature, the α -secondary KIE was determined through a competition experiment. To this end, an approximate 1:1 mixture of **7.1** and **7.1-2'-d₁** and a catalytic amount of HOTf (5 mol %) in toluene was heated at 60 °C and analyzed periodically by LC-MS (Scheme 60, eq. 1). The concentrations of **7.1** and **7.1-2'-d₁** were determined from the total conversion and from the isotopic ratios **7.1/7.1-2'-d₁** and **7.2/7.2-7a-d₁**. Plots of $\ln[\mathbf{7.1}]$ and $\ln[\mathbf{7.1-2'-d_1}]$ versus time were linear to about three half-lives with observed rate constants of $k_{\text{obs}} = (2.19 \pm 0.03) \times 10^{-3}\text{ s}^{-1}$ and $k_{\text{obs}} = (2.51 \pm 0.05) \times 10^{-3}\text{ s}^{-1}$, respectively (Figure 81), which correspond to an inverse KIE of $k_{\text{D}}/k_{\text{H}} = (1.15 \pm 0.03)$. In a separate experiment, treatment of **7.1-2'-d₁** ($75 \pm 1\%$ d_1 by MS) with a catalytic amount of HOTf (5 mol %) at 85 °C in toluene for 48 h led to isolation of **7.2-7a-d₁** ($76 \pm 1\%$ d_1 by MS) as the exclusive

deuterated isotopomer in 77 % yield without detectable loss or scrambling of deuterium as determined by MS and ^2H NMR analysis [Scheme 60, eq. 2; Figure 74f].

Scheme 60: The HOTf-catalyzed hydroamination of a ~1:1 mixture of 7.1 and 7.1-2'- d_1 to 7.2 and 7.2-7a- d_1 (eq. 1) and the HOTf catalyzed isomerization of 7.1-2'- d_1 to 7.2-7a- d_1 (eq. 2).



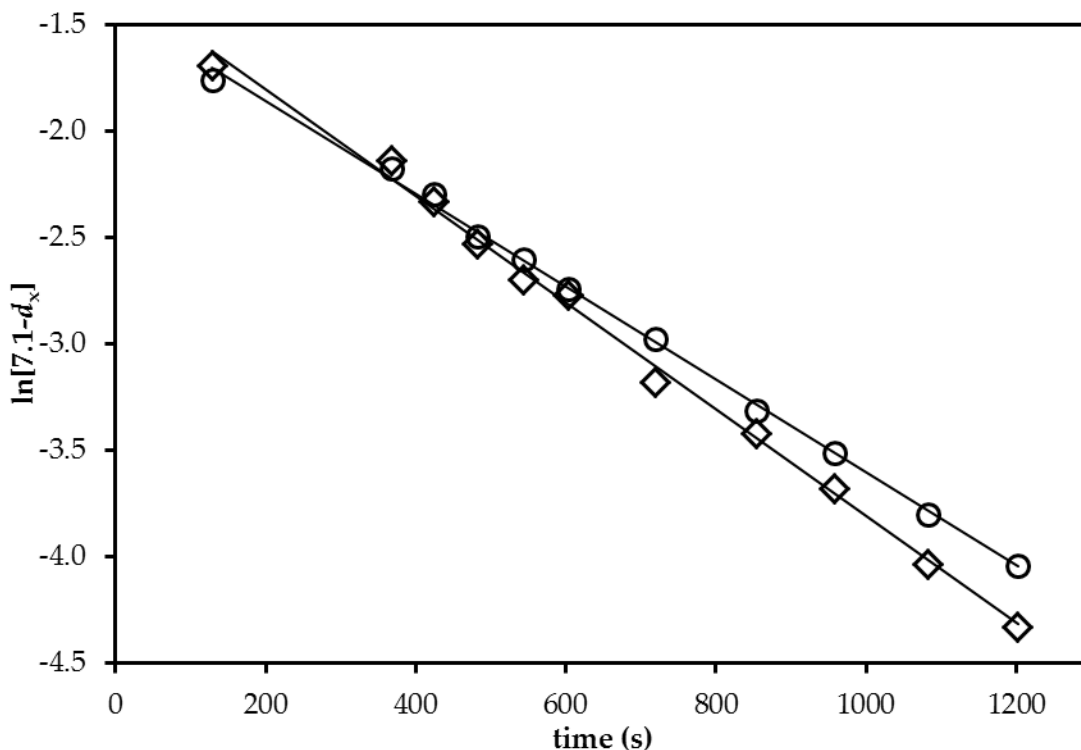


Figure 81: First order plot for the conversion of 7.1 to 7.2 (O) and 7.1-2'- d_1 to 7.2-7a- d_1 (◇) catalyzed by triflic acid (5 mol %) in toluene at 60 °C.

7.2.3 Mechanism of the acid-catalyzed conversion of 7.1 to 7.2

Our experimental observations rule out several potential mechanisms for the acid-catalyzed conversion of 7.1 to 7.2. The absence of deuterium scrambling, alkene isomerization, and/or incorporation of deuterium into unreacted starting material in the acid-catalyzed reactions of isotopomers 7.1-1',3'- d_2 , 7.1-N- d_1 , and 7.1-2'- d_1 argues strongly against mechanisms involving rapid and reversible protonation/deuteration of the C2' or C3' alkenyl carbon atoms followed by turnover-limiting attack of the pendant sulfonamide on a C2' carbenium ion. Furthermore, the *anti* stereoselectivity and the second-order rate law for the conversion of 7.1 to 7.2 rule out a mechanism

analogous to those proposed by Hosomi et al.³⁰⁰⁻³⁰¹ and Hartwig and Schlummer¹⁸⁰ involving intramolecular proton transfer from a protonated sulfonamide to the C3' alkenyl carbon atom followed by trapping of the resulting carbenium ion with the neutral sulfonamide moiety.

We therefore considered mechanisms for the acid-catalyzed conversion of **7.1** to **7.2** initiated by turnover-limiting, irreversible intermolecular proton transfer from a protonated sulfonamide to the C3' alkenyl carbon of **7.1**. Of the possible mechanisms that meet this requirement, stepwise pathways involving a solvationally equilibrated carbenium ion (Ade₂) or a tight ion pair are inconsistent with our experimental observations, as is a stepwise preassociation pathway. Because the regio- and stereoselectivity of the C–N bond formation in the conversion of **7.1** to **7.2** is largely predetermined by the substrate geometry, protonation must occur regio- and stereoselectively at the C3' position of the cyclohexene moiety on the face opposite that occupied by the diphenylethylsulfonamide group. Although delivery of a proton to the less sterically hindered face of the alkene is reasonable, regioselective protonation of the electronically unbiased C=C bond at C3' without participation of the pendant sulfonamide group appears unlikely. Preassociation of the sulfonamide nitrogen atom and the alkene C2' atom prior to intermolecular proton transfer to C3' in a manner analogous to that suggested by Kresge and Chiang²⁶⁸ accounts for the regioselectivity of

the proton transfer only if the nitrogen atom is felt in the transition state for protonation, at which point, the C–H and C–N bond formation become concerted.²⁶⁵⁻²⁶⁷

Key to distinguishing between stepwise and concerted mechanisms for the conversion of **7.1** to **7.2** is the α -secondary KIE of $k_D/k_H = (1.15 \pm 0.03)$ determined for the conversion of **7.1-2'-d₁** to **7.2-7a-d₁**. This observation points to significant C–N bond formation in the turnover-limiting step of the hydroamination and argues strongly against a stepwise pathway involving turnover-limiting carbenium ion formation. The approximation of Streitwieser et al.³¹¹ of the Bigeleisen equation³¹⁵⁻³¹⁷ can be used to calculate a theoretical maximum α -secondary KIE for a re-hybridization event. Using the representative C–H stretching and bending frequencies for the sp² carbon of *cis*-2-butene (2980, 1425, and 852 cm⁻¹ for stretching, in-plane bending, and out of plane bending, respectively) as a model for **7.1** and the sp³ methine carbon of a secondary alcohol as a model for **7.2** (2900, 1340, and 1340 cm⁻¹ for stretching, in-plane bending, and out of plane bending, respectively),³¹⁸ we estimated a maximum α -secondary KIE for the conversion of **7.1** to **7.2** resulting from conversion of an alkene ground state to a tetrahedral transition state of $k_D/k_H \approx 1.20$ at 333 K. Consideration of calculated fractionation factors for the H/D exchange between olefinic and aliphatic positions predicts a similar value.³¹⁹⁻³²¹ Conversely, because conversion of **7.1** to **7.2** through turnover-limiting carbenium ion formation would occur without transition-state rehybridization, such a process should occur without a significant α -secondary KIE.

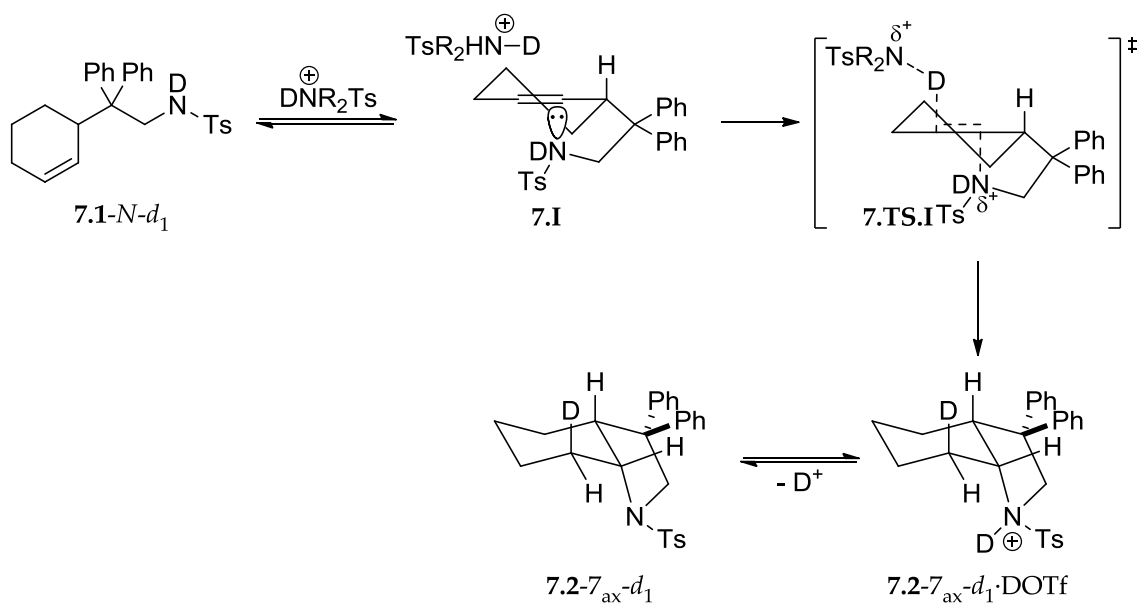
Supporting this contention, the calculated fractionation factor of 1.179 for the H/D exchange between a secondary carbenium ion and secondary alkyl moiety indicates that fractionation factors between an olefinic and carbenium hydrogen differ by only a few percent.³²²

Available experimental data regarding the α -secondary KIEs of the Brønsted acid promoted addition of nucleophiles to alkenes are in accord with the analysis provided above. For example, the thiocyanate-catalyzed isomerization of maleic acid- d_2 to fumaric acid- d_2 displayed an inverse KIE of $k_D/k_H = 1.17$ (corrected for H/D exchange) at 25 °C, attributed to turnover-limiting conjugate addition of thiocyanate to an O-protonated maleic acid.³²³ In contrast, acid-catalyzed hydration of α -deuteriostyrene³²⁴⁻³²⁵ or 4,4-dideuterio-1-phenyl-1,3-butadiene³²⁶ displayed no detectable KIE, consistent with turnover-limiting carbenium ion formation. Acid-catalyzed hydrolysis of ethyl vinyl ether produced a small inverse α -secondary KIE of $k_D/k_H = (1.036 \pm 0.004)$; however, this effect was attributed to an inductive KIE rather than to an α -secondary KIE.³²⁷

All of our experimental observations, including the second-order rate law, activation parameters, inverse α -secondary KIE, and *anti* stereoselectivity are consistent with a concerted mechanism for the conversion of **7.1** to **7.2**. Our proposed mechanism is depicted in Scheme 61 for the DOTf-catalyzed conversion of **7.1-N- d_1** to **7.2-7_{ax}- d_1** . As has been noted by Jencks,²⁶⁵⁻²⁶⁷ preassociation is a necessary prerequisite for concerted reaction pathways, and, as such, conversion of **7.1-N- d_1** to **7.2-7_{ax}- d_1** is likely initiated by

formation of the alkene–sulfonamide encounter complex **7.I**. Intermolecular deuteron transfer from an N-deuterated sulfonamide to the C3' alkenyl carbon atom of **7.1-N-d₁** in concert with an intramolecular *anti* addition of the pendant sulfonamide nitrogen atom to the C2' alkenyl carbon atom through transition state **7.TS.I** would generate the N-deuterated sulfonamide cation **7.2-7_{ax}-d₁·DOTf**. Intermolecular deuteron transfer from **7.2-7_{ax}-d₁·DOTf**, either to a second sulfonamide nitrogen atom or to the C3' carbon atom of a second molecule of **7.1-N-d₁**, would release **7.2-7_{ax}-d₁** and continue the catalytic cycle (Scheme 61).

Scheme 61: Proposed mechanism for the DOTf-catalyzed intramolecular *syn*-hydroamination of **7.1-N-d₁.**



7.3 Summary and conclusions

We have shown that the Brønsted acid catalyzed intramolecular hydrofunctionalization of a cyclohexenyl moiety with a sulfonamide, alcohol, or

carboxylic acid occurs with net *anti* addition of the H-X (X=N, O) bond across the pendant C=C bond of the cyclohexene moiety and without positional isomerization or H/D exchange. Kinetic analysis of the intramolecular hydroamination of the cyclohexenyl sulfonamide derivative **7.1** established a second-order rate law and large negative entropy of activation. Kinetic analysis of the intramolecular hydroamination of deuterated isotopomer **7.1-2'-d₁** revealed an inverse α -secondary KIE of $k_D/k_H = (1.15 \pm 0.03)$, consistent with significant C-N bond formation in the turnover-limiting step of the hydroamination. All of our experimental observations regarding the Brønsted acid catalyzed conversion of **7.1** to **7.2** support a mechanism involving concerted intermolecular transfer of a proton from an *N*-protonated sulfonamide to the C3' carbon atom of **7.1** coupled with intramolecular *anti* addition of the pendant sulfonamide nitrogen atom to the C2' carbon atom. The high *anti* stereoselectivity and the absence of deuterium scrambling in the Brønsted acid catalyzed intramolecular hydroalkoxylation of **7.3-1',3'-d₂** and the hydroacyloxylation of **7.5-1',3'-d₂** suggest that these transformations occur through a similar pathway.

Perhaps the most significant implication of our study is that the stereoselectivity of these Brønsted acid catalyzed intramolecular hydrofunctionalization processes is indistinguishable from that expected for an outer-sphere transition-metal-catalyzed pathway.³²⁸ Furthermore, in the event that Brønsted acids were generated stoichiometrically from a metal precursor, the resulting acid-catalyzed intramolecular

hydrofunctionalization would appear to conform to the second-order rate law: $\text{rate} = [\text{metal}][\text{substrate}]$, apparently consistent with a metal-catalyzed cyclization. The absence of positional isomerization or olefinic H/D exchange would also appear consistent with a metal-catalyzed transformation. As a result, it appears that strong corroborating evidence and/or rigorous control experiments are required to confidently discount the presence of Brønsted acid catalyzed reaction pathways in metal-based alkene hydrofunctionalization processes.

7.4 Experimental

7.4.1 General methods

Acid-catalyzed reactions were performed in glass tubes sealed with a Teflon-coated septum. Room temperature is 23 °C. NMR spectra were obtained on a Varian spectrometer operating at 400 MHz for ^1H NMR and 100 MHz for ^{13}C NMR in CDCl_3 unless noted otherwise. ^2H NMR spectra were recorded in toluene that contained one drop of toluene-*d*8 as reference. IR spectra were obtained on a Bomem MB-100 FT IR spectrometer. Gas chromatography was performed on a Hewlett-Packard 5890 gas chromatograph equipped with a 25 m polydimethylsiloxane capillary column. LCMS was performed on an Agilent Technologies 1100 Series LC/MSD-Trap SL equipped with an Agilent Zorbax C-18 with 3.5 μm particle 1 \times 150 mm column. Flash column chromatography was performed employing 200 - 400 mesh silica gel (EM). Thin layer chromatography (TLC) was performed on silica gel 60 F254. Elemental analyses were

performed by Complete Analysis Laboratories (Parsippany, NJ). Error limits for rate constants refer to the standard deviation of the slope of the respective kinetic plot or from the standard deviation of multiple experiments.

N-(2-Cyclohex-2'-enyl-2,2-diphenylethyl)-*p*-toluenesulfonamide (**7.1**),¹⁴⁰

2-(2'-cyclohexenyl)-2,2-diphenylethanol (**7.3**),³²⁹ 1,3-dideuterio-2-cyclohexen-1-ol,³³⁰ and 2-deuterio-2-cyclohexen-1-ol³³¹ were synthesized employing published procedures.

Ether, methylene chloride, and toluene were purified by passage through columns of activated alumina under nitrogen. Toluene-*d*8 was distilled from sodium/benzophenone ketyl under N₂. Reagents were obtained through major chemical suppliers and were used as received, with the exception of thionylchloride, which was distilled from triphenylphosphite prior to use.

7.4.2 Syntheses of substrates 7.1, 7.3, and 7.5 and isotopomers

7.4.2.1 Syntheses and characterization of isotopomers of 7.1

N-(2-1',3'-Dideuteriocyclohex-2'-enyl-2,2-diphenylethyl)-*p*-toluenesulfonamide

(**7.1-1',3'-d₂**)¹⁴⁰ A solution of 1,3-dideuterio-2-cyclohexen-1-ol (3.0 g, 30 mmol) in ether (80 mL) was added to a solution of thionylchloride (5.2 g, 44 mmol) in ether (30 mL) at room temperature and the resulting solution was stirred for 30 min, quenched with saturated aqueous NaHCO₃, and extracted with ether. The combined ether extracts were washed with brine, dried (MgSO₄), and concentrated to give

1,3-dideuteriod-3-chlorocyclohexene (**7.7**) as a pale yellow oil that used in subsequent steps without further purification.

A solution of diphenylacetonitrile (3.61 g, 18.7 mmol) in DMF (19 mL) was added slowly via syringe to a stirred suspension of sodium hydride (0.45 g, 19 mmol) in DMF (6 mL) at room temperature. The resultant green mixture was stirred for 1 h and cooled to 0 °C. Crude **7.7** (2.22 g, 18.8 mmol) was added dropwise and the mixture was gradually warmed to room temperature and stirred for 8 h. The reaction mixture was poured into an ice/water mixture (100 mL) and extracted with ether (3 x 30 mL). The combined ether extracts were washed with water (2 x 20 mL), dried (MgSO₄), filtered, and concentrated to give diphenyl(1,3-dideuteriocyclohex-2-enyl)acetonitrile (**7.8**) as a white powder that was used in subsequent steps without further purification. ¹H NMR analysis of **7.8** revealed ≥ 95% deuteration at the C1 position and ~85% deuteration at the C3 position.

A solution of crude **7.8** (~18.7 mmol) in diethyl ether (62 mL) was added dropwise to a suspension of LiAlH₄ (2.13 g, 56.1 mmol) in ether (13 mL) at 0 °C. The mixture was refluxed for 16 h, cooled to 0 °C, and treated sequentially with water (2 mL) and 15% aqueous NaOH (2 mL). The resulting suspension was stirred for 30 min, and treated with an additional portion of water (3 mL). The resulting suspension was filtered through a mixture of Celite and MgSO₄, eluting generously with ether. The filtrate was concentrated to give 2-(1',3'-dideuteriocyclohex-2'-enyl)-2,2-diphenylethylamine (**7.9**) as

a viscous yellow oil which was employed in the subsequent step without further purification. ^1H NMR analysis of S3 revealed $\geq 95\%$ deuteration at the C1' position and $\sim 85\%$ deuteration at the C3' position.

A solution of *p*-toluenesulfonyl chloride (3.57 g, 18.7 mmol) and triethylamine (6 mL) in methylene chloride (25 mL) was added via syringe to a solution of crude **7.9** (~ 18.7 mmol). The resultant yellow solution was stirred at room temperature for 6 h and then treated sequentially with water (10 mL) and 1N HCl (10 mL) and extracted with methylene chloride. The combined organic extracts were washed with saturated NaHCO_3 and brine, dried (MgSO_4), and concentrated to give a yellow solid that was recrystallized from hot EtOAc/hexanes to give **7.1-1',3'- d_2** (4.38 g, 54% over 3 steps) as a colorless crystals. Mass spectral analysis of **7.1-1',3'- d_2** (corrected for ^{13}C isotopomers) revealed an 83:17 mixture of d_2 ($m/z = 434.2$) and d_1 ($m/z = 433.3$) isotopomers. ^1H NMR analysis of **1a-1',3'- d_2** revealed $\sim 95\%$ deuteration of the C1' position (δ 3.22) and $\sim 85\%$ deuteration of the C3' ($\delta \sim 5.60$) position of the cyclohexenyl substituent.

For 7.7: ^1H NMR (400 MHz): δ 7.48 (d, $J = 8.4$ Hz, 2 H), 7.37 (d, $J = 8.4$ Hz, 2 H), 7.32-7.15 (m, 6 H), 5.87-5.82 (m, ~ 0.15 H), 5.46 (s, 1 H), 2.07 – 1.91 (m, 2 H), 1.81-1.73 (m, 1 H), 1.54-1.38 (m, 3 H).

For 7.8: ^1H NMR (400 MHz): δ 7.31-7.15 (m, 10 H), 5.78 (s, 1 H), 5.63-5.57 (m, ~ 0.15 H), 4.75(br s, 2 H), 3.42 (d, $J = 13.2$ Hz, 1 H), 3.25 (d, $J = 13.2$ Hz, 1 H), 1.88 – 1.71 (m, 1 H), 1.70-1.36 (m, 4 H), 0.94 (dt, $J = 4, 12$ Hz, 1 H).

For 7.1-1',3'-d₂: ¹H NMR: δ 7.52 (d, *J* = 8.0 Hz, 2 H), 7.28-7.20 (m, 8 H), 7.12-7.08 (m, 4 H), 5.69 (s, 1 H), 5.62-5.58 (m, ~0.17 H), 3.85 (dd, *J* = 5.4, 7.6 Hz, 1 H), 3.61 (dd, *J* = 7.6, 11.6 Hz, 1 H), 3.50 (dd, *J* = 5.4, 11.6 Hz, 1 H), 2.41 (s, 3 H), 1.90-1.72 (m, 2 H), 1.69-1.56 (m, 1 H), 1.55-1.37 (m, 2H), 0.88 (dt, *J* = 2.8, 12.1 Hz, 1 H). ¹³C{¹H} NMR: δ 143.3, 143.1, 141.2, 136.1, 129.6, 129.2, 129.1, 128.3, 128.0, 127.9, 127.4, 127.0, 126.8, 126.5, 54.0, 50.1, 38.7 (t, *J* = 18 Hz), 24.9, 24.7, 24.3, 22.0, 21.5 (C3' carbon not observed). MS (ESI, M⁺): 434.2 (83%), 433.3 (17%).

***N*-Deuterio-*N*-(2-cyclohex-2'-enyl-2,2-diphenylethyl)-*p*-toluenesulfonamide (7.1-*N*-d₁).** A biphasic mixture of **7.1** (220 mg, 0.50 mmol), toluene-*d*₈ (1.0 mL), and D₂O (1.0 mL) was stirred at room temperature for 30 min. An aliquot (0.50 mL) of the organic layer was removed via syringe and transferred to an oven-dried NMR tube capped with a rubber septum and was analyzed by NMR spectroscopy without further isolation. This same sample was employed in acid-catalyzed deuterioamination without further purification. Owing to the nominal solubility of water in toluene (0.033%), this sample also contained 7.9 μmol (~16 mM) D₂O. ¹H NMR analysis of **7.1-*N*-d₁** revealed ~90 % deuteration of the sulfonamide nitrogen atom. ¹H NMR (toluene-*d*₈): δ 7.63 (d, *J* = 7.5 Hz, 2 H), 7.22-7.07 (m, 10 H), 6.90 (d, *J* = 8.0 Hz, 1 H), 5.85 (d, *J* = 10.5 Hz, 1 H), 5.64-5.58 (m, 1 H), 3.82 (d, *J* = 11.8 Hz, 1 H), 3.67 (d, *J* = 11.8 Hz, 1 H), 3.38-3.30 (m, 1 H), 2.09 (s, 3 H), 1.97-1.90 (m, 1 H), 1.84-1.75 (m, 1 H), 1.64-1.42 (m, 3 H), 1.10-1.01 (m, 1 H). ²H NMR (toluene): δ 4.24.

***N*-(2-2'-deuteriocyclohex-2'-enyl-2,2-diphenylethyl)-*p*-toluenesulfonamide (7.1-2'-*d*₁)**. A solution of 2-deuterio-2-cyclohexen-1-ol (2.6 g, 26 mmol) in ether (70 mL) was added to a solution of thionyl chloride (4.7 g, 40 mmol) in ether (16 mL) at room temperature. The resulting solution was stirred for 90 min, quenched with satd. NaHCO₃ (aq), and extracted with ether. The combined ether extracts were washed with brine, dried (MgSO₄), filtered, and concentrated to give 2-deuterio-3-chlorocyclohexene (7.10) as a pale yellow oil that was employed in subsequent steps without further purification.

Isotopomer 7.1-2'-*d*₁ was prepared in 64% yield from 7.10 using a procedure analogous to that used for preparation of sulfonamide 7.1. Mass spectral analysis of 7.1-2'-*d*₁ (corrected for ¹³C isotopomers) revealed a 75:25 mixture of *d*₁ (*m/z* = 433.3) and *d*₀ (*m/z* = 432.2) isotopomers. ¹H NMR: δ 7.48 (d, *J* = 8 Hz, 2 H), 7.24-7.14 (m, 8 H), 7.07-7.00 (m, 4 H), 5.64 (d, *J* = 10.8 Hz, 0.2 H), 5.60-5.48 (m, 1 H), 3.79 (dd, *J* = 5.6, 7.2 Hz, 1 H), 3.55 (dd, *J* = 7.6, 11.6 Hz, 1 H), 3.40 (dd, *J* = 5.2, 11.6 Hz, 1 H), 3.21-3.12 (m, 1 H), 2.35 (s, 3 H), 1.84-1.65 (m, 2 H), 1.62-1.50 (m, 1 H), 1.48-1.32 (m, 2 H), 0.87-0.76 (m, 1 H). ²H NMR (toluene): δ 3.73. ¹³C{¹H} NMR (*d*₁ isotopomer only): δ 143.5, 143.2, 141.4, 136.2, 129.8, 129.5, 129.4, 129.2, 128.5, 127.9 (br m), 127.6, 127.2, 126.9, 126.7, 54.2, 50.2, 39.2, 25.0, 24.5, 22.2, 21.6. MS (ESI, M⁺): 433.3 (75%), 432.2 (25%).

7.4.2.2 Syntheses and characterization of isotopomers of 7.3 and 7.5

2-(1',3'-Dideuteriocyclohex-2'-enyl)-2,2-diphenylethanol (7.3-1',3'-*d*₂).

Isotopomer 7.3-1',3'-*d*₂ was synthesized in 80% yield over two steps from 7.7 using a procedure similar to that used to prepare protio isotopomer 7.3. Mass spectral analysis of 7.3-1',3'-*d*₂ (corrected for ¹³C isotopomers) established a 96:4 mixture of *d*₂ [*m/z* = 263.1 (*M*⁺ - H₂O)] and *d*₁ [*m/z* = 262.1 (*M*⁺ - H₂O)] isotopomers. ¹H NMR analysis of 7.3-1',3'-*d*₂ revealed ≥ 95% deuteration of the C1' and C3' positions of the cyclohexenyl substituent. ¹H NMR: δ 7.37-7.18 (m, 10 H), 5.78 (s, 1 H), 4.20 (dd, *J* = 1.2, 6.8 Hz, 2 H), 1.92-1.47 (m, 5 H), 1.16 (t, *J* = 7.0 Hz, 1 H), 1.04 (dt, *J* = 3.2, 12.4 Hz, 1 H). ¹³C{¹H} NMR: δ 144.2, 124.5, 129.5, 129.4, 128.9, 128.0, 127.5, 126.3, 126.2, 68.1, 56.0, 38.6 (t, *J* = 14.9 Hz), 24.9, 24.8, 22.4, (C3' carbon not observed). MS (ESI, *M*⁺ - H₂O): 263.1 (96%), 262.1 (4%).

2-(2-Cyclohexenyl)-2,2-diphenylacetic acid (7.5). Diisopropylcarbodiimide (0.73 g, 5.8 mmol) was added to a solution of 2-cyclohexen-1-ol (0.50 g, 5.1 mmol), diphenylacetic acid (1.38 g, 6.50 mmol), and DMAP (65 mg, 0.53 mmol) in CH₂Cl₂ (16 mL) at 0 °C and the resulting suspension was stirred for 2 h at 0 °C and 1 h at room temperature. The resulting suspension was filtered and the filtrate was concentrated under vacuum to give an oily residue that was chromatographed (SiO₂; hexanes:EtOAc = 99:1) to give 2-cyclohexenyl-2,2-diphenylacetate (7.11) (1.41 g, 97 %) as a white solid that was used in subsequent steps without further purification.

A solution of *n*-BuLi (3.90 mL, 2.47 M in hexanes, 9.63 mmol) was added dropwise to a stirred solution of diisopropylamine (1.01 g, 9.93 mmol) in THF (20 mL) at -78 °C and stirred for 30 minutes with gradual warming to 0 °C. The resulting solution was then transferred into a solution of **7.11** in THF (50 mL) at -78 °C to form a bright yellow solution that was stirred for 1 h at -78 °C. Chlorotrimethylsilane (1.1 g, 10 mol) was added to the reaction mixture via syringe and the resulting solution was stirred 1 h at -78 °C, warmed to 45 °C over 2 h, and stirred for 10 h. The resulting mixture was cooled to 0 °C, treated with 1N HCl, stirred for 45 min at 0 °C, warmed to room temperature, and extracted with ether. The combined ether extracts were washed with 1N HCl and brine, dried (MgSO₄), and concentrated. Chromatography (SiO₂; 15% ether in pentane) of the residue gave **7.5** (0.96 g, 68 %) as a white solid.

For 7.11: TLC (hexanes:EtOAc = 99:1): R_f = 0.30. ¹H NMR: δ 7.32-7.21 (m, 10 H), 5.92 (dt, J = 1.2, 10 Hz, 1 H), 5.71-5.66 (m, 1 H), 5.32-5.30 (m, 1 H), 5.00 (s, 1 H), 2.09-1.89 (m, 2 H), 1.88-1.79 (m, 1 H), 1.73-1.53 (m, 3 H). ¹³C{¹H} NMR: δ 172.2, 139.0, 133.1, 128.8, 128.7, 128.7, 128.6, 127.3, 125.5, 69.1, 57.4, 28.3, 25.0, 18.9. HRMS calcd (found) for C₂₄H₂₈O₂ (M⁺): 292.1463 (292.1465).

For 7.5: TLC (pentane:ether = 8:1): R_f = 0.30. ¹H NMR: δ 10.8 (br s, 1 H), 7.34-7.23 (m, 10 H), 5.67 (br d, J = 10.5, 1 H), 5.62-5.57 (m, 1 H), 3.81-3.75 (m, 1 H), 1.94-1.81 (m, 2 H), 1.72-1.63 (m, 1 H), 1.58-1.48 (m, 1 H), 1.42 (br s, 1 H), 1.02 (dq, J = 3.0, 12.5 Hz, 1 H).

$^{13}\text{C}\{^1\text{H}\}$ NMR: δ 179.0, 140.8, 139.7, 130.4, 130.4, 129.8, 128.1, 127.8, 127.4, 127.2, 127.0, 64.6, 40.0, 25.8, 25.2, 22.1. HRMS calcd (found) for $\text{C}_{24}\text{H}_{28}\text{O}_2$ (M^+): 292.1463 (292.1465).

2-(1',3'-Dideuteriocyclohex-2'-enyl)-2,2-diphenylacetic acid (7.5-1',3'- d_2).

Isotopomer 7.5-1',3'- d_2 was synthesized in 65 % yield from 1,3-dideuterio-2-cyclohexen-1-ol and employing a procedure analogous to that used for preparation of 7.5. Mass spectral analysis of 7.5-1',3'- d_2 (corrected for ^{13}C isotopomers) established a >99:<1 mixture of d_2 [$m/z = 294.2$ (M^+)] and d_1 [$m/z = 293.2$ (M^+)] isotopomers. ^1H NMR analysis of 7.5-1',3'- d_2 revealed $\geq 95\%$ deuteration of the C1' and C3' positions of the cyclohexenyl substituent.

For 7.11- d_2 : ^1H NMR: δ 7.35-7.23 (m, 10 H), 5.71 (s, 1 H), 5.02 (s, 1 H), 2.10-1.91 (m, 2 H), 1.89-1.81 (m, 1 H), 1.74-1.54 (m, 3 H). $^{13}\text{C}\{^1\text{H}\}$ NMR: δ 172.1, 130.9, 132.7 (t, $J = 18$ Hz), 128.61, 128.56, 128.5, 128.4, 127.1, 125.1, 68.3 (br t), 57.2, 28.0, 24.7, 18.7.

For 7.5-1',3'- d_2 : TLC (hexanes:EtOAc = 4:1): $R_f = 0.25$. ^1H NMR: δ 10.85 (br s, 1 H), 7.38-7.21 (m, 10 H), 5.68 (s, 1 H), 1.97-1.80 (m, 2 H), 1.74-1.62 (m, 1 H), 1.60-1.49 (m, 1 H), 1.48-1.32 (m, 1 H), 1.03 (dt, $J = 2.5, 12.2$ Hz, 1 H). $^{13}\text{C}\{^1\text{H}\}$ NMR: δ 180.4, 140.6, 139.6, 130.5, 130.4, 129.5 (t, $J = 5.3$), 128.0, 127.7, 127.4, 127.1, 127.0, 64.6, 39.5 (t, $J = 14.5$), 25.7, 25.0, 22.0. HRMS calcd (found) for $\text{C}_{20}\text{H}_{18}\text{D}_2\text{O}_2$ (M^+): 294.1589 (294.1587). MS (ESI, M^+): 294.2 (99.5%), 293.2 (0.5%).

7.4.3 Acid-catalyzed hydrofunctionalizations and characterizations of bicyclic products.

7.4.3.1 Synthesis and characterization of 7.2 and isotopomers

rac-(3*aR*,7*aR*)-3,3-Diphenyl-1-(*p*-toluenesulfonyl)-octahydroindole.¹⁴⁰ To a solution of 7.1 (64.7 mg, 0.150 mmol) in toluene (0.3 mL), triflic acid (0.7 μ L, 7.5×10^{-3} mmol) was added through a syringe. The resulting solution was heated at 60 °C for 3 h, cooled to room temperature, and filtered through a plug of silica gel. The solvent was evaporated under vacuum to give pure 7.2 (64.5 mg, 100 %) as a white solid. Slow evaporation of a toluene solution of 7.2 gave crystals of 7.2 suitable of X-ray diffraction (Figure 73) ¹H NMR (800 MHz, CDCl₃, 45 °C): δ = 7.43 (d, J = 8.0 Hz, 2 H), 7.19 (t, J = 8.0 Hz, 2 H), 7.09 (t, J = 8.0 Hz, 1 H), 7.07–6.98 (m, 9 H), 4.48 (d, J = 11.1 Hz, 1 H; H₂), 4.25 (d, J = 11.1 Hz, 1 H; H₂), 3.78 (m, 1 H; H_{7a}), 2.95 (dt, J = 10.4, 4.8 Hz, 1 H; H_{3a}), 2.49 (br d, J = 14.4 Hz, 1 H; H_{7eq}), 2.32 (s, 3 H), 1.58 (m, 1 H; H_{7ax}), 1.55–1.41 (m, 4 H; H₅, H₆), 1.28–1.15 ppm (m, 2 H; H₄); ¹³C{¹H} NMR (126 MHz, CDCl₃, 25 °C): δ = 145.1, 143.8, 142.8, 134.2, 129.3, 128.5, 128.4, 127.6, 127.1, 126.7, 126.1, 125.7, 59.1, 58.2, 55.5, 44.3, 28.8, 25.5, 24.5, 21.5, 20.1 ppm.

All remaining acid-catalyzed hydrofunctionalization reactions were performed employing analogous procedures.

X-ray data for 7.2: Monoclinic, P2(1)/c, $T = 296$ K, $a = 8.8385(10)$ Å, $b = 26.705(3)$ Å, $c = 9.4913(11)$ Å, $\beta = 94.690(8)^\circ$, $V = 2232.8(5)$ Å³, $Z = 4$, $R[F_2 > 2\sigma(F_2)] = 0.042$, $wR(F_2) = 0.138$. CCDC-798744 contains the supplementary crystallographic data for this chapter.

These data can be obtained free of charge from The Cambridge Crystallographic Data Centre via www.ccdc.cam.ac.uk/data_request/cif.

Assignment of aliphatic protons of 7.2. The aliphatic protons of **7.2** were unambiguously assigned on the basis of combined ^1H - ^1H (800 MHz) COSY and ^1H - ^1H NOESY analysis at 45 °C in CDCl_3 (Figures 82 – 84). Relevant $^2J_{\text{HH}}$ and $^3J_{\text{HH}}$ coupling constants (Figures 82 - 83) were determined from these spectra and from ^1H NMR analysis of deuterated isotopomers **7.2-3a,7_{eq}-d₂** and **7.2-7_{ax}-d₁**. Central to the determination of the relative configuration of the deuterated isotopomers **7.2-3a,7_{eq}-d₂** and **7.2-7_{ax}-d₁** is the assignment of protons H7_{ax} and H7_{eq}. As noted in the text, neither the through-bond nor through-space interactions of H7_{ax} and H7_{eq} with H7a proved reliable for assigning H7_{ax} and H7_{eq}. Rather, these protons were assigned by the presence of a strong NOESY cross peak between the axial tertiary proton H3a [δ 2.95 (td, J = 4.8, 10.4 Hz)] and H7_{ax} [δ 1.58 (m, 1 H)] and the absence of a cross peak between H3a and H7_{eq} [δ 2.49 (br d, J = 14.4 Hz)] (Figure 84).

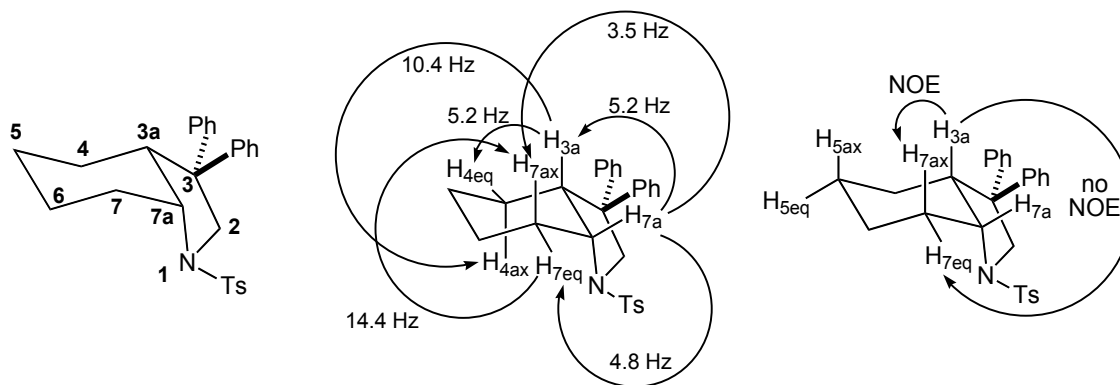


Figure 82: Numbering scheme (left structure), relevant ^1H - ^1H coupling constants (center structure), and key NOESY interactions (right structure) for compound 7.1.

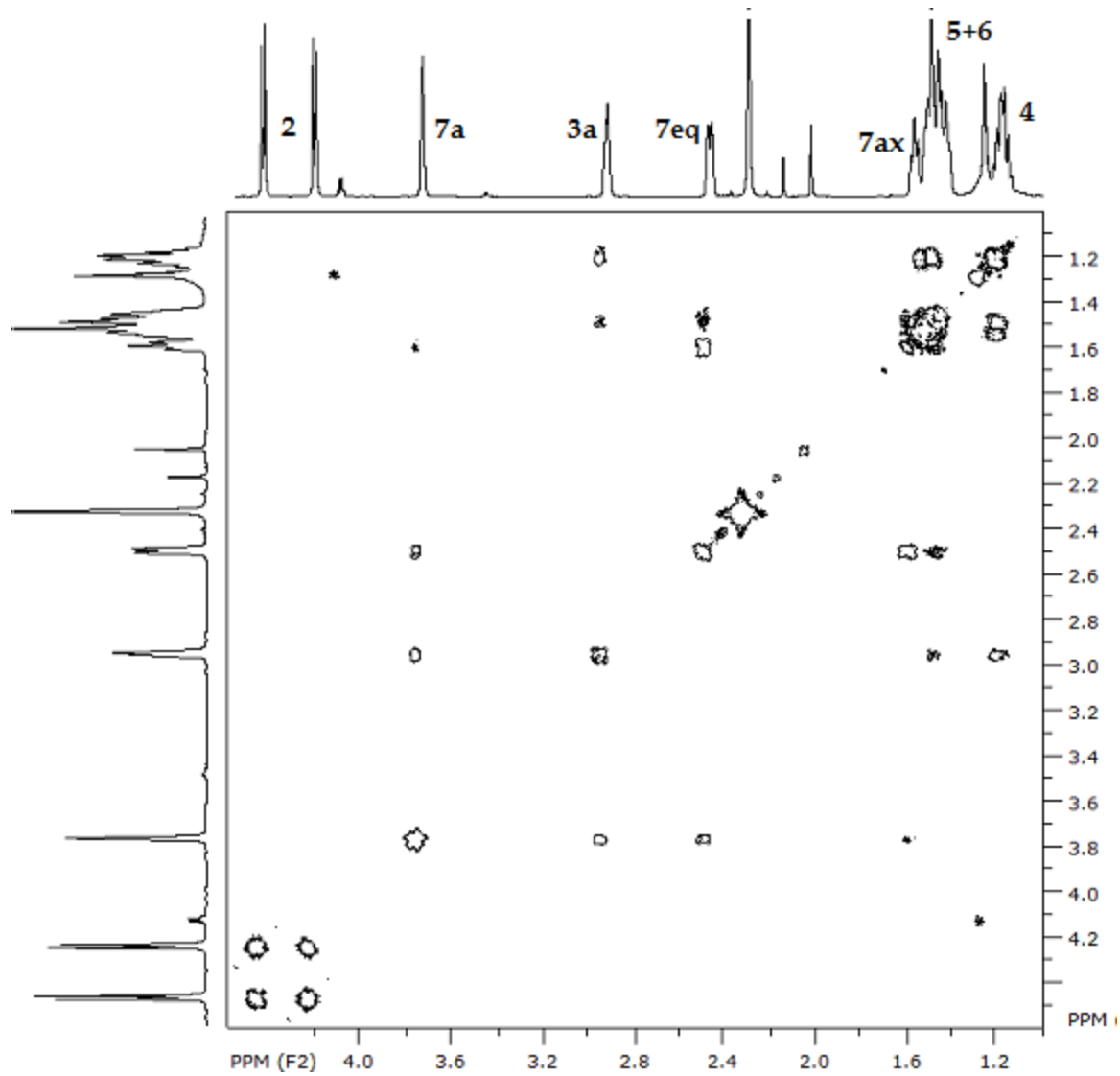


Figure 83: ^1H - ^1H COSY (800 MHz) NMR spectrum of 7.2 at 45 °C in CDCl_3 .

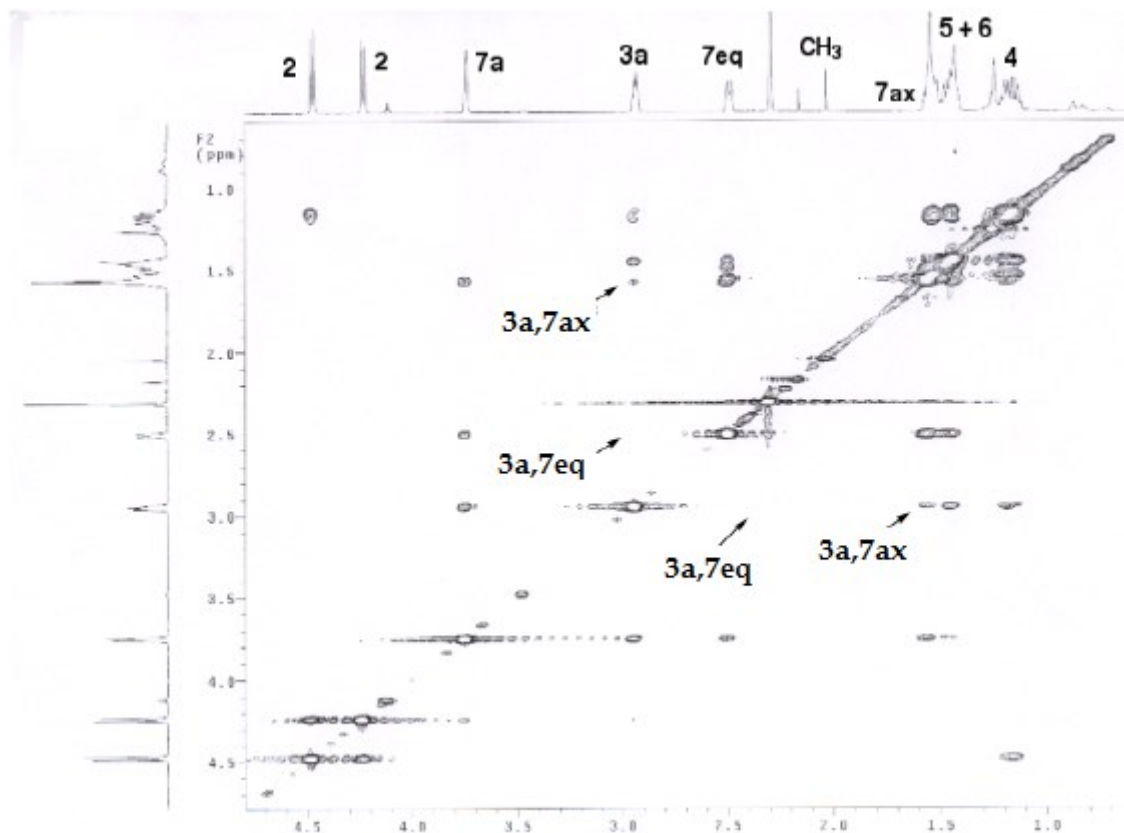


Figure 84: ^1H - ^1H NOESY (800 MHz) NMR spectrum of 7.2 at 25 °C in CDCl_3 .

rac-(3aR,7R,7aR)-3,3-Diphenyl-1-(*p*-toluenesulfonyl)-(3a,7- $^2\text{H}_2$)-octahydro-1H-indole (7.2-3a,7eq- d_2). Reaction of 7.1-1',3'- d_2 (65 mg, 0.15 mmol; 83% d_2 , 17% d_1 by MS) with triflic acid (0.7 μL , 7.5×10^{-3} mol) in toluene (0.3 mL) at 85 °C for 48 h led to isolation of 7.2-3a,7eq- d_2 (62 mg, 96 %) as a white solid. Mass spectral analysis (corrected for ^{13}C isotopomers) established an 83:16 ratio of d_2 [$m/z = 434.2$ (M^+)] and d_1 [$m/z = 433.3$ (M^+)] isotopomers. ^1H NMR analysis of 7.2-3a,7eq- d_2 revealed ~95 % deuteration of the C3a (δ 2.95) position and ~85% deuteration of the C7_{eq} (δ 2.49) position with no detectable (<5 %) accumulation of deuterium at the C7_{ax} or C7a positions (Figure 74,

spectrum b). ^2H NMR displayed a ~1:1 ratio of resonances at δ 2.96 and δ 2.51 corresponding to the C3a and C7_{eq} positions with no detectable (<5 %) accumulation of deuterium at the C7_{ax} or C7a positions (Figure 74, spectrum c). ^1H NMR (500 MHz, 25 °C): δ 7.40 (d, J = 8 Hz, 2 H), 7.17 (t, J = 8 Hz, 2 H), 7.07 (tt, J = 1.0, 6.0 Hz, 1 H), 7.05-6.95 (m, 9 H), 4.47 (d, J = 11.0 Hz, 1 H), 4.22 (d, J = 11.0 Hz, 1 H), 3.73 (d, J = 3.5, 1 H), 2.29 (s, 3 H), 1.60-1.35 (m, 5 H), 1.26-1.08 (m, 2 H). ^2H NMR (76 MHz, CHCl_3): δ 2.96, 2.51 (~1:1). $^{13}\text{C}\{^1\text{H}\}$ NMR (126 MHz, CDCl_3): δ 145.2, 143.9, 142.8, 134.3, 129.4, 128.6, 128.5, 127.6, 127.2, 126.7, 126.2, 125.7, 59.0, 58.2, 55.4, 43.8 (t, J = 16 Hz), 28.5 (t, J = 16 Hz), 25.5, 24.5, 21.5, 20.1. MS (ESI, M^+): 434.2 (83%), 433.3 (16%).

***rac*-(3aR,7S,7aR)-3,3-Diphenyl-1-(*p*-toluenesulfonyl)-(3a,7- $^2\text{H}_2$)-octahydro-1H-indole (7.2-7_{ax}- d_1).** Triflic acid-*O-d* (1.3 μL , 0.015 mmol) was added via syringe to an NMR tube that contained a solution of 7.1-*N-d*₁ (0.25 mmol; 90% *d* by ^1H NMR) in toluene-*d*₈ (0.50 mL). The resulting solution was heated at 60 °C for 3 h and monitored periodically by ^1H NMR spectroscopy. The resulting solution was filtered through a plug of silica gel and solvent was evaporated under vacuum to give pure 7.2-7_{ax}- d_1 (84 mg, 77 %) as a white solid. Mass spectral analysis (corrected for ^{13}C isotopomers) established a 90:10 mixture of d_1 [m/z = 433.3 (M^+)] and d_0 [m/z = 432.2 (M^+)] isotopomers. ^1H NMR analysis of 7.2-7_{ax}- d_1 revealed ~90 % deuteration of the C7_{ax} position with no detectable (< 5%) accumulation of deuterium at the C7_{eq} or C7a positions (Figure 74, spectrum d). Likewise, ^2H NMR analysis of 7.2-7_{ax}- d_1 displayed a single resonance at δ

1.50 corresponding to the C7_{ax} position with no detectable (< 5%) accumulation of deuterium at the C7_{eq} or C7a positions (Figure 74, spectrum e). ¹H NMR: δ 7.41 (d, *J* = 8.4, 2 H), 7.19 (t, *J* = 7.4 Hz, 2 H), 7.12-6.95 (m, 10 H), 4.49 (d, *J* = 11.1 Hz, 1 H), 4.25 (d, *J* = 11.1 Hz, 1 H), 3.75 (t, *J* = 4.8 Hz, 1 H), 2.95 (td, *J* = 5.2, 10.4 Hz, 1 H), 2.51-2.45 (m, 1 H), 2.31 (s, 3 H), 1.57-1.48 (m, 4 H), 1.26-1.08 (m, 2 H). ²H NMR (76 MHz, toluene): δ 1.50. MS (ESI, M⁺): 433.3 (90%), 432.2 (10%).

Analysis of unreacted starting material in the DOTf-catalyzed cyclization of 7.1-*N-d*₁ Triflic acid-*O-d* (1.7 μL, 0.019 mmol) was added via syringe to an NMR tube that contained a solution of 7.1-*N-d*₁ (0.25 mmol) in toluene that contained a drop of toluene-*d*₈. The resulting solution was heated at 60 °C, monitored by ²H NMR to ~ 50% conversion, and quenched by addition of triethylamine (4 μL). A similar experiment that utilized ¹H NMR analysis of a toluene-*d*₈ solution of 7.1-*N-d*₁ and a catalytic amount of DOTf was performed concurrently. ²H NMR analysis of the former solution after quench displayed resonances at δ 4.5, corresponding to the *N-D* resonance of unreacted 7.1-*N-d*₁ and δ 1.58 corresponding to the D7_{ax} resonance of 7.2-7a-*d*₁ (Figure 75). There was no detectable (< 5 %) accumulation of deuterium at the C2' or C3' alkenyl positions of 7.1-*N-d*₁ (δ 5.8 and 5.6) or at the C7_{eq} or C7a position of 7.2-7a-*d*₁. ¹H NMR analysis of the latter solution after quench displayed resonances corresponding to the protons of 7.1-*N-d*₁ and 7.2-7a-*d*₁ with no evidence of positional isomerization of 7.1-*N-d*₁.

***rac*-(3aR,7aR)-3,3-Diphenyl-1-(*p*-toluenesulfonyl)-(7a-²H)-octahydro-1H-indole**

(7.2-7a-*d*₁) Reaction of **7.1-2'-*d*₁** (65 mg, 0.15 mmol; 25% *d*₀, 75% *d*₁ by MS) with triflic acid (0.7 μL, 7.5 × 10⁻³ mol) in toluene (0.3 mL) at 60 °C for 3 h led to isolation of **7.2-7a-*d*₁** (63 mg, 96%) as a white solid. Mass spectral analysis of **7.2-7a-*d*₁** (corrected for ¹³C isotopomers) established a 76:24 mixture of *d*₁ [*m/z* = 433.3 (M⁺)] and *d*₀ [*m/z* = 432.2 (M⁺)] isotopomers. ¹H NMR analysis of **7.2-7a-*d*₁** revealed ~75 % deuteration of the C7a position (δ 3.78) with no detectable (<5%) accumulation of deuterium at the C7_{eq} or C7_{ax} positions (Figure 74, spectrum f). ²H NMR analysis of **7.2-7a-*d*₁** revealed a single resonance corresponding to deuteration of the C7a position at δ 3.78 with no detectable (< 5 %) accumulation of deuterium at the C7_{eq} or C7_{ax} positions. ¹H NMR (500 MHz): δ 7.42 (d, *J* = 8 Hz, 2 H), 7.19 (t, *J* = 7.5 Hz), 7.12-6.94 (m, 10 H), 4.49 (d, *J* = 11 Hz, 1 H), 4.27 (d, *J* = 11 Hz, 1 H), 3.79-3.74 (m, 0.22 H), 2.98-2.93 (m, 1 H), 2.52 (d, *J* = 13.5 Hz, 1 H), 2.31 (s, 3 H), 1.62-1.40 (m, 5 H), 1.29-1.10 (m, 2 H). ²H NMR (CHCl₃): δ 3.78. ¹³C{¹H} NMR: δ 145.2, 143.9, 142.8, 134.3, 129.3, 128.6, 128.4, 127.6, 127.1, 126.7, 126.1, 125.7, 59.1, 58.7 (t, *J* = 21 Hz), 58.2, 55.5, 44.3, 44.2, 28.8, 28.6, 25.5, 24.6, 21.5, 20.1. MS (ESI, M⁺): 433.3 (76%), 432.2 (24%).

7.4.3.2 Synthesis and characterization of 7.4 and isotopomers

***rac*-(3aR,7aR)-3,3-Diphenyloctahydrobenzofuran (7.4)** A solution of **7.3** (42 mg, 0.15 mmol) and triflic acid (0.7 μL, 7.5 × 10⁻³ mol) in toluene (0.3 mL) was heated at 60 °C for 3 h to give **7.4** (39 mg, 93 %) as a white solid. ¹H NMR: δ 7.36 (br d, *J* = 7.5 Hz, 2 H),

7.21-7.15 (m, 4 H), 7.10-7.04 (m, 4 H), 4.78 (d, $J = 8.5$ Hz, 1 H, H_2), 4.66 (d, $J = 8.5$ Hz, 1 H, H_2), 4.14-4.11 (m, 1 H, H_{7a}), 2.71 (ddd, $J = 4.3, 5.7, 10.2$ Hz, 1 H, H_{3a}), 1.89 (br d, $J = 13.5$ Hz, 1 H, H_{7eq}), 1.66 - 1.50 (m, 2 H, H_{4eq} and H_{5eq}), 1.46-1.31 (m, 3 H, H_{7ax} and H_6), 1.11 (tq, $J = 3.2, 12.6$ Hz, 1 H, H_{5ax}), 0.91 (dq, $J = 3.4, 12.9$ Hz, 1 H, H_{4ax}). $^{13}\text{C}\{^1\text{H}\}$ NMR: δ 146.5, 143.7, 128.6, 128.3, 126.9, 126.2, 126.1, 76.4, 74.6, 59.7, 44.6, 29.0, 25.8, 24.6, 20.2, (one carbon resonance obscured).

Assignment of Aliphatic Protons of 7.4 The aliphatic protons of **7.4** were assigned on the basis of combined ^1H , ^1H - ^1H COSY and ^1H - ^1H NOESY analysis (Figures 85 – 87). In contrast to the analyses of **7.2** and **7.4**, the NOESY spectrum of **7.4** displayed no distinguishing cross peak between H_{3a} and H_{7ax} (Figure 87). Rather, these protons were assigned by the presence of a NOESY cross peak between the axial tertiary proton H_{5ax} (δ 1.11) and H_{7ax} (δ 1.4) and the absence of a cross peak between H_{5ax} (δ 1.11) and H_{7eq} (δ 1.89) (Figure 87).

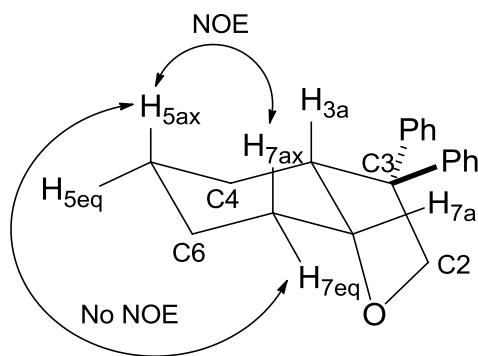


Figure 85: Numbering scheme and key NOESY interactions for compounds 7.4.

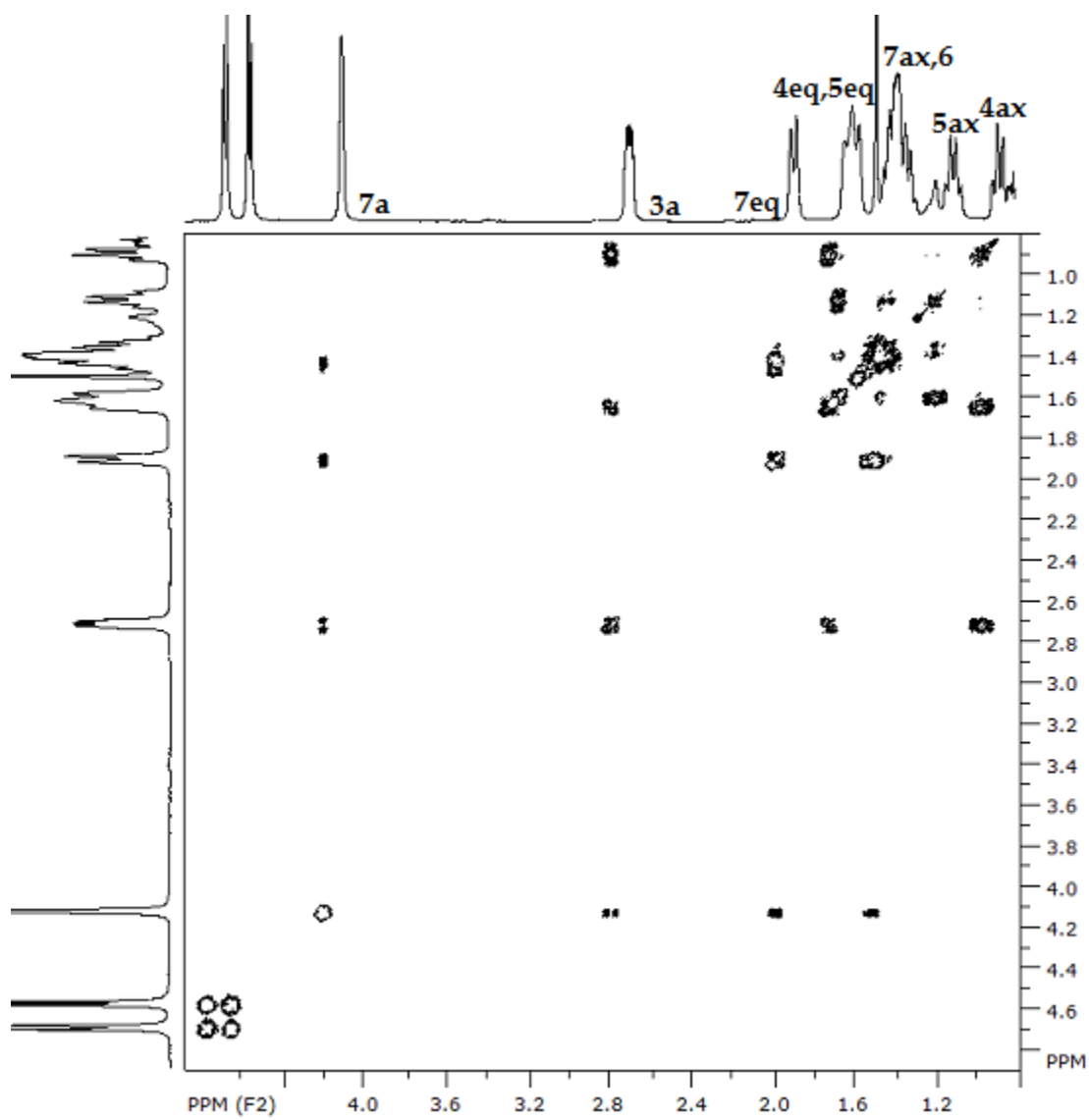


Figure 86: ^1H - ^1H COSY (500 MHz) NMR spectrum of 7.4 at 25 °C in CDCl_3 .

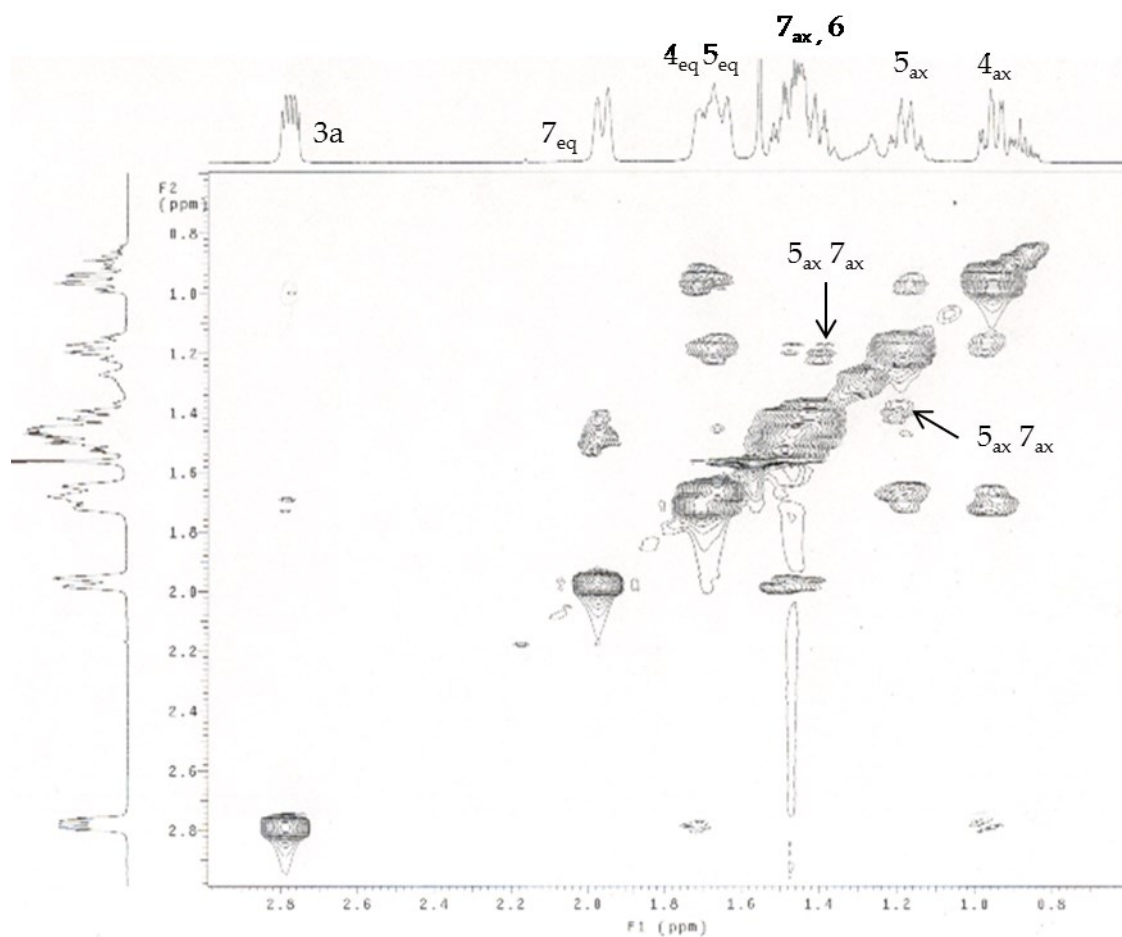


Figure 87: ^1H - ^1H NOESY (500 MHz) NMR spectrum of 7.4 at 25 °C in CDCl_3 .

rac-(3aR,7R,7aR)-3,3-Diphenyl-(3a,7- $^2\text{H}_2$)-octahydrobenzofuran (7.4-3a,7eq- d_2).

Treatment of 7.3-1',3'- d_2 (42 mg, 0.150 mmol, 96% d_2 by MS) with triflic acid (0.7 μL , 7.5×10^{-3} mol) in toluene (0.3 mL) at 85 °C for 48 h led to isolation of 7.4-3a,7eq- d_2 (40 mg, 96%) as a white solid. Mass spectral analysis of 7.4-3a,7eq- d_2 (corrected for ^{13}C isotopomers) established a 95:3:2 ratio of d_2 [$m/z = 281.1$ (M^+)], d_1 [$m/z = 280.1$ (M^+)], and d_0 [$m/z = 279.1$ (M^+)] isotopomers. ^1H and ^2H NMR analysis of 7.4-3a,7eq- d_2 revealed > 95 % deuteration of the C7eq (δ 1.89) and C3a (δ 2.71) positions with no detectable ($\leq 5\%$) deuteration at the

C7_{ax} (δ 1.34) and C7_a (δ 4.11) positions (Figure 76, spectra b and c). ¹H NMR: δ 7.35 (br d, J = 8.4 Hz, 2 H), 7.24-7.02 (m, 8 H), 4.78 (d, J = 8.6 Hz, 1 H), 4.66 (d, J = 8.6 Hz, 1 H), 4.11 (d, J = 2.8 Hz, 1 H), 1.66-1.53 (m, 2 H), 1.44-1.03 (m, 4 H), 0.86 (dt, J = 2.4, 13.6, 1 H). ²H NMR (CHCl₃): δ 2.81, 1.99. ¹³C{¹H} NMR: δ 146.5, 143.7, 128.6, 128.3, 126.9, 126.2, 126.1, 76.3, 74.6, 59.6, 44.1 (t, J = 16 Hz), 28.7 (t, J = 16 Hz), 25.7, 24.6, 20.1, (one carbon resonance obscured). MS (ESI, M⁺): 281.1 (95%), 280.1 (2%), 279.1 (2%).

7.4.3.3 Synthesis and characterization of 7.6 and isotopomers

rac-(3aR,7aR)-3,3-diphenylhexahydrobenzofuran-2(3H)-one (7.6). A solution of 7.5 (45 mg, 0.15 mmol) and triflic acid (0.7 μ L, 7.5×10^{-3} mol) in toluene (0.3 mL) was stirred at 60 °C for 3 h to give 7.6 (43 mg, 96%) as a white solid. ¹H NMR: δ 7.50 (d, J = 7.7 Hz, 2 H), 7.35 (d, J = 7.7 Hz, 2 H), 7.27 (t, J = 7.5 Hz, 2 H), 7.19 (q, J = 8.6, 3 H), 7.10 (t, J = 7.2, 1 H), 4.61 (br s, 1 H, H7_a), 3.07 (td, J = 5.8, 11.6 Hz, 1 H, H3_a), 2.16 (br d, J = 15.1 Hz, 1 H, H7_{eq}), 1.6 (br d, J = 13.0 Hz, 1 H, H6_{ax}), 1.57-1.47 (m, 2 H, H7_{ax} and H5_{eq}), 1.39-1.33 (m, 1 H, H6_{eq}), 1.15-1.06 (m, 2 H, H5_{ax} and H4_{eq}), 1.01-0.95 (m, 1 H, H4_{ax}). ¹³C{¹H} NMR: δ 177.1, 140.0, 138.5, 129.1, 128.5, 128.1, 127.9, 127.7, 126.6, 75.1, 62.7, 43.2, 27.7, 25.8, 24.0, 19.7.

The aliphatic protons of 7.6 were unambiguously assigned on the basis of combined ¹H-¹H COSY and ¹H-¹H NOESY analysis (Figures 88 and 89). Key to the assignment of the aliphatic protons of 7.6 was the presence of strong NOESY cross peak between the axial tertiary proton H3_a (δ 3.07) and H7_{ax} (δ 1.5) and the absence of a cross peak between H3_a and H7_{eq} (δ 2.16) (Figure 89).

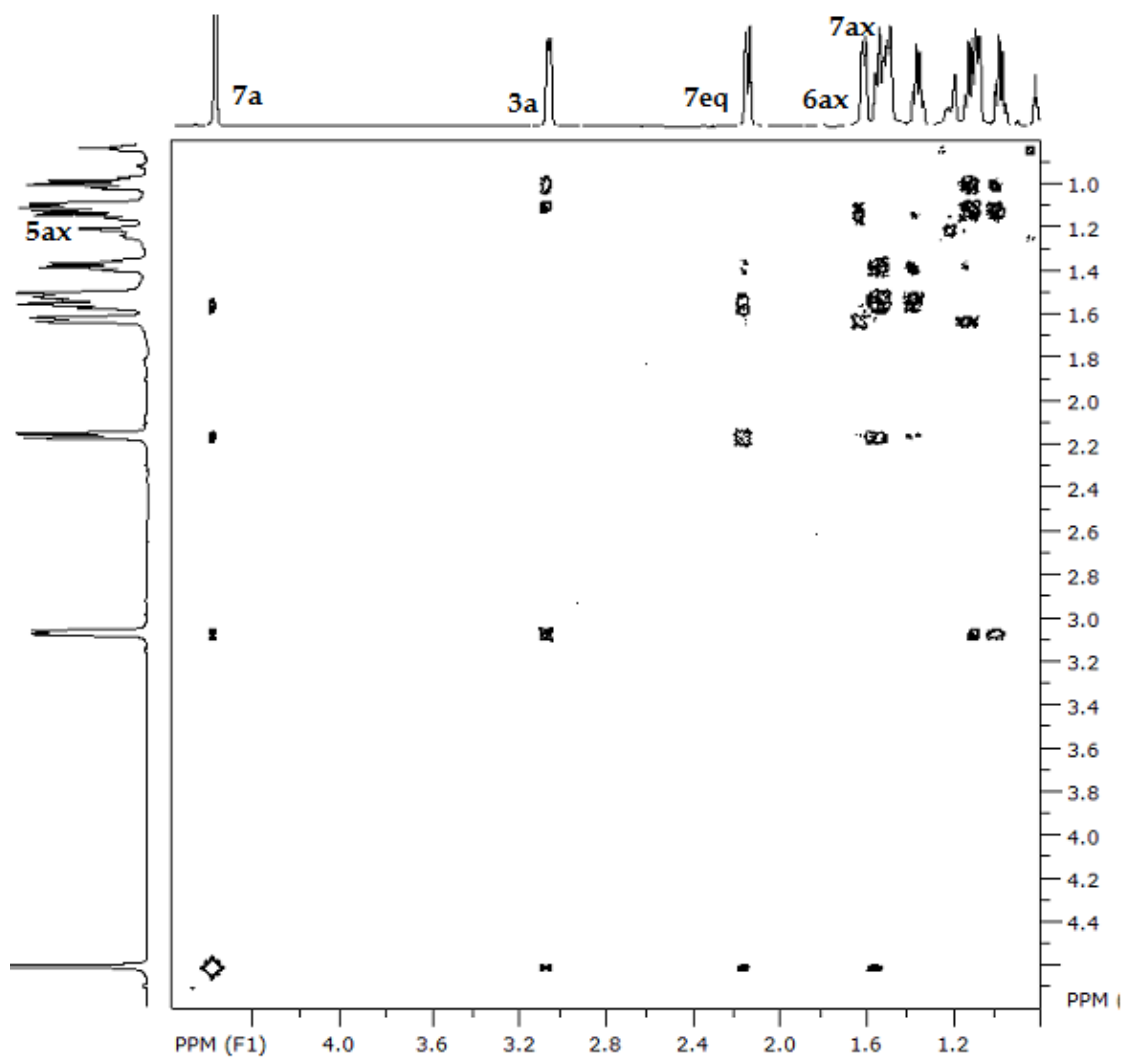


Figure 88: ^1H - ^1H COSY (800 MHz) NMR spectrum of 7.6 at 25 °C in CDCl_3 .

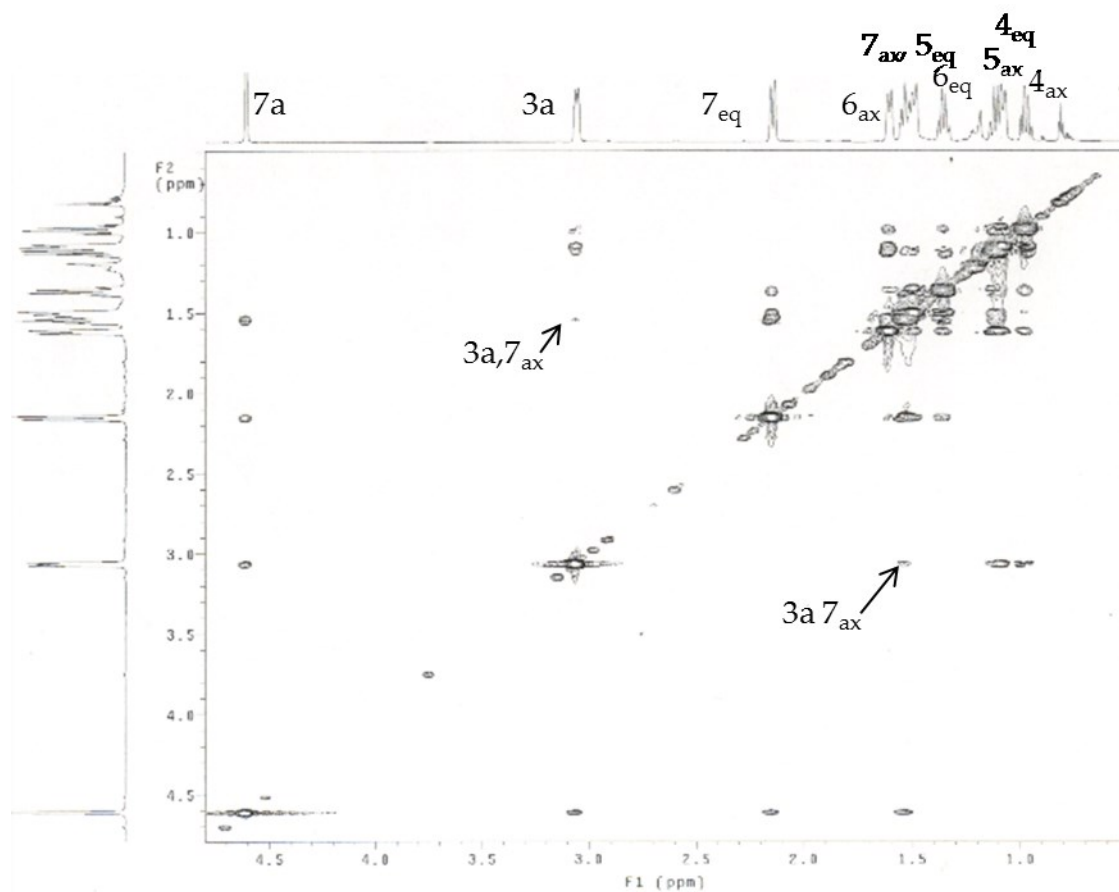


Figure 89: ^1H - ^1H NOESY (800 MHz) NMR spectrum of 7.6 at 25 °C in CDCl_3 .

rac-(3*a*R,7*R*,7*a*R)-3,3-diphenyl-(3*a*,7- $^2\text{H}_2$)-hexahydrobenzofuran-2(3*H*)-one (7.6-3*a*,7 $_{\text{eq}}$ - d_2) A solution of 7.5-1',3'- d_2 (45 mg, 0.15 mmol, > 99 % d_2 by MS) and triflic acid (0.7 μL , 7.5×10^{-3} mol) in toluene (0.3 mL) was stirred at 80 °C for 48 h to give 7.6-3*a*,7 $_{\text{eq}}$ - d_2 (45 mg, 100 %) as a white solid. Mass spectral analysis (corrected for ^{13}C isotopomers) established a > 98:< 2 ratio of d_2 [$m/z = 317.2$ ($\text{M}^+ + \text{Na}$)] and d_1 [$m/z = 316.2$ ($\text{M}^+ + \text{Na}$)] isotopomers. ^1H and ^2H NMR analysis of 7.6-3*a*,7 $_{\text{eq}}$ - d_2 revealed $\geq 95\%$ deuteration of the C7 $_{\text{eq}}$ (δ 2.16) and C3*a* (δ 3.07) positions and $\leq 5\%$ deuteration at the C7 $_{\text{ax}}$ (δ 1.55) position

(Figure 77, spectra b and c), ¹H NMR: δ 7.51 (d, *J* = 8.8 Hz, 2 H), 7.38 (d, *J* = 8.4 Hz, 2 H), 7.28 (t, *J* = 8.0 Hz, 2 H), 7.22-7.17 (m, 3 H), 7.13-7.08 (m, 1 H), 4.61 (br d, *J* = 2.8 Hz, 1 H), 1.66-1.46 (m, 3 H), 1.43-1.30 (m, 1 H), 1.23-1.05 (m, 2 H), 1.04-0.93 (m, 1 H). ²H NMR (CHCl₃): δ 3.14, 2.22. ¹³C{¹H} NMR: δ 177.1, 139.9, 138.5, 129.0, 128.5, 128.1, 127.8, 127.6, 126.6, 75.0, 62.6, 42.7 (t, *J* = 16 Hz), 27.3 (t, *J* = 16 Hz), 25.7, 23.9, 19.6. LCMS (ESI, M⁺ + Na): 317.2 (98.1%), 316 (1.4%).

7.4.3 Kinetic experiments

7.4.3.1 Kinetics of the HOTf catalyzed conversion of 7.1 to 7.2

Triflic acid (5.00 μL, 5.6 × 10⁻² mmol, 25 mM) was added via a gas-tight syringe equipped with a stainless steel needle into a solution of 7.1 (488 mg, 1.13 mmol, 0.50 M) in dry toluene (2.25 mL) that had been pre-equilibrated at 62.5 °C. The reaction mixture was stirred and aliquots were periodically removed via syringe. Aliquots were quenched with saturated aqueous NaHCO₃, extracted with acetonitrile, and analyzed by liquid chromatography equipped with a UV detector. The conversion of 7.1 to 7.2 was quantitative and occurred without formation of intermediates or byproducts.

Furthermore, analysis of stock solutions of 7.1 and 7.2 revealed that the UV response factors of 7.1 and 7.2 were not significantly different (≤ 0.1 %) over the concentration range utilized in these experiments. For these reasons, the concentration of 7.1 was determined from the integration of the peaks in the LC spectrum corresponding to 7.1 and 7.2 according to the formula $[7.1] = 0.50 \text{ M} \times [7.1] / \{[7.1] + [7.2]\}$. A plot of $\ln[7.2]$

versus time was linear to ~3 half-lives (Figure 78, Table 17), with an observed rate constant of $k_{\text{obs}} = 4.2 \pm 0.1 \times 10^{-3} \text{ s}^{-1}$. Employing a similar procedure, observed rate constants for the reaction of **1a** with triflic acid were determined at [HOTf] = 5.0 mM and 12.6 mM at 62 °C in toluene (Figure 78, Table 17). A plot of k_{obs} versus [HOTf] was linear over this range, which provided the second-order rate constant for hydroamination of **7.1** of $k_2 = 3.3 \pm 0.3 \times 10^{-1} \text{ s}^{-1}$ (Figure 79).

Observed rate constants for the reaction of **7.1** (0.5 M) with HOTf (~25 mM) in toluene were determined as a function of temperature from 39-72 °C (Table 17, Figure 90). An Eyring plot of the corresponding second-order rate constants (Figure 80), specifically a plot of $\ln(k_2/T)$ versus $1000/T$, gave a linear regression of $y = -4.88x + 6.66$ (or $y = -4880x + 6.66$ for plot of $\ln(k_2/T)$ versus $1/T$). Activation parameters for the conversion of **7.1** to **7.2** were determined according to the permutations of the Eyring Equation: $\Delta H^\ddagger = -mR$ and $\Delta S^\ddagger = [b - \ln(k_B/h)]R$, where m and b are the slope and y -intercept, respectively, of the linear regression from the Eyring plot, R is the universal gas constant ($1.987 \text{ cal mol}^{-1} \text{ K}^{-1}$), k_B is the Boltzmann constant and h is Planck's constant.

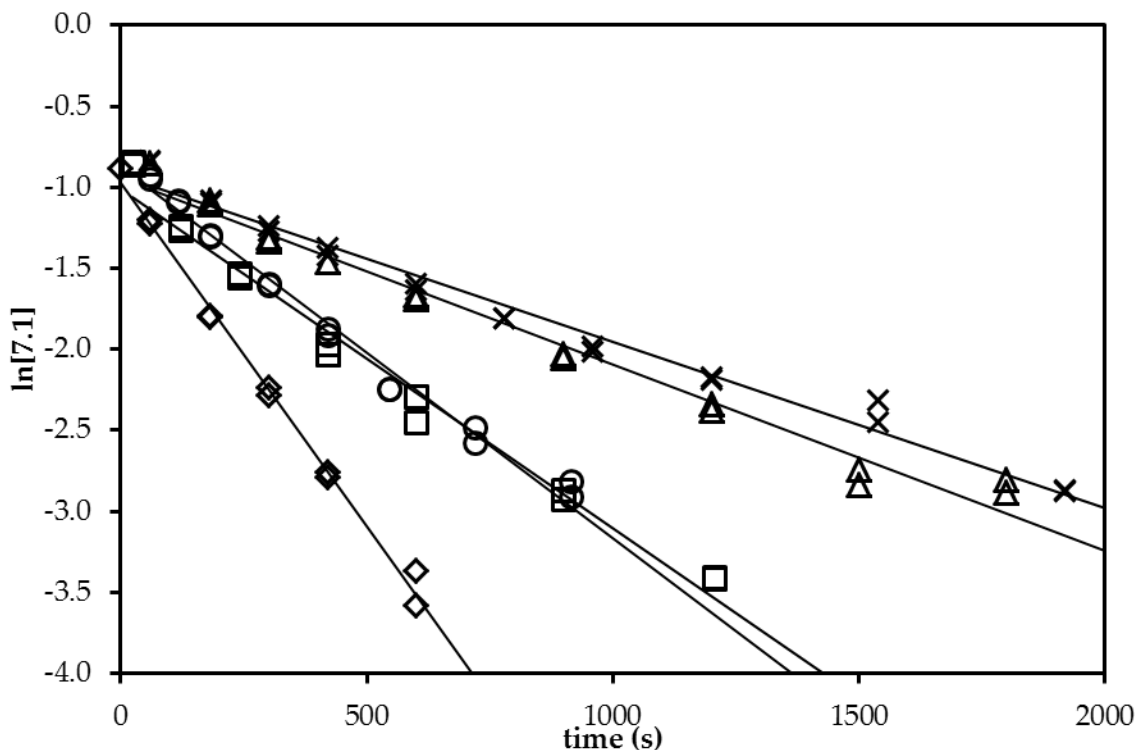


Figure 90: First-order plots for the conversion of 7.1 ($[7.1]_0 = 0.50 \text{ M}$) to 7.2 catalyzed by triflic acid in toluene: $[\text{HOTf}] = 12.6 \text{ mM}$ at $72 \text{ }^\circ\text{C}$ (O); $[\text{HOTf}] = 25.2 \text{ mM}$ at $62.5 \text{ }^\circ\text{C}$ (◇); $[\text{HOTf}] = 25.2 \text{ mM}$ at $53.0 \text{ }^\circ\text{C}$ (□); $[\text{HOTf}] = 25.2 \text{ mM}$ at $39 \text{ }^\circ\text{C}$ (△); and $[\text{HOTf}] = 25.1 \text{ mM}$ at $45.5 \text{ }^\circ\text{C}$ (×).

7.4.3.2 α -Secondary KIE for the conversion of 7.1 to 7.2

A mixture of 7.1 (162 mg, 0.376 mmol) and 7.1-2'- d_1 (74 % d_1 , 326 mg, 0.754 mmol) was dissolved in toluene (2.25 mL). Mass spectral analysis of the resulting solution revealed a 47.6:52.4 mixture of d_0/d_1 isotopomers. The solution was equilibrated at $59.5 \text{ }^\circ\text{C}$ and triflic acid (4.0 mg, $5.7 \times 10^{-2} \text{ mmol}$) was added. The resulting solution was stirred and aliquots were removed periodically using a syringe, quenched with saturated aqueous NaHCO_3 solution, extracted with acetonitrile, and analyzed by LC-MS for conversion and isotopic abundance. The concentrations of 7.1 and 7.1-2'- d_1 were

determined from total conversion, obtained by integration of the peaks in the LC spectrum corresponding to **7.1 + 7.1-2'-d₁** and **7.2 + 7.2-7a-d₁** and from the isotopic ratios **7.1/7.1-2'-d₁** and **7.2/7.2-7a-d₁** determined from MS analysis of the corresponding LC peaks (Table 18). Plots of ln[**7.1**] and ln[**7.1-2'-d₁**] versus time were linear to about three half lives with observed rate constants of $k_{\text{obs}} = (2.19 \pm 0.03) \times 10^{-3} \text{ s}^{-1}$ and $k_{\text{obs}} = (2.51 \pm 0.05) \times 10^{-3} \text{ s}^{-1}$, respectively, (Figure 81) which correspond to an inverse KIE of $k_{\text{D}}/k_{\text{H}} = (1.15 \pm 0.03)$.

Table 18: Total conversion and isotope ratios as a function of time for the reaction of a 47.6:52.4 mixture of 7.1 and 7.1-2'-d₁ catalyzed by HOTf (5 mol %) in toluene at 59.5 °C as determined from LC/MS analysis.

time (s)	7.1-d_x:7.2-d_x	7.1 : 7.1-2'-d₁	7.2 : 7.2-7a-d₁
0	100 : 0	47.6 : 52.4	--
129	71.3 : 28.7	47.9 : 52.1	45.7 : 54.3
368	46.3 : 53.7	48.3 : 51.7	46.3 : 53.7
424	39.6 : 60.4	47.9 : 52.1	45.4 : 54.6
483	32.4 : 67.6	48.4 : 51.6	46.0 : 54.0
554	28.3 : 71.7	48.6 : 51.4	45.7 : 54.3
604	25.4 : 74.6	48.8 : 51.2	46.6 : 53.4
720	18.5 : 81.5	49.1 : 50.9	45.9 : 54.1
853	13.8 : 86.2	49.6 : 50.4	46.8 : 53.2
958	11.0 : 89.0	50.1 : 49.9	46.8 : 53.2
1083	8.0 : 92.0	50.9 : 49.1	46.9 : 53.1
1202	6.1 : 93.9	51.9 : 48.1	47.0 : 53.0

The Streitwieser approximation³¹¹ of the Bigeleisen equation estimates the theoretical maximum kinetic isotope effect by:

$$\left(\frac{k_{\text{H}}}{k_{\text{D}}}\right) = e^{\left[\frac{0.187}{T} \Sigma(v_{\text{H}} - v_{\text{H}}^{\ddagger})\right]}$$

Substituting known stretching and bending frequencies for the sp² carbon of *cis*-2-butene [2980 (stretching), 1425 (in-plane bending), 852 (out-of-plane bending)]³¹⁸ as a model for those of **7.1** and the methyne carbon of a secondary alcohol [2900 (stretching), 1340 (in-plane bending), 1340 (out-of-plane bending)]³¹⁸ as a model for **7.2** the equation becomes:

$$\left(\frac{k_{\text{H}}}{k_{\text{D}}}\right) = e^{\left[\frac{0.187}{T}(2980-2900+1425-1340+852-1340)\right]} = e^{\frac{-60.4}{T}}$$

At $T = 333 \text{ K}$, this equation predicts a maximum KIE for the conversion of **7.1** to **7.2** of $k_{\text{H}}/k_{\text{D}} = 0.834$ or $k_{\text{D}}/k_{\text{H}} = 1.20$.

References

1. Negishi, E.-i. *Angew. Chem. Int. Ed.* **2011**, *50*, 6738.
2. Hegedus, L. S., *Transition metals in the synthesis of complex organic molecules*. University Science Books: Sausalito, Calif., 2010.
3. Teles, J. H.; Brode, S.; Chabanas, M. *Angew. Chem. Int. Ed.* **1998**, *37*, 1415.
4. Bandini, M. *Chem. Soc. Rev.* **2011**, *40*, 1358.
5. Corma, A.; Leyva-Pérez, A.; Sabater, M. J. *Chem. Rev.* **2011**, *111*, 1657.
6. Gorin, D. J.; Sherry, B. D.; Toste, F. D. *Chem. Rev.* **2008**, *108*, 3351.
7. Krause, N.; Winter, C. *Chem. Rev.* **2011**, *111*, 1994.
8. Li, Z.; Brouwer, C.; He, C. *Chem. Rev.* **2008**, *108*, 3239.
9. Fürstner, A.; Davies, P. W. *Angew. Chem. Int. Ed.* **2007**, *46*, 3410.
10. Jiménez-Núñez, E. s.; Echavarren, A. M. *Chem. Rev.* **2008**, *108*, 3326.
11. Toullec, P. Y.; Michelet, V. *Top. Curr. Chem.* **2011**, *302*, 31.
12. Bongers, N.; Krause, N. *Angew. Chem. Int. Ed.* **2008**, *47*, 2178.
13. Sengupta, S.; Shi, X. *ChemCatChem* **2010**, *2*, 609.
14. Widenhofer, R. A. *Chemistry – A European Journal* **2008**, *14*, 5382.

15. Schmidbaur, H.; Schier, A. *Organometallics* **2010**, *29*, 2.
16. Shapiro, N. D.; Toste, F. D. *Synlett* **2010**, *2010*, 675.
17. Hashmi, A. S. K. *Angew. Chem. Int. Ed.* **2010**, *49*, 5232.
18. Bender, C. F.; Widenhoefer, R. A. *J. Am. Chem. Soc.* **2005**, *127*, 1070.
19. Chatt, J. *Chem. Rev.* **1951**, *48*, 7.
20. Chatt, J.; Duncanson, L. A. *Journal of the Chemical Society (Resumed)* **1953**, *0*, 2939.
21. Dewar, M. J. S. *Bull. Soc. Chim. Fr.* **1951**, *18*, C71.
22. Pyykkö, P. *Angew. Chem. Int. Ed.* **2004**, *43*, 4412.
23. Pyykkö, P. *Angew. Chem. Int. Ed.* **2002**, *41*, 3573.
24. Schwerdtfeger, P. *Heteroat. Chem* **2002**, *13*, 578.
25. Gorin, D. J.; Toste, F. D. *Nature* **2007**, *446*, 395.
26. Pyykko, P.; Desclaux, J. P. *Acc. Chem. Res.* **1979**, *12*, 276.
27. Gimeno, M. C.; Laguna, A. *Chem. Rev.* **1997**, *97*, 511.
28. Carvajal, M. A.; Novoa, J. J.; Alvarez, S. J. *Am. Chem. Soc.* **2004**, *126*, 1465.
29. Ziegler, T.; Rauk, A. *Inorg. Chem.* **1979**, *18*, 1558.

30. Hertwig, R. H.; Koch, W.; Schröder, D.; Schwarz, H.; Hrušák, J.; Schwerdtfeger, P. *The Journal of Physical Chemistry* **1996**, *100*, 12253.
31. Nechaev, M. S.; Rayón, V. M.; Frenking, G. *The Journal of Physical Chemistry A* **2004**, *108*, 3134.
32. Kim, C. K.; Lee, K. A.; Kim, C. K.; Lee, B.-S.; Lee, H. W. *Chem. Phys. Lett.* **2004**, *391*, 321.
33. Barnett, N. J.; Slipchenko, L. V.; Gordon, M. S. *The Journal of Physical Chemistry A* **2009**, *113*, 7474.
34. Shapiro, N. D.; Toste, F. D. *Proceedings of the National Academy of Sciences* **2008**, *105*, 2779.
35. Flugge, S.; Anoop, A.; Goddard, R.; Thiel, W.; Furstner, A. *Chemistry* **2009**, *15*, 8558.
36. Hooper, T. N.; Green, M.; McGrady, J. E.; Patel, J. R.; Russell, C. A. *Chem. Commun.* **2009**, 3877.
37. Salvi, N.; Belpassi, L.; Tarantelli, F. *Chemistry* **2010**, *16*, 7231.
38. Herrero-Gomez, E.; Nieto-Oberhuber, C.; Lopez, S.; Benet-Buchholz, J.; Echavarren, A. M. *Angew. Chem. Int. Ed. Engl.* **2006**, *45*, 5455.
39. Akana, J. A.; Bhattacharyya, K. X.; Müller, P.; Sadighi, J. P. *J. Am. Chem. Soc.* **2007**, *129*, 7736.
40. de Frémont, P.; Marion, N.; Nolan, S. P. *J. Organomet. Chem.* **2009**, *694*, 551.
41. Zuccaccia, D.; Belpassi, L.; Tarantelli, F.; Macchioni, A. *J. Am. Chem. Soc.* **2009**, *131*, 3170.

42. Brown, T. J.; Dickens, M. G.; Widenhoefer, R. A. *J. Am. Chem. Soc.* **2009**, *131*, 6350.
43. Fueno, T.; Okuyama, T.; Deguchi, T.; Furukawa, J. *J. Am. Chem. Soc.* **1965**, *87*, 170.
44. Kurosawa, H.; Asada, N. *J. Organomet. Chem.* **1981**, *217*, 259.
45. Kurosawa, H.; Majima, T.; Asada, N. *J. Am. Chem. Soc.* **1980**, *102*, 6996.
46. Brown, T. J.; Dickens, M. G.; Widenhoefer, R. A. *Chem Commun (Camb)* **2009**, 6451.
47. Lavallo, V.; Frey, G. D.; Donnadiou, B.; Soleilhavoup, M.; Bertrand, G. *Angew. Chem. Int. Ed. Engl.* **2008**, *47*, 5224.
48. Zuccaccia, D.; Belpassi, L.; Rocchigiani, L.; Tarantelli, F.; Macchioni, A. *Inorg. Chem.* **2010**, *49*, 3080.
49. Brown, T. J.; Widenhoefer, R. A. *J. Organomet. Chem.* **2011**, *696*, 1216.
50. Celik, M. A.; Dash, C.; Adiraju, V. A.; Das, A.; Yousufuddin, M.; Frenking, G.; Dias, H. V. *Inorg. Chem.* **2013**, *52*, 729.
51. Salvi, N.; Belpassi, L.; Zuccaccia, D.; Tarantelli, F.; Macchioni, A. *J. Organomet. Chem.* **2010**, *695*, 2679.
52. Hooper, T. N.; Green, M.; Russell, C. A. *Chem Commun (Camb)* **2010**, *46*, 2313.
53. Ciancaleoni, G.; Belpassi, L.; Tarantelli, F.; Zuccaccia, D.; Macchioni, A. *Dalton Transactions* **2013**, *42*, 4122.
54. Brouwer, C.; He, C. *Angew. Chem., Int. Ed.* **2006**, *45*, 1744.

55. Giner, X.; Nájera, C. *Org. Lett.* **2008**, *10*, 2919.
56. Brouwer, C.; Rahaman, R.; He, C. *Synlett* **2007**, *11*, 1785.
57. Wang, M. Z.; Wong, M. K.; Che, C. M. *Chem. — Eur. J.* **2008**, *14*, 8353.
58. Yeh, M. C. P.; Pai, H. F.; Lin, Z. J.; Lee, B. R. *Tetrahedron* **2009**, *65*, 4789.
59. Müller, T. E.; Hultsch, K. C.; Yus, M.; Foubelo, F.; Tada, M. *Chem. Rev.* **2008**, *108*, 3795.
60. Dzhemilev, U. M.; Tolstikov, G. A.; Khusnutdinov, R. I. *Russ. J. Org. Chem.* **2009**, *45*, 957.
61. Behr, A.; Becker, M.; Beckmann, T.; Johnen, L.; Leschinski, J.; Reyer, S. *Angew. Chem., Int. Ed.* **2009**, *48*, 3598.
62. Kovács, G.; Ujaque, G.; Lledós, A. *J. Am. Chem. Soc.* **2008**, *130*, 853.
63. Hooper, T. N.; Butts, C. P.; Green, M.; Haddow, M. F.; McGrady, J. E.; Russell, C. A. *Chem-Eur J* **2009**, *15*, 12196.
64. Cinellu, M. A.; Minghetti, G.; Stoccoro, S.; Zucca, A.; Manassero, M. *Chem. Commun.* **2004**, *0*, 1618.
65. Dias, H. V. R.; Fianchini, M.; Cundari, T. R.; Campana, C. F. *Angew. Chem. Int. Ed.* **2008**, *47*, 556.
66. Nakamura, A.; Ueyama, N.; Yamaguchi, K., *Organometallic Conjugation*. 2002.
67. Yasuda, H.; Nakamura, A. *Angew. Chem., Int. Ed. Engl.* **1987**, *26*, 723.

68. Félix, V.; Calhorda, M.; Drew, M.; Gonçalves, I.; Romão, C. *Inorg. Chim. Acta* **1998**, 263.
69. Nakamura, A.; Mashima, K. *J. Organomet. Chem.* **2004**, 689, 4552.
70. Mashima, K.; Nakamura, A. *J. Organomet. Chem.* **2002**, 663, 5.
71. Tsang, J. Y. K.; Buschhaus, M. S. A.; Graham, P. M.; Semiao, C. J.; Semproni, S. P.; Kim, S. J.; Legzdins, P. *J. Am. Chem. Soc.* **2008**, 130, 3652.
72. Tsang, J. Y. K.; Buschhaus, M. S. A.; Legzdins, P. *J. Am. Chem. Soc.* **2007**, 129, 5372.
73. Ng, S. H. K.; Adams, C. S.; Hayton, T. W.; Legzdins, P.; Patrick, B. O. *J. Am. Chem. Soc.* **2003**, 125, 15210.
74. Kreiter, C. G.; Wenz, M.; Bell, P. J. *J. Organomet. Chem.* **1990**, 387, 175.
75. Kreiter, C. G.; Wenz, M.; Bell, P. J. *J. Organomet. Chem.* **1990**, 394, 195.
76. Kreiter, C. J.; Michels, W.; Wenz, M. *Chem. Ber.* **1986**, 119, 1994.
77. Zhuang, J. M.; Sutton, D. *Organometallics* **1991**, 10, 1516.
78. Jzang, T. t.; Liu, C. s. *Organometallics* **1988**, 7, 1271.
79. Christensen, N. J.; Hunter, A. D.; Legzdins, P. *Organometallics* **1989**, 8, 930.
80. Kuo, G. H.; Helquist, P.; Kerber, R. C. *Organometallics* **1984**, 3, 806.
81. Dooling, D.; Joorst, G.; Mapolie, S. F. *Polyhedron* **2001**, 20, 467.

82. Benn, R.; Jolly, W.; Joswig, T.; Mynott, R.; Schick, K. P. *Z. Naturforsch., B: Chem. Sci.* **1986**, *41*, 680.
83. Håkansson*, M.; Brantin, K.; Jagner*, S. *J. Organomet. Chem.* **2000**, *602*, 5.
84. Haakansson, M.; Jagner, S.; Walther, D. *Organometallics* **1991**, *10*, 1317.
85. Song, L.; Trogler, W. C. *J. Organomet. Chem.* **1993**, *452*, 271.
86. Quinn, H. W. *Can. J. Chem.* **1967**, *45*, 1329.
87. Krossing, I. *Angew. Chem. Int. Ed. Engl.* **2011**, *50*, 11576.
88. Sanguramath, R. A.; Hooper, T. N.; Butts, C. P.; Green, M.; McGrady, J. E.; Russell, C. A. *Angew. Chem. Int. Ed. Engl.* **2011**, *50*, 7592.
89. Sanguramath, R. A.; Patra, S. K.; Green, M.; Russell, C. A. *Chem Commun (Camb)* **2012**, *48*, 1060.
90. Perez-Galan, P.; Delpont, N.; Herrero-Gomez, E.; Maseras, F.; Echavarren, A. M. *Chemistry* **2010**, *16*, 5324.
91. Partyka, D. V.; Robilotto, T. J.; Zeller, M.; Hunter, A. D.; Gray, T. G. *Organometallics* **2008**, *27*, 28.
92. Partyka, D. V.; Updegraff, J. B.; Zeller, M.; Hunter, A. D.; Gray, T. G. *Organometallics* **2009**, *28*, 1666.
93. Xu, F. B.; Li, Q. S.; Wu, L. Z.; Leng, X. B.; Li, Z. C.; Zeng, X. S.; Chow, Y. L.; Zhang, Z. Z. *Organometallics* **2003**, *22*, 633.
94. Li, Q. S.; Wang, C. Q.; Zou, R. Y.; Xu, F. B.; Song, H. B.; Wan, X. J.; Zhang, Z. Z. *Inorg. Chem.* **2006**, *45*, 1888.

95. Peng, T. S.; Gladysz, J. A. *J. Am. Chem. Soc.* **1992**, *114*, 4174.
96. Åkermark, B.; Glaser, J.; Ohrström, L.; Zetterberg, K. *Organometallics* **1991**, *10*, 133.
97. Schwerdtfeger, P.; Hermann, H. L.; Schmidbaur, H. *Inorg. Chem.* **2003**, *42*, 1334.
98. Reich, H. J. *WINDNMR-PRo*, 7.1.13; University of Wisconsin: Madison, WI, 2008.
99. Bruker-Nonius *SAINT*, 2009.9; Bruker-Nonius: Madison, WI, USA, 2009.
100. Bruker-Nonius *SADABS*, 2009.9; Bruker-Nonius: Madison, WI, USA, 2009.
101. Bruker-AXS *XS*, Bruker-AXS: Madison, WI, USA, 2009.
102. Altomare, A.; Cascarano, G.; Giacovazzo, C.; Guagliardi, A.; Burla, M. C.; Polidori, G.; Camalli, M. *J. Appl. Crystallogr.* **1994**, *27*, 435.
103. Bruker-AXS *XL*, 2009.9; Bruker-AXS: Madison, WI, USA, 2009.
104. Pradal, A.; Toullec, P. Y.; Michelet, V. *Synthesis* **2011**, *2011*, 1501.
105. Ito, Y.; Sawamura, M.; Hayashi, T. *J. Am. Chem. Soc.* **1986**, *108*, 6405.
106. Muñoz, M. P.; Adrio, J.; Carretero, J. C.; Echavarren, A. M. *Organometallics* **2005**, *24*, 1293.
107. Cheon, C. H.; Kanno, O.; Toste, F. D. *J. Am. Chem. Soc.* **2011**, *133*, 13248.
108. Bandini, M.; Monari, M.; Romaniello, A.; Tragni, M. *Chemistry – A European Journal* **2010**, *16*, 14272.

109. Liu, F.; Qian, D.; Li, L.; Zhao, X.; Zhang, J. *Angew. Chem. Int. Ed.* **2010**, *49*, 6669.
110. Bandini, M.; Gualandi, A.; Monari, M.; Romaniello, A.; Savoia, D.; Tragni, M. J. *Organomet. Chem.* **2011**, *696*, 338.
111. Bandini, M.; Eichholzer, A. *Angew. Chem. Int. Ed.* **2009**, *48*, 9533.
112. Aikawa, K.; Kojima, M.; Mikami, K. *Adv. Synth. Catal.* **2010**, *352*, 3131.
113. Tarselli, M. A.; Chianese, A. R.; Lee, S. J.; Gagné, M. R. *Angew. Chem. Int. Ed.* **2007**, *46*, 6670.
114. Aikawa, K.; Kojima, M.; Mikami, K. *Angew. Chem. Int. Ed.* **2009**, *48*, 6073.
115. Wang, M.-Z.; Zhou, C.-Y.; Guo, Z.; Wong, E. L.-M.; Wong, M.-K.; Che, C.-M. *Chemistry – An Asian Journal* **2011**, *6*, 812.
116. Melhado, A. D.; Amarante, G. W.; Wang, Z. J.; Luparia, M.; Toste, F. D. *J. Am. Chem. Soc.* **2011**, *133*, 3517.
117. Hashmi, A. S. K.; Hamzić, M.; Rominger, F.; Bats, J. W. *Chemistry – A European Journal* **2009**, *15*, 13318.
118. Wheaton, C. A.; Jennings, M. C.; Puddephatt, R. J. *Z Naturforsch B* **2009**, *64*, 1469.
119. Bats, J. W.; Hamzic, M.; Hashmi, A. S. K. *Acta Crystallographica Section E* **2007**, *63*, m2344.
120. Wheaton, C. A.; Jennings, M. C.; Puddephatt, R. J. *J. Am. Chem. Soc.* **2006**, *128*, 15370.
121. Schmidbaur, H. *Chem. Soc. Rev.* **1995**, *24*, 391.

122. Brooner, R. E. M.; Widenhoefer, R. A. *Organometallics* **2011**, *30*, 3182.
123. Herrero-Gómez, E.; Nieto-Oberhuber, C.; López, S.; Benet-Buchholz, J.; Echavarren, A. M. *Angew. Chem. Int. Ed.* **2006**, *45*, 5455.
124. Partyka, D. V.; Updegraff, J. B.; Zeller, M.; Hunter, A. D.; Gray, T. G. *Organometallics* **2009**, *28*, 1666.
125. Jarek, R. L.; Flesher, R. J.; Shin, S. K. J. *Chem. Educ.* **1997**, *74*, 978.
126. Aakermark, B.; Glaser, J.; Oehrstroem, L.; Zetterberg, K. *Organometallics* **1991**, *10*, 733.
127. Bruker-Nonius *TWINABS*, 2009.9; Bruker-Nonius: Madison, WI, USA, 2009.
128. Brooner, R. E. M.; Widenhoefer, R. A. *Organometallics* **2012**, *31*, 768.
129. Grrirane, A.; Garcia, H.; Corma, A.; Álvarez, E. *ACS Catalysis* **2011**, *1*, 1647.
130. Brown, T. J.; Sugie, A.; Dickens, M. G.; Widenhoefer, R. A. *Organometallics* **2010**, *29*, 4207.
131. Brown, T. J.; Sugie, A.; Leed, M. G.; Widenhoefer, R. A. *Chemistry* **2012**, *18*, 6959.
132. Lavallo, V.; Frey, G. D.; Kousar, S.; Donnadiou, B.; Bertrand, G. *Proceedings of the National Academy of Sciences of the United States of America* **2007**, *104*, 13569.
133. Shapiro, N. D.; Toste, F. D. *Proceedings of the National Academy of Sciences* **2008**, *105*, 2779.
134. Furstner, A.; Alcarazo, M.; Goddard, R.; Lehmann, C. W. *Angew. Chem. Int. Ed. Engl.* **2008**, *47*, 3210.

135. Roth, K. E.; Blum, S. A. *Organometallics* **2010**, *29*, 1712.
136. LaLonde, R. L.; Brenzovich, J. W. E.; Benitez, D.; Tkatchouk, E.; Kelley, K.; Goddard, I. I. I. W. A.; Toste, F. D. *Chemical Science* **2010**, *1*, 226.
137. Grisé, C. M.; Rodrigue, E. M.; Barriault, L. *Tetrahedron* **2008**, *64*, 797.
138. Wang, Z. J.; Benitez, D.; Tkatchouk, E.; Goddard Iii, W. A.; Toste, F. D. *J. Am. Chem. Soc.* **2010**, *132*, 13064.
139. Brouwer, C.; He, C. *Angew. Chem. Int. Ed.* **2006**, *45*, 1744.
140. Zhang, J.; Yang, C.-G.; He, C. *J. Am. Chem. Soc.* **2006**, *128*, 1798.
141. Preisenberger, M.; Schier, A.; Schmidbaur, H. *J. Chem. Soc., Dalton Trans.* **1999**, *0*, 1645.
142. Mézailles, N.; Ricard, L.; Gagosz, F. *Org. Lett.* **2005**, *7*, 4133.
143. Wang, W.; Hammond, G. B.; Xu, B. *J. Am. Chem. Soc.* **2012**, *134*, 5697.
144. Schmidbaur, H.; Hamel, A.; Mitzel, N. W.; Schier, A.; Nogai, S. *Proceedings of the National Academy of Sciences* **2002**, *99*, 4916.
145. Vollenbroek, F. A.; Van den Berg, J. P.; Van der Velden, J. W. A.; Bour, J. J. *Inorg. Chem.* **1980**, *19*, 2685.
146. Brown, T. J.; Weber, D.; Gagne, M. R.; Widenhoefer, R. A. *J. Am. Chem. Soc.* **2012**, *134*, 9134.
147. Michelet, V.; Toullec, P. Y.; Genêt, J.-P. *Angew. Chem. Int. Ed.* **2008**, *47*, 4268.

148. Diver, S. T.; Giessert, A. J. *Chem. Rev.* **2004**, *104*, 1317.
149. Lloyd-Jones, G. C. *Organic & Biomolecular Chemistry* **2003**, *1*, 215.
150. Marinetti, A.; Jullien, H.; Voituriez, A. *Chem. Soc. Rev.* **2012**, *41*, 4884.
151. Watson, I. D. G.; Toste, F. D. *Chemical Science* **2012**, *3*, 2899.
152. Nieto-Oberhuber, C.; López, S.; Jiménez-Núñez, E.; Echavarren, A. M. *Chemistry – A European Journal* **2006**, *12*, 5916.
153. Zhang, L.; Sun, J.; Kozmin, S. A. *Adv. Synth. Catal.* **2006**, *348*, 2271.
154. Nieto-Oberhuber, C.; Muñoz, M. P.; Buñuel, E.; Nevado, C.; Cárdenas, D. J.; Echavarren, A. M. *Angew. Chem. Int. Ed.* **2004**, *43*, 2402.
155. Nieto-Oberhuber, C.; López, S.; Echavarren, A. M. *J. Am. Chem. Soc.* **2005**, *127*, 6178.
156. Nieto-Oberhuber, C.; Muñoz, M. P.; López, S.; Jiménez-Núñez, E.; Nevado, C.; Herrero-Gómez, E.; Raducan, M.; Echavarren, A. M. *Chemistry – A European Journal* **2006**, *12*, 1677.
157. Lee, S. I.; Kim, S. M.; Choi, M. R.; Kim, S. Y.; Chung, Y. K.; Han, W.-S.; Kang, S. O. *The Journal of Organic Chemistry* **2006**, *71*, 9366.
158. Lee, S. I.; Kim, S. M.; Kim, S. Y.; Chung, Y. K. *Synlett* **2006**, 2006, 2256.
159. Fürstner, A.; Szillat, H.; Gabor, B.; Mynott, R. J. *Am. Chem. Soc.* **1998**, *120*, 8305.
160. Witham, C. A.; Mauleón, P.; Shapiro, N. D.; Sherry, B. D.; Toste, F. D. *J. Am. Chem. Soc.* **2007**, *129*, 5838.

161. Nieto-Oberhuber, C.; Pérez-Galán, P.; Herrero-Gómez, E.; Lauterbach, T.; Rodríguez, C.; López, S.; Bour, C.; Rosellón, A.; Cárdenas, D. J.; Echavarren, A. M. *J. Am. Chem. Soc.* **2008**, *130*, 269.
162. Escribano-Cuesta, A.; Perez-Galan, P.; Herrero-Gomez, E.; Sekine, M.; Braga, A. A. C.; Maseras, F.; Echavarren, A. M. *Organic & Biomolecular Chemistry* **2012**, *10*, 6105.
163. Fürstner, A.; Davies, P. W.; Gress, T. *J. Am. Chem. Soc.* **2005**, *127*, 8244.
164. Matsuda, T.; Kadowaki, S.; Goya, T.; Murakami, M. *Synlett* **2006**, 2006, 0575.
165. Ota, K.; Lee, S. I.; Tang, J.-M.; Takachi, M.; Nakai, H.; Morimoto, T.; Sakurai, H.; Kataoka, K.; Chatani, N. *J. Am. Chem. Soc.* **2009**, *131*, 15203.
166. Bender, B. R.; Norton, J. R.; Miller, M. M.; Anderson, O. P.; Rappe, A. K. *Organometallics* **1992**, *11*, 3427.
167. Benn, R.; Ruffínska, A. *J. Organomet. Chem.* **1982**, *238*, C27.
168. Fitch, J. W.; Ripplinger, E. B.; Shoulders, B. A.; Sorey, S. D. *J. Organomet. Chem.* **1988**, *352*, C25.
169. Krivdin, L. B.; Kalabin, G. A. *Prog. Nucl. Magn. Reson. Spectrosc.* **1989**, *21*, 293.
170. Maier, W. F.; Schleyer, P. V. R. *J. Am. Chem. Soc.* **1981**, *103*, 1891.
171. Oba, G.; Moreira, G.; Manuel, G.; Koenig, M. *J. Organomet. Chem.* **2002**, *643–644*, 324.
172. Liebman, J. F.; Greenberg, A. *Chem. Rev.* **1976**, *76*, 311.
173. Uddin, J.; Dapprich, S.; Frenking, G.; Yates, B. F. *Organometallics* **1999**, *18*, 457.

174. Liu, C.; Widenhoefer, R. A. *Org. Lett.* **2007**, *9*, 1935.
175. Liu, Z.; Wasmuth, A. S.; Nelson, S. G. *J. Am. Chem. Soc.* **2006**, *128*, 10352.
176. Mo, J.; Eom, D.; Lee, E.; Lee, P. H. *Org. Lett.* **2012**, *14*, 3684.
177. Tarselli, M. A.; Gagne, M. R. *The Journal of Organic Chemistry* **2008**, *73*, 2439.
178. Zhang, Z.; Liu, C.; Kinder, R. E.; Han, X.; Qian, H.; Widenhoefer, R. A. *J. Am. Chem. Soc.* **2006**, *128*, 9066.
179. Ford, W. T. *Acc. Chem. Res.* **1973**, *6*, 410.
180. Schlummer, B.; Hartwig, J. F. *Org. Lett.* **2002**, *4*, 1471.
181. Rosenfeld, D. C.; Shekhar, S.; Takemiya, A.; Utsunomiya, M.; Hartwig, J. F. *Org. Lett.* **2006**, *8*, 4179.
182. McBee, J. L.; Bell, A. T.; Tilley, T. D. *J. Am. Chem. Soc.* **2008**, *130*, 16562.
183. Anderson, L. L.; Arnold, J.; Bergman, R. G. *J. Am. Chem. Soc.* **2005**, *127*, 14542.
184. McKinney Brooner, R. E.; Widenhoefer, R. A. *Chemistry – A European Journal* **2011**, *17*, 6170.
185. Mango, F. D. *Coord. Chem. Rev.* **1975**, *15*, 109.
186. Paquette, L. A.; Zon, G. *J. Am. Chem. Soc.* **1974**, *96*, 203.
187. Zon, G.; Paquette, L. A. *J. Am. Chem. Soc.* **1974**, *96*, 215.

188. Paquette, L. A.; Zon, G. *J. Am. Chem. Soc.* **1974**, *96*, 224.
189. Taylor, R. T.; Paquette, L. A. *J. Org. Chem.* **1978**, *43*, 242.
190. Paquette, L. A.; Allen, G. R.; Henzel, R. P. *J. Am. Chem. Soc.* **1970**, *92*, 7002.
191. Park, K. H.; Chung, Y. K. *Adv. Synth. Catal.* **2005**, *347*, 854.
192. Ichikawa, Y.; Nishimura, T.; Hayashi, T. *Organometallics* **2011**, *30*, 2342.
193. Ooi, T.; Hokke, Y.; Tayama, E.; Maruoka, K. *Tetrahedron* **2001**, *57*, 135.
194. Fedorov, A.; Moret, M.-E.; Chen, P. *J. Am. Chem. Soc.* **2008**, *130*, 8880.
195. Echavarren, A. M. *Nature chemistry* **2009**, *1*, 431.
196. Hashmi, A. S. K. *Angew. Chem. Int. Ed.* **2008**, *47*, 6754.
197. Benitez, D.; Shapiro, N. D.; Tkatchouk, E.; Wang, Y.; Goddard, W. A.; Toste, F. D. *Nature chemistry* **2009**, *1*, 482.
198. Fürstner, A.; Morency, L. *Angew. Chem. Int. Ed.* **2008**, *47*, 5030.
199. Fañanás-Mastral, M. n.; Aznar, F. *Organometallics* **2009**, *28*, 666.
200. Seidel, G.; Mynott, R.; Fürstner, A. *Angew. Chem. Int. Ed.* **2009**, *48*, 2510.
201. Schubert, U.; Ackermann, K.; Aumann, R. *Cryst Struct Commun* **1982**, *11*, 591.
202. Allen, F. H.; Kennard, O.; Watson, D. G.; Brammer, L.; Orpen, A. G.; Taylor, R. *Journal of the Chemical Society, Perkin Transactions 2* **1987**, *0*, S1.

203. Liu, L.-P.; Hammond, G. B. *Chemistry – An Asian Journal* **2009**, *4*, 1230.
204. Liu, L.-P.; Xu, B.; Mashuta, M. S.; Hammond, G. B. *J. Am. Chem. Soc.* **2008**, *130*, 17642.
205. Hansmann, M. M.; Rominger, F.; Hashmi, A. S. K. *Chemical Science* **2013**, *4*, 1552.
206. Fernández, E. J.; Laguna, A.; Olmos, M. E., Recent Developments in Arylgold(I) Chemistry. In *Adv. Organomet. Chem.*, Academic Press: 2004; Vol. Volume 52, pp 77.
207. Lin, I. J. B.; Vasam, C. S. *Can. J. Chem.* **2005**, *83*, 812.
208. Olah, G. A.; Westerman, P. W. *J. Am. Chem. Soc.* **1973**, *95*, 7530.
209. Olah, G. A.; Liang, G. *J. Am. Chem. Soc.* **1973**, *95*, 3792.
210. Olah, G. A.; Westerman, P. W.; Nishimura, J. *J. Am. Chem. Soc.* **1974**, *96*, 3548.
211. Olah, G. A.; Liang, G.; Babiak, K. A.; Murray, R. K. *J. Am. Chem. Soc.* **1974**, *96*, 6794.
212. Olah, G. A.; Prakash, G. K. S.; Liang, G. *The Journal of Organic Chemistry* **1977**, *42*, 2666.
213. Brookhart, M.; Studabaker, W. B.; Husk, G. R. *Organometallics* **1987**, *6*, 1141.
214. Tumer, S. U.; Herndon, J. W.; McMullen, L. *J. Am. Chem. Soc.* **1992**, *114*, 8394.
215. Connor, J. A.; Jones, E. M. *J. Chem. Soc., Dalton Trans.* **1973**, *0*, 2119.
216. Widenhoefer, R. A.; Han, X. *Eur. J. Org. Chem.* **2006**, *2006*, 4555.

217. Pohlki, F.; Doye, S. *Chem. Soc. Rev.* **2003**, 32, 104.
218. Hong, S.; Marks, T. J. *Acc. Chem. Res.* **2004**, 37, 673.
219. Marcseková, K.; Doye, S. *Synthesis* **2007**, 2007, 145.
220. Beller, M.; Thiel, O. R.; Trauthwein, H. *Synlett* **1999**, 1999, 243.
221. Yin, Y.; Zhao, G. *J. Fluorine Chem.* **2007**, 128, 40.
222. Haskins, C. M.; Knight, D. W. *Chem. Commun.* **2002**, 0, 2724.
223. Yin, Y.; Zhao, G. *Heterocycles* **2006**, 68, 23.
224. Motokura, K.; Nakagiri, N.; Mori, K.; Mizugaki, T.; Ebitani, K.; Jitsukawa, K.; Kaneda, K. *Org. Lett.* **2006**, 8, 4617.
225. Yang, L.; Xu, L.-W.; Xia, C.-G. *Tetrahedron Lett.* **2008**, 49, 2882.
226. Jimenez, O.; Müller, T. E.; Schwieger, W.; Lercher, J. A. *J. Catal.* **2006**, 239, 42.
227. Ackermann, L.; Kaspar, L. T.; Althammer, A. *Organic & Biomolecular Chemistry* **2007**, 5, 1975.
228. Jazzar, R.; Dewhurst, R. D.; Bourg, J.-B.; Donnadiou, B.; Canac, Y.; Bertrand, G. *Angew. Chem. Int. Ed.* **2007**, 46, 2899.
229. Lapis, A. A. M.; DaSilveira Neto, B. A.; Scholten, J. D.; Nachtigall, F. M.; Eberlin, M. N.; Dupont, J. *Tetrahedron Lett.* **2006**, 47, 6775.
230. Yadav, J. S.; Reddy, B. V. S.; Raju, A.; Ravindar, K.; Narender, R. *Lett Org Chem* **2008**, 5, 651.

231. Yang, L.; Xu, L. W.; Xia, C. G. *Synthesis-Stuttgart* **2009**, 1969.
232. Griffiths-Jones, C. M.; Knight, D. W. *Tetrahedron* **2010**, *66*, 4150.
233. Ackermann, L.; Althammer, A. *Synlett* **2008**, 2008, 995.
234. Lemechko, P.; Grau, F.; Antoniotti, S.; Duñach, E. *Tetrahedron Lett.* **2007**, *48*, 5731.
235. Coulombel, L.; Dunach, E. *Green Chemistry* **2004**, *6*, 499.
236. Franck, X.; Figadère, B.; Cavé, A. *Tetrahedron Lett.* **1997**, *38*, 1413.
237. Miura, K.; Hondo, T.; Takahashi, T.; Hosomi, A. *Tetrahedron Lett.* **2000**, *41*, 2129.
238. Wang, B.; Gu, Y.; Yang, L.; Suo, J.; Kenichi, O. *Catal. Lett.* **2004**, *96*, 71.
239. Linares-Palomino, P. J.; Salido, S. a.; Altarejos, J. n.; Sánchez, A. *Tetrahedron Lett.* **2003**, *44*, 6651.
240. Coulombel, L.; Duñach, E. *Synth. Commun.* **2005**, *35*, 153.
241. Zhou, Y.; Woo, L. K.; Angelici, R. J. *Applied Catalysis A: General* **2007**, *333*, 238.
242. Li, Z.; Zhang, J.; Brouwer, C.; Yang, C.-G.; Reich, N. W.; He, C. *Org. Lett.* **2006**, *8*, 4175.
243. Yang, C.-G.; He, C. *J. Am. Chem. Soc.* **2005**, *127*, 6966.
244. Taylor, J. G.; Adrio, L. A.; Hii, K. K. *Dalton Transactions* **2010**, *39*, 1171.
245. Adrio, L. A.; Quek, L. S.; Taylor, J. G.; Kuok Hii, K. *Tetrahedron* **2009**, *65*, 10334.

246. Cheng, X.; Xia, Y.; Wei, H.; Xu, B.; Zhang, C.; Li, Y.; Qian, G.; Zhang, X.; Li, K.; Li, W. *Eur. J. Org. Chem.* **2008**, 2008, 1929.
247. Taylor, J. G.; Whittall, N.; Hii, K. K. *Org. Lett.* **2006**, 8, 3561.
248. Wei, H.; Qian, G.; Xia, Y.; Li, K.; Li, Y.; Li, W. *Eur. J. Org. Chem.* **2007**, 2007, 4471.
249. Wabnitz, T. C.; Yu, J.-Q.; Spencer, J. B. *Chemistry – A European Journal* **2004**, 10, 484.
250. Chwang, W. K.; Nowlan, V. J.; Tidwell, T. T. *J. Am. Chem. Soc.* **1977**, 99, 7233.
251. Nowlan, V. J.; Tidwell, T. T. *Acc. Chem. Res.* **1977**, 10, 252.
252. Kresge, A. J.; Chiang, Y.; Fitzgerald, P. H.; McDonald, R. S.; Schmid, G. H. *J. Am. Chem. Soc.* **1971**, 93, 4907.
253. Koshy, K. M.; Roy, D.; Tidwell, T. T. *J. Am. Chem. Soc.* **1979**, 101, 357.
254. Csizmadia, V. M.; Koshy, K. M.; Lau, K. C. M.; McClelland, R. A.; Nowlan, V. J.; Tidwell, T. T. *J. Am. Chem. Soc.* **1979**, 101, 974.
255. Chwang, W. K.; Knittel, P.; Koshy, K. M.; Tidwell, T. T. *J. Am. Chem. Soc.* **1977**, 99, 3395.
256. Taft, R. W. *J. Am. Chem. Soc.* **1952**, 74, 5372.
257. Taft, R. W.; Purlee, E. L.; Riesz, P.; DeFazio, C. A. *J. Am. Chem. Soc.* **1955**, 77, 1584.
258. Boyd, R. H.; Taft, R. W.; Wolf, A. P.; Christman, D. R. *J. Am. Chem. Soc.* **1960**, 82, 4729.

259. Freeman, F. *Chem. Rev.* **1975**, 75, 439.
260. Banthorpe, D. V. *Chem. Rev.* **1970**, 70, 295.
261. Cooper, J. D.; Vitullo, V. P.; Whalen, D. L. *J. Am. Chem. Soc.* **1971**, 93, 6294.
262. Hevesi, L.; Piquard, J. L.; Wautier, H. *J. Am. Chem. Soc.* **1981**, 103, 870.
263. Okuyama, T.; Fueno, T. *J. Am. Chem. Soc.* **1980**, 102, 6590.
264. Wautier, H.; Desauvage, S.; Hevesi, L. *J. Chem. Soc., Chem. Commun.* **1981**, 0, 738.
265. Jencks, W. P. *Chem. Rev.* **1972**, 72, 705.
266. Jencks, W. P. *Acc. Chem. Res.* **1980**, 13, 161.
267. Jencks, W. P. *Chem. Soc. Rev.* **1981**, 10, 345.
268. Chiang, Y.; Kresge, A. J. *J. Am. Chem. Soc.* **1985**, 107, 6363.
269. Dietze, P. E.; Jencks, W. P. *J. Am. Chem. Soc.* **1987**, 109, 2057.
270. Herlihy, K. *Aust. J. Chem.* **1989**, 42, 1345.
271. Fahey, R. C., The Stereochemistry of Electrophilic Additions to Olefins and Acetylenes. In *Topics in Stereochemistry*, John Wiley & Sons, Inc.: 2007; pp 237.
272. Hammond, G. S.; Nevitt, T. D. *J. Am. Chem. Soc.* **1954**, 76, 4121.
273. Hammond, G. S.; Collins, C. H. *J. Am. Chem. Soc.* **1960**, 82, 4323.

274. Pocker, Y.; Stevens, K. D. *J. Am. Chem. Soc.* **1969**, *91*, 4205.
275. M. Weiss, H.; M. Touchette, K. *Journal of the Chemical Society, Perkin Transactions 2* **1998**, *0*, 1517.
276. Fahey, R. C.; McPherson, C. A. *J. Am. Chem. Soc.* **1971**, *93*, 2445.
277. Pasto, D. J.; Meyer, G. R.; Lepeska, B. *J. Am. Chem. Soc.* **1974**, *96*, 1858.
278. Becker, K. B.; Grob, C. A. *Synthesis* **1973**, 1973, 789.
279. Fahey, R. C.; Smith, R. A. *J. Am. Chem. Soc.* **1964**, *86*, 5035.
280. Fahey, R. C.; Monahan, M. W. *J. Am. Chem. Soc.* **1970**, *92*, 2816.
281. Pasto, D. J.; Gadberry, J. F. *J. Am. Chem. Soc.* **1978**, *100*, 1469.
282. Staab, H. A.; Wittig, C. M.; Naab, P. *Chem. Ber.* **1978**, *111*, 2965.
283. Naab, P.; Staab, H. A. *Chem. Ber.* **1978**, *111*, 2982.
284. Pocker, Y.; Stevens, K. D.; Champoux, J. J. *J. Am. Chem. Soc.* **1969**, *91*, 4199.
285. Fahey, R. C.; McPherson, C. A.; Smith, R. A. *J. Am. Chem. Soc.* **1974**, *96*, 4534.
286. Fahey, R. C.; Monahan, M. W.; McPherson, C. A. *J. Am. Chem. Soc.* **1970**, *92*, 2810.
287. Corriu, R.; Guenzet, J. *Tetrahedron* **1970**, *26*, 671.
288. Fahey, R. C.; McPherson, C. A. *J. Am. Chem. Soc.* **1969**, *91*, 3865.

289. Allen, A. D.; Tidwell, T. T. *J. Am. Chem. Soc.* **1982**, *104*, 3145.
290. Roberts, R. M. G. *Journal of the Chemical Society, Perkin Transactions 2* **1976**, *0*, 1183.
291. Dewar, J. S.; Fahey, R. C. *Angewandte Chemie International Edition in English* **1964**, *3*, 245.
292. Dewar, M. J. S.; Fahey, R. C. *J. Am. Chem. Soc.* **1963**, *85*, 3645.
293. Abraham, R. J.; Monasterios, J. R. *Journal of the Chemical Society, Perkin Transactions 2* **1975**, *0*, 574.
294. Berlin, K. D.; Lyerla, R. O.; Gibbs, D. E.; Devlin, J. P. *Journal of the Chemical Society D: Chemical Communications* **1970**, *0*, 1246.
295. Dewar, M. J. S.; Fahey, R. C. *J. Am. Chem. Soc.* **1963**, *85*, 2245.
296. Dewar, M. J. S.; Fahey, R. C. *J. Am. Chem. Soc.* **1963**, *85*, 2248.
297. Izawa, K.; Okuyama, T.; Fueno, T. *Bull. Chem. Soc. Jpn.* **1974**, *47*, 1477.
298. Li, X.; Ye, S.; He, C.; Yu, Z.-X. *Eur. J. Org. Chem.* **2008**, *2008*, 4296.
299. Kovács, G. b.; Lledós, A.; Ujaque, G. *Organometallics* **2010**, *29*, 5919.
300. Miura, K.; Hondo, T.; Nakagawa, T.; Takahashi, T.; Hosomi, A. *Org. Lett.* **2000**, *2*, 385.
301. Miura, K.; Okajima, S.; Hondo, T.; Nakagawa, T.; Takahashi, T.; Hosomi, A. *J. Am. Chem. Soc.* **2000**, *122*, 11348.
302. Howells, R. D.; Mc Cown, J. D. *Chem. Rev.* **1977**, *77*, 69.

303. Laughlin, R. G. *J. Am. Chem. Soc.* **1967**, *89*, 4268.
304. Olavi, P.; Virtanen, I.; Maikkula, M. *Tetrahedron Lett.* **1968**, *9*, 4855.
305. Birchall, T.; Gillespie, R. J. *Can. J. Chem.* **1963**, *41*, 2642.
306. Menger, F. M.; Mandell, L. J. *Am. Chem. Soc.* **1967**, *89*, 4424.
307. Melander, L. C. S., *Reaction rates of isotopic molecules*. Wiley: New York, 1980.
308. Hengge, A. C., *Isotope effects in chemistry and biology*. Taylor & Francis: Boca Raton, 2006.
309. Eaborn, C. J. *Organomet. Chem.* **1988**, *356*, C87.
310. Matsson, O.; Westaway, K. C., Secondary Deuterium Kinetic Isotope Effects and Transition State Structure. In *Adv. Phys. Org. Chem.*, Bethell, D., Ed. Academic Press: 1999; Vol. Volume 31, pp 143.
311. Streitwieser, A.; Jagow, R. H.; Fahey, R. C.; Suzuki, S. *J. Am. Chem. Soc.* **1958**, *80*, 2326.
312. Strausz, O. P.; Safarik, I.; O'Callaghan, W. B.; Gunning, H. E. *J. Am. Chem. Soc.* **1972**, *94*, 1828.
313. Safarik, I.; Strausz, O. P. *The Journal of Physical Chemistry* **1972**, *76*, 3613.
314. Bender, B. R. *J. Am. Chem. Soc.* **1995**, *117*, 11239.
315. Bigeleisen, J. *The Journal of Chemical Physics* **1949**, *17*, 675.
316. Bigeleisen, J.; Mayer, M. G. *The Journal of Chemical Physics* **1947**, *15*, 261.

317. Bigeleisen, J.; Wolfsberg, M., Theoretical and Experimental Aspects of Isotope Effects in Chemical Kinetics. In *Adv. Chem. Phys.*, John Wiley & Sons, Inc.: 1957; pp 15.
318. Roeges, N. P. G., *A guide to the complete interpretation of infrared spectra of organic structures*. Wiley: Chichester ; New York, 1994.
319. Hartshorn, S. R.; Shiner, V. J. *J. Am. Chem. Soc.* **1972**, *94*, 9002.
320. Gajewski, J. J.; Olson, L. P.; Tupper, K. J. *J. Am. Chem. Soc.* **1993**, *115*, 4548.
321. Okuyama, T.; Fueno, T. *J. Am. Chem. Soc.* **1983**, *105*, 4390.
322. Hout, R. F.; Levi, B. A.; Hehre, W. J. *J. Comput. Chem.* **1983**, *4*, 499.
323. Seltzer, S. *J. Am. Chem. Soc.* **1961**, *83*, 1861.
324. Schubert, W. M.; Lamm, B. *J. Am. Chem. Soc.* **1966**, *88*, 120.
325. Schubert, W. M.; Lamm, B.; Keefee, J. R. *J. Am. Chem. Soc.* **1964**, *86*, 4727.
326. Pocker, Y.; Hill, M. J. *J. Am. Chem. Soc.* **1969**, *91*, 7154.
327. Kresge, A. J.; Weeks, D. P. *J. Am. Chem. Soc.* **1984**, *106*, 7140.
328. *Principles and applications of organotransition metal chemistry*. University Science Books: Mill Valley, Calif., 1987.
329. Qian, H.; Han, X.; Widenhoefer, R. A. *J. Am. Chem. Soc.* **2004**, *126*, 9536.
330. Kantner, S. S.; Humski, K.; Goering, H. L. *J. Am. Chem. Soc.* **1982**, *104*, 1693.

331. Braem, D.; Gülaçar, F. O.; Burger, U.; Buchs, A. *Org. Mass Spectrom.* **1979**, *14*, 609.

Biography

Rachel Elizabeth McKinney Brooner was born in Pensacola, Florida in 1985. After earning an International Baccalaureate diploma from Pensacola High School, Rachel received a Bachelors of Arts in Chemistry and a Bachelors of Arts in Psychology from Huntingdon College in Montgomery, Alabama.

After graduation, Rachel accepted entrance into the Duke University Chemistry Department to pursue a PhD in Chemistry as a James B. Duke fellow. Rachel affiliated with the Widenhoefer lab in January of 2009 and began researching the synthesis of organometallic complexes of gold(I) and mechanistic studies in gold(I)- and acid-catalyzed π -activation catalysis.

While at Duke, Rachel has been awarded the Burroughs Welcome Fellowship (2010-2011), the Joe Taylor Adams Fellowship (2013), and the Charles Bradsher Fellowship (2013) by the Duke Chemistry Department. She was also recognized by the Duke chapter of Sigma Xi and the Inorganic division of the American Chemical Society with travel grants for participation in conferences.

Rachel's research in the Widenhoefer lab has been published in a number of original, peer-reviewed research reports and presented at several nationally recognized conferences. In addition, she has co-authored an invited review on gold(I) π -complexes.

Publications

Brooner, R. E. M.; Widenhoefer, R. A. Experimental Studies of Cationic, Two-Coordinate Gold π -Complexes. Invited contribution for *Angew. Chem., Int. Ed.*, *in press*.

Brooner, R. E. M.; Brown, T. J.; Widenhoefer, R. A. Direct Observation of a Cationic Gold(I) Bicyclo-[3.2.0]-hept-1(7)-ene Complex Generated in the Cycloisomerization of a 7-Phenyl-1,6-Enyne. *Angew. Chem., Int. Ed.*, **2013**, *52*, 6259.

Brooner, R. E. M.; Brown, T. J.; Widenhoefer, R. A. Synthesis and Study of Cationic, Two-coordinate Triphenylphosphine Gold π -Complexes. *Chem. Eur. J.*, **2013**, *19*, 8276.

Brooner, R. E. M.; Widenhoefer, R. A. Synthesis and Structure of Dicationic, Bis(gold) π -Alkene Complexes Containing a 2,2'-Bis(phosphino)biphenyl Ligand. *Organometallics* **2012**, *31*, 768.

Brooner, R. E. M.; Widenhoefer, R. A. Syntheses, X-ray Crystal Structures, and Solution Behavior of Cationic, Two-Coordinate Gold(I) η^2 -Diene Complexes. *Organometallics* **2011**, *30*, 3182.

Brooner, R. E. M.; Widenhoefer, R. A. Stereochemistry and Mechanism of the Brønsted Acid Catalyzed Intramolecular Hydrofunctionalization of an Unactivated Cyclic Alkene. *Chem. Eur. J.* **2011**, *17*, 6170.

Research Presentations

Brooner, R. E. M., Widenhoefer, R. A. "Synthesis and Solution Behavior of Cationic, Two-coordinate Gold(I) π -Complexes Bearing a Triphenylphosphine Ligand." 244th National Meeting of the American Chemical Society. August 2012. Poster.

Brooner, R. E. M., Brown, T. J., Widenhoefer, R. A. "Synthesis, Characterization, Structures, and Solution Behavior of Cationic, Monomeric Gold(I) π -Complexes." Gordon Research Conference in Organometallic Chemistry. July 2012. Poster.

Brooner, R. E. M., Widenhoefer, R. A. "Syntheses, X-ray Crystal Structures, and Solution Behavior of Cationic, Two-Coordinate Gold(I) η^2 -Diene Complexes." 242nd National Meeting of the American Chemical Society. August 2011. Oral Presentation.